Physical and Chemical Speciation of Iron in the Polar Oceans

Thuróczy, Charles-Edouard

Physical and Chemical Speciation of Iron in the Polar Oceans

Fysische en Chemische Speciatie Van IJzer in Polaire Wateren

Charles-Edouard Thuróczy

The work presented in this thesis was carried out at the Department of Biological Oceanography of the Royal Netherlands Institute for Sea Research (NIOZ):

Royal Netherlands Institute for Sea Research (NIOZ)
Department of Biological Oceanography
P.O. Box 59
1790 AB Den Burg
The Netherlands

Financial support was provided by the International Polar Year program of the Netherlands Organisation for Scientific Research (NWO) as the subsidy for Geotraces sub-project 851.40.102.

Cover design: Alex-T-/Alex Thuróczy

ISBN: 978-90-367-5141-4

RIJKSUNIVERSITEIT GRONINGEN

Physical and Chemical Speciation of Iron in the Polar Oceans

Proefschrift

ter verkrijging van het doctoraat in de
Wiskunde en Natuurwetenschappen
aan de Rijksuniversiteit Groningen
op gezag van de
Rector Magnificus, dr. E. Sterken,
in het openbaar te verdedigen op
maandag 21 november 2011
om 14:30 uur

door

Charles-Edouard Thuróczy
geboren op 21 januari 1983
te Bois-Colombes, Frankrijk

Promotor:	Prof. dr. ir. H.J.W. De Baar
Copromotor:	Dr. L.J.A. Gerringa
Beoordelingscommissie:	Prof. dr. C.M.G. Van Den Berg
	Prof. dr. A.G.J. Buma
	Prof. dr. S. Blain

To my family

Contents

Chapter 1

Introduction

1. Iron and ligands

Iron (Fe) is a transition metal and is the fourth most abundant element in the Earth's crust (5.6%, Taylor, 1964; Turner *et al.*, 2001) after oxygen (O), silicon (Si) and aluminium (Al). This abundance is due to its very stable nucleus ^{56}Fe which represents 91.66% of the six Fe isotopes (from ^{54}Fe to ^{59}Fe; Turner *et al.*, 2001). In contrast, in the modern ocean Fe is present at very low concentrations. It is such a scarce element, that it is limiting phytoplankton growth in 40% of the world ocean in region known as HNLC (High Nutrient, Low Chlorophyll, De Baar *et al.*, 1990; Martin *et al.*, 1991; De Baar and De Jong, 2001). Despite its very low concentration, Fe is essential for phytoplankton in the euphotic zone of the surface ocean where solar irradiance is present. Phytoplankton is the base of the food web and is responsible for fixation of dissolved carbon dioxide via photosynthesis in the upper euphotic. Photosynthesis is the process that transforms water (H_2O) and carbon dioxide (CO_2) into carbohydrates ($C_6H_{12}O_6$ or CH_2O) and dioxygen (O_2) with presence of light (photons). Microbial communities comprising the bacteria and archaea also need Fe for their functioning. These organisms are, in contrast to phytoplankton, present throughout the whole water column (Tortell *et al.*, 1999; Reinthaler *et al.*, 2006) and are responsible for degradation and remineralisation of sinking organic matter. Part of the organic matter and the products issued from its breakdown constitute an interesting mixture of molecules with a potentially high affinity to bind Fe. These molecules that are able to bind Fe are called ligands and are crucial to keep Fe dissolved in seawater. Due to their strong binding properties, these ligands enhance the solubility of Fe in seawater (as explained in paragraph 3) and thus its bioavailability to micro-organisms.

2. Evolution of the biogeochemistry of iron in the ocean and appearance of the ligands: from the primitive to the modern ocean

During the Archean Era (>2.5 billion years ago), oxygen was absent from the ocean. However, sulphur was dominant, hence governed the redox potentials in the ocean instead of oxygen. Under these conditions, due to the higher solubility, Fe

was abundant (Da Silva and William, 1991) between 10 and 100 μM (Saito *et al.*, 2003). Later in this period, photoautotroph cyanobacteria appeared (Saito *et al.*, 2003; Hunter and Boyd, 2007) and they evolved relying on the most abundant, available and suitable transition metal as an electron mediator for their metabolism.

Iron allows an easy electron transfer in enzymes because of a low energy requirement. Iron has a standard redox potential of 0.77V ($Fe^{3+} + e^- \rightarrow Fe^{2+}$; E^0 = 0.77 V; Hunter and Boyd, 2007). Iron is used in 1) metallo-enzymes (ATP synthase, nitrogen fixation and reduction of nitrate, nitrite and sulphate), 2) in vital processes of living entities, notably for respiration and photosynthesis (Photosystems I and II, cytochromes; Sunda *et al.*, 1991 and 2001; Timmermans *et al.*, 2001 and 2005), and for 3) oxygen transport in higher organisms.

Cyanobacteria evolved during a transition period between the primitive and the modern ocean, the Proterozoic Era (2.5-0.5 billion years ago). At this time, the ocean was even more sulfidic than during the Archean Era (Saito *et al.*, 2003; Hunter and Boyd, 2007) and photosynthesis by the cyanobacteria caused a gradual oxygenation of the oceans, from the surface to the deep followed by transfer of oxygen into the atmosphere. Concentrations of Fe decreased to about 0.1 μM in the ocean (Saito *et al.*, 2003). Eukaryotes also appeared during the Proterozoic; they evolved and diversified through the geological times in a wide range of living entities, from unicellular phytoplankton to multicellular complex organisms, all of them using Fe. The multiplication and diversification of the living entities lead to the increasing production of organic ligands. The gradual ocean oxygenation leaded to massive precipitation of Fe, such that concentrations in seawater decreased to nano-molar values. This massive precipitation formed large and worldwide Fe deposits (Banded Iron Formation, BIF; De Baar and La Roche, 2003). This resulted in a dramatic change in Fe availability over the geological time (Saito *et al.*, 2003), with organic complexation of Fe controlling its availability to the living organisms.

3. The biogeochemistry of iron in the modern ocean

Iron exists in several physical-chemical states in seawater. These states are classified as species and the complete assembly of several species is known as the speciation of Fe (or another trace metal) in seawater. Iron has two oxidation states: the soluble ferrous form Fe(II), which is oxidised into the ferric form Fe(III) under oxic conditions. Under oxic conditions, the ferric form has a low solubility at normal seawater pH~8 (Kuma *et al.*, 1996; Millero, 1998), of 0.08 to 0.2 nM Fe (Liu and Millero, 2002; Wu *et al.*, 2001). However, thanks to the presence of organic molecules (*i.e.* ligands), Fe is found at higher concentrations than expected by its solubility. These ligands form strong Fe(III)-complexes allowing to keep Fe in the dissolved phase, hence enhance Fe solubility, as already mentioned in paragraph 1. The existence of Fe-binding ligands was proven first by Gledhill and Van Den Berg (1994). In oxic seawater, Fe(III) forms strong complexes with donor ligands containing oxygen, nitrogen (N) and fluor (F), whereas in anoxic conditions, Fe(II) forms strong complexes with donor ligands containing phosphorus (P) and sulphur (S) (Ussher *et al.*, 2004).

In seawater, up to 99.9% of dissolved Fe(III) (DFe) is bound to organic ligands (Gledhill and Van Den Berg, 1994; Rue and Bruland, 1995; Wu and Luther, 1995; Nolting *et al.*, 1998; Hutchins *et al.*, 1999a and 1999b; Powell and Donat, 2001; Gerringa *et al.*, 2006 and 2007), which are mainly originating from living organisms (Dissolved Organic Matter, DOM; Hirose, 2007). These ligands are either originating from the degradation of organic matter, like algae and fecal pellets, or other biologic products, like sugars and siderophores. Siderophore are molecules produced by prokaryotes and enhance the availability of Fe under Fe-stress conditions (Butler, 1998 and 2005; Barbeau *et al.*, 2001; Maldonado *et al.*, 2005). Recent studies allowed assigning a large variety of molecules as being Fe-binding ligands like humic substances, which seem to be very refractory in the deep oceans (Laglera *et al.*, 2007). Among others, siderophores (Rue and Bruland, 1995; Lewis *et al.*, 1995; Hudson, 1998; Hutchins *et al.*, 1999; Witter *et al.*, 2000; Macrellis *et al.*, 2001; Martinez *et al.*, 2007; Gledhill *et al.*, 2004; Haygood *et al.*, 1993; Reid *et al.*, 1993; Wilhelm and Trick, 1994; Wilhelm, 1995; Wilhelm *et al.*,

1996 and 1998), transparent exopolymer particles (TEP, Logan *et al.*, 1995), and saccharides (Van Der Merwe *et al.*, 2009; Hassler *et al.*, 2009 and 2011) have proven to be of importance in the Fe binding ligand pool and having a potential to enhance Fe bioavailability.

Under the term "ligand", one should read "ligand soup" since there may actually be hundreds, thousands yet more different ligands in seawater over a wide size spectrum of size classes and Fe-binding functional groups (Buffle and Leppard, 1995a and 1995b). In oceanography, this metal complexation is commonly measured using voltammetric methods (Gledhill and Van Den Berg, 1994; Wu and Luther, 1995; Rue and Bruland, 1995 and 1997; Lewis *et al.*, 1995; Nolting *et al.*, 1998; Hutchins *et al.*, 1999a and 1999b; Witter *et al.*, 2000; Barbeau *et al.*, 2001; Boye *et al.*, 2001; Powell and Donat, 2001; van Leeuwen and Raewyn, 2005; van Leeuwen and Jansen, 2005; Gerringa *et al.*, 2006, 2007 and 2008). The ligands are described using one ligand class (Gledhill and Van Den Berg, 1994; Wu and Luther, 1995; Boye *et al.*, 2001; Powell and Donat, 2001; Gerringa *et al.*, 2006, 2007 and 2008) or two classes of ligands (Rue and Bruland, 1995 and 1997; Lewis *et al.*, 1995; Nolting *et al.*, 1998; Hutchins *et al.*, 1999a and 1999b; Barbeau *et al.*, 2001), the distinction between one or two ligand classes also depending on the method of measurement. In the case of two ligand classes, most authors discuss a relatively strong class L1 (siderophore like) mainly found in surface waters. This L1 ligand is attributed to bacterial/microbial activity, but exists at lower concentrations than the second class of ligands L2. This second class of L2 ligands is relatively weak but found in the whole water column and originates from degradation of organic matter (breakdown of biological material) in sinking particles (dying plankton, fecal pellets) and terrestrial organic matter transported from the shelves. Moreover, Rijkenberg *et al.* (2008b) measured weaker ligands in surface waters which were attributed to bacterial breakdown of phytoplankton blooms.

Nevertheless, Fe is not only bound to organic ligands, but also forms inorganic complexes (Fe-oxy(hydr)-oxides) defining the inorganic Fe speciation (Millero, 1998; Hudson *et al.*, 2003). The main inorganic complexes may be the oxy-oxide

$[Fe(CO_3)_2]^{2-}$ for Fe(II) and the hydr-oxides $[Fe(OH)]^{2+}$, $[Fe(OH)_2]^{+}$, $[Fe(OH)_3]^{0}$, $[Fe(OH)_4]^{-}$ and $[FeCl]^{2+}$ for Fe(III). At normal seawater pH, about 60% of inorganic dissolved Fe may be in the $[Fe(OH)_3]^{0}$ form as predicted by a model for inorganic Fe(III) speciation in seawater (Liu and Millero, 2002; Millero *et al.*, 1995). This chemical species is very sensitive to precipitation.

4. Processes controlling the fate of iron in the ocean: the main parameters of the Fe cycle

The distribution of Fe is controlled by the competition between stabilisation and removal processes within the oceans and by the presence of external sources of Fe to the ocean (De Baar and De Jong, 2001).

The external sources of Fe to the oceans are predominantly inputs from the river runoff and continental margin, sediment re-suspension and upwelling (Johnson *et al.*, 1997; De Baar and De Jong, 2001; Moore and Braucher, 2008; Klunder *et al.*, 2011), aerosols deposition at the surface (Duce and Tindale, 1991; Jickells *et al.*, 2005), ice melting (Lannuzel *et al.*, 2007, 2008 and 2010) and hydrothermal vents (Klunder *et al.*, 2011). The residence time of Fe has been estimated from 20 to 200 days in surface waters, where mixing and biologic activity are very dynamic, to 70-200 yr in deep waters (Ussher *et al.*, 2004). Stabilisation of Fe in seawater is ensured by organic complexation with natural ligands, which increases the residence time of Fe in seawater, hence enhances its potential bioavailability. Iron can be removed from the water column by precipitation as oxy-hydroxides and by adsorption and scavenging on settling particles (>0.2 μm). In seawater, the majority of Fe is actually present in the particulate phase (Cullen *et al.*, 2006; Vraspir and Butler, 2009). Terrigenous particles from lands (*i.e.* earth crust) are very rich in Fe but only release a small percentage of metals (*e.g.* Fe) in seawater (Desboeufs and Losno, 2001; Bonnet and Guieu, 2004; Journet *et al.*, 2008) and have a short residence time in the water column. Fine colloids are known to be very reactive (Wells *et al.*, 1993 and 2000: Nishioka *et al.*, 2001 and 2005) and can have a long residence time in seawater.

These fine colloids can be the first step in the removal of Fe in the deep ocean by next forming larger aggregates that by Stokes Law can sink more rapidly (Kepkay *et al.*, 1994; Logan *et al.*, 1995; Wu *et al.*, 2001; Cullen *et al.*, 2006).

5. Physical and chemical speciation of Fe in this study

Since size fractionation gives information on the concentrations of Fe and ligands and on the conditional stability constant of the ligands with Fe, it informs us on the processes controlling the distribution of Fe in the Ocean, for example solubilisation of Fe via organic complexation and Fe removal via colloid aggregation, export via scavenging and precipitation.

The speciation of Fe comprises the investigation of the different forms of Fe in seawater within a size spectrum. Different size fractions are separated by mean of filtrations (*i.e.* physical speciation). In each of the size fractions, chemical analyses are used to determine different parameters which characterize the Fe binding ligands (*i.e.* chemical speciation).

Three size fractions were studied during this thesis: 1) the total fraction using unfiltered samples, which contains the particulate fraction (>0.2 μm), 2) the dissolved fraction (<0.2 μm); and 3) a fraction smaller than 1000 kDa which contains the truly soluble (<10 kDa) and the small colloidal fraction. Upon such size fractionation, one or more fractions were subjected to voltammetric analyses in order to obtain results on the concentrations and conditional stability constant of the Fe-binding ligands in seawater. The filtrations and analytical procedures involved here are described in Chapter 2.

The physical and chemical speciation of Fe was investigated first in the Eastern North Atlantic Ocean at a station off the coast of Portugal (Chapter 3). Following this cruise, three polar cruises were completed: the first one in the Arctic Ocean in 2007 (Chapter 6); a second one in the Atlantic sector of the Southern Ocean in 2008 (Chapter 4 and 5) along the Zero Meridian from Cape Town to the Antarctic continent, through the Weddell Sea and through the Drake Passage; and the third one in the Amundsen Sea (Southern Ocean), west of the Antarctic Peninsula in 2009 during the phytoplankton blooms (Chapter 7). The major findings and an

overview of the processes involved in the cycling of Fe regarding the organic complexation, as well as recommendations for future research, are summarised in the final synthesis (Chapter 8).

6. Importance and objectives of the GEOTRACES program during the International Polar Year

Geotraces is an international program which aims to study the large-scale distribution of the key trace elements and isotopes in order to understand their biogeochemical cycles in the oceans in relation to a changing environment (GEOTRACES Science Plan). The key trace elements are iron (Fe), aluminium (Al), manganese (Mn), zinc (Zn), cadmium (Cd) and copper (Cu). These metals can either be essential (Fe, Mn, Zn) and/or toxic (Cd and Cu) for the marine organisms and thus directly influencing their ecosystems, hence the global carbon cycle. Moreover Al and some other trace elements show intriguing correlations with the overall ocean biological cycle (Middag *et al.*, 2009) that deserve further unraveling by investigation. The cycling of the trace elements depends on the sources to the oceans (notably continental runoff, sediments, atmosphere, ocean crust, hydrothermal activity), on internal processes taking place within the ocean (uptake, regeneration, burial, and circulation), and on their chemical speciation.

The International Polar Year (IPY) is a scientific framework aiming to study the Arctic and Antarctic regions. The fourth IPY, after those in 1882-1883, 1932-1933 and 1957-1958, took place between March 2007 and March 2009 in order to cover 2 complete annual cycles. Very diverse social, physical, biological and chemical subjects were investigated by over 60 nations. The Arctic and the Antarctic Peninsula regions are among the most affected by the warming climate. These sensitive polar ecosystems are therefore are threatened by the rapid changing environment. It is therefore of our duty to observe, understand and explain the mechanisms involved in order to predict future changes and limit the negative effects on our planet.

Chapter 2

Materials and methods

1. Seawater fractions studied for the speciation of Fe

Analyses of Fe concentrations, ligand concentrations and their characteristics were done in unfiltered samples and in two size fractions:

1. Unfiltered samples (UNF), containing the total dissolvable fraction of Fe, which consist of the particulate fraction (>0.2 μm) and the dissolved fraction (<0.2 μm);
2. The dissolved fraction, by convention defined as <0.2 μm;
3. The fraction smaller than 1000 kDa (<1000 kDa), containing the truly soluble and the small colloidal fraction.

Note that the fraction comprised between 1000 kDa and 0.2 μm is called larger colloidal fraction in this thesis. In chapters 4 and 7, only the dissolved fraction was analysed and discussed.

2. Parameters commonly used

The following parameters were used to describe and interpret the results obtained during this thesis:

- Iron concentrations [Fe]: Fe in the unfiltered fraction is called Total Dissolvable Fe **[TDFe]** and represents the concentration of the Fe that has been dissolved after acidification and one year storage of the sample at pH 1.8. Iron in the dissolved fraction is denoted as [**DFe]** and is analysed in a sample that after the filtration was acidified to pH 1.8 and next analysed within 24 hours. The Fe in the fraction smaller than 1000 kDa as [$\mathbf{Fe_{<1000\ kDa}}$] was also acidified to pH 1.8 and analysed within 24 hours.
- Note that **particulate Fe** (>0.2 μm) is sometimes mentioned, and corresponds to [TDFe]-[DFe]. Similarly, **larger colloidal Fe** (between 1000 kDa and 0.2 μm) corresponds to [DFe]-[$Fe_{<1000\ kDa}$].
- Total ligand concentration (per fraction) is **[Lt]**: $\mathbf{[Lt]_{<0.2\ \mu m}}$ in the dissolved fraction, and $\mathbf{[Lt]_{<1000\ kDa}}$ in the fraction <1000 kDa.

- Excess ligand concentration (**[Excess L]** or **[L']**): Excess L corresponds to the empty ligand sites and thus expresses the binding potential of the ligands and is calculated by [Lt]-[Fe] for each size fraction.
- The conditional stability constant **K'** (**log K'** or **$\log_{10}$ K'** in its logarithmic form) reflects the binding strength of the natural ligands with Fe.
- The ratio **[Excess L]/[Fe]** (Chapter 3, 5 and 6) or **[Lt]/[Fe]** (Chapter 4 and 7) represent the relative saturation state of the ligands with Fe (per fraction). Note that the ratio [Excess L]/[Fe] is always >0 and the ratio [Lt]/[Fe] is always >1 as the ligands are in excess of Fe, otherwise Fe would immediately precipitate. A low ratio (close to 0 for [Excess L]/[Fe] or close to 1 for [Lt]/[Fe]) corresponds to ligands saturated with Fe and indicates a low capacity of the ligands to bind and buffer additional Fe input. Higher is the ratio, lesser the ligands become saturated with Fe, thus buffering Fe inputs, hence increasing the solubility of Fe.
- Alpha **α** (**log α** or **$\log_{10}$ α** in its logarithm form) is the product of K' and Excess L. Alpha expresses the reactivity of the ligands.
- The concentration of Fe^{3+} expressed by pFe, the negative logarithm of [Fe^{3+}]. A low pFe value corresponds to a high concentration of free Fe, and reversely.

3. Cleaning procedures

All sample bottles (Nalgene, Low-Density Polyethylene, LDPE) were cleaned according to the following procedure: first the bottles were rinsed with demineralised water, then filled with a detergent solution (5% concentrated, Micro-90, International Products Corporation). Next, the bottles were soaked for 24 h in a hot bath (60-70ºC). After this, each bottle was rinsed with demineralised water to remove the soap and rinsed 2 times with MQ water (Millipore Milli-Q deionised water, R >18.2 MΩ cm^{-1}). Subsequently the bottles were filled with 6 M HCl (diluted from 37% HCl, reagent grade, J.T. Baker) and soaked during 24 h in a 60-70ºC bath. Next the bottles were rinsed 3 timed with MQ water. This acid-wash procedure was repeated, but then using a 3 M nitric acid (diluted from 65%, reagent grade, J.T. Baker). Finally, the bottles were stored filled with 0.2 M 3QD-

HNO3 (from 65% reagent grade, J.T. Baker) and each packed in two LDPE plastic bags. All the filling/emptying and rinsing steps were done in a clean room (class 100).

4. Sampling systems

Onboard R.V. *Pelagia* (Chapter 3) and R.V. *Polarstern* (Chapters 4, 5 and 6) the seawater samples were taken from the surface to the bottom using the Titan Mk. II frame which was connected to a Kevlar hydrowire (De Baar *et al.*, 2008a). On the frame were attached 24 internally Teflon-coated PVC 12 L GO-FLO samplers (General Oceanics Inc.). Immediately upon recovery the frame was placed inside a clean container for a direct sub-sampling from each GO-FLO sampler: "In fact this is within the more stringent criteria of an ISO Class 6 clean room (formerly US FED STD 209E Class 1000)", in De Baar *et al.*, 2008a.

Onboard R.V. *Nathaniel B. Palmer* (Chapter 7) in the Amundsen Sea (Southern Ocean) samples were taken in the upper 300 meters of the water column (typically at 10, 25, 50, 100, 200, 300 m) using the same type of modified Teflon coated GO-FLO samplers as used above on the frame, but here attached to a non-metal 6 mm diameter Dyneema wire. The samplers were closed using messengers.

5. Sampling procedures and filtrations

All samples were collected in acid-cleaned LDPE bottles after 5 times rinsing of the bottles with the sample itself (UNF, dissolved or <1000 kDa samples).

Unfiltered samples were taken first (Figure 1, step 1), then the rest of seawater was directly filtered in-line (0.2 μm pore size, Sartorius Sartobran-300) from the GO-FLO using slight nitrogen gas overpressure of 1.5 atm (Figure 1, step 2). Ultra-filtration of the 0.2 μm filtered water (Figure 1, step 3) was performed immediately after the first filtration in a laminary flow bench (class 0). Onboard R.V. *Nathaniel B. Palmer* (Chapter 7), the GO-FLO samplers were brought one by one to a trace metal clean container and linked to a tubing extension for sub-

sampling under a clean laminar down flow bench. Samples were filtered (0.2 µm pore size, Sartorius Sartobran-300) using N_2 overpressure (1.5 atm).

Ultrafiltration was performed using hollow-fibre-filters (Sterapore, Mitsubishi-rayon Co., Ltd.) with a size cut-off of 1000 kDa (Nishioka *et al.*, 2001). A 12-channels peristaltic pump (ISM 937, Ismatec, IPC-N) with Tygon® LFL (Long Flex Life) tubing was used for the ultra-filtration with a flow rate of 5-7 $ml.min^{-1}$.

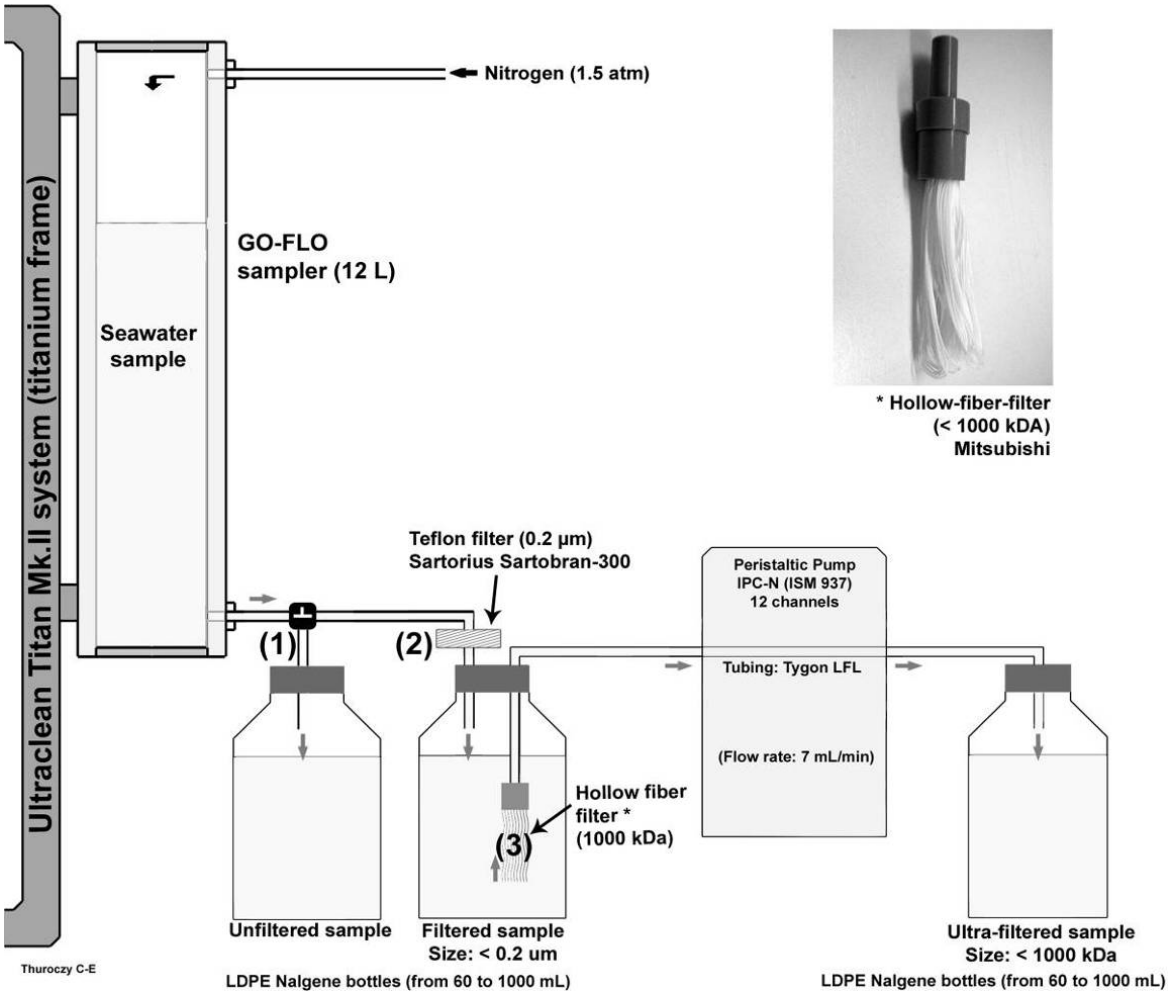

Figure 1: *Sampling using the Titan Mk. II frame and size fractionation of seawater:* ***1:*** *Unfiltered sampling.* ***2:*** *Filtration of seawater sample over 0.2 µm pore size filter.* ***3:*** *Ultra-filtration of the seawater sample over 1000 kDa pore size filter. Steps 1 and 2 were done in the titanium-frame clean air container. Step 3 was performed in a laminary flow bench (class 0) in another clean room.*

The polyethylene hollow-fibre-filters were activated and cleaned in the home laboratory before use on board according to the following protocol adapted from Nishioka *et al.* (2001).

The filters were activated by pumping 15 ml of three times quartz distilled (3QD-) methanol (flow rate of 5 $ml.min^{-1}$), then rinsed with 30 ml MQ water. They were left soaking for 3 days in an HCl bath (1 M, Suprapur, Merck) during which each day 25 ml of HCl 1 M was pumped through the filter (5 $ml.min^{-1}$). Then, they were rinsed with MQ water (140 ml, 7 $ml.min^{-1}$) and stored in acid-cleaned polypropylene tubes closed by caps and filled with acidified MQ water (0.02 M HCl, Suprapur, Merck). Before use on board, the filters were rinsed by pumping MQ water (300 ml, 7 $ml.min^{-1}$) and the sample itself (200 ml, 7 $ml.min^{-1}$).

A mass balance verification for Fe as well as for the ligands was done with 4 samples from the Southern Ocean (cruise ANTXXIV/3). Two samples, one from the surface layer, containing 0.162 nM Fe, and one deep sample near the sediment containing 0.994 nM Fe, were used. The sum of the larger colloidal (here assumed to be between 1000 kDa and 0.2 µm) and <1000 kDa fractions was compared with the dissolved fraction (<0.2 µm). This resulted in a perfect mass balance for Fe concentrations in both samples. Regarding the ligand concentrations, in surface samples a gain of Excess L concentration of 0.10 Eq of nM Fe was measured whereas in the deep samples a loss of Excess L of 0.05 Eq of nM Fe. These results were of the same order of magnitude as the detection limit (0.04 Eq of nM Fe) as mentioned in paragraph 7.1. Moreover, no Fe contamination was detected in the filtrate and in the retentate. Therefore the filters were considered to function properly.

6. Samples conservation and storage

Samples taken for Fe analysis by FIA were immediately acidified to pH 1.8 using 12 M ultraclean HCl (Baseline® Hydrochloric Acid, Seastar Chemicals Inc.). The dissolved and <1000 kDa filtered samples were left acidified for at least 12 h

before analysing. The unfiltered samples were acidified in the same way, but they were stored one year before being analysed in the home laboratory.

Samples taken for the analysis of the Fe speciation were stored at 4ºC when their analysis could be performed within 3 days; otherwise they were immediately frozen at -20ºC in the dark. Unfiltered samples were kept in the dark at 4ºC and measured within 3 days to avoid any influence of biological activity. They were discarded beyond 3 days storage in case that the analysis could not be performed.

7. Iron analyses

Iron analyses were done by an in-line flow injection analysis (FIA) system using chemiluminescence as a detection method (De Jong *et al.*, 1998) and is described by Klunder *et al.* (2011). Samples were acidified to pH 1.8 using 12 M ultraclean HCl (Baseline® Hydrochloric Acid, Seastar Chemicals Inc.). The filtered samples (<0.2 μm and <1000 kDa fractions) were measured directly onboard and left acidified for at least 12 h before analysing. The unfiltered samples were acidified in the same way, but they were stored one year before being analysed in the home laboratory using the same system and procedure in a class 100 clean-room.

The samples for Fe analysis by FIA and Fe speciation were taken from the same station, cast, GO-FLO sampler and using the same filter cartridge, but in different sub-sampling bottle (*i.e.* duplicate bottles).

The method analyses Fe(III), therefore hydrogen peroxide (Merck suprapur 30%) solution was added (60 μl of a 1‰) at least one hour before analysis to ensure oxidation any Fe(II) present (Lohan *et al.*, 2005). The acidified samples were pre-concentrated over a Toyopearl AFChelate 650M (TesoHaas Germany) column during 120 s. Subsequently the column was rinsed with MQ for 60 s, after which Fe was eluted with 0.4 M HCl (Suprapur, Merck) for 120 s and injected in the photon counter (Hamamatsu HC 135). The system was controlled by an interface developed in LabView. The standard deviation of the duplicate measurements (dissolved fraction) or triplicate measurements (<1000 kDa fraction and unfiltered samples) of one sample was lower than 5%. The blank, *i.e.* the background value of Fe in the MQ water and chemicals, is defined as the

calculated amount of photons measured at 0 s loading time. Blank values varied slightly between the different days, but did not exceed 80 pM. The lowest detection limit, defined as three times the standard deviation of the blank (De Jong *et al.*, 1998), was 11, 1 and 8 pM for the measurements of the unfiltered, dissolved and <1000 kDa fractions, respectively.

For the validation of the measurements and for the long term consistency, a certified SAFe reference water was regularly measured. The measured Fe concentrations (Table 1) were in accordance with the community consensus values (Johnson *et al.*, 2007).

Table 1: Validation of the measurements using certified SAFe water for each cruise. Concentrations of Fe measured in SAFe water are in nM ± Standard Deviation (S.D.); n is the number of measurements.

	S1	**D2**
Published value (Johnson *et al.*, 2007)	0.097 ± 0.043; n=140	0.91 ± 0.17; n=168
Arctic Ocean (ARK XXII/2)		0.92 ± 0.06; n=24
Southern Ocean (ANT XXIV/3)	0,101 ± 0,034; n=34	0,97 ± 0,07 ; n=20
Southern Ocean (NBP09-01)	0.078 ± 0.012; n=10	0.942 ± 0.043; n=13

8. Determination of iron speciation

8.1. Voltammetric procedure and sample treatment

Organic complexation of iron was determined by competing ligand exchange – adsorptive stripping voltammetry (CLE-AdSV) using 2-(2-Thiazolylazo)-p-cresol (TAC) as a competing ligand (Croot and Johansson, 2000). The voltammetric equipment consisted of a μAutolab potentiostat (Type II, Ecochemie, The Netherlands), a mercury drop electrode (model VA 663 from Metrohm). The mercury drop size was approximately 0.25 mm^2. The reference electrode was double-junction, Ag/AgCl, 3 M KCl, with a salt bridge filled with 3 M KCl and a glassy carbon counter-electrode. Samples were stirred with a PTFE Teflon stirrer (3000 rpm). A current filter (Fortress 750, Best Power) to which the equipment was linked was used to prevent electrical noise.

The seawater sample was buffered to pH 8.05 by adding a mixed NH_3/NH_4OH borate buffer (final concentration 5 mM). The buffer stock was 1 M boric acid, (Suprapur, Merck) in 0.25 M ammonia (Suprapur, Merck) cleaned through a

SepPak C18 column with 20 µM TAC (2-(2-Thiazolylazo)-p-cresol). A stock of 0.02 M TAC was prepared in 3QD-Methanol for a final concentration of 10 µM in the seawater sample (Croot and Johansson, 2000).

Additions of Fe(III) standard (0, 0.33, 0.5, 0.67, 1, 1.5, 2, 2.5, 3, 4, 6, 8 nM, Chapter 2, 3, 4, 5 and 6; and 0, 0.2, 0.4, 0.6, 0.8, 1, 1.2, 1.5, 2, 2.5, 3, 4, 6, 8 and 10 nM, Chapter 7) were done with a stock of 1 µM Fe(III) (prepared in 0.03 M HCl, Seastar chemicals Inc.) in a series of Teflon PFA vials (Savillex, 30 ml volume) including 2 blanks (0 nM Fe addition). The seawater sample was poured into the Teflon PFA vials (15 ml per vial). The titration series was left overnight to equilibrate before measuring.

Before preparing the first titration series (true sample), all Teflon vials were conditioned two times beforehand by preparing a titration with iron additions using filtered (<0.2 µm or <1000 kDa) seawater containing the lowest concentration of Fe possible.

Before each titration series, the voltammetric Teflon cell was cleaned using a blank solution. The chemical blank was below the detection limit of the method, being 0.027 nM [$Fe(TAC)_2$] obtained by calculating three times the noise.

Each equilibrated aliquot was transferred into the voltammetric Teflon cell and purged with nitrogen for 180 s. The differential pulse method was used. The deposition potential of -0.4 V was applied during 140 to 240 s (depending on the sample and on the sensitivity of the equipment) and the sample was stirred to allow a better adsorption of Fe-$(TAC)_2$ on the mercury drop. An equilibration time of 5 s without stirring was done before scanning between -0.4 to -0.7 V at 1.95 $mV.s^{-1}$ (modulation amplitude was 25.05 mV). Modulation time was 0.01 s and interval time was 0.1 s. The visible peak due to the dissociation of the Fe-complex was found between -0.460 V and -0.500 V. Each measurement was done at least twice.

The detection limit of the method was determined as 3 times the standard deviation of several blank measurements and was 0.040 Eq of nM Fe (n = 11). The chemical blank was below this detection limit.

8.2. Calculation of iron speciation

Ligand concentrations [Lt] (in Equivalent of nano Molar of Fe, Eq of nM Fe), conditional stability constants K' and their respective standard deviations were calculated using the Langmuir model (Eq.1, non-linear regression of the Langmuir isotherm, Gerringa *et al.*, 1995). By using the Langmuir model (Gledhill and Van Den Berg, 1994) it is assumed that equilibrium between all Fe(III) species exists, all binding sites between Fe and the unknown ligand Lt are equal and binding is reversible, as follows:

$$[FeL] = \frac{K' \times [Fe^{3+}] \times [Lt]}{1 + K' \times [Fe^{3+}]} \qquad \text{(Eq.1)}$$

Here [FeL] is the concentration of natural iron-ligand complexes assuming the existence of one organic ligand, and a one to one coordination, $[Fe^{3+}]$ is the ionic iron concentration, K' and [Lt] are two unknown parameters that need to be determined.

K' is the conditional stability constant of Fe with the natural ligand:

$$K' = [FeL] / ([Fe^{3+}] \times [L']) \qquad \text{(Eq.2)}$$

With [L'] being the concentration of empty ligand sites (excess ligand concentration); and assuming equilibrium as follows:

$$Fe^{3+} + L' \leftrightarrow FeL \qquad \text{(Eq.3)}$$

And [Lt] represents the total ligand concentration assuming equilibrium as follows:

$$[Lt] = [FeL] + [L'] \qquad \text{(Eq.4)}$$

Equation 1 is obtained using equations 2 and 4 as follows:

$$\text{From Eq. 4, } [L'] = [Lt] - [FeL] \qquad \text{(Eq.5)}$$

$$\text{So, Eq.2 becomes } K' = \frac{[FeL]}{[Fe^{3+}] \times ([Lt] - [FeL])} \qquad \text{(Eq.6)}$$

When Eq.6 is writen as function of [FeL], it becomes Eq.1.

In order to solve Equation 1 which has two unknowns, K' and [Lt], a titration of the empty ligand sites with different standard Fe additions is needed to obtain a series of $[Fe^{3+}]$ and [FeL]. To do so, the competing ligand TAC is used. Like the natural ligand, TAC is in equilibrium with Fe^{3+}:

$$Fe^{3+} + 2\ TAC' \leftrightarrow Fe(TAC)_2 \qquad \text{(Eq.7)}$$

$$\text{And } \beta_{Fe(TAC)2} = [Fe(TAC)_2] / ([Fe^{3+}] \times [TAC]^2) \qquad \text{(Eq.8)}$$

With $\beta_{Fe(TAC)2}$ being the conditional stability constant of Fe with TAC assuming equilibrium and TAC' being free TAC defined here as the concentration of TAC that is not bound to Fe.
It is assumed that [TAC'] = [TAC] (total) since TAC is largely in excess:
[TAC] = 10 µM ($\beta_{Fe(TAC)2} = 10^{22.4}$, Croot and Johansson, 2000).

$$\text{Using Eq.8:} \qquad [Fe^{3+}] = [Fe(TAC)_2] / (\alpha_{Fe(TAC)2}) \qquad \text{(Eq.9)}$$

$$\text{With } \alpha_{Fe(TAC)2} = \beta_{Fe(TAC)2} \times [TAC]^2 = 10^{12.4} \qquad \text{(Eq.10)}$$

According to the mass balance of Fe,

$$[FeL] = [Fe_{fraction}] + [Fe_{added}] - [Fe(TAC)_2] \qquad \text{(Eq.11)}$$

Where $[Fe_{fraction}]$ is the iron concentration measured by FIA in either the unfiltered (TDFe), orthe dissolved (DFe) or the <1000 kDa fractions ($Fe_{<1000\ kDa}$); $[Fe_{added}]$ is the concentration of iron added for the titration and $[Fe(TAC)_2]$ represents the concentration of iron bound to TAC. The latter $[Fe(TAC)_2]$ is calculated for every Fe addition by dividing the peak height (nA) by the slope (S = sensitivity) of the straight part of the titration curve. The sensitivity S (in $Amper.mol^{-1}$) of the method is influenced by ligand sites not yet saturated with Fe as explained by Turoczy and Sherwood (1997) and Hudson *et al.* (2003). This is accounted for by an algebraic solution of the equilibrium equations including the Langmuir

isotherm, in which S is determined together with Lt and K'. The estimated parameters are given with standard deviation from the fit of the model to the data.

For the calculation of pFe, the negative logarithm of $[Fe^{3+}]$, the sum of the measured alpha of the natural organic ligands (product of the concentration of excess L and K' = [L'] x K') and that of the alpha of the inorganic ligands ($\alpha_{inorg} = 10^{10}$ after Millero, 1998) were used as follows:

$$pFe = -\log [Fe^{3+}] = -\log\{[Fe_{fraction}] / (\alpha_{org}+\alpha_{inorg})\} \quad \text{(Eq.12)}$$

8.3. Estimation of the ligand characteristics in unfiltered samples

The ligand concentration [Lt] and stability constant K' are variables which depend on the Fe concentration used in the calculations. However under natural conditions (seawater pH ~8), part of Fe in unfiltered (UNF) samples is irreversibly bound in colloids or into mineral particles which are refractory (not dissolvable). This refractory Fe (unknown percentage of TDFe) does not participate in the speciation of Fe determined here. Moreover, phytoplankton cells and micro-organisms contain Fe which is released in seawater after acidification, thus over-estimating the Fe concentration in the sample. Therefore, for UNF samples, the concentrations of Lt and Excess L were estimated in two ways: an upper limit using [TDFe] and a lower limit using [DFe] in the calculations (Paragraph 7.2. above).

Note that the ligand concentration [Lt] and stability constant K' are artificially increased when using [TDFe] (assumed to be exchangeable for the calculations). However, the concentration of Excess L ([Lt]-[Fe]), is hardly influenced by the Fe concentration (Thuróczy *et al.*, 2010b, Chapter 3 and 2011a).

Chapter 3

Speciation of iron in the Eastern North Atlantic Ocean

This chapter is adapted from: Thuróczy, C.-E., Gerringa, L.J.A., Klunder, M.B., Middag, R., Laan, P., Timmermans, K.R., De Baar, H.J.W, 2010b. Speciation of Fe in the Eastern North Atlantic Ocean. Deep-Sea Research I 57 (11), 1444-1453. doi: 10.1016/j.dsr.2010.08.004.

Abstract

In the Eastern North Atlantic Ocean iron (Fe) speciation was investigated in three size fractions: the dissolvable from unfiltered samples, the dissolved fraction (<0.2 μm) and the fraction smaller than 1000 kDa (<1000 kDa). Fe concentrations were measured by flow injection analysis and the organic Fe complexation by voltammetry. In the research area the water column consisted of North Atlantic Central Water (NACW), below which Mediterranean Overflow Water (MOW) was found with the core between 800 and 1000 m depth. Below 2000 m depth the North Atlantic Deep Water (NADW) proper was recognised. Dissolved Fe and Fe in the <1000 kDa fraction showed a nutrient like profile, depleted at the surface, increasing until 500-1000 m depth below which the concentration remained constant. Fe in unfiltered samples clearly showed the MOW with high concentrations (4 nM) compared to the overlying NACW and the underlying NADW, with 0.9 nM and 2 nM Fe, respectively. By using Excess ligand (Excess L) concentrations as parameter we show a potential to bind Fe. The surface mixed layer had the highest excess ligand concentrations in all size fractions due to phytoplankton uptake and possible ligand production. The ratio of Excess L over Fe proved to be a complementary tool in revealing the relative saturation state of the ligands with Fe. In the whole water column, the organic ligands in the larger colloidal fraction (between 0.2 μm and 1000 kDa) were saturated with Fe, whereas those in the smallest fraction (<1000 kDa) were not saturated with Fe, confirming that this fraction was the most reactive one and regulates dissolution and colloid aggregation and scavenging processes. This regulation was remarkably stable with depth since the alpha factor (product of Excess L and K'), expressing the reactivity of the ligands, did not vary and was 10^{13}. Whereas, in the NACW and the MOW, the ligands in the particulate (>0.2 μm) fraction were unsaturated with Fe with respect to the dissolved fraction, thus these waters had a scavenging potential.

1. Introduction

Dissolved iron (DFe) in seawater (<0.2 μm) consists of several size classes of colloidal Fe next to an operationally defined soluble pool (<smallest size cut-off ultra-filtration; Nishioka *et al.*, 2005). Organic Fe(III)-complexes exist within both the colloid pool(s) and the soluble pool (Boye *et al.*, 2005) and are characterised by a very high conditional binding strength (logK' ≈ 20-23; Gledhill and Van Den Berg, 1994). These organic ligands bind Fe(III) so strongly that more than 99% of Fe in the oceans is in the organically complexed form (Rue and Bruland, 1997; Boye and Van Den Berg, 2000; Croot *et al.*, 2001; Gerringa *et al.*, 2006). Therefore ligands prevent Fe(III) from precipitating as oxyhydroxides and enable Fe to remain dissolved above concentrations determined by the solubility product (Kuma *et al.*, 1996; Millero, 1998). In the ocean surface layer the speciation of Fe regulates its availability to phytoplankton and other micro-organisms, which also influence the Fe speciation: on the one hand Fe is consumed by these micro-organisms, on the other hand they can produce organic ligands (Rue and Bruland, 1997; Boye and Van Den Berg, 2000; Croot *et al.*, 2001; Gerringa *et al.*, 2006). In the deep ocean, organic complexation and the distribution over different size fractions determines precipitation and adsorption on particles. The quasi-equilibrium competition between dissolved organic complexation, colloid size class particles and fine suspended particles is deemed to control the removal by scavenging via settling of large particles and thus the deep ocean residence time of Fe (Figure 1, made after De Baar and De Jong, 2001). According to Nishioka and Takeda (2000) and Nishioka *et al.* (2005) the small colloidal fraction (in their papers defined as between 200 kDa and 0.2 μm) is a very reactive fraction. Moreover Bergquist *et al.* (2007) concluded that variations in dissolved Fe are due to changes in the colloidal fraction (in their paper between 0.02 μm and 0.4 μm) in the Atlantic Ocean.

Here we investigate the processes of solubilisation through complexation versus scavenging and precipitation (Figure 1) to gain insight into the cycling of Fe by sampling a deep profile at a station in the Eastern North Atlantic Ocean. Therefore we focus on size fractionation within the Fe-pool to study the organic

complexation of Fe in three size fractions: the unfiltered samples (UNF), the dissolved fraction (< 0.2 µm), and the fraction smaller than 1000 kDa.

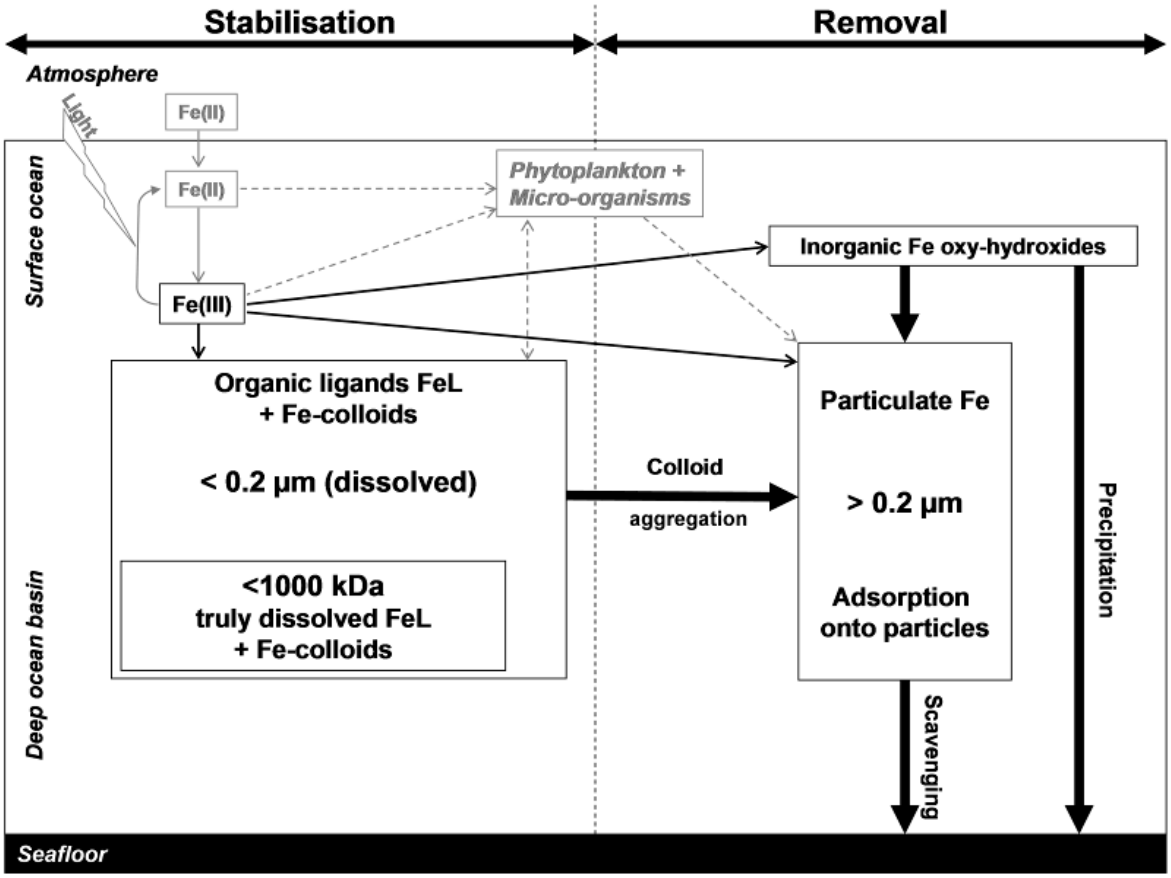

Figure 1: *Schematic representation of the Fe chemistry in the ocean. In the surface layer phytoplankton consume Fe and produce organic ligands. Photo-reduction of Fe is indicated in grey since it is not considered in this paper. Organic ligands in the dissolved fraction (<0.2 µm) and within the smaller fraction (<1000 kDa) increase the residence time of Fe in the ocean by binding Fe, thus keeping the concentration of inorganic Fe low, preventing from precipitation as oxy-hydroxides, and restricting scavenging via adsorption onto particles. Finally, colloid aggregation is a possible pathway for removing Fe from the dissolved phase.*

2. Additional details on the materials and methods

Samples were collected aboard R.V. *Pelagia* between April 11 and April 26, 2007, during the IPY-Geotraces (Geotraces Science Plan, 2006) cruise (64PE267) in the Eastern North Atlantic Ocean off the coast of Portugal (Figure 2). Water samples were collected from station 14 (39°44'N-14°10'W), where six hydrocasts were

performed for trace metals and nutrients (casts 1, 4, 5, 7, 18 and 20, Middag *et al.*, personal communication). The first cast was sampled on April 19 for size fractionation and the measurements of organic speciation of Fe.

Analyses of Fe and the ligand characteristics were done on samples in three different size fractions as explained in Chapter 2: Unfiltered samples (UNF), the dissolved fraction, defined as <0.2 μm and the fraction smaller than 1000 kDa (<1000 kDa),

Iron analysis in unfiltered (TDFe) samples and samples <1000 kDa was done from the same cast (Cast 1). Unfortunately, the results of DFe from this cast could not be used due to a contamination of the FIA chemuluminescence system by the buffer; therefore, the DFe concentrations from cast 18 (April 24) were used to calculate the speciation (see next).

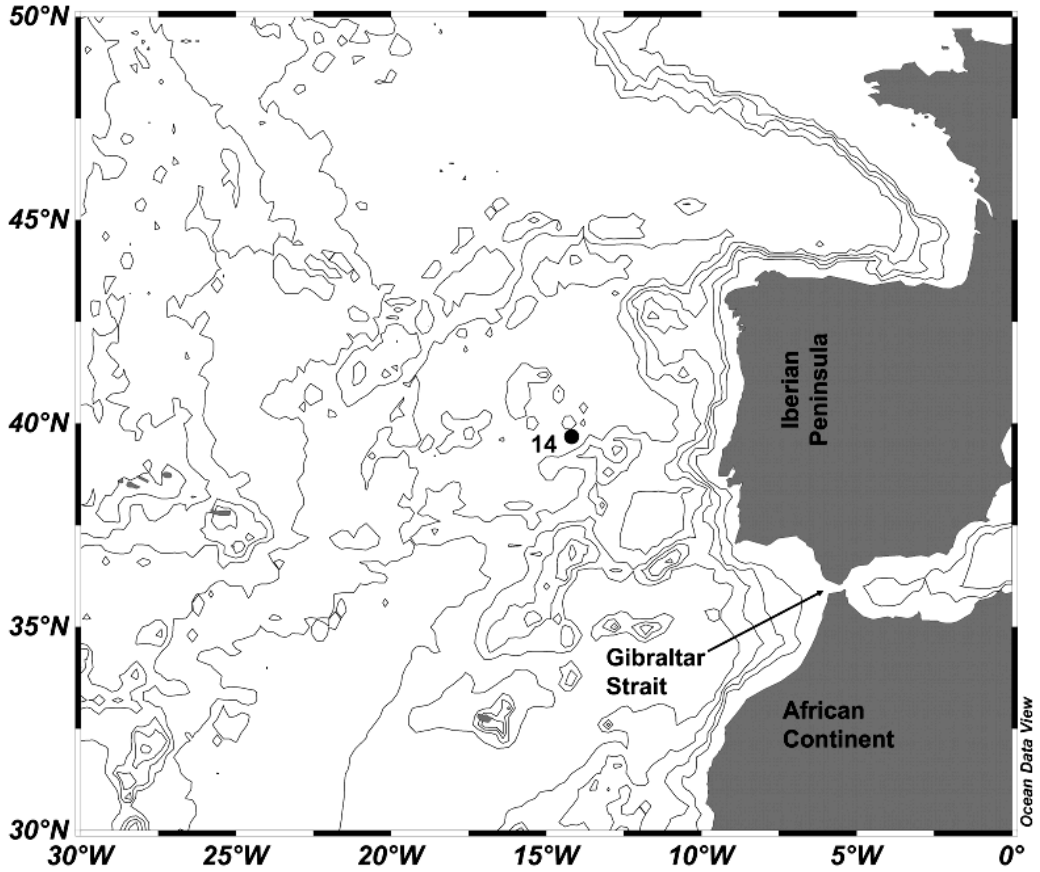

Figure 2: *Chart showing station 14 (39°44'N-14°10'W). The displayed isobaths are 1000, 2000, 3000, 4000 and 5000 m depth.*

To overcome problems with the interpretation of the results due to variations between casts in DFe over the period of sampling, speciation data was interpreted as "Excess L" concentrations ($[\text{Excess L}]_{\text{fraction}} = [\text{Lt}]_{\text{fraction}} - [\text{Fe}]_{\text{fraction}}$). Excess L represents the empty binding sites for Fe (concentration of empty ligand sites for Fe), thus a potential for binding Fe. The use of Excess L for interpretation of the organic complexation of Fe was also used by others (Rijkenberg *et al.*, 2008a and Boye *et al.*, 2001).

Nutrient, DFe, dissolved Mn and dissolved Al data showed very little variation between the different casts (Middag *et al.*, personal communication) indicating that water masses did not change in time. Indeed, standard deviations in DFe between casts 18 and 20 were very small (0.04 nM Fe on average).

Salinity (conductivity), temperature and depth (pressure) were measured with the CTD (Seabird SBE 911+) mounted on the titanium frame (De Baar *et al.*, 2008a).

3. Results

Station 14 was located west of the coast of Portugal, north of the Strait of Gibraltar (Figure 2). A surface mixed layer (SML) of about 50 m depth existed with relatively constant salinity (36.05) and decreasing potential temperature (15.3 to 14.8º C, Figure 3). Below the SML both the potential temperature and salinity decreased to a minimum of 11.5º C and 35.7, respectively, at about 550 m depth. Below this depth, both salinity and potential temperature increased again, but to separate maxima around 1100 and 800 m depth, respectively, representing the lower and upper cores of the Mediterranean Overflow Water (MOW, Ambar *et al.*, 2008; Figure 3). The minimum of salinity and potential temperature at 550 m depth separated the MOW and the NACW (van Aken *et al.,* 2001). At about 2000 m depth the NADW proper was found and below 4000 m Low Deep Water was recognised, with Antarctic Bottom Water (AABW) influence (for more details, see Measures *et al.,* 1995; Laës *et al.*, 2003).

The fluorescence (given by the CTD sensor in relative arbitrary units) showed maximum values of 0.8 at 38 m depth, and decreased to values <0.1 below 120 m

depth (Figure 4). The fluorescence provides an indication of the abundance of Chlorophyll a, *i.e.* the abundance of phytoplankton.

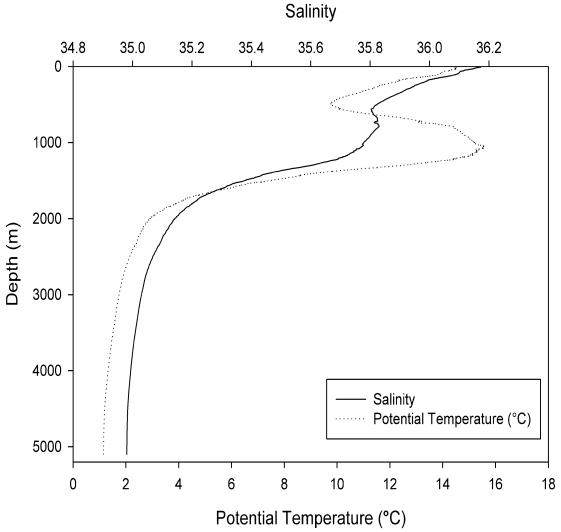

Figure 3: *Vertical profile of mean values of salinity and temperature from six hydrocasts at station 14 (1, 4, 7, 15, 18 and 20).*

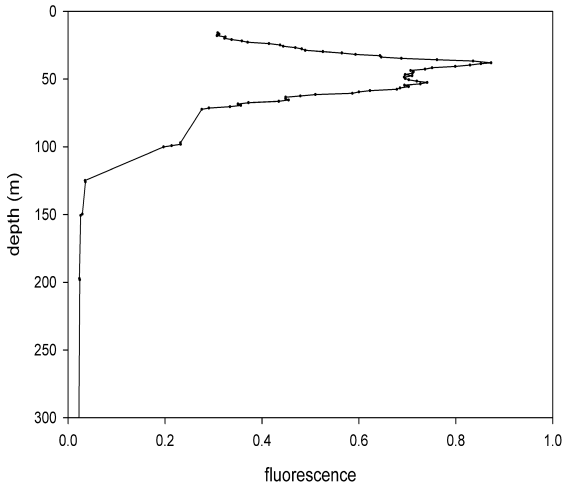

Figure 4: *Fluorescence (arbitrary units, a.u.) with depth (m) at station 14, cast 1..*

Iron was measured in three size fractions (Tables 1A, 1B, 2B, Figure 5). The $Fe_{<1000\ kDa}$ concentrations (Table 1B) were very low; 0.02 nM in the SML increasing gradually to 0.22 nM at 2000 m and to 0.143 nM at 4000 m depth (bottom depth at station 14 was 5300 m). The concentrations of DFe showed a typical Fe profile shape, with very low values (0.1 nM) in the SML The concentrations of DFe increased to a maximum of 0.69 nM at 500 m. Slightly lower concentrations were measured at mid-depth in the MOW (0.57 nM at 1000 to 2000 m depth) below which they increased again to concentrations of 0.65-0.7 nM at 3000-4000 m depth. Iron in the unfiltered (TDFe) samples was measured at the lowest concentrations in the SML (0.95 nM). A broad maximum concentration was found in the MOW (4.1 nM). Below the MOW the concentrations decreased to values close to and lower than 2 nM. A small maximum of 2.77 nM (one data point only) was also measured at 200 m depth.

The ligand characteristics are presented in tables 1 and 2, where the total ligand concentration Lt is shown together with Excess L concentrations. The total ligand

concentrations Lt more or less followed the Fe concentrations from the same fraction. Showing Excess L (Figure 6) the data is made almost (see discussion) independent of the used Fe concentration. In this study this was relevant for two reasons: first because DFe concentration was measured, although at the same station, in samples from a different cast (18) than the cast (1) in which the speciation measurements were done; second because the measured TDFe (dissolvable) was not necessarily the reversibly complexed Fe in those unfiltered samples. It is to be expected that not all TDFe is bound reversibly to ligand and adsorption sites. However, it is unknown which percentage is irreversibly bound. For example inside mineral particles Fe is refractory (not dissolvable) at normal ocean pH conditions (pH~8) but may (partly) have dissolved during the one year acidification at the pH 1.8. In order to better understand the influence of an unknown concentration of Fe (not participating in reversible adsorption and ligand binding) on the results of the concentrations of ligand and Excess L and on K', the speciation data of the unfiltered fraction was calculated with the two extreme Fe concentrations, the minimum being the DFe concentration and the maximum being TDFe concentrations (dissolvable).

Table 1 (Next page): *Results of Fe and Fe speciation measurements for two size fractions: <0.2 µm (Table 1A) and <1000 kDa (Table 1B).*
** Standard deviation and R^2 of the fit of the parameters Lt, K' and S using the nonlinear Langmuir model.*
*** Mean value of upper and lower concentrations: 0.64 and 0.7 nM at 3000 and 4000 m, respectively.*

A	Depth (m)	[DFe]$_{cast18}$ (nM)	SD	[Lt] (Eq of nM Fe)	SD*	logK' (mol^{-1})	SD*	[Excess L] (Eq of nM Fe)	log alpha	Excess L /DFe	S	SD*	R^2*
<0.2 µm	26	*0.130*	*0.002*	1.21	0.31	21.68	0.31	1.08	12.71	8.31	2.62	0.11	0.997
	102	*0.200*	*0.012*	0.65	0.19	21.93	0.31	0.45	12.58	2.25	2.00	0.07	0.997
	202	*0.460*	*0.046*	0.87	0.07	22.64	0.41	0.41	13.25	0.89	2.19	0.03	0.999
	501	*0.690*	*0.014*	1.00	0.08	22.71	0.37	0.31	13.20	0.45	2.09	0.04	0.998
	800	*0.670*	*0.005*	0.93	0.08	22.57	0.37	0.26	12.98	0.39	2.10	0.03	0.999
	999	*0.570*	*0.002*	0.80	0.08	23.00	0.36	0.23	13.36	0.40	1.31	0.03	0.998
	1998	*0.580*	*0.018*	1.59	0.26	21.83	0.23	1.01	12.83	1.74	2.18	0.09	0.997
	3497	*0.670*	**	1.76	0.13	22.11	0.13	1.09	13.15	1.63	2.46	0.07	0.998
	3998	*0.700*	*0.019*	1.54	0.06	22.91	0.29	0.84	13.83	1.20	1.14	0.02	0.999

B	Depth (m)	[Fe$_{<1000\ kDa}$] (nM)	SD	[Lt] (Eq of nM Fe)	SD*	logK' (mol^{-1})	SD*	[Excess L] (Eq of nM Fe)	log alpha	Excess L /Fe$_{<1000\ kDa}$	S	SD*	R^2*
<1000 kDa	26	0.029	0.008	1.35	0.18	22.02	0.25	1.32	13.14	45.52	1.06	0.03	0.998
	102	0.019	0.159	0.42	0.11	22.47	0.43	0.40	13.08	21.31	1.58	0.04	0.998
	202	0.047	0.083	0.51	0.12	22.32	0.34	0.46	12.99	9.68	2.16	0.05	0.998
	501	0.088	0.051	1.10	0.06	22.45	0.13	1.01	13.46	11.48	0.50	0.01	0.999
	800	0.077	0.083	0.61	0.12	21.98	0.40	0.53	12.71	6.83	2.28	0.05	0.997
	999	0.129	0.051	0.70	0.14	22.04	0.34	0.57	12.80	4.46	2.51	0.06	0.999
	1998	0.220	0.014	0.93	0.14	22.14	0.29	0.71	13.00	3.23	2.48	0.07	0.999
	3497	0.164	0.067	1.19	0.07	22.32	0.15	1.03	13.33	6.24	0.49	0.01	0.999
	3998	0.143	0.025	0.89	0.08	22.20	0.20	0.75	13.07	5.20	0.61	0.01	0.999

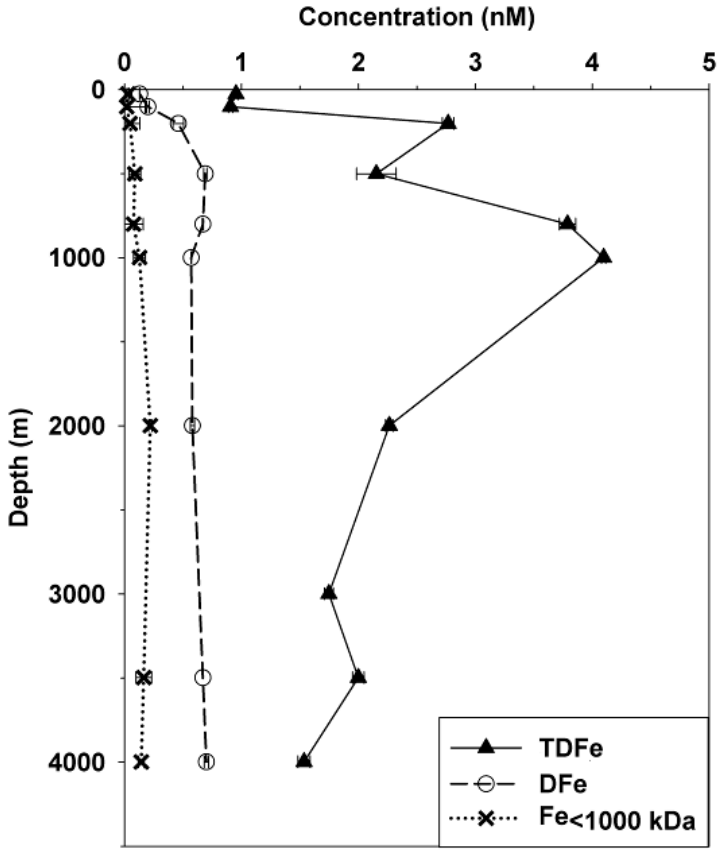

Figure 5: *Concentrations of Fe (in nM) with depth in the three size fractions: in unfiltered samples, <0.2 µm and <1000 kDa. TDFe and* $Fe_{<1000\ kDa}$ *concentrations are from cast 1, DFe concentrations are from cast 18. The standard deviation of the duplicate measurements (<0.2 µm fraction) or triplicate measurements (<1000 kDa and unfiltered fractions) is given.*

The Excess L concentrations of the dissolved and <1000 kDa fractions were relatively high in the surface SML, 1.08 and 1.32 Eq of nM Fe, respectively (Tables 1, 2 and Figure 6). Below the SML Excess L concentrations in both fractions decreased steeply to 0.45 and 0.40 Eq of nM Fe, respectively. Excess L in the <1000 kDa fraction had a small maximum at 500 m depth (near 1 Eq of nM Fe). Both fractions (dissolved and <1000 kDa) showed an increase in Excess L concentrations from the MOW to 2000 m depth from 0.2 to 1 and 0.5 to 0.7 Eq of nM Fe, respectively, and remained more or less constant with depth below 2000 m. Excess L in the unfiltered samples have comparable concentrations for the calculations using two different Fe concentrations (DFe and TDFe), thus proving that the Excess L concentration as such is independent of the Fe concentration. Compared to the two smaller size fractions Excess L concentrations were larger in

the layer between 100 m and 2000 m. This layer comprised the MOW proper (800-1000 m), and MOW mixed with NACW above it and with NADW below it. In the deep waters of the NADW proper, Excess L concentrations in unfiltered samples were comparable to the other two smaller size fractions.

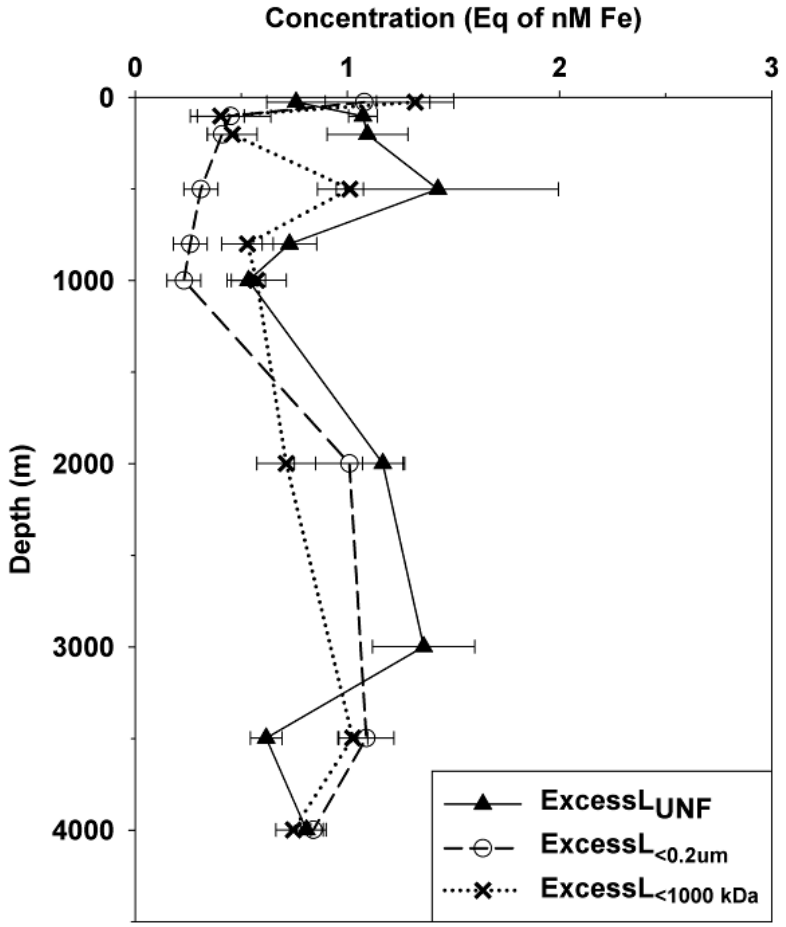

Figure 6: *Concentrations with depth of excess ligands ([Excess L]) in Equivalents of nano-Molar iron (Eq of nM Fe) in the three size fractions: unfiltered samples, <0.2 μm and <1000 kDa. The estimated parameters are given with standard deviation of the fit of the model to the data.*

To determine the relation between the concentration of Excess L and Fe within the same fraction, the ratio of the two concentrations ([Excess L]/[Fe]) was used (Figure 7, Tables 1 and 2). The Excess L over Fe was evident in the surface layer for all fractions (Thuróczy *et al.*, 2011a and Chapter 4). Relatively more Excess L sites were present in the smallest size fractions.

The conditional stability constant K' of the binding between the ligands and Fe was more or less equal for the two finer fractions, average values being $10^{22.38}$ and $10^{22.22}$ for dissolved and <1000 kDa, respectively (Tables 1A, 1B). The K' of the unfiltered samples was comparable when DFe concentrations were used (average K' = $10^{22.39}$) but higher (average K' = $10^{22.86}$) when the TDFe concentrations were used (Tables 2A and 2B).

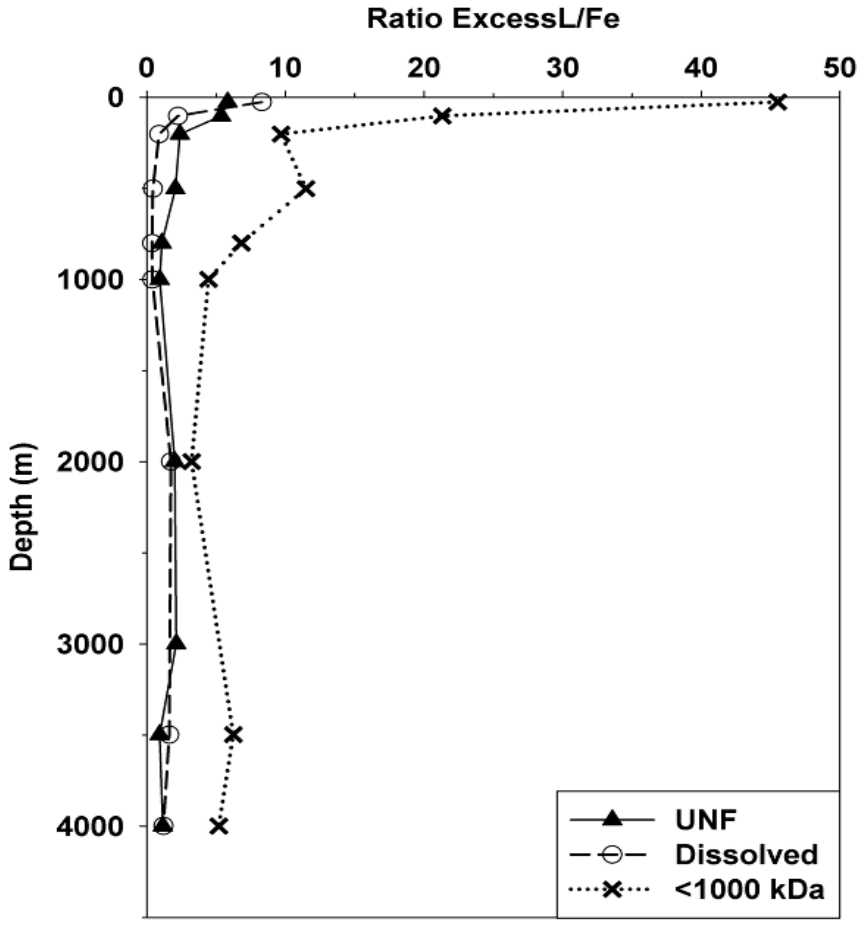

Figure 7: *The ratio of Excess L and Fe concentrations ([Excess L]/[Fe]) per size fraction with depth.*

4. Discussion

4.1. Iron

The concentrations of DFe measured here were comparable to Fe profiles more to the south west of the Canary Islands reported by Sarthou *et al.* (2007), De Baar *et al.* (2008a) and Rijkenberg *et al.* (2008a) in surface waters. The deep water concentration of DFe was also consistent with those reported by Ussher *et al.*

(2007) on a transect in the Eastern North Atlantic Ocean (46°N, 8°W to 52°N, 4°E), and values of DFe (<0.4 μm) in the upper 1000 m at a station (40°N, 20°W) reported by Measures *et al.* (2008). The mean concentration of 0.7 nM for DFe between 2000-4000 m depth in this study was very close to DFe (<0.4 μm) concentrations measured by Wu *et al.* (2001; 0.6-0.7nM Fe) in the north Atlantic Ocean and Bergquist *et al.* (2007; 0.4-0.8 nM Fe) in the western North Atlantic Ocean.

Wu *et al.* (2001), Cullen *et al.* (2006) and Bergquist *et al.* (2007) also measured soluble Fe (their fraction was <0.02 μm). Below 2000 m depth we measured 0.13-0.22 nM Fe which was slightly lower than those found by Wu *et al.* (2001, 0.2-0.3 nM Fe), Bergquist *et al.* (2007, 0.2-0.4 nM Fe), and the deep data from Cullen *et al.* (2006, 0.22-0.28 nM Fe).

No distinction between MOW and the other water masses could be made in the concentrations of DFe. However, there was a strong signal in Fe concentrations of the unfiltered samples. The TDFe concentration was much higher in the MOW than in the Atlantic water masses, which was not observed Sarthou *et al.* (2007) because of a different sampling strategy.

The position of the MOW in the water column did not make possible the interpretation of processes occurring as gradual trends with increasing depth, as discussed by Wu *et al.* (2001). Apparently the high TDFe in the MOW was transported mainly laterally. Our station was located relatively far away from the Mediterranean outlet. The net horizontal velocity of lenses of MOW is of the order of a few cm/s (after Ambar *et al.*, 2008), although the velocity within the whirls is much larger (up to 60 cm/s; Ambar *et al.*, 2008). The MOW would have taken at least a few months if not more than a year to reach our sampling location. The vertical sinking velocity of diatoms is a relatively high (15-100 m per day for *Chaetoceros sp.* according to Passow, 1991 and Van Haren *et al.*, 1998). Within 50 days they would have sunk out of the MOW. Therefore, the particles containing Fe remaining in the MOW must be of a colloidal nature. It must be noted that the sparse sampling below the MOW did not permit further interpretation of these processes.

4.2. Fe-binding ligands

High concentrations of Fe-binding ligands in the surface layer have also been observed by Gerringa *et al.* (2006) in the Atlantic Ocean west of the Canary Islands and by Thuróczy *et al.* (2011a and Chapter 4) in the Atlantic sector of the Southern Ocean, who found high concentrations but also large variations in the dissolved organic ligand concentration above the chlorophyll maximum. A relation between phytoplankton characteristics and ligand concentrations existed within and below the chlorophyll maximum (Gerringa *et al.*, 2006). In the present study, although the sampling was not directed towards small scale differences in the vertical upper layer of the ocean, the highest concentrations of ligands were found at 50 m depth in the dissolved and <1000 kDa fractions, indicating that phytoplankton could be the source of dissolved organic ligands, as observed by others (Rue and Bruland, 1997; Boye *et al.*, 2001; Croot *et al.*, 2001). In the upper 100 m, the K' values in the dissolved fraction of this research ($10^{20.9}$-$10^{21.7}$) fitted the range of those found by Gerringa *et al.* in the upper 150 m (2006; $10^{19.8}$-$10^{22.7}$) in the same fraction. Also Boye *et al.* (2003) found relatively low K' values in surface waters at 41ºN ($10^{20.6}$-10^{21}). This indicated that the ligands presumably coming from the phytoplankton are relatively weak, supporting the conclusion of Rijkenberg *et al.* (2008b) that phytoplankton can modify ligand characteristics. Others stated that ligands related to phytoplankton activity belong to the relatively strong ligand group (Rue and Bruland, 1997; Cullen *et al.*, 2006; Hunter and Boyd, 2007).

Table 2 (Next page): *Results of Fe and Fe speciation measurements for the unfiltered samples.*
Table 2A shows the results of the speciation calculations using DFe concentrations (<0.2 µm from cast 18). Table 2B shows the speciation results using the TDFe concentrations.
** Standard deviation and R^2 of the fit of the parameters Lt, K' and S using the nonlinear Langmuir model.*
*** Mean value of upper and lower concentrations: 0.64 and 0.7 nM at 3000 and 4000 m, respectively.*

A	Depth (m)	$[DFe]_{cast18}$ (nM)	SD	[Lt] (Eq of nM Fe)	SD*	logK' (mol^{-1})	SD*	[Excess L] (Eq of nM Fe)	log alpha	Excess L /DFe	S	SD*	R^2*
	26	*0.130*	*0.002*	0.89	0.14	22.28	0.53	0.76	13.16	5.83	2.53	0.07	0.997
	102	*0.200*	*0.012*	1.27	0.07	22.71	0.24	1.07	13.74	5.37	1.06	0.02	0.994
	202	*0.460*	*0.046*	1.55	0.19	22.46	0.73	1.09	13.50	2.38	2.20	0.08	0.997
	501	*0.690*	*0.014*	2.12	0.57	21.55	0.21	1.43	12.70	2.07	2.33	0.21	0.997
	800	*0.670*	*0.005*	1.40	0.13	22.78	0.32	0.73	13.64	1.09	1.10	0.03	0.996
	999	*0.570*	*0.002*	1.10	0.08	22.27	0.15	0.53	13.00	0.94	4.13	0.08	0.999
	1998	*0.580*	*0.018*	1.75	0.10	22.70	0.31	1.17	13.76	2.01	0.61	0.01	0.997
	2998	*0.640*	*0.005*	2.00	0.24	21.75	0.14	1.36	12.88	2.12	2.37	0.08	0.998
	3497	*0.670*	**	1.29	0.07	22.85	0.40	0.62	13.64	0.92	1.21	0.02	0.998
	3998	*0.700*	*0.019*	1.51	0.08	23.07	0.54	0.81	13.97	1.15	1.10	0.03	0.997

B	Depth (m)	$[Fe_{UNF}]$ (nM)	SD	[Lt] (Eq of nM Fe)	SD*	logK' (mol^{-1})	SD*	[Excess L] (Eq of nM Fe)	log alpha	Excess L /Fe_{UNF}	S	SD*	R^2*
	26	0.953	0.016	1.74	0.12	22.52	0.28	0.79	13.42	0.82	2.54	0.07	0.997
	102	0.906	0.018	1.96	0.06	23.01	0.23	1.06	14.03	1.17	1.06	0.02	0.998
	202	2.767	0.049	3.89	0.16	22.82	0.31	1.12	13.87	0.41	2.21	0.08	0.994
	501	2.153	0.169	3.33	0.24	22.10	0.14	1.17	13.17	0.54	2.37	0.09	0.997
	800	3.788	0.069	4.50	0.11	23.40	0.71	0.71	14.26	0.19	1.09	0.03	0.996
	999	4.097	0.018	4.56	0.06	23.17	0.15	0.46	13.84	0.11	4.07	0.07	0.999
	1998	2.264	0.032	3.41	0.08	23.10	0.28	1.15	14.16	0.51	0.61	0.01	0.997
	2998	1.747	0.038	2.84	0.13	22.23	0.11	1.10	13.27	0.63	2.30	0.05	0.999
	3497	1.999	0.049	2.71	0.06	23.13	0.26	0.71	13.98	0.35	1.24	0.02	0.999
	3998	1.535	0.052	2.47	0.07	23.14	0.26	0.93	14.11	0.61	1.15	0.03	0.998

The results in table 2 from the calculation of the ligand characteristics of unfiltered samples using two different Fe concentrations, DFe and TDFe, illustrated that Excess L concentration was hardly influenced by the Fe concentration. This is valid as long as the titration data fits well to the model of Langmuir. Indeed, the discrepancies in Excess L concentrations at 500 and 3000 m depth for unfiltered sample were caused by a relatively bad fit of the model. By adding TDFe to the Excess L concentration, the upper limit of the total ligand concentration was obtained (Table 2B), whereas the lower limit was obtained by the addition of the DFe (Table 2A). However, the K' values were quite different between the two calculations (Table 2). Consequently, a 2.2 to 7.3 times higher [$Fe_{fraction}$] (Eq 2) resulted in a 1.24 to 7.16 higher K' value leading to a difference in logK' of 0.09 to 0.85. Therefore the calculation of K' is sensitive to refractive Fe that is irreversibly bound in colloids or particles and can be artificially increased by a too high [$Fe_{fraction}$]. Part of Fe bound in the high molecular weight fraction (between 1000 kDa and 0.2 μm) may be not exchangeable, as already suggested by Cullen *et al.* (2006). Hitherto it was assumed that all Fe in the samples was reversibly bound by ligands. This assumption has consequences on parameters as the alpha factor which would be overestimated. Alpha (Tables 1 and 2), the product of K' and the Excess L, represents the reactivity of the ligands and reflects the equilibrium between Fe and ligands. A high alpha favours Fe solubilisation via organic complexation (large Excess L, or strong ligands, or both). Reversely, a low alpha favours Fe loss from solution via precipitation and or scavenging.

4.3. Complexation versus scavenging in the water column

Wu *et al.* (2001) showed that soluble Fe (defined as <10 kDa) and soluble ligands were depleted in surface waters, then increased to a maximum at 100 m depth, after which they both decreased most likely due to colloid aggregation and scavenging of Fe. They concluded that a competition exists between empty soluble ligand sites and adsorption sites on colloids and particles, and that colloid aggregation may cause a net export of Fe from the water column to the sediments

(Figure 1). Although we do not have the smallest size fraction of the truly soluble (<10 kDa), the two dissolved size fractions and the unfiltered samples allow us to see trends due to colloid aggregation or solubilisation with depth. The ratio of Excess L over Fe ([Excess L]/[Fe]) per size fraction indicates a relative competitive force (Thuróczy *et al.*, 2011a and Chapter 4, using [Lt]/[Fe]) since it reflects the relative saturation of the natural ligands with Fe. A ratio near 0 means saturation of the Excess L that can lead to Fe precipitation if Fe is dissolved and scavenging if Fe is in the particulate fraction (>0.2 µm). Reversely, high ratios in the dissolved fractions mean Fe depletion and a high potential for Fe solubilisation. For the two smaller size fractions (<0.2 µm and <1000 kDa, Figure 7, Table 1), [Excess L]/[Fe] was high in the surface followed by a steep decrease to reach low and more or less constant values with depth. Surface ratios of 11 and 45 decreased to 2-0.4 and 3-10 (for <0.2 µm and <1000 kDa, respectively); thus a high potential for binding Fe inputs (by rain, dust or remineralisation) existed. Ligands were unsaturated because of Fe uptake by phytoplankton.

According to Bergquist *et al.* (2007), the variability of DFe with depth is due to the variability of the colloidal Fe (between 0.02 and 0.4 µm; here colloidal Fe is assumed to be between 1000 kDa and 0.2 µm), illustrated by the linear relationship $[Fe_{<0.4\ \mu m}] = 1.18\ [Fe_{0.02\ -0.4\ \mu m}] + 0.29$ ($R^2 = 0.85$). A slope of 1.18 being near 1 showed that the changes in concentrations were attributed to the colloidal Fe pool, and that the soluble Fe concentration remained 0.29 nM. We also found a similar relationship: $[Fe_{<0.2\ \mu m}] = 1.16\ [Fe_{1000\ kDa-0.2\ \mu m}] + 0.03$ ($R^2 = 0.93$, n = 9). The slopes were identical; however the y-cut-off was ten times lower, nearly zero. Therefore we can conclude that colloidal Fe determines the changes in dissolved concentration, but then soluble Fe (here <1000 kDa) does not a play any role.

Since the ligands are assumed to be organic, the presence of phytoplankton and co-existing organisms like bacteria is one of the possible sources (Rue and Bruland, 1997; Butler, 1998 and 2005; Boye and Van Den Berg, 2000; Croot *et al.*, 2001; Barbeau *et al.*, 2001; Maldonado *et al.*, 2005; Gerringa *et al.*, 2006). The trend of the [Excess L]/[Fe] with depth was the same for the different fractions, but

the absolute values heavily depend on the Fe concentration used in the calculation for the unfiltered sample (Tables 2A and 2B).

The ratio of Excess L between the fractions <0.2 µm and <1000 kDa (Figure 8) was near 1 in the whole water column. It was even slightly below 1 in samples from the upper 1000 m, which is in theory not possible, as empty sites present in the smaller fraction should also be present in the total sample. Filtration might cause a disequilibrium in the samples, in which the smallest and most reactive fraction (Nishioka *et al.*, 2001, 2005; Cullen *et al.*, 2006) exchanges Fe during filtration. Thus empty ligand sites occur predominantly in the fraction <1000 kDa. The disequilibrium might be caused by colloidal formation as suggested by Kondo *et al.* (2008). Contamination is to be excluded since [$Fe_{<0.2\ \mu m}$] is always larger than [$Fe_{<1000\ kDa}$].

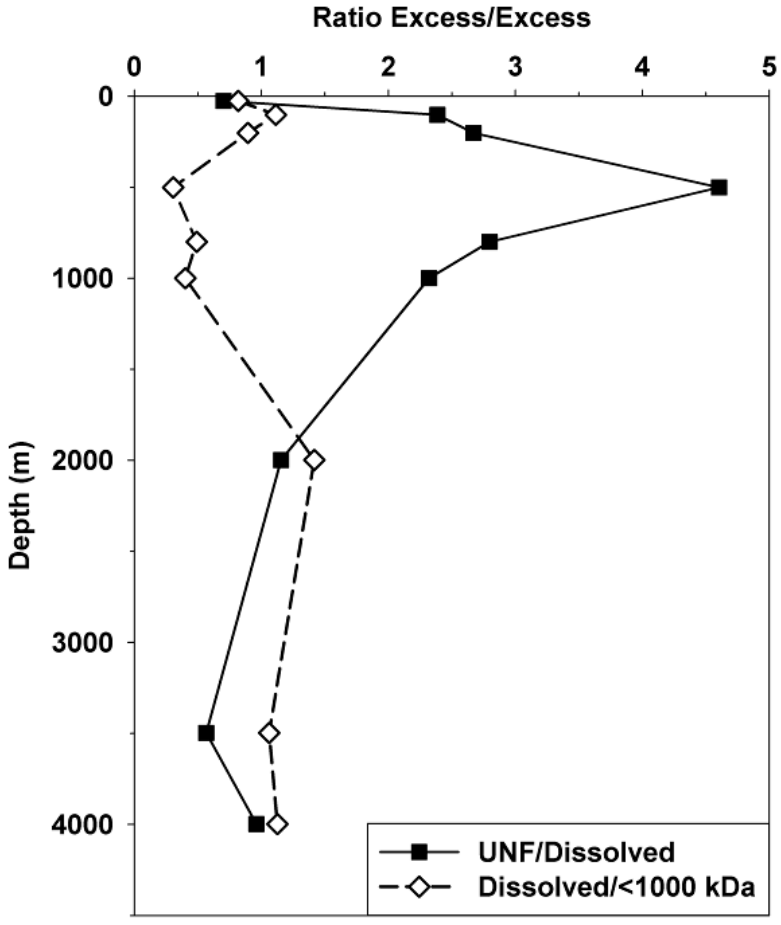

Figure 8: *Ratios [Excess L_{UNF}]/[Excess $L_{<0.2\ \mu m}$] and [Excess $L_{<0.2\ \mu m}$]/[Excess $L_{<1000\ kDa}$] with depth.*

According to the temperature / salinity diagram presented by Middag *et al.* (personal communication), the NADW started at 1750-2000 m, which was also the boundary for the changes in iron parameters such as TDFe and the ratio of Excess L between the fractions [Excess L_{UNF}]/[Excess $L_{<0.2\ \mu m}$] and [Excess $L_{<0.2\ \mu m}$]/[Excess $L_{<1000\ kDa}$] (Figures 5 and 8). The ratio of Excess L between the fractions [Excess L_{UNF}]/[Excess $L_{<0.2\ \mu m}$] and [Excess $L_{<0.2\ \mu m}$]/[Excess $L_{<1000\ kDa}$] informs us which size fraction has the highest potential to bind Fe.

Theoretically these ratios should be equal or higher than 1. When the ratio is larger than one, the larger fraction has more empty ligand sites (*i.e.* Excess L) which are not present in the smaller fraction and has a potential to bind Fe. Between 50 m and 2000 m (comprising the NACW and the MOW) a significant amount of Excess L existed in the unfiltered water (Figure 8) and thus pointed to processes of reversible adsorption (complexation in the dissolved fraction). This was especially the case in the NACW, and to a lesser extent in the MOW (but the ratio was still 2). Thus the potential for scavenging was larger than for solubilisation between 50 and 2000 m.

High scavenging potential above the MOW can be explained by a previous dust deposition but also by sinking phytoplankton. Although the station was not located in the centre of the Sahara dust plumes (Bowie *et al.*, 2002; Croot *et al.*, 2004a), Middag *et al.* (personal communication) detected the influence of dust input on dissolved Al, Mn and Fe concentrations. According to Bergquist and Boyle (2006) the residence time of TDFe due to dust input is 1 to 5 months, thus dust input could explain the high concentrations of TDFe. A contribution of sinking phytoplankton may partly explain the TDFe maximum at a depth of 200 m. Mixing with more Fe-saturated particles (ratio 2-2.5 compared to 4, Figure 8) coupled with remineralisation might have resulted in solubilisation of Fe, explaining the small maximum in DFe at 500 m depth.

Scavenging only occurs if the adsorption sites on colloids or larger particles bind stronger than the dissolved organic ligands. This control can be expressed by the alpha factor of the organic ligands. Below 800 m depth, alpha of the ligands in the <1000 kDa fraction was remarkably constant at 10^{13} (Table 1). These ligands

were unsaturated in the whole water column (Figure 7) and thus 10^{13} as alpha factor seems to be an equilibrium value controlling scavenging and precipitation of Fe below 800-1000 m depth (Figure 8). Colloid aggregation can occur in the fraction between 1000 kDa and 0.2 µm which was saturated with Fe over the whole water column.

Together with the conclusion from Wu *et al.* (2001), that Fe uptake by phytoplankton is preferably done from the soluble fraction, that part of the colloidal fraction is inert, and that the same organic ligands are present in both fractions, we come to a different conclusion than Bergquist *et al.* (2007) who suggested that the colloidal fraction is the one that changes, whereas the soluble one does not. The saturation of the ligands in both size fractions regulates the formation of inorganic Fe-colloids and particles, in which Fe is irreversibly bound. From our research we show that the ligands in the colloidal fraction were saturated, whereas in the whole water column the ligands in the soluble fraction were not saturated (here <1000 kDa). Thus the Excess L in the soluble fraction regulates dissolution and colloid aggregation with a remarkably stable alpha factor of 10^{13}. Is thus the solubility product or better the colloid aggregation product of Fe 10^{13}?

5. Conclusions

The concentrations of DFe and $Fe_{<1000\ kDa}$ followed a nutrient-type profile with depth: depleted at the surface by phytoplankton uptake, a modest increase until 500-1000 m, and more or less constant concentrations below. The Excess L concentrations of the dissolved and <1000 kDa fractions were relatively high in the SML, 1.08 and 1.32 Eq of nM Fe, respectively. These high Excess L concentrations can be explained by Fe uptake increasing the empty ligand sites but also by ligand production by phytoplankton and bacteria.

The MOW was recognised by TDFe concentrations twice higher than in the overlying and underlying Atlantic Water masses. Here the ligands were not completely saturated, thus equilibrium between adsorption and complexation existed.

Excess L proved to be a very useful parameter since it is independent of the Fe concentration, which is not the case for total ligand concentration, alpha factor and conditional stability constant. Excess L gives information on the binding potential of the ligands, especially when expressed in the ratio [Excess L]/[Fe] which reflects the relative saturation of the ligands.

The smallest size fraction which was less saturated with Fe had relatively more Excess L (<1000 kDa fraction >> dissolved fraction >> unfiltered sample), and consequently had the largest capacity to bind more Fe, confirming that this is the most reactive fraction. The ratio $ExcessL_{UNF}/ExcessL_{<0.2\mu m}$ being larger than 1clearly showed that above 1000-2000 m unsaturated ligands existed in the unfiltered fraction, suggesting the removal of Fe from the dissolved phase by processes of reversible adsorption; whereas below 2000 m depth precipitation would be the major process of Fe removal. In the whole water column, the organic ligands in the larger colloidal fraction (between 1000 kDa and 0.2 μm) were saturated with Fe. The controlling alpha factor of the ligands ([Excess L] * K') of the <1000 kDa fraction was relatively constant at 10^{13} in the NADW and in the MOW, and might reflect the equilibrium between dissolved and particulate in these water masses.

Chapter 4

Observation of consistent trends in the organic complexation of dissolved iron in the Atlantic sector of the Southern Ocean

This chapter is adapted from: Thuróczy, C.-E., Gerringa, L.J.A., Klunder, M.B., Laan, P., De Baar, H.J.W., 2011a. Observation of consistent trends in the organic complexation of dissolved iron in the Atlantic sector of the Southern Ocean. Deep-Sea Research II. doi: 10.1016/j.dsr2.2011.01.002.

Abstract

Organic complexation of dissolved iron (DFe) was investigated in the Atlantic sector of the Southern Ocean in order to understand the distribution of Fe over the whole water column. The total concentration of dissolved organic ligands ([Lt]) measured by voltammetry ranged between 0.54 and 1.84 Eq of nM Fe whereas the conditional binding strength (K') ranged between $10^{21.4}$ and $10^{22.8}$. For the first time, trends in Fe-organic complexation were observed in an ocean basin by examining the ratio ([Lt]/[DFe]), defined as the organic ligand concentration divided by the dissolved Fe concentration. The [Lt]/[DFe] ratio indicates the saturation state of the natural ligands with Fe; a ratio near 1 means saturation of the ligands leading to precipitation of Fe. Reversely, high ratios mean Fe depletion and show a high potential for Fe solubilisation. In surface waters where phytoplankton is present low dissolved Fe and high variable ligand concentrations were found. Here the [Lt]/[DFe] ratio was on average 4.4. It was especially high (5.6-26.7) in the HNLC (High Nutrient, Low Chlorophyll) regions, where Fe was depleted. The [Lt]/[DFe] ratio decreased with depth due to increasing dissolved Fe concentrations and became constant below 450 m, indicating a steady state between ligand and Fe. Relatively low [Lt]/[DFe] ratios (between 1.1 and 2.7) existed in deep water north of the Southern Boundary, facilitating Fe precipitation. The [Lt]/[DFe] ratio increased southwards from the Southern Boundary on the Zero Meridian and from east to west in the Weddell Gyre due to changes both in ligand characteristics and in dissolved iron concentration. High [Lt]/[DFe] ratio expresses Fe depletion versus ligand production in the surface. The decrease with depth reflects the increase of [DFe] which favours scavenging and (co-) precipitation, whereas a horizontal increase in the deep waters results from an increasing distance from Fe sources. This increase in the [Lt]/[DFe] ratio at depth shows the very resistant nature of the dissolved organic ligands.

1. Introduction

The presence and availability of iron (Fe) is vital for life in the ocean. This trace nutrient is used by most organisms in seawater including phytoplankton in the euphotic zone. Phytoplankton is not only the base of the food web; it is also largely responsible for the fixation of dissolved carbon dioxide and the production of dissolved oxygen. Iron is used in phytoplankton cells in different locations and processes (Sunda *et al.* 1991 and 2001), notably in photosynthesis (photosystems) and in enzymes (*e.g.* nitrate-reductase). Due to its low concentration in seawater, iron is a limiting factor of primary production (Martin and Gordon, 1988, Martin *et al.*, 1991; De Baar *et al.*, 1990 and 1995; Buma *et al.*, 1991; Coale *et al.*, 1996; Fitzwater *et al.*, 1996; Timmermans *et al.*, 1998, 2001 and 2004), especially in HNLC (High Nutrient, Low Chlorophyll, Martin *et al.*, 1991) regions such as those in the Southern Ocean. Iron is used in the surface by phytoplankton but also over the whole water column by microbial communities (Bacteria and Archaea; Tortell *et al.*, 1996 and 1999) responsible for the degradation and remineralisation of sinking organic matter. Iron is found in seawater at concentrations above those determined by the solubility product (Kuma *et al.*, 1996; Millero, 1998). This is due to Fe binding organic ligands. Indeed 95 to 99.9 % of the dissolved Fe is strongly complexed by natural organic ligands (Gledhill and Van Den Berg, 1994; Rue and Bruland, 1995; Wu and Luther, 1995; Nolting *et al.*, 1998; Powell and Donat, 2001) allowing Fe to remain in solution, yet possibly limiting its availability for direct biological uptake.

The knowledge of the chemistry of Fe is important to understand its cycle in the world ocean which determines its distribution over the water column. The distribution of Fe in the oceans is controlled by its sources (aerosols deposition to the surface ocean, upwelling, ice melting and hydrothermal events), and by competition between processes which stabilise and remove it. Organic complexation stabilises Fe in seawater by keeping it in solution thus increasing its residence time. Fe removal is mainly caused by precipitation as oxy-hydroxides, adsorption onto large particles or colloid aggregation. (Alldredge *et al.*, 1993; Wells *et al.*, 1993, 1994 and 2000; Kepkay *et al.*, 1994; Logan *et al.*, 1995; Wu *et al.*, 2001; Cullen *et al.*, 2006).

The work presented here forms part of the GEOTRACES program (www.geotraces.org, Geotraces Science Plan, 2006). As part of this program, the

distribution of Fe along the Zero Meridian (Klunder *et al.*, 2011) and several other trace elements, including dissolved aluminium and manganese (Middag *et al.*, 2011a and 2011b), were also investigated.

This study describes the organically complexed state of Fe over the whole water column and the observed changes in the Fe chemistry when passing from the Sub-Antarctic Ocean into the Weddell Gyre (HNLC regions). With the knowledge of the Fe chemistry and of the organically complexed Fe in the whole water column, the processes controlling the Fe distribution in the world oceans can be better understood.

2. Description of the Southern Ocean

2.1. General aspects of the Southern Ocean

Many special aspects of the Southern Ocean give it a unique status. First of all, it is the only ocean with a permanent water flow around the globe (Antarctic Circumpolar Current, ACC), and the only ocean that communicates directly with the Atlantic Ocean, the Pacific Ocean and the Indian Ocean. The Southern Ocean is a key place for the deep water formation and thus for thermohaline circulation (Carmack, 1977; Mantyla and Reid, 1983; Foldvik and Gammelrød, 1988; Orsi *et al.*, 1999).

2.2. Fronts and zones

Several fronts (Figure 1) separate the Southern Ocean in different zones (Pollard *et al.*, 2002). The bottom topography contributes in maintaining the division of these zones with ridges separating different basins. Along the Zero Meridian, the Sub-Tropical Front (STF) with a surface salinity of 34.8 (Whitworth and Nowlin, 1987) and a temperature of 10-12ºC at 200 m depth separates warmer South Atlantic Surface Water (SASW) from the cooler and fresher Sub-Antarctic Surface Water (SAASW) in the Sub-Antarctic Zone (SAZ). Southwards, the Sub-Antarctic Front (SAF) separates the SAZ from the Polar Frontal Zone (PFZ) with a drop in salinity (Whitworth and Nowlin, 1987). During the ANTXXIV/3 cruise the SAF was located north of station 103 at ~46ºS (Figure 1). The PF is defined by a temperature of 2ºC at 200 m (Pollard *et al.*, 2002) and was located at 50º16'S just north of station 107. The Antarctic Zone (AAZ) is located on the Bouvet Triple Junction region (Atlantic-Indian Ridge which

separates the South Atlantic Basin and the Weddell Basin) and is delimited northwards by the Polar Front (PF) and southwards by the Southern Boundary (SB). The SB was located between 55º30'S and 56ºS on the Zero Meridian. The eastwards flowing ACC is found between the SAF and the SB. The Weddell Gyre is located between the SB and the Antarctic continent (Pollard *et al.*, 2002).

2.3. Water masses

2.3.1. Along the Zero Meridian

At the surface, the South Atlantic Surface Water (SASW, warm >12ºC, Whitworth and Nowlin, 1987) is found north of the STF and the Sub-Antarctic Surface Water (SSW) is found in the SAZ. The North Atlantic Deep Water (NADW, colder and more saline) flows along the bottom in the SAZ and PFZ. The Antarctic Intermediate Water (AAIW) flows northwards between the NADW and the surface water north of the PF. In the AAZ, the Circumpolar Deep Water is the main water mass present and is divided into the Upper Circumpolar Deep Water (UCDW) and the Lower Circumpolar Deep Water (LCDW). South of the SB (55ºS), in the Weddell Gyre the Antarctic Surface Water (AASW) coming from the ice melting during the summer (<5ºC) and the Antarctic deep water (colder and more saline) are found. This last water mass is divided into 3 separated water masses (Carmack and Foster, 1975; Fahrbach *et al.*, 2004; Klatt *et al.*, 2005), the Warm Deep Water (WDW) between ~200-1000 m with positive temperatures, the Weddell Sea Deep Water (WSDW, temperatures between 0ºC and -0.7ºC) and the Weddell Sea Bottom Water (WSBW, temperature below -0.7ºC).

2.3.2. In the Weddell Gyre

The Weddell Sea is an important region in the Southern Ocean because it is the main location where the Antarctic bottom water is formed (Klatt *et al.*, 2005). The cold surface water sinks along the continental slope of the Antarctic Peninsula towards the bottom and circulates eastwards along the North Weddell Ridge and the Southern Indian Ridge. The Weddell Gyre is limited westwards by the Antarctic Peninsula (60ºW) and extends eastwards along the North Weddell Ridge (60ºS) and along the

Southwest Indian Ridge (50-55ºS) until the Enderby Basin at 30ºE (Deacon, 1979; Gouretski and Danilov, 1993). The circulation of the water in the Weddell Gyre is cyclonic. The Weddell Sea is mainly constituted of the WDW, WSDW and WSBW. On top is the surface water (SW) about 100-200 m thick, with negative temperatures due to sea-ice melting.

2.3.3. Through the Drake Passage

The Drake Passage is a relatively narrow pathway between South America and the Antarctic Peninsula where the Antarctic Circumpolar Current and the South Pacific Currents converge. In this passage, the ACC is the main water mass present and is divided into the UCDW and the LCDW. The South Pacific Deep Water (SPDW), dense and characterised by high concentration of SiO_4, is also found (Sievers *et al.*, 1984). The Weddell Sea Bottom Water is also found in the Drake Passage. After bypassing the Antarctic Peninsula, the WSBW follows the bottom topography and circulates westwards along the continental slope in the Drake Passage.

3. Additional details on the materials and methods

3.1. Cruise track and sampling strategy

The ANT XXIV/3 expedition onboard R.V. *Polarstern* started from Cape Town, South Africa (February 2008), going south-westwards and reached the Zero Meridian at ~50ºS (Figure 1). The Sub-Tropical Front (STF), the Sub-Antarctic Front (SAF), the Polar Front (PF) and the Southern boundary of the Antarctic Circumpolar Current (SB in the present study) were successively crossed on the Zero Meridian. The Southern Boundary is also called SBdy in the Drake Passage by others (Barré *et al.*, 2008). The expedition continued across the Weddell Sea to King Georges Island, and finally traversed the Drake Passage until arrival in Punta Arenas, Chile (April 2008).

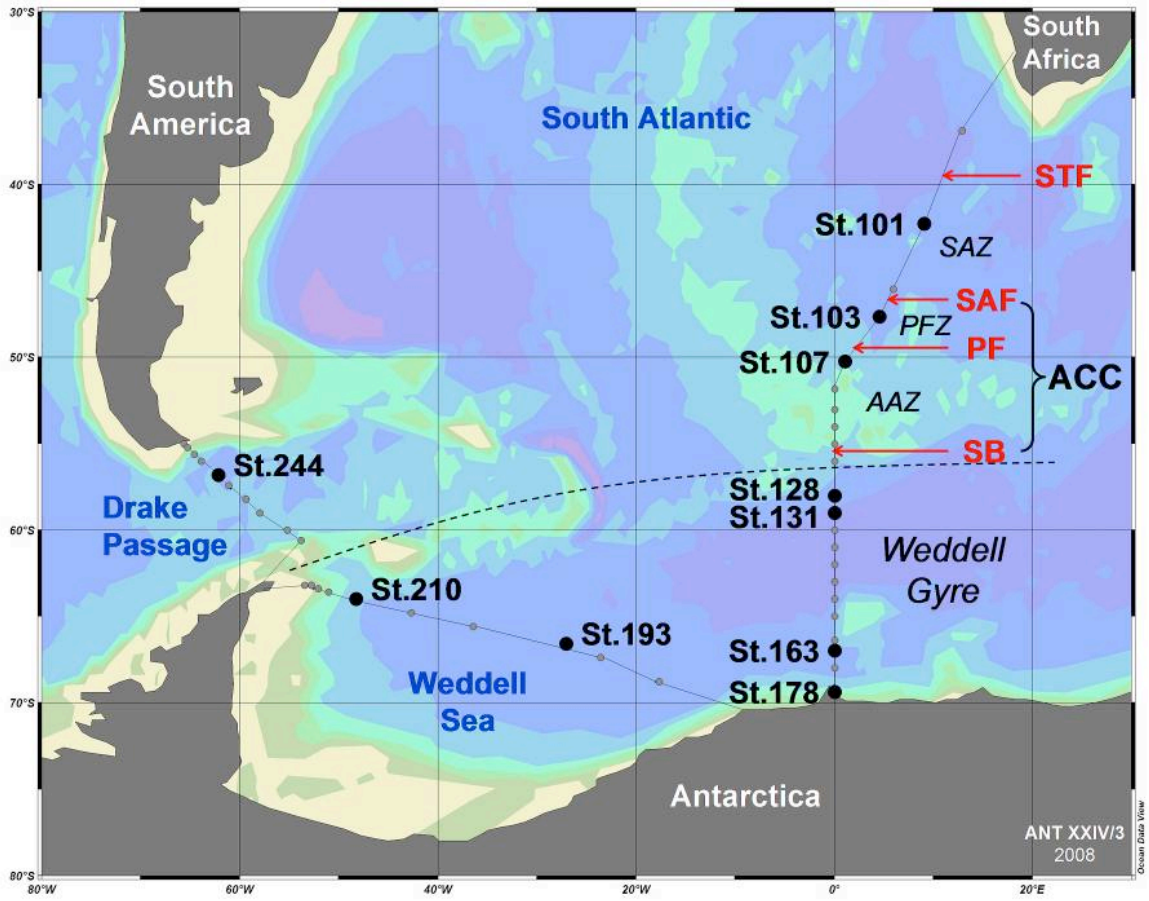

Figure 1: *Chart of the Atlantic sector of the Southern Ocean and location of the fronts and zones. The 10 stations sampled for this study are indicated by large black dots with station numbers. The small grey dots represent the additional stations also sampled with the titanium frame from NIOZ. The dashed line delimits the Weddell Gyre. STF = Sub-Tropical Front; SAF = Sub-Antarctic Front; PF = Polar Front; SB = Southern Boundary; SAZ = Sub-Antarctic Zone (St. 101); PFZ = Polar Frontal Zone (St. 103); AAZ = Antarctic Zone (St. 107); ACC = Antarctic Circumpolar Current; Weddell Gyre (St. 128, 131, 163, 178, 193 and 210.*

Overall 10 stations were sampled (Figure 1), for a total of 82 samples: 7 stations along the Zero Meridian, 2 stations in the Weddell Sea and 1 station in the Drake Passage. Station 101 was located in the SAZ (42.34ºS), station 103 in the PFZ (46ºS), station 107 in the AAZ south of the PF (50.27ºS). Stations 128 (58ºS), 131 (59ºS), 163 (67ºS) and 178 (69.4ºS) were situated in the eastern part of Weddell Gyre on the Zero Meridian. The stations 193 and 210 were taken in the Weddle Sea. The station 244 was located north of the PF in the Drake Passage (between 57º41'S and 57º51'S) and south of the SAF. Each sample was taken at judiciously chosen depths in order to sample all the different water masses present.

3.2. Fluorescence

Fluorescence, given in arbitrary unit (a.u.), was obtained from the NIOZ CTD sensor installed on the titanium frame. It corresponds to chlorophyll-a and is an indicator of phytoplankton abundance in seawater (Kiefer *et al.*, 1973; Babin *et al.*, 1996). Note that we discuss the layer where the fluorescence is >0.1 a.u. as the euphotic layer (this chapter and next chapters). The euphotic layer is defined as the depth range where the measured Photosynthetic Active Radiation (PAR) is more than 1 % of the incoming PAR at the sea surface (*i.e.* from sea surface until the 1% light depth) and is slightly different to the depth where the fluorescence was >0.1 a.u.. We did so to combine the influence of the light irradiance and of the presence of phytoplankton.

Table 1: *Averaged fluorescence (arbitrary unit, a.u.) in the surface layer per station. Standard deviations (S.D.), the number of samples (n) and the maximum depth (m) where* fluorescence > 0.1 a.u. are shown.

Stations	Fluorescence (a.u.)	S.D.	n	Maximum depth (m)
101	0.41	0.21	6	100
103	0.59	0.26	5	75
107	0.30	0.02	6	100
128	0.27	0.04	5	90
131	0.11	0.01	4	100
163	0.94	0.51	6	100
178	1.01	0.97	7	140
193	0.42	0.17	6	100
210	0.16	0.01	4	50
244	0.24	0.02	7	100

Relatively high values in surface waters corresponding to a chlorophyll maximum at about 50 m depth (euphotic zone) and a decrease with depth towards the aphotic zone were observed. At station 178 the fluorescence could even be detected at ~140 m depth.

Table 1 shows the average of fluorescence in the surface layer per station when it was > 0.1 a.u.. Stations 101 and 103 had relatively high fluorescence compared to stations 131 and 210 where lower fluorescence was recorded. Close to the ice edge

(St. 163 and 178) the highest fluorescence of all stations was measured due to a phytoplankton bloom.

4. Results

4.1. Dissolved Fe distribution

The concentrations of dissolved Fe along the Zero Meridian (Figure 2 and Table 2) from the same expedition are shown in detail by Klunder *et al.* (2011). At the stations presented here, the concentration of dissolved Fe was always below the nano-molar level and showed a nutrient-like vertical profile.

With a surface minimum at all stations (between 0.02 and 0.19 nM) the concentration of dissolved Fe increased with depth with a maximum just above the seafloor (St. 163: 0.58 nM; St. 193: 0.59 nM), or became more or less constant below 500-1000 m (St. 101: 0.63 nM; St. 103: 0.56 nM; St. 131: 0.36 nM; St. 244: 0.40 nM). Station 107 located south of the PF showed variability in the concentrations of dissolved Fe in the upper layers (0-450 m). It remained constant below 450 m at ~0.55 nM. At station 128 a steep increase was found from the surface until 450 m (until 0.76 nM) followed by a minimum at 1000 m (0.35 nM), and by a second maximum at 2500 m (0.68 nM) and a decrease towards the bottom. Two samples were taken at station 178 in the upper water at 137 and 451 m depth with 0.08 and 0.17 nM of Fe, respectively. Station 210 close to the Antarctic Peninsula slope had a maximum concentration of Fe between 1000 and 1500 m (0.46 nM) ascribed to hydrothermal input (Klunder *et al.*, 2011).

Table 2 (Below and next page): *Dissolved Fe and the characteristics of the dissolved Fe binding ligands of all samples. Dissolved Fe concentrations [DFe] are in nM (± standard deviations). Concentrations of the ligand [Lt] and the excess ligand [L'] are in Eq of nM Fe (± standard deviations). Conditional stability constants K' are in mol^{-1} with standard deviations.*
At station 101 the deepest samples collected at 3505 m and 4353 m had higher values of dissolved Fe, 0.630 nM and 0.572 nM, respectively, as compared with the duplicate sub-samples reported by Klunder et al. (2011), 0.401 nM and 0.280 nM, respectively.

The cause for this discrepancy is not known; perhaps our samples were contaminated. Nevertheless here we use our values, 0.63 nM and 0.572 nM in further interpretation. At station 178 Klunder et al. (2011) measured a complete vertical profile and found elevated concentrations of dissolved Fe between 300 and 800 m depth due to melted ice (1.50 nM of Fe at 451 m). The cause for the discrepancy with our sample at 451 m (0.171 nM) is not known.

** when the [DFe] was not determined in the same sample and therefore the concentration [DFe] was averaged from the samples above and under it; this was used for the calculation of the ligand characteristics (Eq. 2).*

***The standard deviation for Fe concentrations is missing when there was not enough sample volume to determine the concentration in triplicate.*

Station	Depth (m)	DFe (nM)	S.D.	[Lt] (Eq of nM Fe)	S.D.	log K' (mol^{-1})	S.D.	[L'] (Eq of nM Fe)	logα	pFe (M)	[Lt]/[DFe]
101											
	48	0.180	0.010	0.71	0.13	22.00	0.35	0.53	12.72	22.47	3.9
	76	0.105	0.007	0.53	0.10	22.12	0.24	0.43	12.76	22.73	5.1
	199	0.270	0.000	0.78	0.37	21.45	0.27	0.51	12.15	21.72	2.9
	502	0.377	0.004	0.70	0.18	21.69	0.33	0.32	12.19	21.62	1.9
	1001	0.587	0.017	1.17	0.11	21.66	0.09	0.59	12.43	21.66	2.0
	1502	0.540	0.020	1.25	0.13	22.16	0.21	0.71	13.02	22.28	2.3
	2501	0.630	0.030	1.26	0.11	21.91	0.13	0.63	12.71	21.91	2.0
	3505	0.630	0.000	1.07	0.05	22.61	0.20	0.44	13.26	22.46	1.7
	4353	0.572	0.039	0.92	0.09	22.42	0.29	0.35	12.97	22.21	1.6
103											
	45	0.187	0.005	0.70	0.20	22.39	0.41	0.51	13.10	22.82	3.7
	73	0.280	0.020	1.44	0.17	22.11	0.19	1.16	13.17	22.72	5.1
	203	0.318	0.015	1.12	0.14	22.40	0.25	0.81	13.30	22.80	3.5
	404	0.522	0.004	1.08	0.14	22.21	0.32	0.56	12.96	22.24	2.1
	499	0.536*	**	1.11	0.10	22.59	0.30	0.57	13.35	22.62	2.1
	751	0.551	0.025	0.90	0.16	22.18	0.35	0.35	12.72	21.98	1.6
	1253	0.532	0.008	0.90	0.08	22.38	0.26	0.37	12.94	22.22	1.7
	1747	0.540	**	1.13	0.10	22.74	0.28	0.59	13.51	22.78	2.1
	2001	0.582	0.009	1.55	0.18	21.93	0.18	0.96	12.92	22.15	2.7
	3099	0.560	0.006	0.99	0.08	22.34	0.22	0.43	12.98	22.23	1.8
107											
	49	0.096	0.002	0.87	0.19	21.84	0.36	0.77	12.73	22.75	9.1
	75	0.540	0.030	1.11	0.17	22.16	0.35	0.57	12.92	22.18	2.1
	199	0.199	0.008	0.84	0.16	21.69	0.16	0.64	12.50	22.20	4.2
	301	0.246	0.013	0.61	0.06	22.49	0.33	0.37	13.06	22.67	2.5
	499	0.520	0.020	0.97	0.07	22.31	0.17	0.45	12.96	22.25	1.9
	749	0.370	0.020	0.97	0.15	21.91	0.24	0.60	12.68	22.11	2.6
	1250	0.560	0.050	0.80	0.06	22.48	0.16	0.24	12.86	22.11	1.4
	1749	0.507	0.006	0.85	0.08	22.54	0.36	0.35	13.08	22.38	1.7
	3500	0.508	0.020	0.68	0.05	22.94	0.31	0.08	12.85	22.07	1.1

Station	Depth (m)	DFe (nM)	S.D.	[Lt] (Eq of nM Fe)	S.D.	log K' (mol^{-1})	S.D.	[L'] (Eq of nM Fe)	logα	pFe (M)	[Lt]/[DFe]
128											
	87	0.162	0.017	0.90	0.15	21.86	0.23	0.74	12.73	22.52	5.6
	311	0.490	0.010	1.84	0.33	21.74	0.23	1.35	12.87	22.18	3.8
	498	0.759	0.020	1.33	0.15	21.97	0.17	0.57	12.72	21.84	1.7
	1001	0.345	0.005	1.30	0.12	21.95	0.15	0.96	12.93	22.40	3.8
	1744	0.439	0.012	0.90	0.11	22.18	0.28	0.46	12.84	22.20	2.0
	2498	0.682	0.044	1.08	0.17	22.23	0.47	0.40	12.83	22.00	1.6
	3497	0.640	0.036	0.92	0.10	22.58	0.28	0.28	13.03	22.22	1.4
	4466	0.481	0.014	0.71	0.13	22.29	0.28	0.23	12.64	21.96	1.5
131											
	50	0.100	0.010	0.81	0.10	22.40	0.43	0.71	13.25	23.25	8.1
	152	0.133	0.003	0.98	0.19	21.68	0.21	0.84	12.60	22.48	7.3
	748	0.235	0.001	0.66	0.19	21.84	0.40	0.43	12.47	22.10	2.8
	1250	0.473	0.009	1.27	0.12	21.86	0.13	0.79	12.76	22.08	2.7
	1750	0.348	0.001	0.87	0.09	22.53	0.40	0.53	13.26	22.71	2.5
	3495	0.362	0.002	0.66	0.07	22.10	0.21	0.30	12.58	22.02	1.8
	4245	0.453	0.002	1.14	0.21	21.87	0.22	0.69	12.71	22.05	2.5
	4514	0.307	0.004	1.03	0.10	22.22	0.23	0.72	13.07	22.59	3.3
163											
	44	0.045	0.001	0.73	0.07	22.50	0.39	0.68	13.33	23.68	16.2
	101	0.107	0.006	0.67	0.13	22.16	0.54	0.56	12.91	22.88	6.3
	210	0.180	0.001	0.88	0.15	22.04	0.30	0.70	12.89	22.63	4.9
	300	0.192	0.001	0.75	0.10	22.32	0.35	0.56	13.07	22.78	3.9
	748	0.201	0.003	0.71	0.08	22.36	0.33	0.51	13.07	22.77	3.6
	1001	0.235	0.013	1.00	0.06	22.37	0.15	0.77	13.26	22.89	4.3
	1501	0.270	0.014	1.01	0.12	22.53	0.61	0.74	13.40	22.96	3.7
	2501	0.418	0.012	1.26	0.16	22.30	0.40	0.84	13.23	22.61	3.0
	4499	0.581	0.051	0.87	0.06	22.51	0.25	0.29	12.98	22.21	1.5
178											
	137	0.081	0.007	1.08	0.23	21.60	0.18	1.00	12.59	22.69	13.3
	451	0.171	0.005	0.88	0.14	21.93	0.24	0.71	12.79	22.55	5.2

Station	Depth (m)	DFe (nM)	S.D.	[Lt] (Eq of nM Fe)	S.D.	log K' (mol^{-1})	S.D.	[L'] (Eq of nM Fe)	logα	pFe (M)	[Lt]/[DFe]
193											
	50	0.045	0.001	1.33	0.17	22.20	0.35	1.28	13.31	23.66	26.7
	101	0.094	0.003	0.69	0.07	22.60	0.46	0.59	13.38	23.40	8.3
	402	0.192	0.009	1.31	0.13	22.24	0.25	1.11	13.29	23.00	6.7
	1000	0.211	0.006	1.25	0.11	22.18	0.19	1.04	13.20	22.87	5.8
	2001	0.327	0.002	1.32	0.19	22.12	0.26	0.99	13.12	22.60	4.0
	2998	0.390	0.021	1.10	0.09	22.76	0.55	0.71	13.61	23.02	2.8
	3997	0.534	0.003	1.39	0.09	22.43	0.21	0.86	13.36	22.63	2.6
	4799	0.592	0.015	1.52	0.09	22.34	0.16	0.93	13.31	22.53	2.6
210											
	30	0.030	0.010	0.49	0.06	22.56	0.43	0.46	13.22	23.73	15.8
	99	0.060	0.010	0.80	0.13	22.16	0.46	0.75	13.04	23.28	13.9
	249	0.160	0.000	1.24	0.09	22.34	0.20	1.08	13.37	23.16	7.7
	351	0.150	0.010	0.92	0.06	22.23	0.16	0.77	13.12	22.94	6.2
	750	0.240	0.010	1.03	0.15	22.17	0.21	0.79	13.07	22.70	4.3
	1000	0.460	0.020	1.16	0.06	22.64	0.23	0.69	13.48	22.81	2.5
	1501	0.460	0.020	1.20	0.07	22.44	0.12	0.75	13.31	22.66	2.6
	2000	0.310	0.020	1.54	0.07	22.24	0.10	1.23	13.33	22.84	5.0
	3500	0.320	0.010	1.08	0.10	22.12	0.19	0.76	13.00	22.50	3.4
	3946	0.360	0.010	1.13	0.05	22.34	0.11	0.77	13.22	22.67	3.2
244											
	38	0.021	0.001	1.38	0.11	21.90	0.12	1.36	13.03	23.71	66.9
	73	0.172	0.005	1.38	0.06	22.78	0.30	1.21	13.87	23.63	8.0
	147	0.128	0.011	1.38	0.11	22.30	0.22	1.25	13.40	23.29	10.8
	748	0.276	0.005	1.45	0.10	22.14	0.15	1.17	13.21	22.76	5.2
	1250	0.381	0.007	1.32	0.13	22.50	0.36	0.94	13.47	22.89	3.5
	1749	0.405	0.024	1.36	0.08	22.11	0.12	0.96	13.09	22.48	3.4
	2497	0.361	0.019	1.34	0.10	22.16	0.16	0.98	13.15	22.59	3.7
	3501	0.441	0.021	1.37	0.08	22.18	0.12	0.93	13.15	22.51	3.1
	4002	0.362	0.002	1.00	0.08	22.59	0.33	0.64	13.40	22.84	2.8

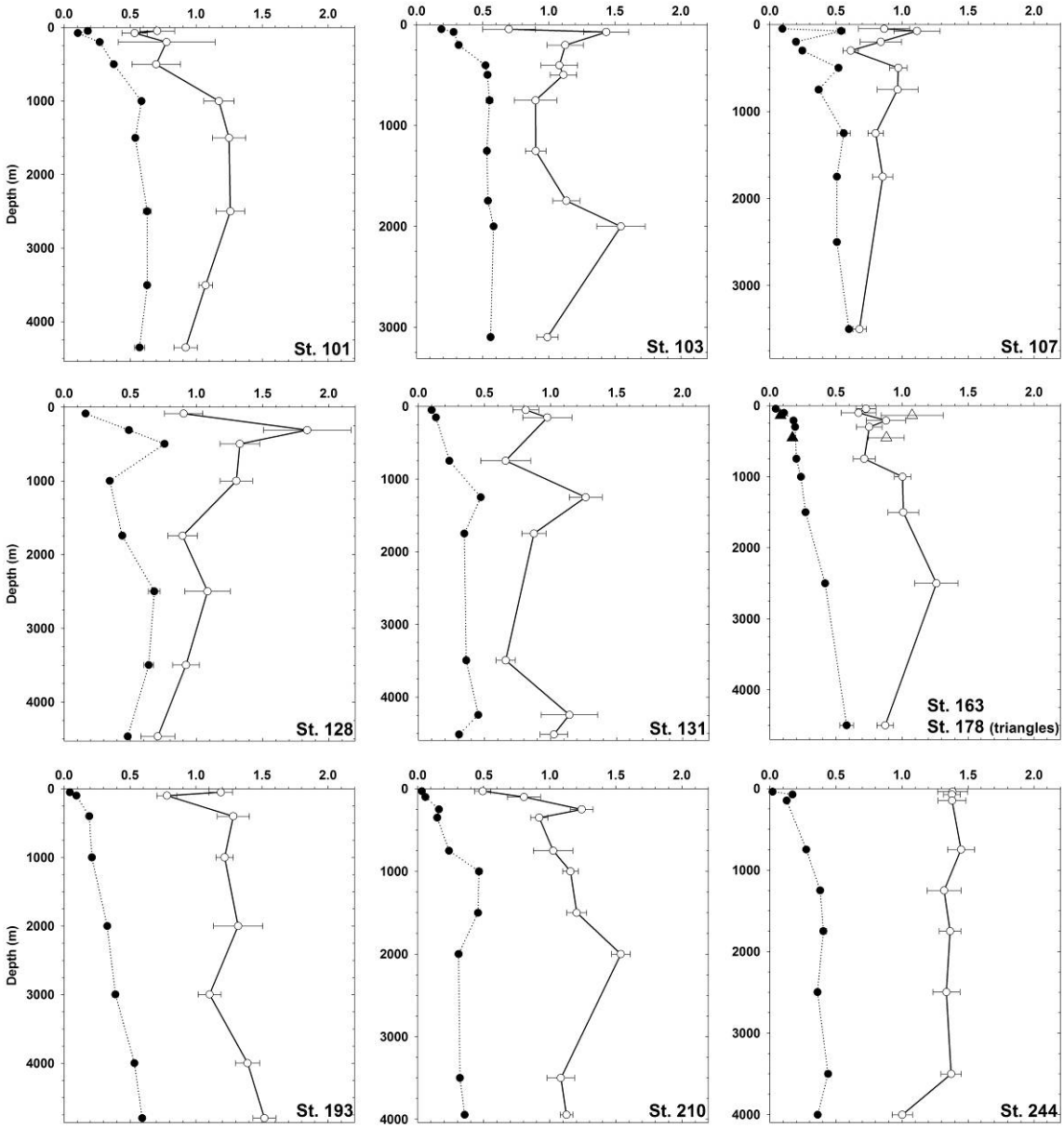

Figure 2: *Vertical distribution of organic ligands (white dots, solid line) and of dissolved Fe (black dots, dotted line) for the 10 stations. Station 163 and 178 (triangles at 137 and 451 m) are plotted in the same graph. Ligand concentrations are in Eq of nM Fe and dissolved Fe concentrations are in nM. The vertical axes are extended until the bottom depth.*

4.2. Organic ligand distribution and characteristics

The concentration of ligands (Figure 2 and Tables 2 and 3) throughout the water column ranged between 0.49 and 1.84 Eq of nM Fe (nano Equivalents of molar Fe). The upper 450 m showed relatively variable ligand concentrations. At stations 101, 131, 163 and 193 the concentrations were between 0.5 and 1.2 Eq of nM Fe in the first

450 meters. At stations 103, 107, 128 and 210 a maximum (1.1-1.9 Eq of nM Fe) was observed between 70 and 310 m depth after a surface minimum (0.5-0.9 Eq of nM Fe). Below 450 m depth the concentration of ligand decreased towards the bottom at station 101, 107 and 128. The ligand concentration was relatively constant at station 163. Station 131 showed higher concentrations of ligand near the seafloor (around 1.09 Eq of nM Fe). The concentration of ligand increased gradually towards the seafloor in the Weddell Sea at stations 193 and 210. At station 244, the concentration of ligand was stable from the surface until 3500 m around 1.33 Eq of nM Fe. Near the seafloor it was about 1.00 Eq of nM Fe.

The concentration of excess ligand (Excess L = L') with respect to Fe ([Lt]-[DFe], Table 2) corresponds to the concentration of free Fe binding sites. A small value of excess L means a near saturation of the ligand. In the upper layer (0-450 m) the mean values of excess L were 0.62 Eq of nM Fe north of the SB, 0.79 Eq of nM Fe in the Weddell Gyre on the Zero Meridian, 0.85 Eq of nM Fe in the Weddell Sea and 1.27 Eq of nM Fe in the Drake Passage (Table 3). Below 450 m depth, the averaged concentrations of excess L were 0.47, 0.56, 0.86 and 0.94, respectively, for the same zones. A surface maximum in excess L was usually found (St. 101, 107, 131, 163, 193 and 244). This excess L increased on average southwards the Southern Boundary on the Zero Meridian. More excess L was found close to the Antarctic ice-edge as well as in the Weddell Sea and in the Drake Passage.

The binding strength is defined by the conditional stability constant K' (Table 2). The K' ranged between $10^{21.45}$ and $10^{22.94}$. The value of K' was variable in the first 500-1000 m in all stations and it slightly increased with depth on the Zero Meridian. At station 193 in the Weddell Sea, K' was also variable with high values of K' at 750 m depth ($10^{22.82}$) and at 3000 m depth ($10^{22.76}$). At station 210, K' was constant over the water column, except at the surface and at 1000 m where higher values were found. In the Drake Passage, the value of K' was constant ($10^{22.15}$) over the water column except for the shallowest and deepest samples.

The organic alpha was relatively constant (about 10^{13}) from 450 m depth towards the bottom at all stations. Variable values of organic alpha were found in the first 450 m layer, ranging from 10^{12} at station 101 to $10^{13.5}$ at station 244. Below 450 m depth at

the stations north of the SB and in the north part of the Weddell Gyre (until station 131) the values of organic alpha were smaller than 10^{13}. Below 450 m depth at the stations close to the Antarctic ice edge, in the Weddell Sea and in the Drake Passage the values of organic alpha were larger than 10^{13} due to higher excess L in these regions.

Relatively low pFe values (Table 2) corresponding to relatively high Fe^{3+} concentrations are due to lower organic alpha values and thus either weaker ligands or lower concentrations of excess L. At stations 101 until 131, pFe decreased from 22.5-23 at the surface to approximately 22 at 450 m depth and remained constant towards the bottom. At stations 163, 193, 210 and 244, a decrease in pFe from 23.7-23.8 at the surface to 22.2-22.5 near the seafloor was found.

The ratio [Lt]/[DFe] (Figures 3 and 4, Tables 2 and 3) shows how much more ligand there is compared to the dissolved Fe. If [Lt]/[DFe] = 1, the ligand sites are fully saturated with Fe. The ratio [Lt]/[DFe] is a useful concept to highlight differences in ligand saturation throughout the water column and between different geographical locations (Thuroczy *et al.*, 2010b and Chapter 3). In order to discuss separately the phenomena and processes occurring in the ocean, the boundary between the upper and deeper ocean was operationally defined at 450 m depth. This choice was dictated by the sampling depths, as the samples were usually taken at fixed depth (…400, 500, 750 m depth…).

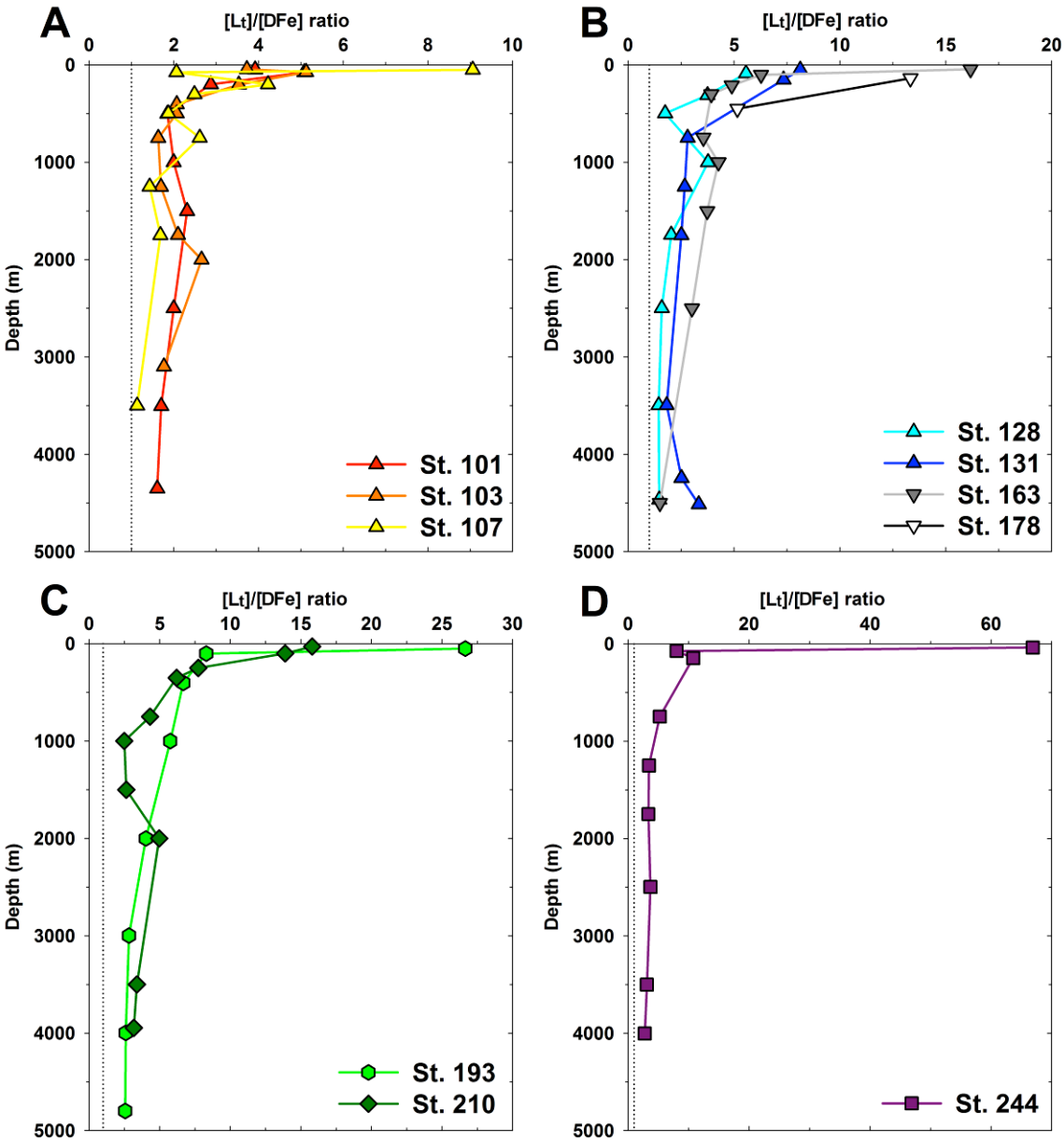

Figure 3: *Ratio values of [Lt]/[DFe]. **A:** North of the SB; **B:** Weddell Gyre on the Zero Meridian; **C:** Weddell Sea; **D:** Drake Passage. The dotted line marks exact saturation of the ligand with [Lt]/[DFe] = 1. Note the different scales on the horizontal axis for the ratio values.*

Table 3: *Average and standard deviation of [Lt] (Eq of nM Fe), [DFe] (nM), [L'] (Eq of nM Fe) and the ratio [Lt]/[DFe] per station and per zone.* ***A:*** *in the upper layer (0-450 m).* ***B:*** *in the deeper part of the ocean (below 450 m depth).* ***C:*** *subdivision of the upper layer for [Lt]/[DFe]: samples from the surface are shown separately from those in the euphotic layer (where fluorescence > 0.1 a.u., surface sample included) and in the layer below it until 450 m depth (Intermediate layer).*
** indicates large standard deviation (Station 244) due to the extremely high surface ratio [Lt]/[DFe] (66.9) compared to the value below this.*

A			Upper layer (0 - 450 m)							
Zones		Stations	Number of samples	Average [Lt]	S.D.	Average [DFe]	S.D.	Average [L']	S.D.	Average [Lt]/[DFe]	S.D.
↑	North of SB	101	n = 3	0.67	0.12	0.185	0.083	0.49	0.05	4.0	1.1
		103	n = 4	1.08	0.30	0.327	0.141	0.76	0.29	3.6	1.2
		107	n = 4	0.86	0.21	0.270	0.191	0.59	0.17	4.5	3.2
Prime Meridian		Average	n = 11	**0.89**	**0.27**	**0.267**	**0.147**	**0.62**	**0.22**	**4.0**	**2.0**
	↑	128	n = 2	1.37	0.66	0.326	0.232	1.04	0.43	4.7	1.3
		131	n = 2	0.89	0.12	0.116	0.023	0.78	0.09	7.7	0.6
		163	n = 4	0.76	0.09	0.131	0.068	0.63	0.07	7.8	5.7
↓	Weddell Gyre	178	n = 2	0.98	0.14	0.126	0.064	0.85	0.20	9.2	5.8
		Average	n = 10	**0.95**	**0.33**	**0.166**	**0.123**	**0.79**	**0.23**	**7.5**	**4.1**
Weddell Sea		193	n = 3	1.08	0.27	0.110	0.075	0.97	0.25	13.9	11.1
		210	n = 4	0.86	0.31	0.099	0.064	0.77	0.25	10.9	4.7
	↓	Average	n = 7	**0.96**	**0.29**	**0.104**	**0.063**	**0.85**	**0.26**	**12.2**	**7.4**
Drake Passage		244	n = 3	1.29	0.18	0.131	0.079	1.27	0.08	28.6	33.2*

B			Deeper layer (below 450 m)							
Zones		Stations	Number of samples	Average [Lt]	S.D.	Average [DFe]	S.D.	Average [L']	S.D.	Average [Lt]/[DFe]	S.D.
↑	North of SB	101	n = 6	1.06	0.22	0.556	0.094	0.51	0.16	1.9	0.3
		103	n = 6	1.10	0.24	0.550	0.019	0.55	0.23	2.0	0.4
		107	n = 5	0.85	0.12	0.511	0.077	0.34	0.20	1.7	0.6
Prime Meridian		Average	n = 17	**1.01**	**0.22**	**0.539**	**0.070**	**0.47**	**0.20**	**1.9**	**0.4**
	↑	128	n = 6	1.04	0.24	0.558	0.160	0.48	0.26	2.0	0.9
		131	n = 6	0.94	0.25	0.363	0.089	0.58	0.19	2.6	0.5
		163	n = 5	0.97	0.20	0.341	0.158	0.63	0.23	3.2	1.1
↓	Weddell Gyre	Average	n = 17	**0.98**	**0.22**	**0.425**	**0.164**	**0.56**	**0.22**	**2.6**	**0.9**
Weddell Sea		193	n = 5	1.25	0.20	0.376	0.162	0.90	0.12	3.6	1.4
		210	n = 6	1.19	0.18	0.357	0.089	0.83	0.20	3.5	1.0
	↓	Average	n = 11	**1.24**	**0.17**	**0.382**	**0.119**	**0.86**	**0.16**	**3.5**	**1.1**
Drake Passage		244	n = 6	1.31	0.16	0.371	0.055	0.94	0.17	3.6	0.9

C			Subdivision of the upper 450 m in:								
			Surface sample			Euphotic layer (where fluorescence > 0.1 a.u.)			Intermediate layer (where fluorescence < 0.1 a.u.)		
Zones		Stations	Depth (m)	Number of samples	[Lt]/[DFe]	Depth (m)	Number of samples	Average [Lt]/[DFe]	Depth (m)	Number of samples	Average [Lt]/[DFe]
↑	North of SB	101	48	n = 1	3.9	0 - 100	n = 2	4.5 ± 0.8	100 - 450	n = 1	2.9
		103	45	n = 1	3.7	0 - 75	n = 2	4.4 ± 1.0	75 - 450	n = 2	2.8 ± 1.0
		107	49	n = 1	9.1	0 - 100	n = 2	5.6 ± 4.9	100 - 450	n = 2	3.4 ± 1.2
Prime Meridian		Average		n = 3	**5.6 ± 3.0**		n = 6	**4.8 ± 2.4**		n = 5	**3.0 ± 0.9**
	↑	128	87	n = 1	5.6	0 - 90	n = 1	5.6	90 - 450	n = 1	3.8
		131	50	n = 1	8.1	0 - 100	n = 1	8.1	100 - 450	n = 1	7.3
		163	44	n = 1	16.2	0 - 100	n = 2	11.2 ± 7.0	100 - 450	n = 2	4.4 ± 0.7
↓	Weddell Gyre	178				0 - 140	n = 1	13.3	140 - 450	n = 1	5.2
		Average		n = 3	**10.0 ± 5.5**		n = 5	**9.9 ± 4.6**		n = 5	**5.0 ± 1.4**
Weddell Sea		193	50	n = 1	26.7	0 - 100	n = 2	17.5 ± 13	100 - 450	n = 1	6.7
		210	30	n = 1	15.8	0 - 50	n = 1	15.8	50 - 450	n = 3	9.3 ± 4.2
	↓	Average		n = 2	**21.2 ± 7.7**		n = 3	**16.9 ± 9.2**		n = 4	**8.6 ± 3.6**
Drake Passage		244	38	n = 1	66.9	0 - 100	n = 2	37.5 ± 41.6*	100 - 450	n = 1	10.8

A trend was seen in the [Lt]/[DFe] ratio with depth in the water column. High [Lt]/[DFe] ratio values were found at the surface with a decrease until 450 m (Figures 3 and 4, Table 3). The upper layer (0-450 m) was characterised by low dissolved Fe

concentrations (surface minima) and variable ligand concentrations. To highlight the steep decrease of the ratio [Lt]/[DFe] from the upper layer downwards, the ratios of the samples from the surface, *i.e.* the samples where phytoplankton grew (fluorescence > 0.1 a.u., Table 1) and of the layer underneath until 450 m depth (fluorescence < 0.1 a.u.) are shown separately in Table 3C.

Below 450 m depth the ratios [Lt]/[DFe] were lower and more constant with depth. This deeper part appeared to be a relatively stable environment (constant concentrations of dissolved Fe and of ligand) where degradation and remineralisation of the organic matter were the dominant chemical processes. A trend in [Lt]/[DFe] between geographical locations was also seen (Figures 3 and 4, Table 3). The ratio values [Lt]/[DFe] increased on average over the whole water column southwards the Southern Boundary on the Zero Meridian and from east to west in the Weddell Gyre.

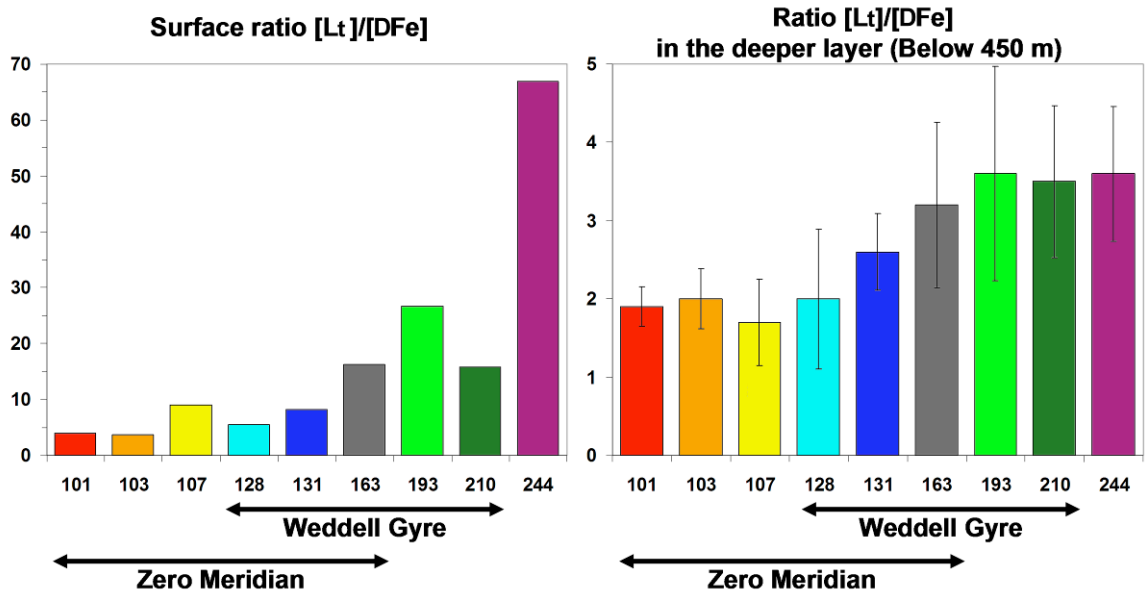

Figure 4: *Values of [Lt]/[DFe] per station. On the left side: surface values of [Lt]/[DFe]. On the right side: averaged values of [Lt]/[DFe] with standard deviations in the layer below 450 m depth. Station 178 is not shown here since only 2 samples were taken (137 m and 451 m depth).*

5. Discussion

5.1. Comparison with literature

The ligand concentrations presented here are similar to the 0.4 and 1.4 Eq of nM Fe reported for the upper 1000 m at 2 stations close to the ice edge at 0º and 10ºW by Boye *et al.* (2001) and along the 20ºE in the ACC. Surface water (until 100 m depth) ligand and Fe concentrations published by Boye *et al.* (2005) from the EisenEx experiment were also comparable at 0.5-0.7 Eq of nM Fe and 0.05 nM, respectively. In addition, similar Fe speciation was estimated (between 0.5 and 1.5 Eq of nM Fe) for the Kerguelen Archipelago Plateau in the Southern Ocean by Gerringa *et al.* (2008), with the exception of the deepest samples. These higher ligand concentrations at depth were attributed to the influence of the sediments. Only at station 131 were the ligand concentrations found below 4000 m similar to those measured by Gerringa *et al.* (2008).

The K' values for the entire water column calculated by Gerringa *et al.* (2008) using the same method were lower ($< 10^{22}$) than the K' values estimated here (mainly $> 10^{22}$). At 55º49'S-6º1'E Croot *et al.* (2004b) found, below a surface minimum (1 Eq of nM Fe), a decrease in the concentration of ligand from 2.5 Eq of nM Fe at 30 m depth to 1.2 Eq of nM Fe at 400 m. This result is comparable to station 128 located in the same area. The K' values found by Croot *et al.* (2004b) were also similar (around 10^{22}) to those found here in the upper 400 m. The dissolved organic ligand characteristics observed during the present study and by others (Powell and Donat, 2001; Gerringa *et al.*, 2008) did not indicate differences between water masses.

5.2. Upper layer of the ocean (0-450 m)

The trend of an increasing [Lt]/[DFe] ratio in the upper waters (Tables 3A and 3C, Figure 4) from north to south on the Zero Meridian and from east to west in the Weddell Gyre probably reflects the existing phytoplankton regimes (Sub-Antarctic region and HNLC region). The high surface ratio confirms the importance of phytoplankton in increasing the ratio [Lt]/[DFe], by Fe uptake and probably ligand production. Both the concentrations of dissolved Fe and of ligands explain the difference in ratios [Lt]/[DFe], lower north of the SB and higher in the Weddell Gyre.

Within the Weddell Gyre, the increase in [Lt]/[DFe] ratio from east to west was due to a decrease in the concentration of dissolved Fe only. Lower concentrations of dissolved Fe were found in the Weddell Sea proper (0.10 nM, n = 7) as compared to those found in the Weddell Gyre on the Zero Meridian (0.17 nM, n = 10). The concentrations of ligand and excess L were relatively constant in the Weddell Gyre. The values of organic alpha and pFe also showed a trend in the upper layer between geographical locations. The increase of organic alpha from north to south on the Zero Meridian and from east to west in the Weddell Gyre was due to an increase in excess L, whereas the increase in pFe value in the upper layer was due to a decrease of the dissolved Fe concentration and an increase of the organic alpha. Station 244, located in the Drake Passage, showed the highest [Lt]/[DFe] ratio at the surface caused by both a high ligand concentration relative to a very low dissolved Fe concentration (0.021 nM). The trend of the ratio [Lt]/[DFe] between geographical locations is seen in the ratio [Lt]/[DFe] of the surface samples (0-50 m) (Table 3C), but also in the euphotic layer (fluorescence > 0.1 a.u.) and in the layer below this (fluorescence < 0.1 a.u.).

The high [Lt]/[DFe] at the surface can be explained by the uptake of Fe and production of ligands (relatively high and variable ligand concentrations) by phytoplankton in the euphotic layer and by the microbial activity degrading the non-resistant ligands (Rue and Bruland, 1997; Tortell *et al.*, 1999; Boye and Van Den Berg, 2000; Croot *et al.*, 2001; Gerringa *et al.*, 2006). The ligand concentration represents the difference between the production and the degradation of the Fe-binding molecules (Boye *et al.*, 2001).

The stations were located in regions influenced by different “regimes” in terms of primary production. The regime in the surface waters at stations 101, 103 and 107 (Sub-Antarctic region) is thus very different from the other stations. Relatively low [Lt]/[DFe] ratio values were found at these stations. Relatively high fluorescence was measured here and Fe was not a limiting factor for phytoplankton growth at these 3 stations. Moreover, the dissolved organic ligand concentration was lower here. This indicated that there was no (need for) production of ligands like siderophores by prokaryotes.

The stations located in the HNLC regions (128, 131, 163, 178, 193 and 210) had low dissolved Fe concentrations and relatively constant ligand concentrations, resulting in higher [Lt]/[DFe] ratio values. Near the edge of the Antarctic ice sheet even higher [Lt]/[DFe] ratio values were found. Here a phytoplankton bloom was clearly observed by high fluorescence at station 163 and 178 (Table 1): a source of Fe was apparently available since the bloom had started. The melting of the Antarctic ice-sheet, its calving icebergs and of the seasonal sea-ice was shown to be a source of dissolved Fe in seawater by Klunder *et al.* (2011). This extra Fe was consumed resulting in low dissolved Fe concentrations. Here, the ligand concentration was relatively constant and was not responsible for the high [Lt]/[DFe] ratio values. However, in the Weddell Sea, even higher ratios [Lt]/[DFe] were found at the surface, whereas, the fluorescence in the water was low. Low dissolved Fe concentrations occurring here explained this high ratio [Lt]/[DFe]. The low dissolved Fe concentration might be caused by a phytoplankton bloom in the recent past or more probably Fe is taken up by phytoplankton living in the sea-ice. The Weddell Sea is known to be a productive area with high biological diversity supported by the growth of phytoplankton in the sea-ice (Arrigo *et al.*, 1997; Flores, 2009). So, even if relatively low fluorescence was measured in the water, Fe consumption should be high.

The particulate fraction, an important part of the Fe cycle, is still missing in the present study and should help to explain the processes occurring in the upper ocean. Adsorption sites on suspended particles compete with empty ligand sites in the dissolved fraction for Fe (Thuróczy *et al*, 2010b and Chapter 3). The adsorption on suspended particles followed by aggregation and downward settling of these particles is deemed to be responsible for the removal of Fe by scavenging.

5.3. Deeper part of the ocean (below 450 m)

Below 450 m depth, the values of [Lt]/[DFe] were low and constant with depth. Like the upper layer (0-450 m depth), the deeper part of the water column also showed a geographical trend: an increase of the ratio [Lt]/[DFe] southwards the Southern Boundary on the Zero Meridian and from east to west in the Weddell Gyre.

The difference between Zero Meridian and Weddell Sea was due to a lower concentration of ligand (1.00 of Eq of nM Fe, n = 34; versus 1.24 Eq of nM Fe, n = 11, respectively). The southward decrease in dissolved Fe concentration on the Zero Meridian was due to an absence of Fe sources (Klunder *et al.*, 2011). Moreover, excess L increased southwards along the Zero Meridian, thus reinforcing the same trend in [Lt]/[DFe]. Within the Weddell Gyre, the increase of [Lt]/[DFe] ratios from east to west was caused by both the concentrations of dissolved Fe (decrease) and the ligand concentration (increase). Obviously the excess ligand concentration also increased from east to west in the Weddell Gyre resulting in the increase of organic alpha value and combined with the decrease in the dissolved Fe concentration, an increase in pFe. Finally, the relatively high ratios of [Lt]/[DFe] in the deep part of the Drake Passage were due to high concentrations of ligand (1.31 Eq of nM Fe, n = 6) and remarkably constant excess L with depth.

The ratio [Lt]/[DFe] was constant below 450 m. Hunter and Boyd (2007) suggested that Fe-binding ligands in the deep ocean are refractory humic materials that originate from degradation of organic matter in the surface layer. The degradation would generate ligand functional groups in the deep ocean (Kuma *et al.*, 1996; Chen *et al.*, 2003) where only one dominant group of ligands is present (Rue and Bruland, 1995; Hunter and Boyd, 2007). The ligand characteristics found in the deep ocean in our samples were indeed relatively constant with depth (constant pFe and organic alpha reflecting an equilibrium between ligands, precipitation and adsorption of Fe) or showed a slight vertical trend, with increasing depth a decrease of excess L, and slight increase of K' value (Tables 2 and 3; Figures 2, 3 and 4). The ligand characteristics in the deep ocean reflect either a balance between production and degradation of dissolved organic ligands or a constant very refractory type/group of ligands. If constant production of ligands by microbial activity with depth exists (Reid *et al.*, 1993) it must be balanced by a constant degradation of ligands (Powell and Donat, 2001). Witter and Luther (1998) showed with a kinetic approach a change in the formation rate of Fe-ligand complexes and consequently the change of the dissociation rate (slower in the deep). They suggested that very slow degradation of ligands results in long residence time of the ligands (up to 1000 yr). Our data could

confirm this statement since the southward flowing water is depleted in Fe but not in ligand: Our study showed a uniform concentration of dissolved organic ligand and a rather uniform K' in deep waters, causing constant organic alpha and pFe values, not suggesting transformation of ligand characteristics with time as suggested by Witter and Luther (1998). Since the trend in [Lt]/[DFe] ratio in the deep waters between geographical locations (Figures 1, 3 and 4, Table 3) was a consequence of what happened in the surface layer, the export of particulate organic matter is important. Knowledge of Fe in other size fractions, like the particulate fraction from unfiltered water and different colloidal size fractions would help to understand which processes control the ligands and the Fe distribution in the deep ocean.

6. Conclusions

Overall the observed trends in [Lt]/[DFe] ratio values with depth and geographical location were consistent with the changes in ligand characteristics (excess L, organic alpha and resulting pFe) but showed a much clearer trend than the separate other parameters and confirmed that the ratio [Lt]/[DFe] is a reliable concept to study the chemistry of Fe in the oceans. This study has shown clear differences between upper waters (until 450 m depth), influenced by the presence of the phytoplankton, and deeper waters (below 450 m depth) in dissolved organic ligand characteristics and in the distribution of dissolved Fe. These high ratios (3.7-66.9) at the surface decreased to a nearly constant value below 450 m (1.7-3.6). Both the upper (0-450 m) and deeper (below 450 m) parts of the ocean showed an increasing trend southwards. In the upper 450 m this trend reflected the increasing depletion of Fe resulting in HNLC waters with increasing distance from Fe sources. However, the ligands also showed an increasing trend southwards showing that they are very resistant to degradation. In the upper layer of the Weddell Gyre, the increase in [Lt]/[DFe] ratio values from east to west is due to a decrease in dissolved Fe concentrations. In the deeper waters of the Weddell Gyre it is due to both the increase of ligand and the decrease of dissolved Fe concentrations. In the deep waters (below 450 m depth) a steady state between dissolved organic ligand and dissolved Fe was found at any location reflecting a balance between production and degradation of the organic matter. With the increase

of dissolved Fe concentrations with depth, the ligand sites for binding Fe are getting filled, and even almost saturated (North of the SB on the Zero Meridian). This near-saturation is deemed to be consistent with the precipitation of Fe as insoluble oxyhydroxide and its removal to the deep ocean. It confirms the important role of the organic ligands in keeping Fe in the soluble phase, thus avoiding its precipitation, and increasing its residence time in the water column. In the deeper layer (> 450 m) the increase in the [Lt]/[DFe] ratio is caused by a decrease in dissolved Fe concentrations only. A consistent trend in [Lt]/[DFe] values, at various depths and locations, is in itself impressive since nobody, to our knowledge, ever found clear trends in ligand characteristics other than a general decrease in ligand concentration with depth. However, the explanation is not still completely clear. The competition in the overall Fe budget between stabilisation by organic ligands and the removal by scavenging (adsorption onto particulate matter and colloid aggregation with or without oxidative precipitation) needs to be taken into account in order to better understand the Fe cycle in the ocean.

Chapter 5

Physical and chemical speciation of iron in the Atlantic sector of the Southern Ocean

Abstract

The geographical trends in the complexation of Fe in the dissolved fraction found in the previous chapter were attributed to changes in the small colloidal fraction only (<1000 kDa). The larger colloidal ligands were found to be saturated with Fe and probably not acting as reversible ligands that participate in the stabilisation of Fe in seawater. Morever, in the upper waters, a large proportion of DFe (70 to 80%) was in fact in the smaller colloidal fraction, whereas in the deeper waters between 50 to 70% of DFe was in this smaller fraction, confirming the crucial role of the small colloidal ligands in solubilising Fe in seawater. No excess ligands were found in the particulate fraction when analyzing unfiltered samples. However, the increasing concentrations of TDFe towards the seafloor found everywhere confirmed that the particulate fraction only plays a role in scavenging and removal of Fe.

1. Introduction

The complexation of dissolved Fe in the Atlantic sector of the Southern Ocean is described in Chapter 4 (Thuróczy *et al.,* 2011). Consistent trends in the saturation state of the organic ligands between depth and locations were discovered, along the Zero Meridian, in the Weddell Sea and in the Drake Passage. In surface waters the unsaturated ligands were found to have a high ratio [Lt]/[DFe] that was related to biota, especially in HNLC regions (Fe uptake and ligand production). On the other hand, the organic ligands were constantly and almost saturated with Fe towards the seafloor, revealing a balance between stabilisation and removal of Fe processes. Precipitation and scavenging must be in equilibrium with production and degradation of organic matter generated from the surface and exported to the deep waters.

In the present chapter, in addition to the dissolved fraction (<0.2 μm), we investigated Fe and Fe binding ligands in the fraction <1000 kDa, which contains the truly soluble Fe and small colloidal Fe, and in unfiltered samples with Total Dissolvable Fe (TDFe), which contain the particulate fraction (>0.2 μm). Together with the work of Klunder *et al.* (2011 and in prep) on the distribution and cycling of dissolved Fe in the same area, the results bring here more information on the differences between these size fractions (dominance, reactivity and saturation state of the ligands) and on the processes involved like solubilisation via organic complexation, and scavenging via large particles in relation with the presence of Fe sources in the Southern Ocean.

2. Description of additional parameters

2.1. Sea-ice conditions

As the expedition was conducted during austral summer, during the time of minimum sea-ice extent, the sea-ice coverage was rather small around Antarctica. On the Zero Meridian no significant sea-ice cover was encountered until the Antarctic coast. However, the sea-ice conditions in the Weddell Sea were particularly extreme. The evaluation of satellite data by the National Snow and Ice Data Center (NSIDC) clearly indicated that the Antarctic summer 2007/2008 was the one with the largest sea-ice

extent ever registered. This trend was particularly strong in the Atlantic sector of the Southern Ocean.

2.2. Temperature and salinity

Temperature and salinity (conductivity) were measured directly from 2 CTD systems (Sea Bird SBE 911+, regularly calibrated using salinity samples) on the sampling frames (a normal rosette from Alfred-Wegener-Institute and the titanium frame from NIOZ).

The temperature range (Figure 1) varied between locations and depths from more than 10ºC in the north and surface layer of the first station to the seawater freezing point (-1.85ºC) in the surface layer in the Weddell Sea or close to the ice edge. This southwards decrease in temperature of the upper waters went stepwise through the frontal zones (Whitworth and Nowlin, 1995; Pollard *et al.*, 2002). At stations 101 and 103 the vertical distributions of temperature had a surface maximum (12.4ºC and 8ºC, respectively) followed by a strong thermocline and a uniform temperature around 0.7ºC in deep waters towards the bottom. The station 107 located south of the PF showed a transition between the warmer northern part and the colder southern part. Indeed a surface maximum (+3ºC until 100 m depth) and a sub-surface minimum (+1.1ºC at 180 m, corresponding to the AAIW) were seen on the profile (Figure 1). In the deep the temperature is more uniform from 1.8ºC to 0.4ºC. For stations located in the Weddell Gyre, a sub-surface minimum with negative temperatures (between 100-200 m) and an underlying maximum between 250 and 500 m, with temperatures above 0°C were found. Then the temperature decreased with depth to become more or less uniform around -0.2 to -0.8ºC.

Salinity increased towards the bottom (from approximately 33.7-34.1 in the surface to 34.6-34.8 at the bottom) with a more or less strong halocline (Figure 1). This halocline was stronger in the upper water column (above 250 m) in the Weddell Gyre (St. 128, 131, 163, 193 and 210) where freshwater was abundant due to ice melting. At the other stations (101, 103, 107 and 244), this gradient was less pronounced.

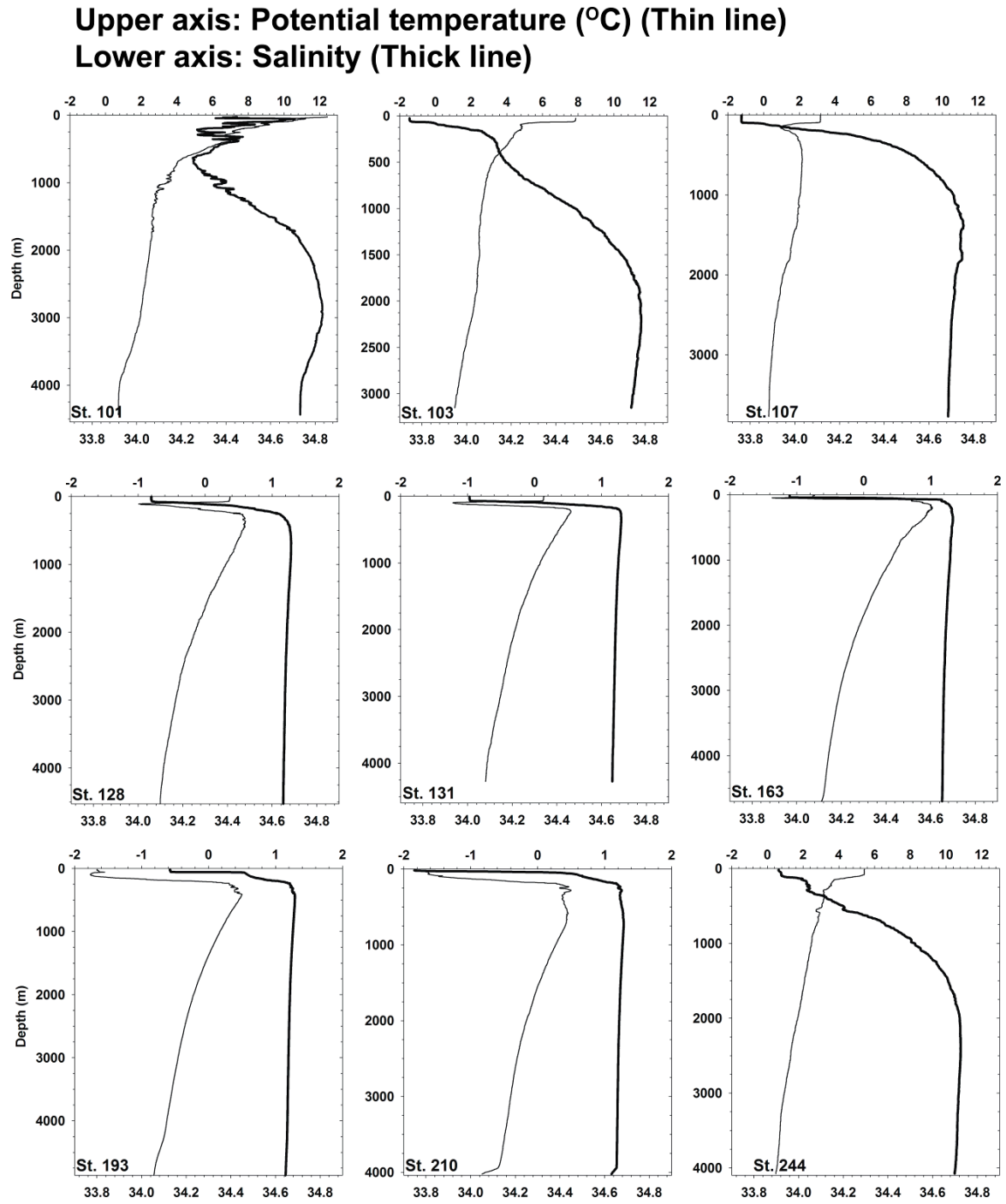

Figure 1: *Potential temperature (ºC, thin line, upper X-axis) and salinity (thick line, lower X-axis) versus depth for the 10 stations studied. Station numbers are in the left bottom corner of the graphs. Note the difference in the scale for the potential temperature at stations 101, 103, 107 and 244 (from -2 to 12ºC) with respect to the other stations. The vertical axes are extended until the bottom depth.*

2.3. Nutrients distributions

The inorganic dissolved nutrients nitrate + nitrite (NO_3 + NO2), phosphate (PO_4) and silicate (SiO_4) were measured directly onboard according to the procedure detailed by Grashoff *et al.* (1983). The concentrations of nitrite (NO_2) were very low or below detection limit, and from here on we will simply refer to only nitrate (NO_3) for the sum of nitrate + nitrite.

The distribution of nutrients (Figure 2) also showed a distinction between the basins in which the stations were situated north of the SB and those located in the Weddell Gyre. At stations 101, 103 107 and 244, the three nutrients (nitrate NO_3, phosphate: PO_4 and silicate: SiO_4) were found at relatively low concentrations at the surface due to depletion by phytoplankton. Nutrient concentrations increased with depth to reach a maximum at 500-1000 m and decreased to become constant in the NADW (NO_3 and PO_4), or increased with depth (SiO_4) in the NADW. Stations located in the Weddell Gyre showed uniform concentrations of NO_x in the entire water column (around 33 µmol/kg) below a surface minimum (25-30 µmol/kg). At these stations the SiO_4 concentration increased from ~70 µmol/kg in the surface water to ~124 µmol/kg at 1000 m depth in the WDW and remained constant within the WSDW and WSBW. The PO_4 concentration showed a similar trend as SiO_4, with a surface value of 1.8-2 µmol/kg and a maximum of 2.3 µmol/kg reached in the WDW for the same stations. The fact that nutrients were not depleted in the surface layer of the Weddell Gyre confirms that it is a High-Nutrient Low-Chlorophyll (HNLC) region (Martin *et al.*, 1988). The Sub-Antarctic stations 101, 103, 107 and 244 were depleted in SiO_4 at the surface but not in NO_3 and PO_4. The low concentrations of SiO_4 found here at the surface are likely due to the intensive removal of SiO_4 by blooms of large diatoms at the Polar Front.

2.4. Fluorescence

The fluorescence in the Southern Ocean during the ANT XXIV/3 expedition is described in chapter 4.

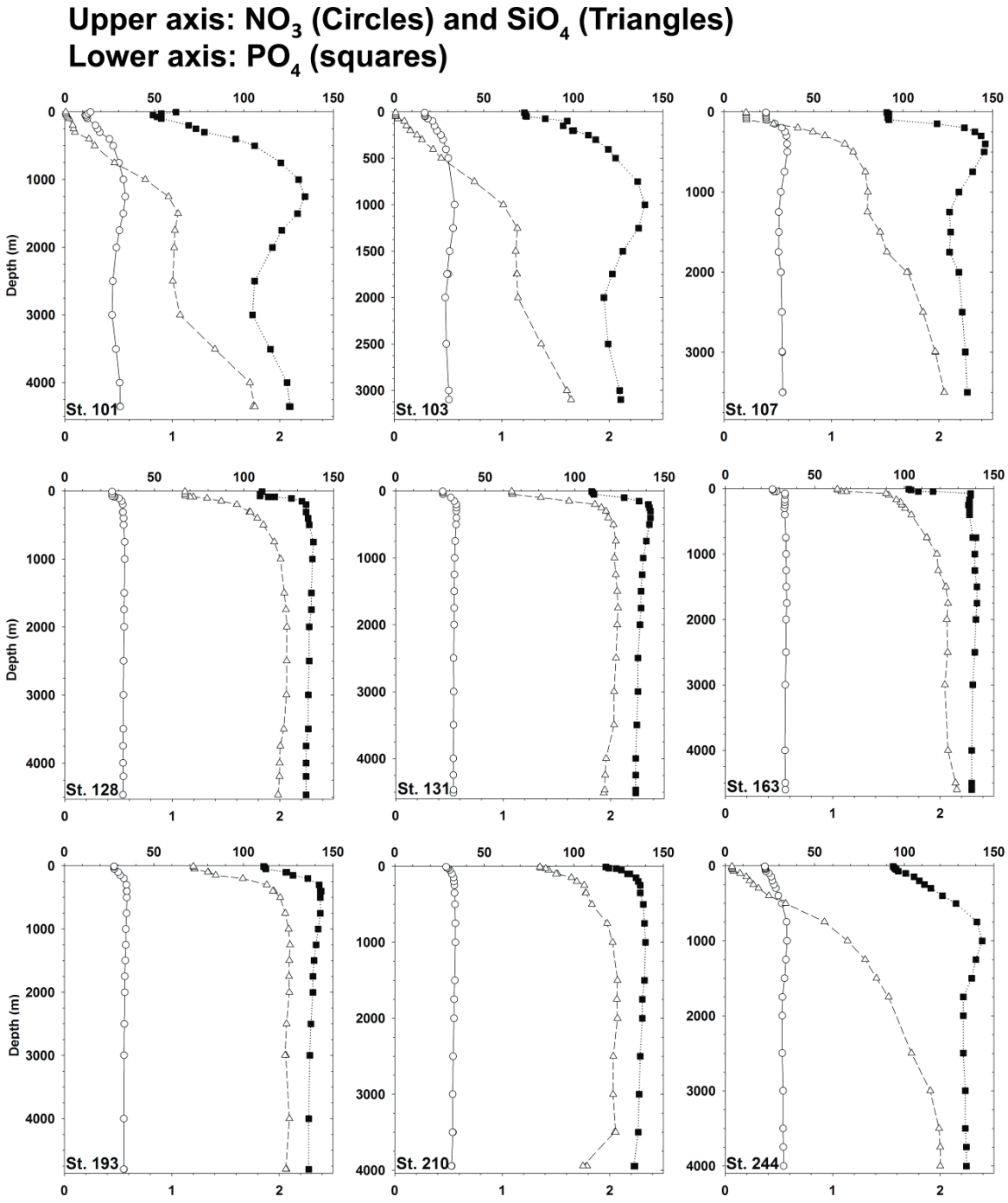

Figure 2: *Concentrations [µmol/kg] versus depth (m) of nitrate (NO_3, circles, upper X-axis), silicate (SiO_4, triangles, upper X-axis) and phosphate (PO_4, squares, lower X-axis) for each station sampled. Station numbers in the left bottom corner of the graphs. The vertical axes are extended until the bottom depth.*

3. Results

3.1. The dissolved and <1000 kDa fractions

The results concerning the dissolved fraction are described in the previous chapter (Chapter 4, Thuróczy *et al.,* 2011).

Table 1 (Below and next page): *Concentrations in the fraction <1000 kDa of Fe and of the ligands and their characteristics. Concentrations of* $Fe_{<1000\ kDa}$ *are in nM (± standard deviations). Concentrations of the ligand* $[L_{<1000\ kDa}]$ *and the excess ligand [L'] are in Eq of nM Fe (± standard deviations). Conditional stability constants K' are in* mol^{-1} *with standard deviations.*
**The standard deviation for Fe concentrations is missing when there was not enough sample volume to determine the concentration in triplicate.*
ND: Not determined.

Station	Depth (m)	[Fe<1000 kDa] (nM)	S.D.	[L<1000kDa] (nEq of M Fe)	S.D.	log K' (mol-1)	S.D.	Sensitivity A.mol-1	S.D.	[L'] (nEq of M Fe])	logα	[L<1000 kDa] / [Fe<1000 kDa]
101												
	48	0.102	0.004	0.38	0.06	22.50	0.32	9.16	0.11	0.28	12.94	3.7
	76	0.073	0.004	0.14	0.08	22.17	0.52	15.98	0.21	0.07	12.00	1.9
	199	0.253	0.016	0.46	0.14	22.30	0.41	7.76	0.18	0.20	12.61	1.8
	502	0.307	0.002	ND	ND	ND	ND	ND	ND	ND	ND	ND
	1001	0.230	0.003	0.78	0.15	22.12	0.49	9.90	0.26	0.55	12.87	3.4
	1502	0.240	0.009	0.71	0.08	22.36	0.37	0.98	0.02	0.47	13.03	3.0
	2501	0.359	0.005	0.83	0.20	21.58	0.20	11.12	0.27	0.47	12.25	2.3
	3505	0.250	0.003	1.05	0.18	21.93	0.20	10.57	0.27	0.80	12.83	4.2
	4353	0.205	0.001	0.58	0.05	23.49	0.48	0.71	0.01	0.38	14.07	2.8
103												
	45	0.172	0.005	0.67	0.09	23.25	0.46	0.70	0.03	0.50	13.94	3.9
	73	0.193	0.005	0.94	0.19	21.61	0.19	0.87	0.02	0.75	12.49	4.9
	203	0.211	0.002	1.03	0.14	22.09	0.19	1.03	0.03	0.82	13.01	4.9
	404	0.339	0.008	1.01	0.13	22.25	0.41	1.03	0.03	0.67	13.08	3.0
	499	0.447	0.008	0.95	0.15	22.31	0.49	1.42	0.04	0.51	13.01	2.1
	751	0.362	0.003	0.78	0.09	22.88	0.31	0.63	0.02	0.42	13.50	2.2
	1253	0.389	0.007	0.80	0.09	22.45	0.24	0.89	0.02	0.41	13.06	2.1
	2001	0.447	0.003	ND	ND	ND	ND	ND	ND	ND	ND	ND
	3099	0.405	0.005	0.91	0.10	22.31	0.18	1.20	0.03	0.50	13.01	2.2
107												
	49	0.078	0.005	0.69	0.07	22.36	0.31	1.30	0.02	0.61	13.15	8.8
	75	0.263	0.007	ND	ND	ND	ND	ND	ND	ND	ND	ND
	199	0.137	0.004	0.78	0.18	22.07	0.27	1.04	0.04	0.65	12.88	5.7
	301	0.214	0.024	0.50	0.10	22.20	0.28	1.07	0.02	0.28	12.66	2.3
	499	0.332	0.007	0.96	0.07	22.58	0.22	0.93	0.01	0.63	13.38	2.9
	749	0.259	0.005	ND	ND	ND	ND	ND	ND	ND	ND	ND
	1250	0.356	0.012	ND	ND	ND	ND	ND	ND	ND	ND	ND
	1749	0.376	0.003	ND	ND	ND	ND	ND	ND	ND	ND	ND
	2500	0.393	0.003	ND	ND	ND	ND	ND	ND	ND	ND	ND
	3500	0.454	0.006	0.54	0.11	22.47	0.35	1.15	0.03	0.09	12.40	1.2

Station	Depth (m)	[Fe<1000 kDa] (nM)	S.D.	[L<1000kDa] (nEq of MFe)	S.D.	log K' (mol-1)	S.D.	Sensitivity A.mol-1	S.D.	[L'] (nEq of MFe])	logα	[L<1000 kDa] / [Fe<1000 kDa]
128												
	87	0.096	0.005									
	311	0.378	0.028	1.65	0.22	21.63	0.13	1.53	0.05	1.28	12.74	4.4
	498	0.629	0.028	1.06	0.12	22.25	0.28	3.58	0.08	0.43	12.88	1.7
	1001	0.163	0.006	0.92	0.22	21.78	0.34	3.87	0.12	0.76	12.66	5.6
	1744	0.263	0.029	0.87	0.05	23.13	0.60	1.15	0.01	0.61	13.92	3.3
	2498	0.478	0.018	1.08	0.16	21.94	0.21	1.19	0.03	0.60	12.72	2.3
	3497	0.319	0.014	0.92	0.13	22.16	0.31	1.72	0.04	0.60	12.94	2.9
	4466	0.345	0.023	0.71	0.09	22.07	0.18	3.17	0.07	0.36	12.63	2.1
131												
	50	0.097	0.004	0.79	0.11	22.15	0.28	1.64	0.03	0.70	12.99	8.2
	748	0.192	0.009	0.38	0.12	22.39	0.46	1.97	0.05	0.19	12.67	2.0
	1250	0.321	0.026	1.20	0.15	21.85	0.16	0.91	0.02	0.88	12.79	3.7
	1750	0.224	0.006	0.47	0.11	22.42	0.38	1.55	0.03	0.25	12.81	2.1
	3495	0.099	0.001	0.39	0.07	22.23	0.50	1.41	0.02	0.29	12.70	4.0
	4245	0.370	0.014	0.74	0.09	22.24	0.29	2.02	0.03	0.37	12.81	2.0
	4514	0.234	0.006	0.81	0.14	21.78	0.22	1.63	0.03	0.58	12.54	3.5
163												
	44	0.043	0.002	0.70	0.05	22.96	0.81	1.17	0.01	0.66	13.78	16.3
	210	0.107	0.002	0.78	0.07	22.56	0.42	0.85	0.01	0.68	13.39	7.3
	300	0.118	0.002	ND	ND	ND	ND	ND	ND	ND	ND	ND
	1001	0.141	0.006	0.99	0.07	22.39	0.23	1.18	0.02	0.85	13.32	7.0
	1501	0.199	0.004	0.90	0.11	21.89	0.16	1.95	0.03	0.70	12.74	4.5
	2501	0.174	0.000	1.09	0.10	22.23	0.21	2.25	0.04	0.91	13.19	6.3
	4499	0.217	0.005	0.82	0.06	22.65	0.30	1.67	0.02	0.61	13.43	3.8
178												
	137	0.075	0.003	0.79	0.15	22.22	0.72	1.39	0.04	0.72	13.08	10.7
	451	0.17	*	0.51	0.09	22.61	0.40	1.68	0.03	0.34	13.14	3.0

Station	Depth (m)	[Fe<1000 kDa] (nM)	S.D.	[L<1000kDa] (nEq of MFe)	S.D.	log K' (mol-1)	S.D.	Sensitivity A.mol-1	S.D.	[L'] (nEq of MFe])	logα	[L<1000 kDa] / [Fe<1000 kDa]
193												
	101	0.069	0.011	0.68	0.06	23.11	0.37	1.79	0.02	0.61	13.89	9.8
	402	0.132	0.003	1.26	0.09	22.40	0.22	2.09	0.04	1.13	13.45	9.6
	3997	0.492	0.007	1.29	0.07	22.50	0.15	1.23	0.03	0.80	13.41	2.6
	4799	0.382	0.007	1.38	0.10	22.30	0.20	0.74	0.01	1.00	13.30	3.6
210												
	99	0.057	0.002	0.65	0.07	23.51	0.57	0.76	0.01	0.60	14.29	11.4
	249	0.140	0.003	0.99	0.10	22.10	0.18	1.58	0.03	0.85	13.03	7.1
	351	0.085	0.004	0.88	0.05	22.44	0.17	0.81	0.01	0.79	13.34	10.3
	750	0.132	0.002	0.99	0.09	22.35	0.26	1.50	0.03	0.85	13.29	7.5
	1000	0.133	0.002	0.85	0.07	22.72	0.30	0.85	0.01	0.72	13.57	6.4
	1501	0.154	0.002	1.17	0.05	22.43	0.13	0.88	0.01	1.02	13.44	7.6
	2000	0.175	0.003	0.92	0.05	22.48	0.17	0.42	0.00	0.74	13.35	5.2
	3500	0.188	0.006	1.04	0.06	22.42	0.16	2.46	0.03	0.85	13.35	5.5
	3946	0.209	0.013	ND	ND	ND	ND	ND	ND	ND	ND	ND
244												
	73	0.024	0.001	1.12	0.07	22.21	0.15	1.21	0.02	1.09	13.25	45.6
	147	0.025	0.001	1.07	0.09	22.05	0.15	2.14	0.04	1.04	13.07	43.0
	748	0.103	0.003	0.62	0.05	22.92	0.61	1.74	0.02	0.52	13.63	6.0
	1250	0.195	0.005	0.77	0.08	22.21	0.23	1.42	0.02	0.57	12.97	3.9
	1749	0.260	0.003	1.00	0.06	22.12	0.10	2.19	0.03	0.74	12.99	3.9
	2497	0.173	0.004	0.64	0.08	21.98	0.20	1.25	0.02	0.47	12.65	3.7
	3501	0.195	0.006	1.04	0.11	22.21	0.18	2.46	0.06	0.84	13.13	5.3
	4002	0.164	0.002	ND	ND	ND	ND	ND	ND	ND	ND	ND

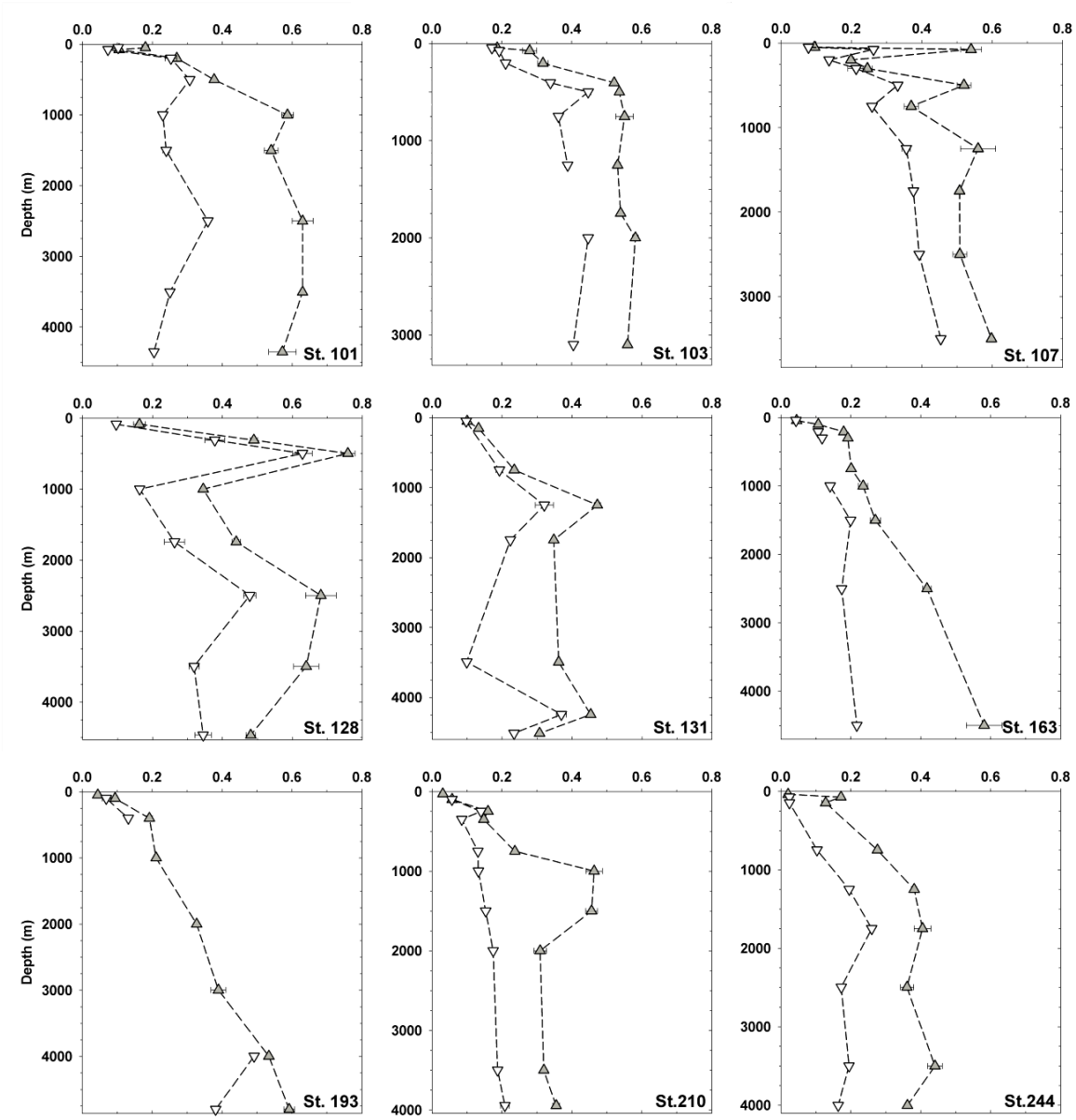

Figure 3: *Concentrations of Fe (nM) in the dissolved fraction (grey triangles, upwards looking) and <1000 kDa fraction (white triangles, downwards looking) with depth (m) at all stations sampled. Standard deviation of duplicate or triplicate measurements are too small to be seen on the graph (<5%).*

The concentrations of Fe in the <1000 kDa fraction (Table 1) were, as expected, lower than the DFe concentrations, and followed more or less the same vertical distribution as seen in Figure 3. This underlines the overall integrity of the filtration methods in terms of valid size cut-off of the filters and avoidance of inadvertent Fe contamination. In the upper layer of the water column (upper 450 m), 68.2 to 81.3% (on average) of DFe was in fact in the <1000 kDa fraction (Table 2) except at St.131,

where the only value present in this layer was 97.4% (in the euphotic layer), and at St. 244 in the Drake Passage were only 16.8% of DFe was present in the smaller fraction. In the euphotic layer where fluorescence was measured >0.1 a.u., no clear trend between the different locations was seen (Figure 3), neither in the layer below (intermediate layer, where fluorescence <0.1 a.u.). In the deeper ocean (below 450 m, Table 2), the percentages of DFe in the <1000 kDa fraction were lower (between 50 and 70%), revealing an increase of large colloidal Fe (between 1000 kDa and 0.2 µm). The lowest percentages in deep waters were found at St. 101, St. 244 in the Drake Passage and St. 210 in the Weddell Sea. The highest value (78.3%) found in the Weddell Sea at St. 193 is only due to a lack of values for the concentrations of $Fe_{<1000\ kDa}$, thus increasing the average percentage in the deeper layer.

Table 2: *Percentages of dissolved Fe present in the fraction <1000 kDa. Average values per layer at each stations, with standard deviation and number of sample (n). The upper layer (above 450 m depth), which includes the Euphotic layer (where fluorescence was measured >0.1 a.u.) and the intermediate layer (where fluorescence was measured <0.1 a.u.), and the deeper layer (below 450 m depth).*

			Euphotic layer (where fluorescence >0.1)			Intermediate layer (where fluorescence <0.1)		
Zones		**Station**	**Average**	**S.D.**	**n**	**Average**	**S.D.**	**n**
	North	**101**	63.2	9.0	2	93.8		1
	of	**103**	80.3	16.2	2	65.7	1.0	2
Prime	**SB**	**107**	65.2	23.4	2	77.9	12.8	2
Meridian		**128**	59.3		1	77.2		1
		131	97.4		1			
	Weddell	**163**	96.1		1	60.5	1.6	2
Weddell	**Gyre**	**193**	73.1		1	68.6		1
Sea		**210**			1	81.3	21.3	2
Drake Passage		**244**	14.2		1	19.4		1

			Upper 450m (euphotic + intermediate layer)			Deeper layer (below 450 m)		
Zones		**Station**	**Average**	**S.D.**	**n**	**Average**	**S.D.**	**n**
	North	**101**	73.4	18.8	3	49.6	17.3	6
	of	**103**	73.0	12.6	4	66.2	20.7	6
Prime	**SB**	**107**	71.5	17.0	4	69.5	5.7	5
Meridian		**128**	68.2	12.6	2	63.6	13.8	6
		131	97.4		1	66.5	20.5	6
	Weddell	**163**	72.4	20.6	3	53.2	16.9	4
Weddell	**Gyre**	**193**	70.8	3.2	2	78.3	19.5	2
Sea		**210**	81.3	21.3	3	48.7	13.7	6
Drake Passage		**244**	16.8	3.6	2	48.4	9.0	6

Excess L concentrations were relatively variable with depth and between locations on the Zero Meridian (St. 101 to 163, Figure 4), with an apparent decrease with depth at St. 107 and 128. At St. 103, below a subsurface maximum of 1.16 Eq of nM Fe in the dissolved fraction (73 m depth) and 0.75 nM Fe in the <1000 kDa fraction, a clear decrease of Excess L was measured and a minimum was reached in both size fractions (between 0.35 and 0.42 Eq of nM Fe) between 750 and 1250 m depth. The concentrations of Excess L were relatively constant with depth at St. 131, except at 1250 m depth with a single maximum (between 0.79-0.88 Eq of nM Fe) in both fractions, where also the concentrations of Fe were slightly higher (Figure 4) than the depths taken above and below. At St. 163, Excess L concentrations were also relatively constant with depth as seen in Figure 4, with a minimum close to the bottom at 4500 m depth (0.61 and 0.29 Eq of nM Fe in the <1000 kDa and dissolved fractions, respectively). In the Weddell Sea, the Excess L concentrations in both fractions (Figure 4, Table 1) appeared to be relatively constant with depth below the euphotic layer. In the Drake Passage at St. 244, below the highest concentrations of Excess L in the dissolved fraction at the surface (up to 1.36 Eq of nM Fe), a constant decrease was measured towards the bottom, for example in the <1000 kDa fraction until 2500 m depth. At 3500 m depth, Excess L concentrations were very similar in both fraction (0.84 and 0.93 Eq of nM in the <1000 kDa and dissolved fractions, respectively).

The binding strength (log K' values) and the reactivity of the ligands (expressed using log alpha values) were variable in the upper layer (above 450 m) and more constant below, in the deeper layer. On the other hand, the log K’ values were rather similar between the dissolved and the <1000 kDa fractions. As already discussed in Chapter 4, geographical trends were observed for the alpha values in the dissolved fraction, with an increase of the ligand reactivity towards the Antarctic continent on the Zero Meridian, and relatively high values measured in the Weddell Sea and in the Drake Passage.

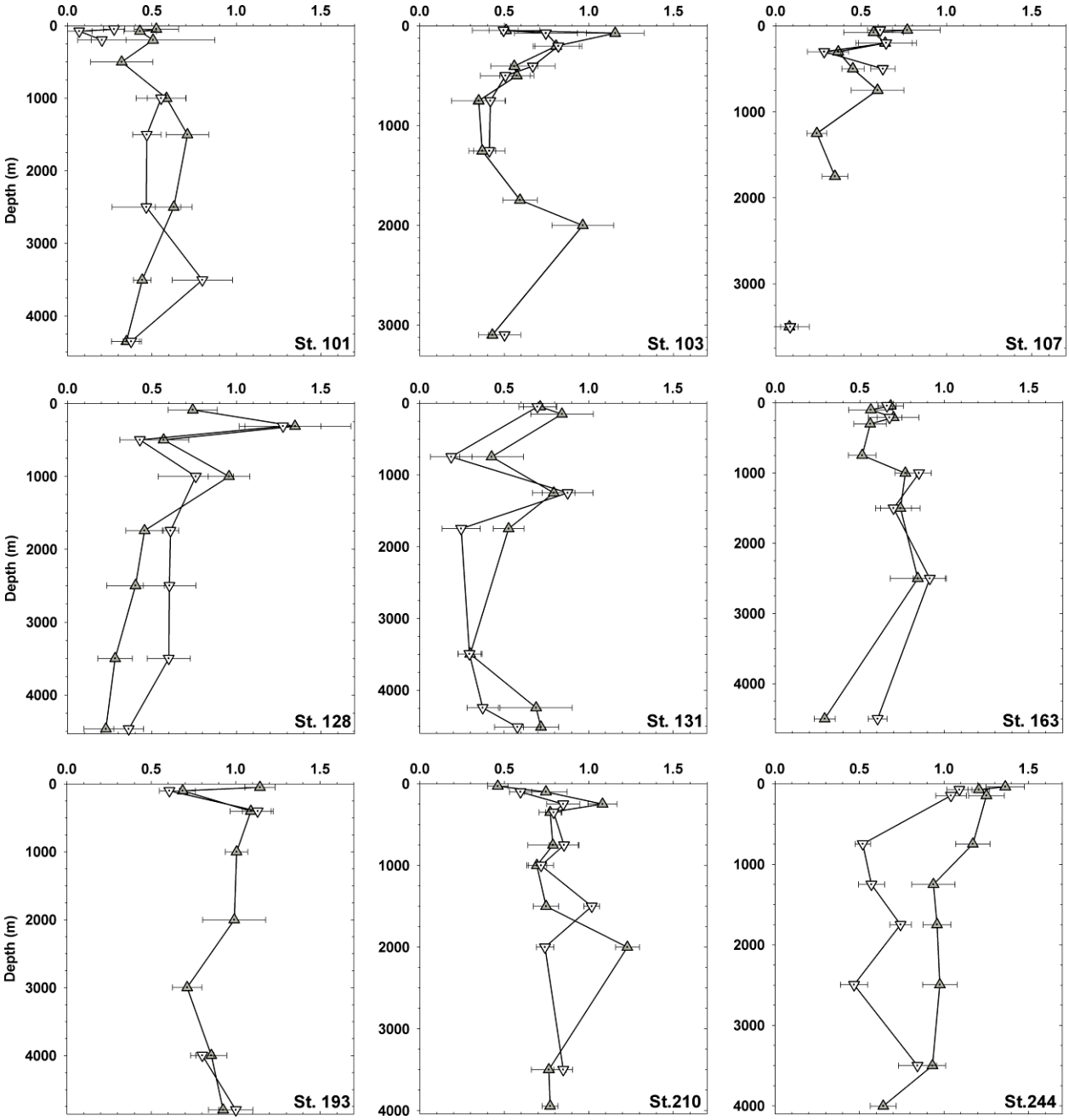

Figure 4: *Concentrations of excess ligands (Excess L, Eq of nM Fe) in the dissolved fraction (grey triangles, upwards looking) and <1000 kDa fraction (white triangles, downwards looking) with depth (m) at all stations sampled. Standard deviations are indicated.*

Results from the saturation of the ligands, expressed by the ratio [Excess L]/[Fe] per fraction (Table 1) show that the ligands in the smaller fraction (<1000 kDa) were less saturated with Fe than ligands in the dissolved fraction. That means that the large colloidal Fe (between 1000 kDa and 0.2 μm) must be almost saturated with Fe.

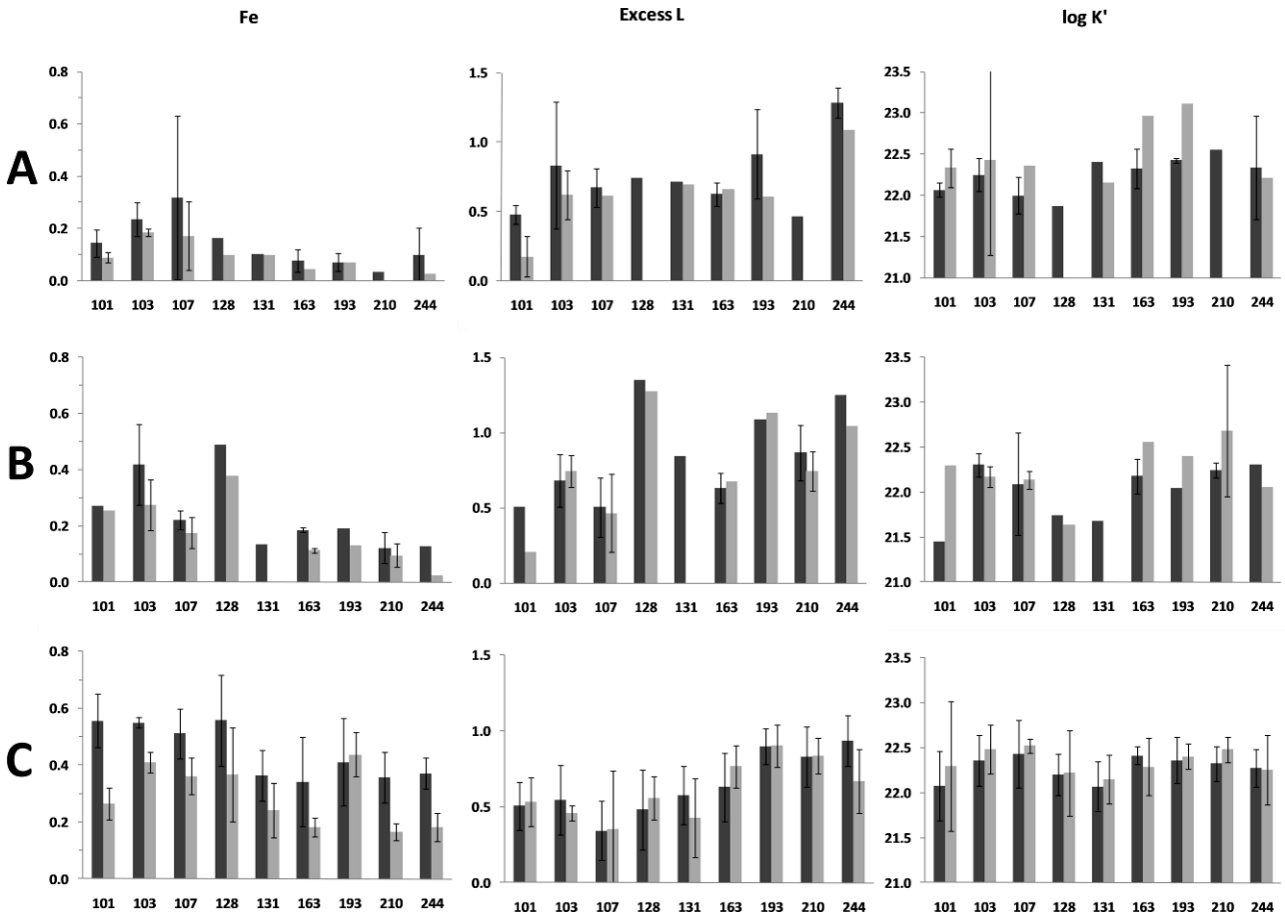

Figure 5: *Average and standard deviation per layer of [Fe] (nM), [Excess L] (Eq of nM Fe) and conditional stability constant (log K', mol^{-1}) per station for the dissolved fraction (dark grey) and for the fraction <1000 kDa (light grey):*
A: *euphotic layer, where fluorescence <0.1 a..u.;* ***B:*** *intermediate layer (below the euphotic layer and above 450 m depth);* ***C:*** *deeper layer (below 450 m). Where there is no standard deviation indicated, only one value was measured in the layer. Notice the average concentration of* $Fe_{<1000\ kDa}$ *larger than DFe at St.193 in the deeper layer: this is due to the only 2 values used in the <1000 fraction against 5 in the dissolved fraction that are relatively low at the depth taken above (see Figure 3).*

Figure 5 summarizes trends in concentrations of Fe and Excess L and binding strength in the 3 layers at each stations sampled for both fractions. Between the two fractions, no distinct difference was seen for Excess L concentrations. Where the binding strength appears higher in the <1000 kDa fraction than in the dissolved fraction, only one value is taken into account in the average. As noted in Chapter 4, a decreasing trend in Fe concentrations was found in the deeper layer between stations north of the SB and those located in HNLC regions. In addition, Excess L concentrations showed an opposite trend, with lower concentrations at the stations

located north of the SB. The geographical changes in the 3 parameters presented in figure 5 are similar in both fractions, meaning that the fraction responsible of these changes is probably the smaller one.

3.2. Unfiltered samples

The concentrations of Total Dissolvable Fe (TDFe, Figure 6) increased with depth at all stations sampled, with maximum concentrations measured at the deepest samples taken. A maximum in TDFe concentration was measured at 500 m depth at St. 128 (2.2 nM Fe) as also found in the smaller fractions at this depth corresponding to the temperature maximum in the Warm Deep Water (WDW). At the closest station, St. 131, no sample was taken at 500 m depth in the same water mass; we cannot confirm here a specific signature of the WDW with TDFe concentration as found for the MOW in the Eastern-North Atlantic Ocean (Chapter 3). However, no clear explanation for the maximum in TDFe concentration at 400 m depth at St. 193 (2.8 nM Fe) can be given since only 3 depths were sampled for unfiltered samples and no other station was taken in the neighbourhood. The concentrations of TDFe (Figure 6, Table 3) appeared to follow the same geographical trends although not as clear, as discussed in Chapter 4: a slight general decrease of TDFe concentrations southwards on the Zero Meridian and from East to West in the Weddell Sea (Figure 6).

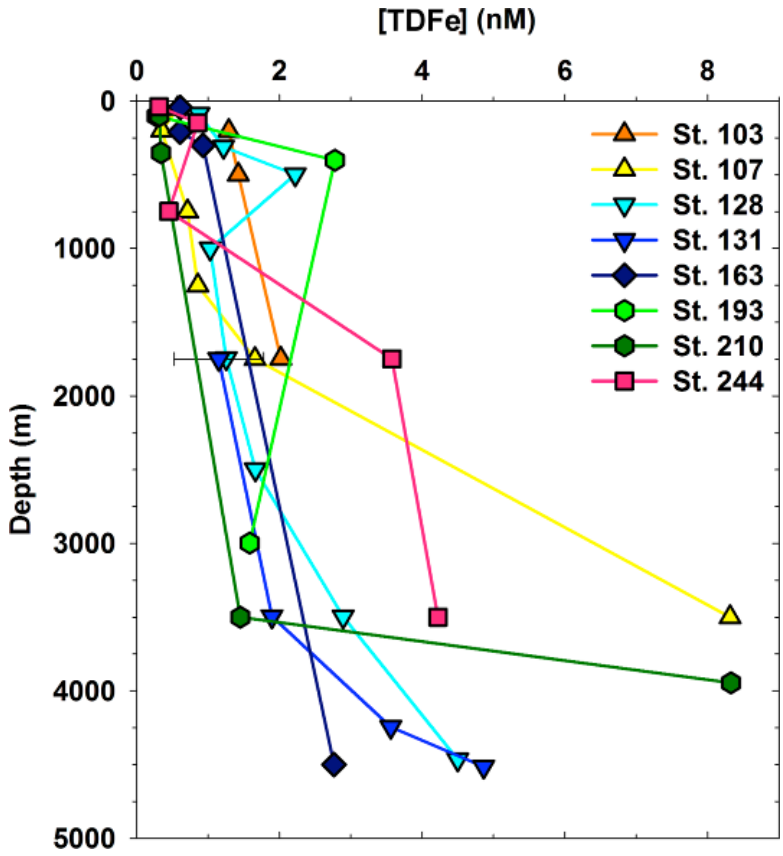

Figure 6: *Concentrations (nM) of Total Dissolvable Fe (TDFe) concentrations with depth at 8 stations sampled. Standard deviation of triplicate measurements are too small to be seen on the graph (<5%).*

The estimation of the concentrations of Excess L was done using the lower limit using DFe concentrations in the calculations (Table 3) as discussed in Chapter 2 and in Thuróczy *et al.* (2010b). Excess L concentrations in unfiltered samples using the lower limit were often lower than those in the dissolved fraction. Assuming that all the organic ligands are present in the total (unfiltered) sample, concentrations of Excess L should be higher than those in smaller fractions, or at least equal within analytical uncertainties. These discrepancies can be explained from two opposite views: one that filtrations probably causes extra complexation sites because colloids and particles may have disintegrated as also discussed in chapters 3 and 7. On the other hand, the particles might have hindered the voltammetric analysis by creating disturbances like aggregation, adsorption and sinking particles, or simply by the presence of living organisms.

Table 3: *Concentrations of TDFe and determination of the ligand characteristics in unfiltered samples using [DFe] in the calculations (lower limit, Chapter 2).*
** The standard deviation for Fe concentrations is missing when there was not enough sample volume to determine the concentration in triplicate.*
*** When the model could not fit the data.*

Station	Depth (m)	[TDFe] (nM)	S.D.	[DFe] (nM)	S.D.	[Lt] (Eq of nM Fe)	S.D.	logK' (mol^{-1})	S.D.	Sensitivity S ($A.mol^{-1}$)	S.D.	[L'] (Eq of nM Fe)	[L']/ [DFe]
103													
	203	1.292	0.005	0.318	0.015	0.73	0.11	22.09	0.31	1.36	0.03	0.42	2.3
	499	1.425	0.010	0.536	*	1.89	0.40	21.33	0.12	1.30	0.07	1.36	3.5
	1747	2.021	0.013	0.540	*	0.68	0.08	23.39	0.64	1.24	0.02	0.14	1.3
107													
	49	0.574	0.010	0.096	0.002	1.21	0.57	21.33	0.35	1.58	0.10	1.11	12.6
	199	0.352	0.011	0.199	0.008	0.99	0.17	21.67	0.20	9.03	0.22	0.79	5.0
	749	0.714	0.013	0.370	0.020	**	**	**	**	**	**	**	**
	1250	0.858	0.014	0.560	0.050	**	**	**	**	**	**	**	**
	1749	1.659	0.006	0.507	0.006	**	**	**	**	**	**	**	**
	3500	8.315	0.022	0.598	0.005	0.87	0.33	21.57	0.53	2.25	0.09	0.28	1.5
128													
	87	0.873	0.005	0.162	0.017	0.77	0.15	21.85	0.30	1.45	0.03	0.61	4.8
	311	1.217	0.035	0.490	0.010	0.70	0.13	22.11	0.50	1.53	0.04	0.21	1.4
	498	2.223	0.003	0.759	0.020	1.11	0.12	22.04	0.20	1.38	0.03	0.35	1.5
	1001	1.031	0.007	0.345	0.005	0.49	0.06	22.68	0.36	1.32	0.02	0.15	1.4
	1744	1.256	0.010	0.439	0.012	1.06	0.11	22.09	0.19	1.35	0.02	0.62	2.4
	2498	1.664	0.009	0.682	0.044	0.69	0.06	23.41	0.51	0.90	0.01	0.01	1.0
	3497	2.893	0.013	0.640	0.036	0.77	0.06	22.85	0.32	1.31	0.02	0.13	1.2
	4466	4.499	0.020	0.481	0.014	1.19	0.30	21.72	0.34	1.34	0.06	0.71	2.5
131													
	1750	1.152	0.628	0.348	0.001	0.76	0.09	23.02	0.39	0.95	0.02	0.42	2.2
	3495	1.896	0.011	0.362	0.002	0.59	0.06	22.32	0.28	1.52	0.02	0.23	1.6
	4245	3.561	0.045	0.453	0.002	1.09	0.20	21.88	0.29	1.44	0.04	0.64	2.4
	4514	4.862	0.035	0.307	0.004	0.67	0.16	21.97	0.64	1.34	0.03	0.36	2.2
163													
	44	0.611	0.004	0.045	0.001	0.84	0.14	21.74	0.20	1.64	0.03	0.80	18.7
	210	0.607	0.005	0.180	0.001	0.90	0.12	21.91	0.20	1.50	0.03	0.72	5.0
	300	0.930	0.015	0.192	0.001	0.99	0.26	21.50	0.22	2.02	0.07	0.80	5.2
	4499	2.766	0.034	0.581	0.051	0.60	0.04	23.55	0.50	1.50	0.01	0.02	1.0
193													
	101	0.279	0.007	0.094	0.003	0.65	0.19	21.66	0.30	3.16	0.08	0.55	6.9
	402	2.778	0.037	0.192	0.009	0.78	0.12	21.77	0.20	2.71	0.05	0.59	4.1
	2998	1.584	0.009	0.390	0.021	1.08	0.17	21.65	0.14	3.47	0.10	0.69	2.8
210													
	99	0.319	0.004	0.058	0.007	0.38	0.12	22.14	0.40	2.41	0.05	0.32	6.6
	351	0.342	0.002	0.148	0.006	1.05	0.42	21.45	0.38	2.47	0.12	0.90	7.1
	3500	1.454	0.028	0.320	0.006	0.54	0.12	21.89	0.37	2.38	0.05	0.22	1.7
	3946	8.327	0.107	0.355	0.010	0.90	0.27	21.54	0.30	2.67	0.09	0.54	2.5
244													
	38	0.314	0.034	0.021	0.001	0.81	0.18	22.18	0.87	1.08	0.03	0.79	39.4
	147	0.858	0.006	0.128	0.011	0.44	0.09	22.25	0.31	1.43	0.02	0.32	3.5
	748	0.450	0.002	0.276	0.005	1.01	0.32	21.69	0.37	1.87	0.08	0.73	3.7
	1749	3.577	0.034	0.405	0.024	1.24	0.11	22.26	0.24	2.16	0.04	0.84	3.1
	3501	4.222	0.026	0.441	0.021	0.61	0.10	22.61	0.38	1.88	0.04	0.16	1.4

4. Discussion

4.1. Size-fractionation

Regarding unfiltered samples, Excess L concentrations calculated using the lower limit were often lower than those in the dissolved fraction confirming that within the measuring detection window established by the use of TAC, the particulate fraction (>0.2 µm) did not contain reversible adsorption sites (no Excess L). Therefore, the particulate fraction only has a role in scavenging and removal processes, as seen everywhere with the increasing concentrations of TDFe with depth.

Additionally, the fraction <1000 kDa proved to be comparable to the whole dissolved fraction regarding the complexation of Fe at most of the locations sampled

(Except St. 244 in the Drake Passage). These similarities shows that the small colloidal fraction (<1000 kDa) is thus the main responsible of the complexation of Fe within the dissolved fraction, thus responsible of the fate of Fe in seawater. Moreover, this smaller fraction was less saturated with Fe than the whole dissolved fraction. Thus, the larger colloidal ligands saturated with Fe, did not appear to compete with the added ligand TAC while titrating compared to the smaller colloidal ligands. This reveals that larger colloids were probably not reversible ligands that participate in the stabilisation of Fe in seawater, hence confirming the major role of the smaller fraction in stabilising Fe via reversible complexation. However, at a station in the Eastern-North Atlantic Ocean (Chapter 3), a large portion of DFe was found to be larger colloidal Fe in the whole water column (up to 80% of DFe), as also found here at St. 244 in the Drake Passage (50-80% of DFe). It is probably characteristic of places dominated by one water mass. Here, the Antarctic Circumpolar Current is composed of the upper and lower Circumpolar Deep Water (UCDW and LCDW), and in the Eastern-North Atlantic Ocean (Chapter 3), with the North Atlantic Central Water (NACW) and the North Atlantic Deep Water (NADW).

In rare cases, concentrations of Excess L were measured higher in the smaller fraction than in the dissolved one considering the analytical uncertainties, like at St. 128 below 1500 m depth. Here no contamination during filtration was seen (*cf.* Fe concentrations in both fractions). A plausible disequilibrium was generated in ultra-filtered samples, as already found and discussed at a station on the shelf sea of the Arctic Ocean (Chapter 6), and earlier (3.2.) when discussing about unfiltered samples.

4.2. Upper layer of the ocean (0-450 m)

In the upper waters (0-450 m), large differences were measured in the excess ligand concentrations and in the binding strength between depth and stations. These observations reflect a variable and changing environment as seen in the potential temperature, salinity and nutrient vertical distributions (Figures 1 and 2). Along the Zero Meridian, several water masses with very different properties meet, as explained in the chapter 4. Colder and fresher water is found south of the Southern Boundary

(SB), due to sea-ice when approaching the Antarctic continent. There, in HNLC regions, the nutrients abundance is higher.

In surface waters, the primary productivity plays an important role in the chemistry of Fe. Blooms produce important amounts of organic matter like dead phytoplankton, and remineralised biogenic material (Eppley *et al.*, 1979; Kepkay *et al.*, 1994; Fisher *et al.*, 2000) representing a potential large variety of Fe-binding ligands (variable ligand concentrations in the upper layer). Part of the organic matter produced can be trapped in sea-ice to be released again later in seawater together with Fe (Fisher *et al.*, 1988; Pusceddu *et al.*, 1999; Thomas *et al.*, 2001; Lannuzel *et al.*, 2008a and 2008b). Iron released from sea-ice is quickly used by phytoplankton living in the water beneath the ice and is therefore found at very low concentrations. Phytoplankton is a food resource for higher trophic levels, especially for the krill, which can play a role in the Fe biogeochemical cycle (Tovar-Sanchez *et al.*, 2007) when releasing important amounts of Fe.

Several other phenomena could explain the variability in the dissolved organic Fe-binding ligands at the surface. Few samples only were taken in the upper water column in our study. However, there, we did find lower amount of large colloidal Fe (between 1000 kDa and 0.2 μm), and slightly stronger ligands in the small fraction (<1000 kDa) than samples taken deeper, most likely due to the influence of biota. Phytoplankton, bacteria and viruses use Fe but only prokaryotes are known to release siderophores under Fe-limited conditions (Butler, 1998 and 2005; Barbeau *et al.*, 2001; Maldonado *et al.*, 2005) facilitating the acquisition of Fe. Moreover viral lysis of plankton cells is known to release dissolved and particulate components containing Fe which can be easily assimilated by other micro-organisms (Poorvin *et al.,* 2004). However, in our surface samples, the TDFe concentrations were not measured higher than deeper samples. Siderophores produced by bacteria may represent 0.2 to 4.6% of the dissolved Fe pool (Mawji *et al.*, 2008), and can therefore play a little role in the speciation and the solubility of Fe in seawater (Tortell *et al.*, 1999).

Verdugo *et al.* (2004) suggested that fibrillar material like polysaccharides can form gels in seawater and can be an important step between truly dissolved and particulate phase. Those colloidal polysaccharides that can act as organic ligands were

found in relatively high concentrations but with relatively low binding constant as already seen by Hassler *et al*. (2011), Benner (2011) and in the Arctic sea-ice by Meiners *et al*. (2008) and Riedel *et al*. (2007). In our samples from the upper waters, the ligand concentrations were not clearly higher than in deeper samples, as for the binding strengths that were not lower, but even slightly higher. Obviously, there was no sign of presence of polysaccharides in our samples, or they were probably outside of our measuring detection window.

4.3. Deeper layer (below 450 m depth)

The ligand characteristics in the deep ocean reflect either a balance between production (remineralisation) and degradation of dissolved organic matter or a constant very refractory type/group of ligands. The constant and ubiquitous presence of organic ligands, in deep water must be due to a permanent input of organic matter from living organisms generated at the surface. Thus, the decomposition by the microbial activity of sinking organic matter may increase the pool of organic ligands, thus enhancing the solubility of Fe in the deep oceans. This hypothesis was confirmed by a good relationship between the solubility of Fe and the concentrations of major nutrients as discussed by Kuma (2002) and Tani *et al.* (2003). During the degradation of organic matter, regeneration of humic substances has also been observed (Hayase and Shinozuka, 1995; Hayase *et al.*, 1988). In addition, humic substances are known to be very refractory (Laglera *et al.*, 2007). Our results on the organic complexation of Fe in the dissolved and <1000 kDa fractions match these explanations. Indeed, in the deeper layer of the water column, the concentration, strength, saturation and reactivity of the ligands in the dissolved and <1000 kDa were pretty stable and constant with depth. Differences were observed between the stations sampled that may be a consequence of the primary production in the surface waters in relation with their respective environments, and the consequent export of organic matter towards deeper waters.

Adsorption sites on sinking particles compete with empty ligand sites in the dissolved fraction for Fe (Thuróczy *et al.*, 2010b and Chapter 3). This adsorption on suspended particles (scavenging) is responsible for export of Fe in deeper waters. In

our study, decrease of TDFe concentrations (Figure 6) following the same geographical trends, as discussed in Chapter 4 for DFe and organic ligands, were found. Despite the limited number of unfiltered samples measured, a decrease of TDFe concentrations southwards on the Zero Meridian and from East to West in the Weddell Sea was observed. In addition, along the same geographical trends, the saturation of the ligands decreased in the deeper waters (Table 1). This observation support the results found in the Arctic Ocean (Chapter 6, Thuróczy *et al.*, 2011b) where the saturation of the ligands and the concentrations of TDFe decreased toward the central Arctic (Makarov Basin). These results were attributed to a lack of Fe sources and a continuous export of Fe via scavenging by large particles. Sources of Fe in the Southern Ocean are known to be relatively modest (De Baar and De Jong, 2001; Klunder *et al.*, 2011) and confirm our observations. The high concentrations of TDFe measured close to the bottom were probably caused by sediment resuspension due to deep water formation in the Weddell Sea and close to the Antarctic continent as seen also for the dissolved Fe distribution by Klunder *et al*. (2011), the dissolved Mn and dissolved Al distributions by Middag *et al.* (2011a and 2011b).

5. Conclusions

The geographical trends in the complexation of Fe in the dissolved fraction found in the previous chapter (Chapter 4 and Thuróczy *et al.,* 2011) appeared to be mainly due to changes in the small colloidal fraction (<1000 kDa). Moreover, these larger colloidal ligands are saturated with Fe and appeared not to compete with the added ligand TAC while titrating compared to the smaller colloidal ligands. This reveals that larger colloids were probably not reversible ligands that participate in the stabilisation of Fe in seawater. Morever, approximately 70-80% of DFe was present as truly dissolved and small colloidal Fe in the upper waters, and between 50 to 70% of DFe in the deeper waters, confirming the crucial role of the small colloidal ligands in solubilising and maintaining a certain stock of Fe in seawater. Only the upper waters of the Drake Passage were found to be very different, with only 17% of DFe as truly dissolved and small colloidal Fe.

In unfiltered samples, the particulate fraction appeared to react in the same way as the larger colloidal ligands, with no excess ligands found in the particulate fraction. In addition, the increasing concentrations of TDFe towards the seafloor confirmed that the particulate fraction only plays a role in scavenging of Fe.

The geographical trends in the saturation state of the dissolved organic ligands was due to the different regimes in terms of primary production in the upper waters and to a continuous export of Fe via scavenging, as explained by the TDFe concentrations, associated to a lack of sources of Fe close to the Antarctic continent in deeper waters. However, a time dimension is missing here to explain the apparent higher scavenging influence far from the sources of Fe. Indeed, the organic ligands are less saturated with Fe in deep waters far from the Fe sources, because of a permanent scavenging that keep emptying the ligands sites, and because of the long time needed for Fe to be transported far from the sources.

Chapter 6

Distinct trends in the speciation of iron between the shelf seas and the deep basins of the Arctic Ocean

This chapter is adapted from: Thuróczy, C.-E., Gerringa, L.J.A., Klunder, M.B., Laan, P., Le Guitton, M., De Baar, H.J.W. 2011b. Distinct trends in the speciation of iron between the shelf seas and the deep basins of the Arctic Ocean. Journal of Geophysical Research-Oceans. doi:10.1029/2010JC006835.

Abstract

The speciation of iron (Fe) was investigated in three shelf seas and three deep basins of the Arctic Ocean in 2007. Two fractions were considered: the dissolved fraction (<0.2 μm), and a fraction <1000 kDa. In addition, unfiltered samples were analysed. Between 74 and 83% of dissolved iron (DFe) was present in the fraction <1000 kDa at all stations and depth, except at the chlorophyll maximum (between 42 and 64%). Distinct trends in Fe concentrations and ligand characteristics were observed from the Barents Sea towards the Amundsen and Makarov Basins (central Arctic). A general decrease of total dissolvable iron (TDFe) was seen from the seas and continental slope ([TDFe]>3nM) towards the Makarov Basin ([TDFe]<2nM). The ratio [TDFe]/[DFe] revealed a relative enrichment of particulate Fe towards the bottom at all stations, indicating Fe export towards the deep ocean. In the deep waters, the ligands in the dissolved fractions became less saturated with Fe (increase of the ratio [Excess L]/[Fe]) from the Nansen Basin via the Amundsen Basin towards the Makarov Basin. This trend was explained the reactivity of the ligands (alpha value), which was higher (log alpha>13.5) in the Nansen and Amundsen basins than in the Makarov Basin, where the ligands were less reactive (log alpha <13) and where the sources of Fe and ligands were limited. The ligands became nearly saturated with depth in the Amundsen and Nansen Basins ([ExcessL]/[Fe] decreased with depth), favouring Fe removal in the deep ocean, whereas in the deep Makarov Basin in contrast to all other observations in the Arctic but also in the Southern Ocean, the ratio [ExcessL]/[Fe] did not decrease, but even increased with depth. Still here scavenging occurred. Although scavenging of Fe was attenuated by the presence of relatively unsaturated organic ligands, the low reactivity of the ligands in combination with the lack of sources of Fe in the Makarov Basin might be the reason of a net export of Fe to the sediment.

1. Introduction

Iron (Fe) is the fourth most abundant element (5% in weight) in the earth's crust (Turner *et al.*, 2001). However, it is found at very low concentrations in seawater. This was due to oxygenation of the ocean during the early life evolution when photosynthetic microalgae appeared (Turner *et al.*, 2001; De Baar and De Jong, 2001), leading to massive precipitation of iron. Nowadays, Fe is such a scarce element, that it is limiting phytoplankton growth in 40% of the world ocean (High Nutrient, Low Chlorophyll, HNLC; De Baar *et al.*, 1990; Martin *et al.*, 1991; De Baar and De Jong, 2001).

Despite its very low concentrations, Fe is essential for phytoplankton in euphotic zones of the surface ocean. It is used in enzymes and in vital processes in cells like photosynthesis (Sunda *et al.*, 1991, 2001; Timmermans *et al.*, 2001, 2005). Phytoplankton, which is the base of the food web in the ocean, is also responsible for fixation of dissolved carbon dioxide. Microbial communities such as bacteria and archaea also need Fe for their functioning (Tortell *et al.*, 1999). These organisms are, in contrast to phytoplankton, present throughout the whole water column (Reinthaler *et al.*, 2006) and are responsible for degradation and remineralisation of sinking organic matter.

Dissolved Fe exists in seawater above concentrations determined by the solubility product of its oxy-(hydr)oxides (Kuma *et al.*, 1996; Millero, 1998) due to the presence of natural ligands. These ligands are mainly organics (Dissolved Organic Matter, DOM; Hirose, 2007) originated from living organisms, and bind up to 99.9% of Fe (Gledhill and Van Den Berg, 1994; Rue and Bruland, 1995; Wu and Luther, 1995; Nolting *et al.*, 1998; Powell and Donat, 2001; Gerringa *et al.*, 2006, 2007).

The distribution of Fe is controlled by the competition between stabilisation and removal processes and by the presence of external sources of Fe to the ocean (De Baar and De Jong, 2001). Stabilisation of Fe in seawater is ensured by organic complexation with natural ligands, which increases the residence time of Fe in seawater, hence enhances its potential bioavailability. Iron can be removed from the water column by precipitation as oxy-hydroxides and by adsorption and

scavenging on settling particles (>0.2 μm). Fine colloids are known to be very reactive (Wells *et al.*, 1993, 2000: Nishioka *et al.*, 2001, 2005) and can have a long residence time in seawater. These fine colloids can be the first step in the removal of Fe in the deep ocean by forming larger aggregates able to sink rapidly (Kepkay *et al.*, 1994; Logan *et al.*, 1995; Wu *et al.*, 2001; Cullen *et al.*, 2006). The main Fe sources in the Arctic Ocean are predominantly inputs from the Eurasian and Canadian rivers, sediment re-suspension occurring on the shelves and continental slopes, sea-ice melting, upwelling and hydrothermal vents (Measures, 1999; De Baar and De Jong, 2001; Moore and Braucher, 2008; Klunder *et al.*, submitted a and b). Aerosols deposition to the surface Arctic Ocean is not a major source of Fe (Moore and Braucher, 2008) as also detailed in Klunder *et al.* (submitted a and b).

The Arctic Ocean is a relatively enclosed ocean, surrounded by lands, and has restricted connections with the Atlantic and Pacific Oceans via the Fram Strait (approximately 2500 m deep) and the Bering Strait (approximately 40 m deep), respectively. The Arctic Ocean plays a key role in the deep water formation, where cold and saline Arctic water sinks contributing to the thermo-haline circulation around the globe. The Arctic Ocean is threatened by quick climate change, with melting of sea-ice due to global warming which directly affects its seasonal variations and life cycles, such as phytoplankton blooms. Therefore it is an interesting environment which needs to be investigated before and during major changes take place.

The Eurasian shelf seas (Figure 1), mainly composed by the Barents Sea, the Kara Sea, the Laptev Sea, the East Siberian Sea and the Chukchi Sea, represent nearly 70% of the surface of the Arctic Ocean (Tomczak and Godfrey, 2001). These shallow areas (10-350 m depth) are strongly influenced by freshwater inputs from the Eurasian and Canadian rivers (Guay and Falkner, 1997). Four major deep basins compose the deep Arctic Ocean: the Nansen Basin, the Amundsen Basin, the Makarov Basin and the Canadian Basin (Figure 1), all separated by ridges.

This study aimed to investigate the speciation of Fe at several locations of the Arctic Ocean, which are very different in terms of geographical situation, water depth and external influences. With this aim, seven stations were sampled during

the ARK XXII/2 cruise on board R.V. *Polarstern* in 2007 (Figure 1); three stations were taken in different seas of the Eurasian continental shelves (Barents Sea, Kara Sea and Laptev Sea), one was chosen on the continental slope of the Nansen Basin, and three were taken in deep basins (Nansen, Amundsen and Makarov basins, Figure 1). Three different size fractions were considered in this study: (1) unfiltered samples (UNF, which contains the particulate fraction >0.2 µm and the dissolved fraction <0.2 µm); (2) the dissolved fraction consisting of a truly dissolved fraction and of several colloidal pools, (Nishioka *et al.*, 2005, Thuróczy *et al.*, 2010b; Boye *et al.*, in press); and (3) the fraction smaller than 1000 kDa which contains the fine colloids and the truly soluble phase. The knowledge of Fe concentrations and ligand characteristics in different sizes-fractions will provide valuable information to explain the processes controlling stabilisation of Fe via organic complexation versus removal of Fe via precipitation and scavenging of Fe, hence better understand the cycle of Fe in the oceans.

This work was part of the GEOTRACES program (Geotraces Science Plan, 2006). The distribution of dissolved Fe (DFe) over the whole water column was investigated on the same cruise (Klunder *et al.*, submitted a and b). In addition to that, other trace elements were analysed during this expedition like dissolved aluminium and manganese as tracers of Fe sources (Middag *et al.*, 2009).

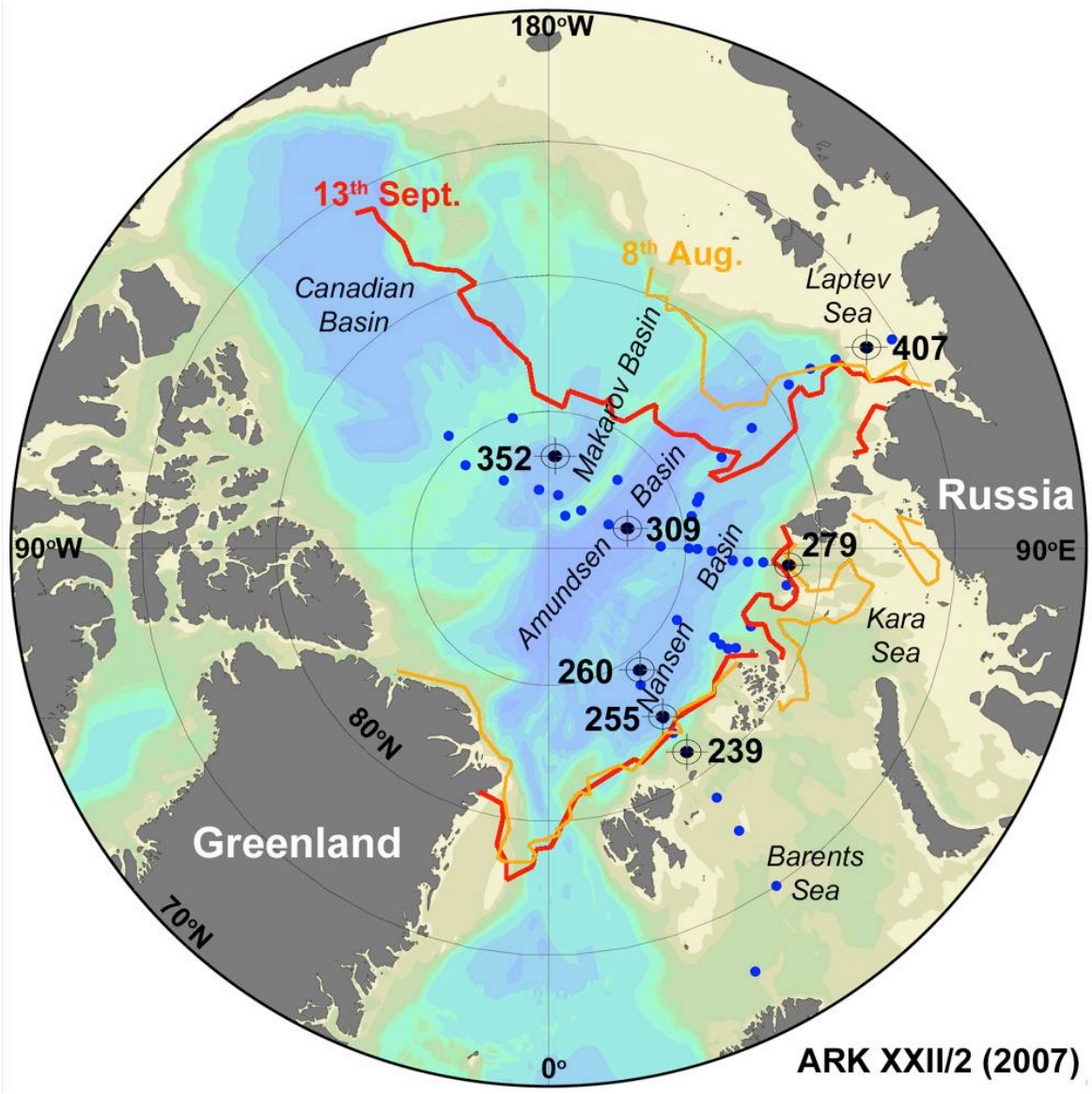

Figure 1: *Chart of the Arctic Ocean with the stations sampled during the ARK XXII/2 cruise. Black target dots represent the 7 stations sampled for this study:* ***St. 239*** *in the Barents Sea (80°59.6'N-33°59'E);* ***St. 255*** *on the slope of the Nansen Basin (82°30.2'N-33°57.1'E);* ***St. 260*** *in the Nansen Basin (84°29.5'N-36°6.9'E);* ***St. 279*** *in the Kara Sea (81°12.3'N-81°12.3'E);* ***St. 309*** *in the Amundsen Basin (87°1.9'N-104°56.7'E);* ***St. 352*** *in the Makarov Basin (86°38.3'N -177°33.3'E) and* ***St. 407*** *in the Laptev Sea (76°10.8'N-122°7.7'E). Blue dots are stations sampled with the titanium frame for trace element analyses. The orange line corresponds to the sea-ice extend on the 8th of August and the red line to the sea-ice extend on the 13th of September 2007.*

2. Additional details on the materials and methods

Samples for Fe and ligand characteristics were collected in the Arctic Ocean during the ARK XXII/2 cruise (28 July-7 October 2007, Figure 1) on-board the German Research Vessel *Polarstern*. Three shelf sea stations were sampled: one in the Barents Sea (St. 239), one in the Kara Sea (St. 279), and one in the Laptev Sea (St. 407). Moreover, four deep stations were sampled: two in the Nansen Basin (St. 255 and 260), one in the Amundsen Basin (St. 309) and one in the Makarov Basin (St. 352).

The first voltammetric analyses (St. 239 in the Barents Sea) showed interferences due to vibrations of the ship while breaking sea-ice since the laboratory container, in which the analyses were performed, was placed in the bow of the ship. This resulted in large standard deviations of the ligand characteristics at this station. In order to avoid these disturbances further analyses were performed in the middle of the ship with a soft mattress placed under the mercury drop electrode.

Temperature, conductivity (salinity), dissolved oxygen (ml.l-1) and fluorescence (given in arbitrary units, a.u.) were measured from the CTD systems (Sea Bird SBE 911+) installed on the titanium frame. These 3 parameters are plotted together in Figures 2A and 2B for each station sampled. Light transmission (in percentage, %) was measured by the transmissiometer (SN 946) installed on the sampling system from the Alfred Wegener Institute (AWI) at the same stations studied here but at different casts.

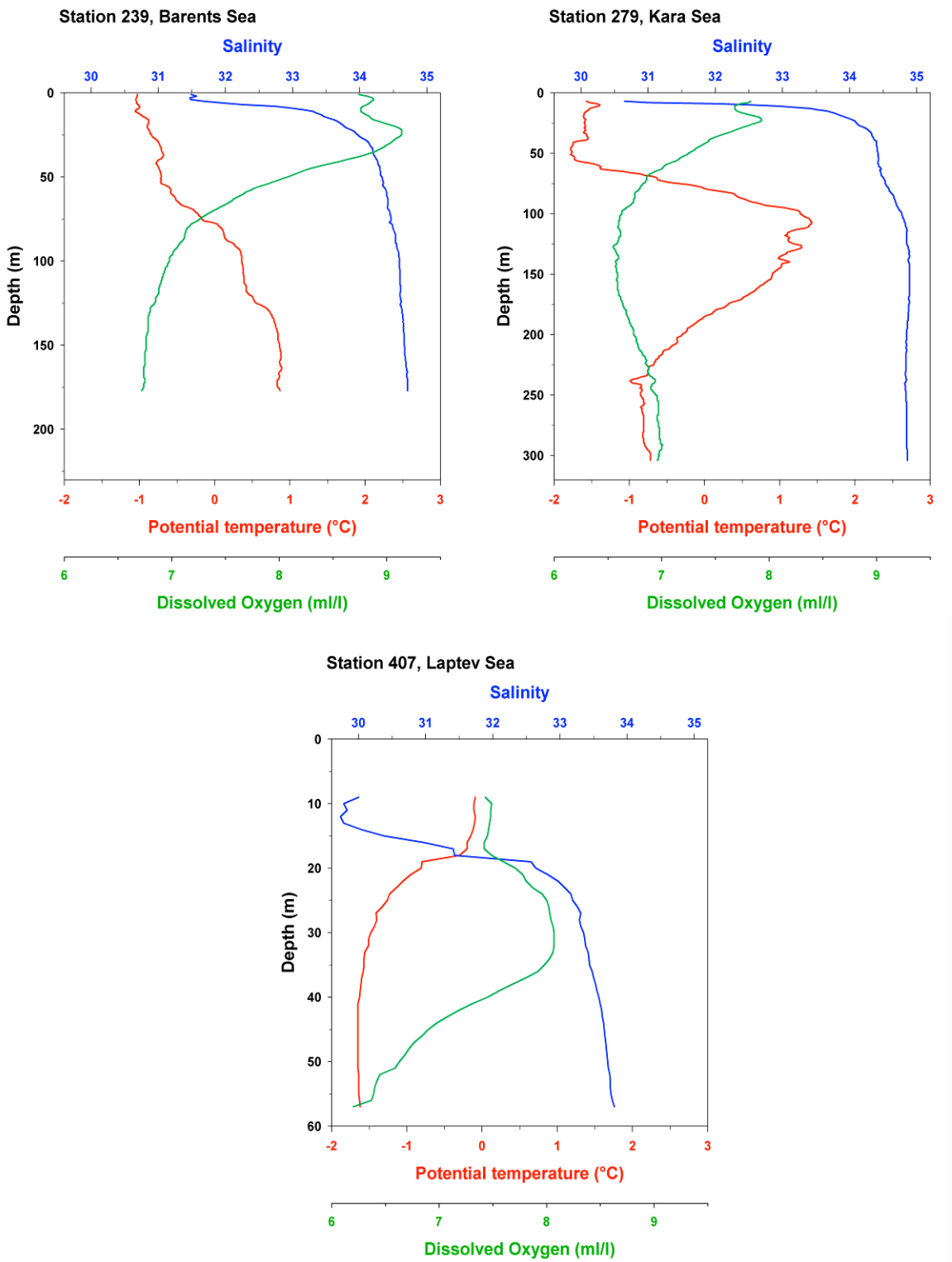

Figure 2A: *Vertical distribution of potential temperature (°C, red), salinity (blue) and dissolved oxygen (ml/l, green) at the shelf sea stations: St. 239 in the Barents Sea, St. 279 in the Kara Sea, and St. 407 in the Laptev Sea.*

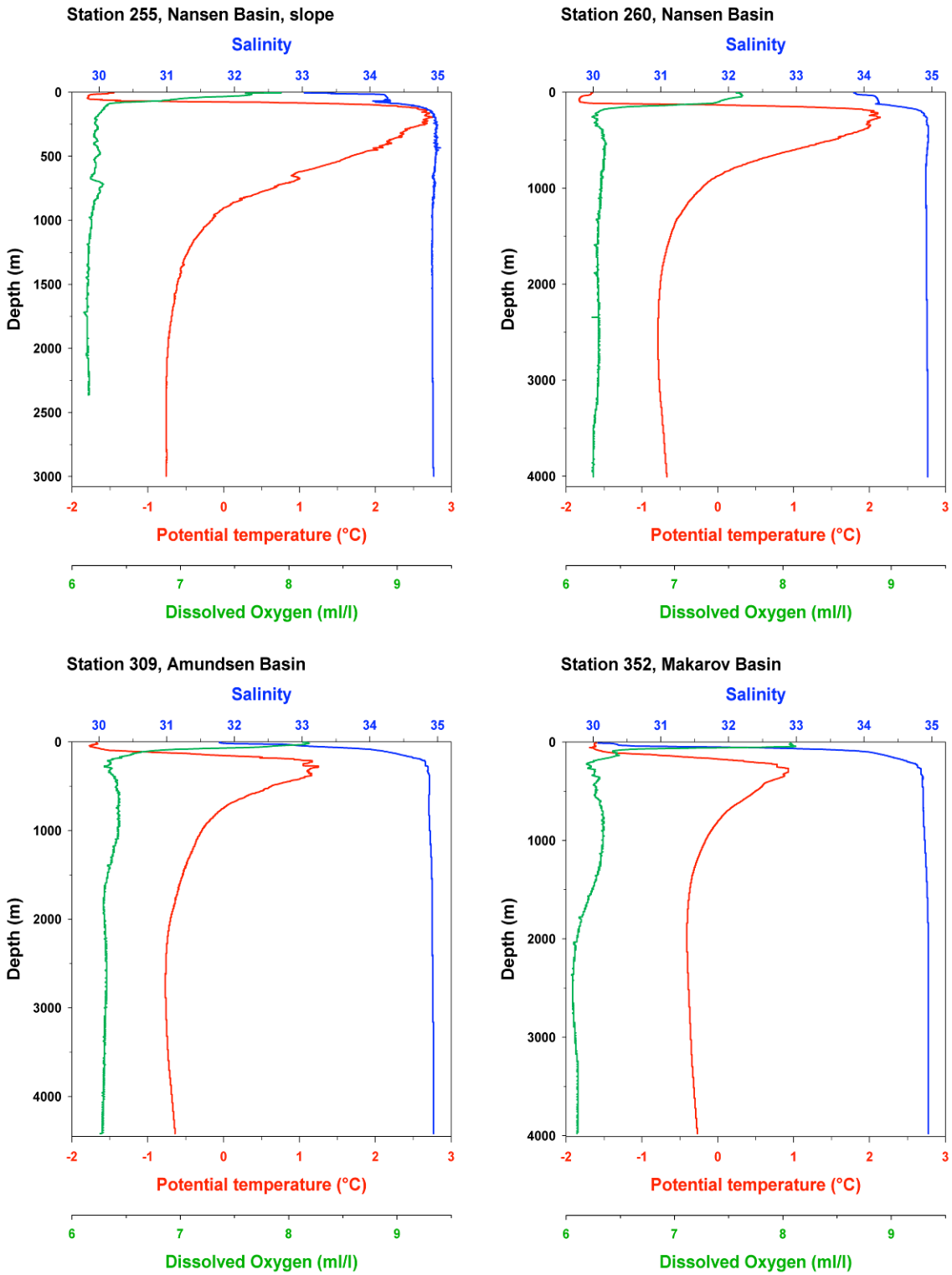

Figure 2B: *Vertical distribution of potential temperature (°C, red), salinity (blue) and dissolved oxygen (ml/l, green) at the deep basin stations: St. 260 in the Nansen Basin, St. 255 at the continental slope of the Nansen Basin, St. 309 in the Amundsen Basin, and St. 352 in the Makarov Basin.*

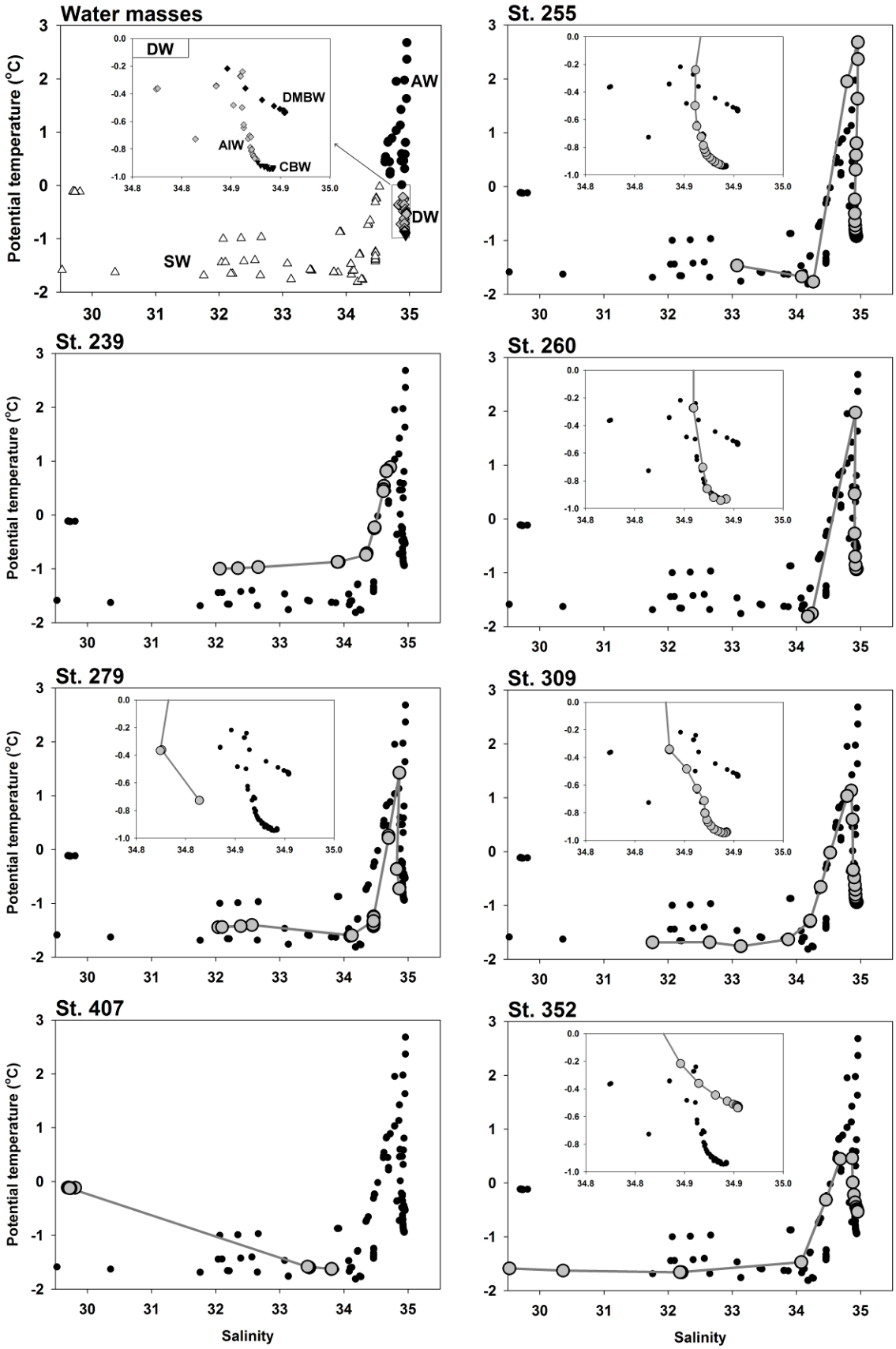
Water masses
DW
DMBW
AIW
CBW
AW
DW
SW
St. 255
St. 239
St. 260
St. 279
St. 309
St. 407
St. 352
Potential temperature (°C)
Salinity

Figure 3 (Left page): *Potential temperature/Salinity diagram (θ/S) for the 7 stations sampled. In the top left graph the corresponding water masses present at the 7 stations are indicated, with the deep waters in the enlarged box. SW: Surface Water; AW: Atlantic Water; DW: Deep Water; AIW: Arctic Intermediate Water; CBW; Cold Bottom Water; DMBW: Deep Makarov Basin Water. The other graphs show the results of the separate stations with a grey line and large grey dots; the small black dots represent the 6 other stations for comparison. On the left side, the shelf sea stations (St. 239 in the Barents Sea; St. 279 in the Kara Sea and St. 407 in the Laptev Sea); on the right side, the deep basins (St. 255 on the slope of the Nansen Basin; St. 260 in the Nansen Basin; St. 309 in the Amundsen Basin and St. 352 in the Makarov Basin). When deep waters are present, they are shown in enlarged boxes.*

3. Results

3.1. Sea-ice coverage, hydrography, fluorescence and light transmission

In winter the Arctic Ocean is completely covered by sea-ice, which partly melts during spring and summer. Between the end of July 2007 (start of the cruise) and the end of August 2007, the sea-ice extent severely decreased in the south part of the Amundsen and Makarov basins and in the Kara Sea (Figure 1). At the time of sampling, the stations in the Barents Sea and in Laptev Sea were ice-free (St. 239 and 407, respectively). At St. 279 in the Kara Sea, approximately 50% of the sea-surface was covered by sea-ice. At the other stations (St. 255, 260, 309 and 352) the sea-surface was totally covered with a relatively thick layer of ice.

Different water masses of the Arctic Ocean can be distinguished as shown in potential temperature versus salinity plots (θ/S diagrams, Figure 3). The Surface Water (SW) from the surface to 100-150 m depth has negative temperatures (<0ºC) and salinities below 34.5. It is influenced by melted sea-ice and river inputs. The distinction between sea-ice melt and river input is explained by Klunder *et al.* (submitted) for the present study. Yamamoto-Kawai *et al.* (2005) could also distinguish the influence of sea-ice and and river fresh water in the Arctic Ocean using δ18O and alkalinity. The Atlantic Water (AW), flowing eastwards along the slope of the Eurasian continental shelves at approximately 100-900 m depth, is characterised by positive temperatures (>0ºC) and salinities between 34.5 and 35 (Figure 3). Below the AW, the Eurasian Basin Deep Water

(EBDW) is found (below 800 m). The EBDW comprises the Arctic Intermediate Water (AIW) found at around 800-2000 m and the Cold Bottom Water (CBW) below 2000 m depth. The AIW and CBW have negative temperatures and salinities above 34.8 (Figure 3). The CBW with temperatures below -0.9ºC is present in the Nansen and Amundsen basins (Figure 3). In the Makarov Basin, the deep water has different properties (temperatures between -0.6 and 0ºC) and is called the Deep Makarov Basin Water (DMBW). The DMBW is influenced by water derived from the Pacific Ocean, which is characterised by concentrations of silicate higher than 10 µM (Anderson *et al.*, 1994). Details about the hydrography of the Arctic basins were described by Anderson *et al.* (1994) and Rudels *et al.* (2000).

Fluorescence (Figure 4) corresponds to chlorophyll-a content and is an indicator of phytoplankton abundance (Kiefer *et al.*, 1973; Babin *et al.*, 1996). At St. 407 in the Laptev Sea, the signal was saturated due to the presence of a great amount of suspended material; therefore the data is not shown here. In the Barents Sea (St.239) and in the Kara Sea (St. 279) the fluorescence was high (1.5 and 0.8 a.u., respectively). The other stations had a lower fluorescence signal, below 0.5 a.u..

Low light transmission (Figure 4) was found at the surface where fluorescence was high. In the Barents Sea (St.239) and in the Kara Sea (St. 279) lower light transmission was measured at the chlorophyll maximum (85% and 88%, respectively). In the deep basins, light transmission was relatively constant below 200 m depth, between 91-92%. Near the seafloor, light transmission was often lower due to the influence of sediments re-suspension.

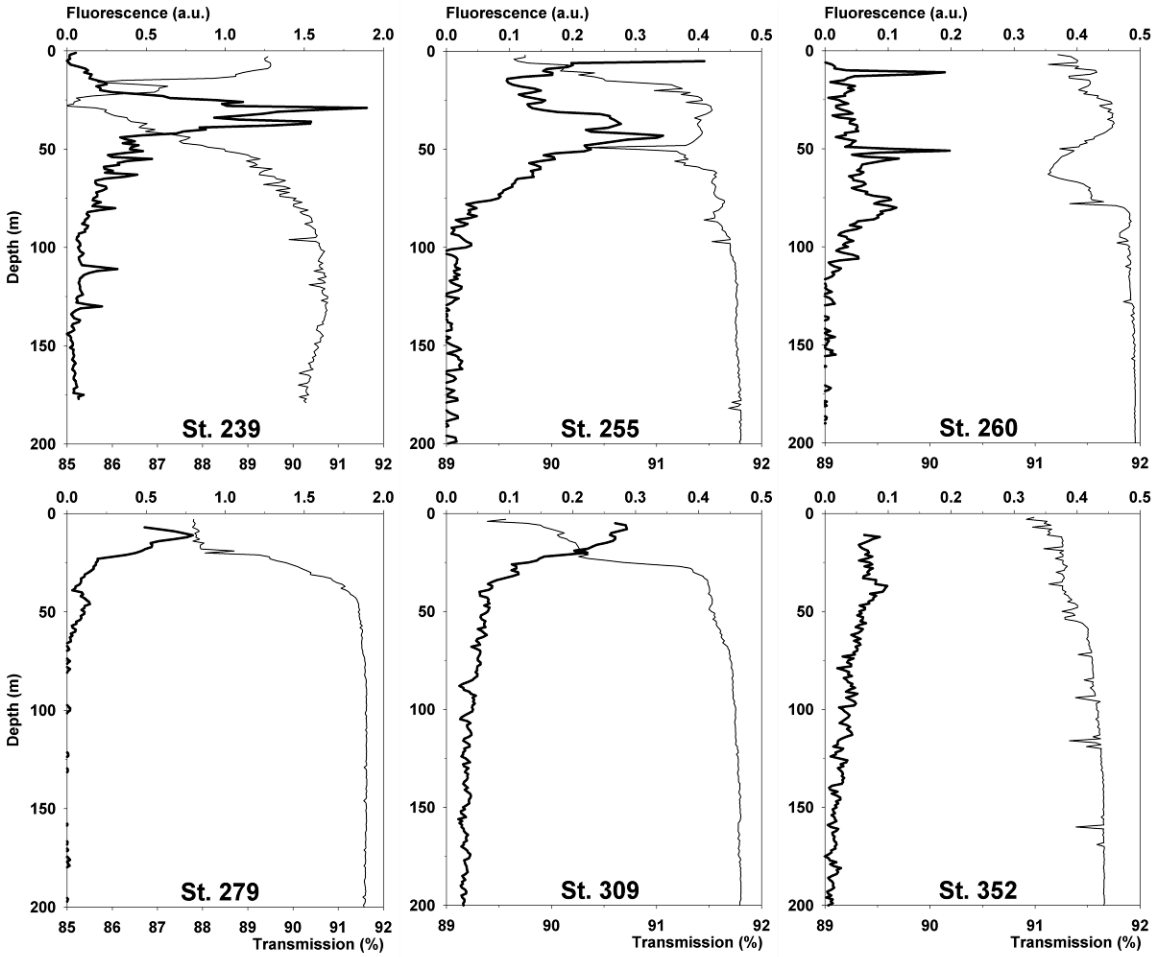

Figure 4: *Fluorescence (a.u., top axis, thick line) and light transmission (%, bottom axis, thin line) in the upper 200 meters at 6 stations sampled. Note the different scales for the fluorescence and for the light transmission between the shelf seas (left side: St. 239 in the Barents Sea and St. 279 in the Kara Sea) and the deep basins (St. 255 on the slope of the Nansen Basin; St. 260 in the Nansen Basin; St. 309 in the Amundsen Basin and St. 352 in the Makarov Basin).*

3.2. Iron concentrations

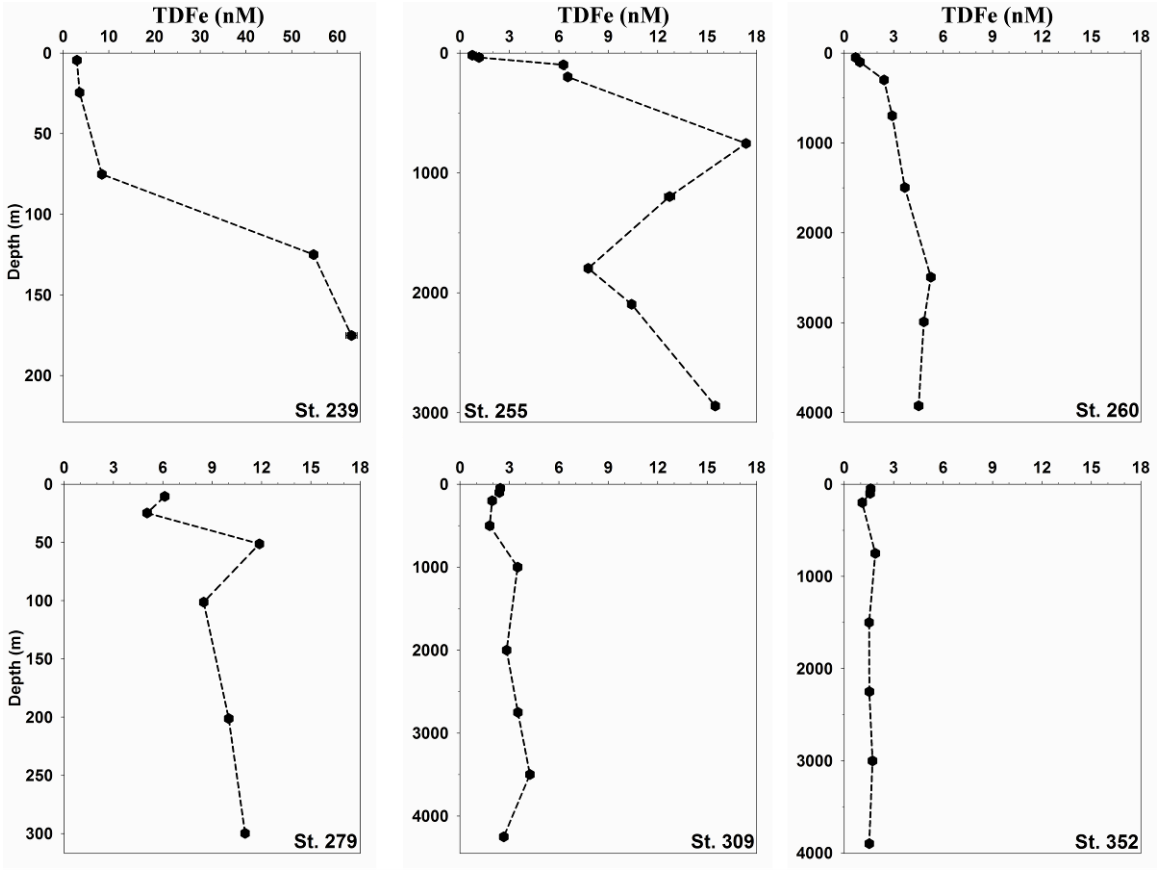

Figure 5: *TDFe concentrations (nM, ± standard deviation of triplicate measurements) from unfiltered samples (with depth at 6 stations sampled. Shelf sea stations are on the left side. The depth axes are extended until the bottom depth: St. 239 at 229 m (Barents Sea); St. 255 at 3078 m (Nansen Basin slope); St. 260 at 4109 m (Nansen Basin); St. 279 at 317 m (Kara Sea); St. 309 at 4449 m (Amundsen Basin); St. 352 at 4005 m (Makarov Basin). Note the different scales for the concentrations at St. 239 (0-65 nM). Error bars are too small (<5%) to be seen on the graphs*

The concentrations of TDFe (Figure 5, Table 2A) varied between 0.7 and 63 nM. The very high concentrations were measured at shelf seas stations (up to 63 nM Fe at St. 239 and up to 11.9 nM Fe at St. 279) and above the slope of the Nansen Basin (St. 255) between 500 and 1200 m depth where [TDFe] was maximum (18 nM) 100 km away horizontally from the bottom slope. In surface waters (SW), average [TDFe] was 0.82 nM ±0.18 (n=2) in the Nansen Basin (St. 260), 2.42 nM ±0.04 (n=2) in the Amundsen Basin (St. 309), and 1.60 nM ±0.02

(n=2) in the Makarov Basin (St. 352). In the layer influenced by the AW, average [TDFe] were 1.74 nM ±0.35 (n=2), 1.88 nM ±0.11 (n=2) and 1.50 nM ±0.56 (n=2) in the same basins, respectively. Finally, below 800 m depth (AIW and CBW), average [TDFe] were 4.57 nM ±0.67 (n=4), 3.35 nM ±0.63 (n=5) and 1.57 nM ±0.10 (n=4) in the Nansen, Amundsen and Makarov basins, respectively.

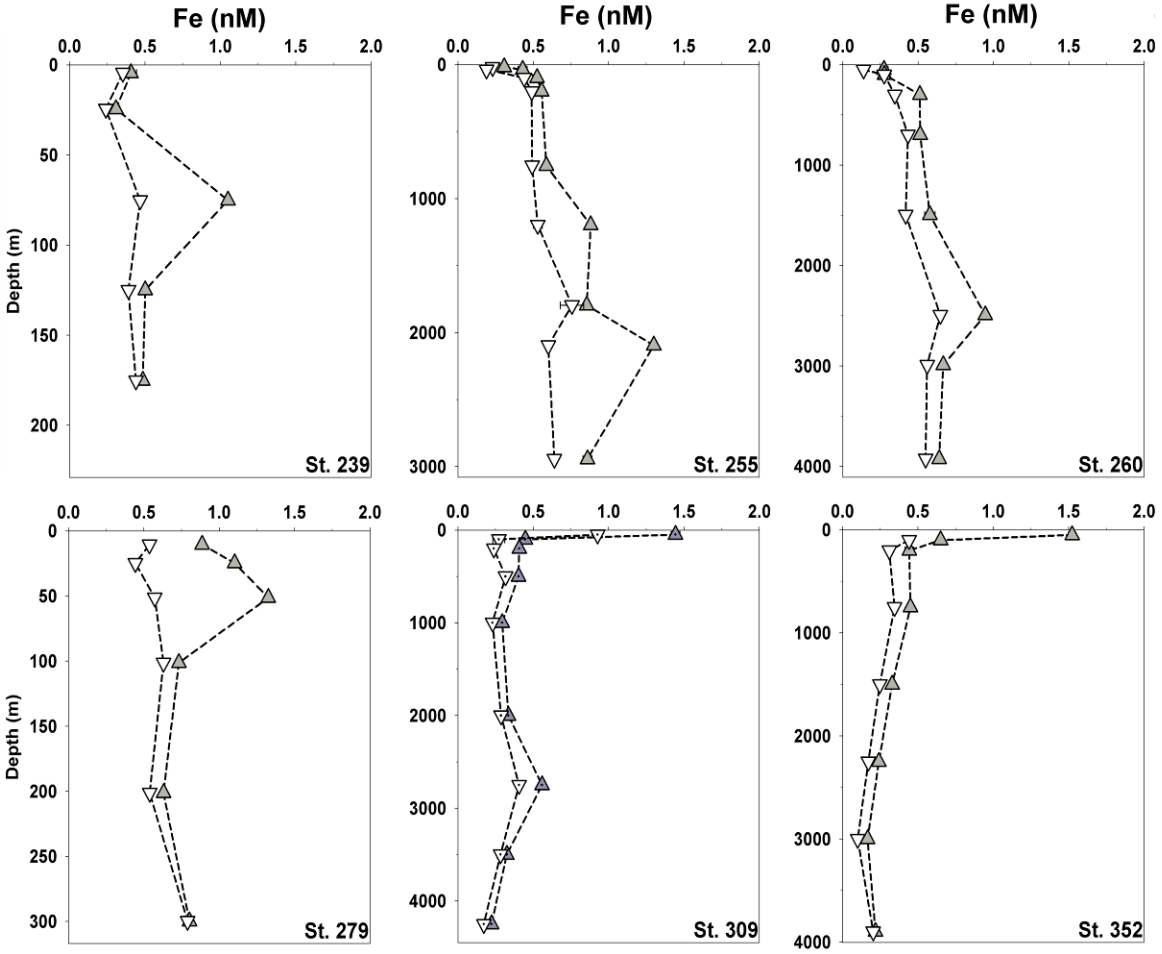

Figure 6A: *Concentrations of Fe with depth at 6 stations sampled (same as in figure 5) and for 2 size fractions: Dissolved fraction (<0.2 µm, grey triangles upwards looking) and fraction <1000 kDa (white triangles downwards looking). Fe concentrations are in nM (± standard deviation of duplicate or triplicate measurements). Error bars for Fe concentrations are too small (<5%) to be seen on the graphs. Shelf sea stations are on the left side. The depth axes are extended until the bottom depth.*

The concentration of DFe (Figure 6A, Table 1) ranged from 0.17 to 1.52 nM. At the shelf sea stations [DFe] were relatively high and constant with depth; average [DFe] were 0.55 nM ±0.29 (n=5) in the Barents Sea (St. 239) and 0.91 nM

±0.26 (n=6) in the Kara Sea (St. 279) with a respective maximum of 1.0 and 1.3 nM Fe below the chlorophyll maximum. In the Laptev Sea (St. 407), average [DFe] was 0.88 nM ±0.21 (n=3). In the Nansen Basin (St. 255 and 260), [DFe] increased from 0.31 and 0.27 nM Fe, respectively at the surface, to 1.30 and 0.95 nM Fe at 2100 and 2500 m depth. In the deepest sample, [DFe] were lower, with 0.86 and 0.64 nM Fe, respectively. Conversely, in the Amundsen Basin (St.309), [DFe] decreased steeply from 1.44 at the surface to 0.22-0.32 nM Fe at depth; and a same trend was observed in the Makarov Basin (St.352) with a decrease of [DFe] from 1.52 nM Fe at surface to 0.17-0.22 nM Fe at depth. The detailed distribution of DFe from the same cruise is presented by Klunder *et al.* (submitted a and b].

The concentration of Fe in the fraction <1000 kDa ([$Fe_{<1000\ kDa}$], Figure 6A, Table 1) accounted for approximately 74 to 83% of the concentration of Fe in the dissolved fraction in the whole water column. Exceptions were the samples taken from the chlorophyll maximum, where 42 to 64% of DFe was present in the fraction <1000 kDa.

3.3. Ligand characteristics

The ligands in the dissolved and <1000 kDa fractions were always found in excess with respect to the Fe concentrations (Tables 1 and 2, Figure 7). At St. 239 in the Barents Sea, [$Lt_{<0.2\ \mu m}$] were higher (4.54 Eq of nM Fe ±0.14, n=3) between 25 and 125 m depth compared to the surface (5 m, 2.75 Eq of nM Fe) and deepest samples (175 m, 2.51 Eq of nM Fe). In the fraction <1000 kDa the ligand concentrations were, as expected, lower than in the dissolved fraction and [$Lt_{<1000\ kDa}$] was relatively constant with depth (2.80 Eq of nM Fe ±0.37 n=5). However, the Kara Sea (St. 279) was an exception since below 25 m depth the ligand concentrations <1000kDa were higher than in the fraction <0.2 µm. No contamination was seen here (Table 1) and each sample was filtered with a different filter to avoid cross contamination. The 5 samples where [$Lt_{<1000\ kDa}$]>[$Lt_{<0.2\ \mu m}$] appeared to be correct (see discussion). Filtration could cause disequilibrium in seawater by removal of constituents. One possible reason is that the smallest and most reactive fraction (Nishioka *et al.*, 2001, 2005; Cullen *et al.*, 2006) could have exchanged Fe during

filtration and/or colloids or colloid aggregates might break and/or disperse during filtration, increasing the active surface and leading to disequilibrium between Fe and ligands in the filtrate (here <1000 kDa). The results from the Laptev Sea (St. 407) are reported in Table 1 but not in Figure 7, because of the limited number of samples. Here [$Lt_{<0.2\ \mu m}$] were above 2 Eq of nM Fe and [$Lt_{<1000\ kDa}$] were below 2 Eq of nM Fe. A maximum was measured in both dissolved and <1000 kDa fractions (between 2.3 and 3.1 Eq of nM Fe). In the deep basins, distinct maxima in [$Lt_{<0.2\ \mu m}$] and in [$Lt_{<1000\ kDa}$] were measured. At the slope of the Nansen Basin (St. 255) a maximum in the ligand concentration existed at 100-200 m depth with 5.2 Eq of nM Fe in the dissolved fraction. At St. 260 in the Nansen Basin and St. 309 in the Amundsen Basin, a maximum was measured in both dissolved and <1000 kDa fractions (between 2.6 and 2 Eq of nM Fe; 3.5 and 2.1 Eq of nM Fe, respectively). In the Amundsen Basin (St. 309) a second maximum was observed in the dissolved fraction with 2.1 Eq of nM Fe at 2750 m depth. The Makarov Basin (St. 352) also had 2 maxima in the dissolved fraction but at different depths (Figure 6B): one at the surface (2.08 Eq of nM Fe) and one between 750 and 1500 m depth (2.16 Eq of nM Fe).

Excess L expresses the binding potential of the ligands by showing the empty sites without relation to the parameter for which these sites are used. Trends with depth of Excess L were relatively similar to trends in total ligand concentrations (Figure 7 and Table 1). Excess L in the UNF fraction followed Excess L in the smaller fractions (within the analytical uncertainty). At St. 255 and 260 in the Nansen Basin, much larger Excess L in the UNF fraction were observed at the surface where they were minimal in the dissolved and <1000 kDa fractions. In the deep Makarov Basin (at 1500 and 2250 m depth) Excess L concentrations in the UNF fraction were lower (0.3 Eq of nM Fe) than Excess L in the dissolved fraction.

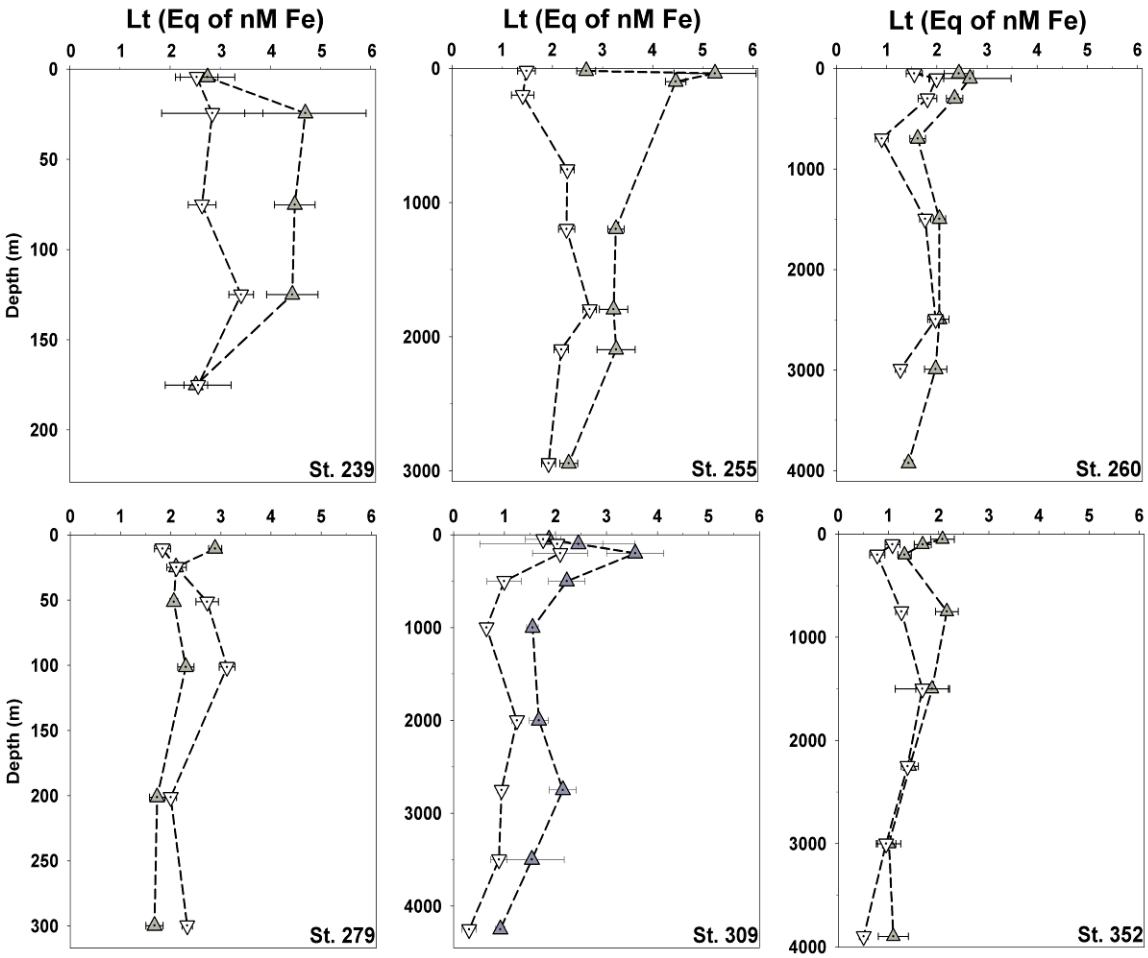

Figure 6B: *Concentrations of Lt with depth at 6 stations sampled (same as in figure 5) and for 2 size fractions: Dissolved fraction (<0.2 µm, grey triangles upwards looking) and fraction <1000 kDa (white triangles downwards looking). Ligand concentrations are in Eq of nM Fe (± standard deviation of the fit of the data to the model). Shelf sea stations are on the left side. The depth axes are extended until the bottom depth.*

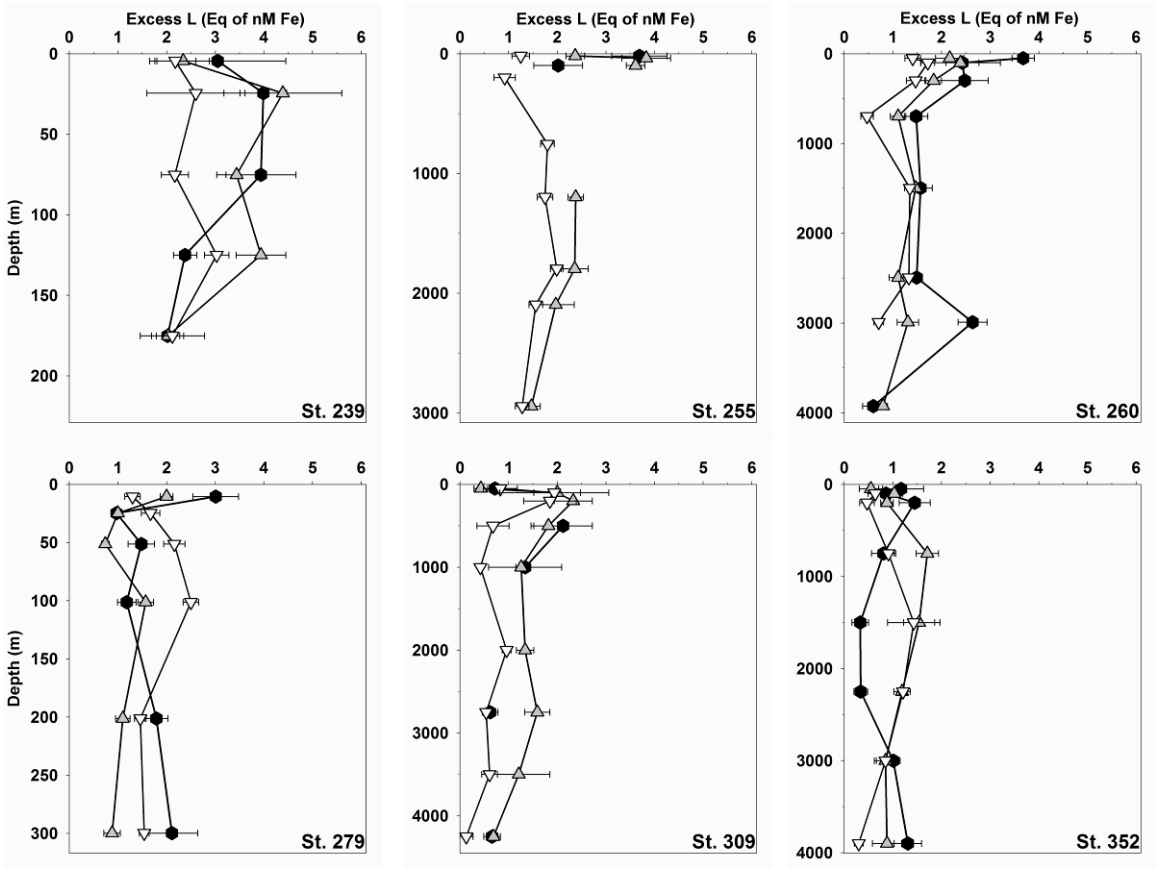

Figure 7: *Excess L concentrations (Eq of nM Fe, ± standard deviation of the fit of the data to the model) with depth at 6 stations sampled (same as in figure 5). Unfiltered samples using the lower limit (black dots), dissolved fraction (<0.2 µm; grey triangles upwards looking) and fraction <1000 kDa; (white triangles downwards looking). Shelf sea stations are on the left side. The depth axes are extended until the bottom depth.*

The conditional stability constant K' (Tables 1 and 2) reflects the binding strength of the natural ligands with Fe. The K' values in all fractions were relatively constant or increased slightly with depth. Average of K' values in the fraction <1000 kDa were $10^{21.96}$ ± 0.36 (n=43) and in the dissolved fraction $10^{21.86}$ ± 0.35 (n=45). The differences between the K' values in the fraction <1000 kDa and those in the dissolved fraction were not significant even if they were often found slightly higher in the fraction <1000 kDa.

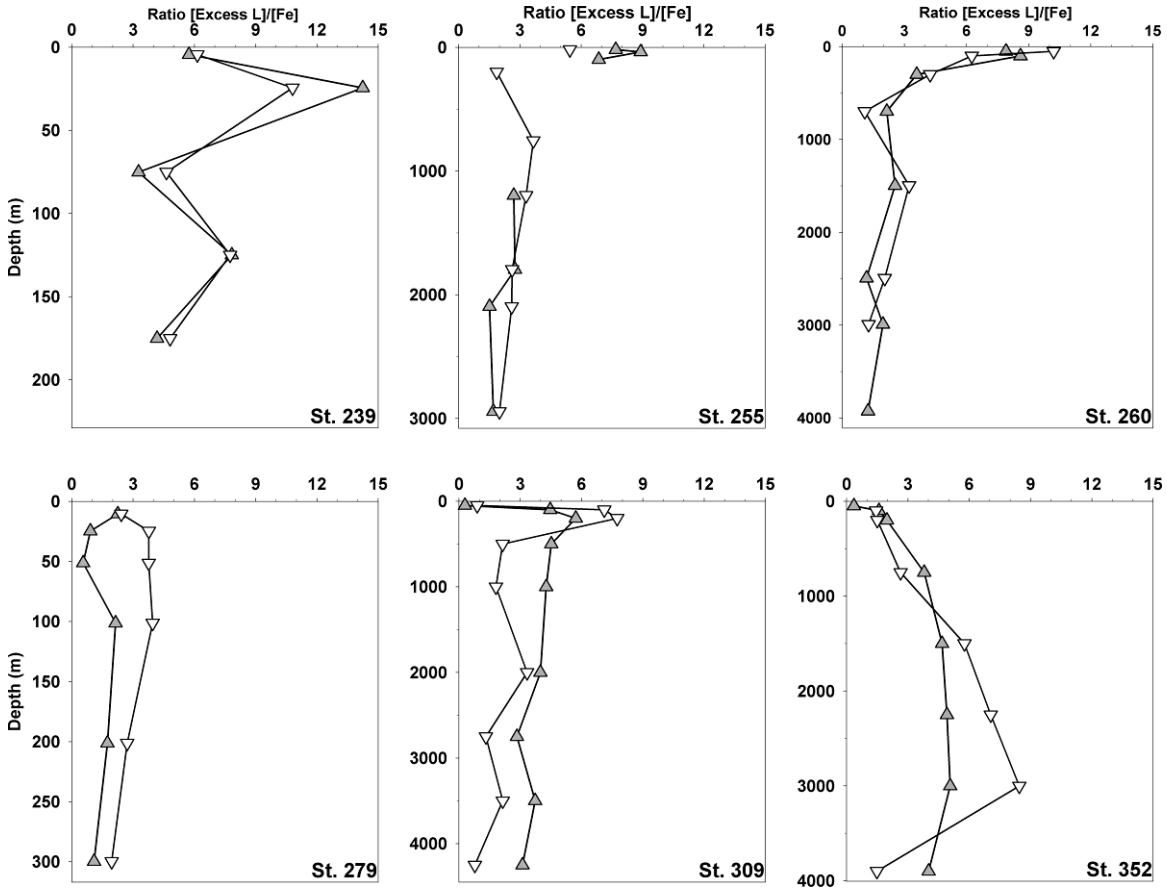

Figure 8: *Ratio values [Excess L]/[Fe] for 6 stations sampled and for the 3 size fractions: Unfiltered samples using the lower limit (black dots), dissolved fraction (<0.2 µm; grey triangles upwards looking) and fraction <1000 kDa; white triangles downwards looking). A ratio of 0 means saturation of the ligands with Fe. Shelf sea stations are on the left side. The depth axes are extended until the bottom depth.*

The ratio [Excess L]/[Fe] (Figure 8, Table 1) represents the relative saturation state of the ligands (*cf.* [Lt]/[Fe] ratio as explained in Chapter 2 and 4). They were relatively high (~5-6) in the Barents Sea (St. 239), with a maximum at 25 m depth (~15). At St. 279 in the Kara Sea, the ratio values were relatively low (<1) between 25 and 50 m depth in the UNF samples and dissolved fractions, whereas higher ratio values were present in the fraction <1000 kDa (~4). The ratio [Excess L]/[Fe] in the Nansen Basin (St. 255 and 260) was high (>6) in the SW, decreasing with depth and remained low and relatively constant (~2-3) in deeper waters. Very low surface ratio values (<1) were seen in the Amundsen and Makarov basins (St. 309 and 352) where high Fe concentrations were measured at 50 m below the sea-ice. Below the surface minimum in the Amundsen basin, high ratio values (>5) in the

SW existed which decreased slightly with depth. In the fraction <1000 kDa the ratio values were lower than in the dissolved fraction below 500 m depth. The Makarov Basin (St. 352) showed a reversed trend with depth, with a surface minimum (~0-1.5) and an increase of [Excess L]/[Fe] with depth in all size fractions. The ratio values in the fraction <1000 kDa were higher than those in the dissolved fraction and in UNF samples.

Alpha, expressed here in its logarithm form (log10 α), is the product of K' and Excess L. Alpha expresses the reactivity of the ligands. A high alpha favours Fe solubilisation via organic complexation (large Excess L, or high K', or both). Reversely, a low alpha makes relatively easier the export and loss of Fe via precipitation and or scavenging. High alpha values were found on the slope of the Nansen Basin (St. 255, logα >13.5). Lower alpha values were found towards the central Arctic (at St. 309 in the Amundsen Basin and at St. 352 in the Makarov Basin, logα <13) (Table 1 and 2, Figure 9).

Table 1 (Next pages): *Fe concentrations (nM), ± standard deviation (S.D.) of duplicate or triplicate measurements, and ligand characteristics (concentrations in Eq of nM Fe) for two size fractions (<0.2 µm and <1000 kDa), ± standard deviation (S.D.) of the fit of the Langmuir model to the data. Conditional stability constant K' are in mol^{-1}. S is the sensitivity of the titration measurement (slope of the straight part of the titration curve, in $Amp.mol^{-1}$).*
**** The standard deviation for Fe concentrations is missing when there was not enough sample volume to determine the concentration in duplicate or triplicate.*
ND: Not determined.

Station	Fraction	Depth (m)	[Fe] (nM)	S.D.	Ligand [Lt] (Eq of nM Fe)	S.D.	logK' (mol^{-1})	S.D.	Sensitivity S ($A.mol^{-1}$)	S.D.	[Excess L] (Eq of nM Fe)	logα	pFe (M)	[Excess L]/[Fe]
239														
Barents	**< 0.2 µm**	**5**	0.408	0.036	2.75	0.54	21.94	0.29	0.98	0.09	2.34	13.31	22.70	5.7
Sea		**25**	0.308	0.025	4.70	1.21	21.39	0.21	0.51	0.06	4.39	13.04	22.55	14.2
		75	1.051	0.002	4.49	0.41	21.81	0.08	1.02	0.07	3.44	13.35	22.33	3.3
		125	0.502	0.005	4.44	0.51	21.61	0.07	1.37	0.11	3.94	13.21	22.50	7.8
		175	0.486	0.017	2.51	0.24	21.69	0.09	1.63	0.06	2.03	12.99	22.31	4.2
	< 1000 kDa	**5**	0.354	***	2.53	0.42	21.96	0.25	0.95	0.07	2.18	13.30	22.75	6.1
		25	0.241	0.004	2.84	1.01	21.49	0.20	0.89	0.15	2.60	12.91	22.53	10.8
		75	0.469	0.002	2.64	0.28	22.09	0.19	0.72	0.04	2.17	13.42	22.75	4.6
		125	0.391	0.011	3.42	0.25	22.47	0.21	0.79	0.04	3.03	13.96	23.36	7.7
		175	0.441	0.005	2.56	0.66	21.90	0.42	2.11	0.21	2.12	13.22	22.58	4.8
255														
Nansen	**< 0.2 µm**	**19**	0.308	0.010	2.67	0.19	22.45	0.23	0.56	0.02	2.37	13.83	23.34	7.7
Slope		**37**	0.430	0.030	4.26	0.50	21.93	0.13	0.39	0.04	3.83	13.51	22.88	8.9
		98	0.526	0.010	4.13	0.19	22.28	0.08	1.30	0.06	3.61	13.84	23.12	6.9
		200	0.556	0.020	ND	ND	ND	ND	ND	ND	ND	ND	ND	ND
		754	0.587	0.010	ND	ND	ND	ND	ND	ND	ND	ND	ND	ND
		1198	0.882	0.011	3.27	0.16	22.30	0.12	1.36	0.04	2.38	13.68	22.74	2.7
		1796	0.855	0.020	3.22	0.28	22.37	0.24	0.66	0.04	2.36	13.75	22.81	2.8
		2096	1.300	0.020	3.27	0.38	21.96	0.13	0.60	0.05	1.97	13.25	22.14	1.5
		2944	0.860	0.030	2.33	0.18	22.15	0.16	1.24	0.04	1.47	13.31	22.38	1.7
	< 1000 kDa	**19**	0.230	0.000	1.48	0.18	22.18	0.28	1.39	0.04	1.25	13.27	22.91	5.5
		37	0.190	0.000	ND	ND	ND	ND	ND	ND	ND	ND	ND	ND
		98	0.440	0.000	ND	ND	ND	ND	ND	ND	ND	ND	ND	ND
		200	0.490	0.010	1.41	0.22	22.49	0.31	0.66	0.04	0.92	13.45	22.76	1.9
		754	0.493	0.023	2.30	0.14	22.18	0.13	0.73	0.02	1.80	13.43	22.74	3.7
		1198	0.530	0.030	2.28	0.16	22.08	0.13	0.61	0.02	1.75	13.33	22.60	3.3
		1796	0.757	0.078	2.74	0.13	22.36	0.12	1.43	0.04	1.99	13.65	22.78	2.6
		2096	0.600	0.020	2.16	0.14	21.97	0.08	1.10	0.03	1.56	13.16	22.38	2.6
		2944	0.640	0.010	1.92	0.14	22.36	0.23	0.79	0.02	1.28	13.47	22.66	2.0
260														
Nansen	**< 0.2 µm**	**50**	0.274	0.027	2.44	0.29	21.64	0.11	1.02	0.04	2.17	12.98	22.54	7.9
Basin		**100**	0.277	0.035	2.66	0.82	21.15	0.15	1.39	0.11	2.39	12.53	22.09	8.6
		300	0.512	0.007	2.36	0.16	22.27	0.17	0.81	0.03	1.84	13.53	22.82	3.6
		698	0.514	0.006	1.62	0.16	21.84	0.12	2.04	0.05	1.11	12.88	22.17	2.1
		1497	0.578	0.034	2.05	0.12	22.56	0.27	0.93	0.02	1.47	13.73	22.97	2.5
		2494	0.946	0.010	2.05	0.19	22.08	0.15	1.54	0.05	1.11	13.13	22.15	1.2
		2991	0.667	0.012	1.98	0.22	21.87	0.15	2.30	0.08	1.31	12.99	22.16	2.0
		3926	0.640	***	1.44	0.09	22.17	0.13	2.07	0.03	0.80	13.07	22.26	1.2
	< 1000 kDa	**50**	0.138	0.006	1.55	0.16	22.23	0.25	0.68	0.02	1.41	13.38	23.24	10.2
		100	0.275	0.036	2.00	0.14	22.04	0.13	0.87	0.02	1.72	13.27	22.83	6.3
		300	0.346	0.002	1.82	0.19	22.10	0.21	0.92	0.03	1.47	13.26	22.72	4.2
		698	0.433	0.022	0.90	0.13	21.77	0.16	2.13	0.04	0.47	12.44	21.81	1.1
		1497	0.418	0.007	1.77	0.11	22.32	0.18	0.76	0.02	1.35	13.45	22.83	3.2
		2494	0.648	0.017	1.98	0.16	22.24	0.15	0.78	0.03	1.33	13.36	22.55	2.1
		2991	0.561	0.003	1.27	0.10	22.11	0.09	1.34	0.04	0.71	12.96	22.22	1.3
		3926	0.550	***	ND	ND	ND	ND	ND	ND	ND	ND	ND	ND

Station	Fraction	Depth (m)	[Fe] (nM)	S.D.	Ligand [Lt] (Eq of nM Fe)	S.D.	logK' (mol^{-1})	S.D.	Sensitivity S ($A.mol^{-1}$)	S.D.	[Excess L] (Eq of nM Fe)	logα	pFe (M)	[Excess L]/[Fe]
279														
Kara	**< 0.2 µm**	**11**	0.887	0.008	2.89	0.13	21.79	0.05	1.16	0.02	2.00	13.09	22.14	2.3
Sea		**25**	1.102	0.007	2.11	0.08	22.10	0.08	1.67	0.02	1.00	13.10	22.06	0.9
		51	1.326	0.005	2.06	0.08	22.46	0.13	1.69	0.03	0.74	13.33	22.21	0.6
		101	0.733	0.008	2.30	0.16	21.79	0.08	2.10	0.05	1.57	12.99	22.12	2.1
		201	0.631	0.002	1.73	0.15	21.94	0.13	1.63	0.04	1.10	12.98	22.18	1.7
		300	0.802	0.013	1.68	0.17	21.87	0.15	1.90	0.05	0.88	12.82	21.91	1.1
	< 1000 kDa	**11**	0.537	0.016	1.84	0.16	22.05	0.16	0.99	0.03	1.30	13.16	22.43	2.4
		25	0.444	0.004	2.12	0.19	22.23	0.22	1.13	0.04	1.67	13.45	22.81	3.8
		51	0.572	0.017	2.73	0.22	22.00	0.13	1.01	0.04	2.16	13.34	22.58	3.8
		101	0.630	0.004	3.13	0.16	22.04	0.09	1.31	0.04	2.50	13.44	22.64	4.0
		201	0.539	0.017	2.00	0.12	22.25	0.14	0.89	0.02	1.46	13.42	22.69	2.7
		300	0.790	0.001	2.33	0.10	22.21	0.10	1.07	0.02	1.54	13.40	22.50	2.0
309														
Amundsen	**< 0.2 µm**	**50**	1.444	0.030	1.87	0.14	22.57	0.33	0.82	0.03	0.43	13.21	22.05	0.3
Basin		**101**	0.448	0.004	2.45	0.48	21.45	0.11	1.94	0.14	2.00	12.75	22.10	4.5
		201	0.407	0.006	2.74	0.39	21.60	0.09	2.76	0.14	2.33	12.97	22.36	5.7
		501	0.403	0.010	2.22	0.36	21.35	0.10	2.26	0.09	1.82	12.61	22.01	4.5
		1001	0.294	***	1.55	0.11	21.85	0.10	2.34	0.04	1.26	12.95	22.48	4.3
		2001	0.336	0.000	1.68	0.18	21.41	0.08	2.31	0.05	1.34	12.54	22.01	4.0
		2750	0.559	0.019	2.14	0.26	21.76	0.14	2.65	0.10	1.59	12.96	22.21	2.8
		3499	0.325	0.006	1.54	0.64	21.18	0.25	2.11	0.13	1.21	12.27	21.75	3.7
		4251	0.223	0.012	0.92	0.09	22.01	0.16	2.17	0.03	0.69	12.85	22.51	3.1
	< 1000 kDa	**50**	0.927	0.026	1.76	0.35	22.04	0.36	1.64	0.12	0.83	12.96	21.99	0.9
		101	0.272	0.039	2.21	1.12	21.03	0.24	2.03	0.19	1.94	12.32	21.88	7.1
		201	0.239	0.003	2.09	0.54	21.16	0.11	2.34	0.12	1.85	12.43	22.05	7.7
		501	0.316	0.000	0.99	0.33	21.29	0.24	2.32	0.08	0.68	12.12	21.62	2.1
		1001	0.230	***	0.65	0.05	22.43	0.22	2.16	0.02	0.42	13.05	22.69	1.8
		2001	0.287	0.020	1.24	0.09	22.26	0.19	2.24	0.04	0.96	13.24	22.79	3.3
		2750	0.406	0.008	0.94	0.08	22.13	0.14	1.24	0.02	0.54	12.86	22.25	1.3
		3499	0.283	0.025	0.89	0.16	21.90	0.23	1.75	0.05	0.61	12.69	22.23	2.1
		4251	0.172	0.005	0.31	0.14	21.67	0.33	1.80	0.04	0.13	11.80	21.57	0.8
352														
Makarov	**< 0.2 µm**	**50**	1.520	0.000	2.08	0.24	21.65	0.13	1.31	0.04	0.55	12.40	21.10	0.4
Basin		**100**	0.651	0.018	1.68	0.17	21.85	0.12	1.08	0.04	1.03	12.87	22.05	1.6
		200	0.444	0.029	1.32	0.13	22.11	0.18	1.75	0.05	0.88	13.05	22.41	2.0
		751	0.451	0.009	2.16	0.23	21.71	0.11	1.50	0.05	1.71	12.94	22.29	3.8
		1500	0.330	0.006	1.87	0.32	21.47	0.13	1.95	0.05	1.54	12.66	22.14	4.7
		2251	0.241	0.013	1.43	0.17	21.77	0.14	1.79	0.04	1.19	12.84	22.46	4.9
		3001	0.167	0.002	1.01	0.23	21.69	0.28	1.90	0.06	0.85	12.62	22.40	5.1
		3900	0.219	0.010	1.10	0.30	21.61	0.31	1.85	0.08	0.88	12.55	22.21	4.0
	< 1000 kDa	**100**	0.442	***	1.08	0.15	21.98	0.23	1.61	0.04	0.64	12.79	22.14	1.4
		200	0.310	0.011	0.78	0.15	21.76	0.25	1.64	0.04	0.47	12.43	21.94	1.5
		751	0.345	0.002	1.26	0.12	21.91	0.13	1.85	0.03	0.91	12.87	22.33	2.6
		1500	0.248	0.012	1.68	0.54	21.20	0.15	1.96	0.13	1.43	12.35	21.96	5.8
		2251	0.172	0.009	1.38	0.08	22.10	0.10	1.77	0.03	1.21	13.18	22.94	7.1
		3001	0.101	0.011	0.95	0.19	21.52	0.17	1.73	0.04	0.85	12.45	22.45	8.5
		3900	0.204	0.004	0.51	0.09	21.99	0.24	1.77	0.03	0.30	12.47	22.16	1.5
407														
Laptev	**< 0.2 µm**	**10**	0.819	0.012	ND	ND	ND	ND	ND	ND	ND	ND	ND	ND
Sea		**30**	0.715	0.009	2.15	0.28	21.57	0.12	1.24	0.04	1.43	12.73	21.88	2.0
		56	1.112	0.000	2.00	0.30	21.59	0.14	1.51	0.06	0.89	12.54	21.50	0.8
	< 1000 kDa	**10**	0.698	0.029	ND	ND	ND	ND	ND	ND	ND	ND	ND	ND
		30	0.563	0.011	1.66	0.41	21.32	0.16	0.67	0.03	1.10	12.36	21.61	2.0
		56	1.004	0.027	1.96	0.25	21.58	0.10	0.75	0.02	0.96	12.56	21.56	1.0

4. Discussion

4.1. Iron over the different fractions

Large freshwater inputs from the Eurasian rivers bring organic matter, sediments and terrigenous materials containing Fe towards the central Arctic. Part of these materials is trapped in the forming sea-ice (Klunder *et al.*, submitted a and b) and transported away from the lands. During summer, this stock of Fe trapped in sea-ice is released in seawater later in time and farther in place when melting occurs, and is responsible for the elevated concentrations of DFe (around 1.5 nM Fe, Figure 6A, Table 1) measured at the surface in the Amundsen and Makarov basins (St. 309 and 352, respectively) as also shown by Klunder *et al.* (submitted a and b). This was also observed in the Southern Ocean by Lannuzel *et al.* (2007, 2008). Measures (1999) also investigated the influence of sediments in sea-ice on surface water Fe concentrations along a US-Canadian section across the Arctic Ocean. He suggested that sediment trapped into sea-ice may be of importance in transporting high Fe and Al concentrations to the surface waters of the central Arctic Ocean.

Wu *et al.* (2001) showed that 30 to 70% of DFe in deep waters was present in colloidal form (between 0.02-0.4 µm). At all stations in our study, Fe concentrations in the fraction <1000 kDa accounted for approximately 74 to 83% of the concentration of Fe in the dissolved fraction in the whole water column, thus 26 to 17% of DFe were present in the larger colloidal fraction (between 1000 kDa and 0.2 µm). Exception existed for the samples taken at the chlorophyll maximum where 42 to 64 % of DFe was present in the fraction <1000 kDa. These results showed that variations of the Fe pool in waters with phytoplankton activity was either due to the decrease (consumption) of Fe concentration in the smaller fraction (here <1000kDa) and/or due to presence or formation of larger Fe colloids. Boye *et al.* (2010) also found in the Southern Polar Frontal Zone (between 20-21°E and 47.7-49.3°S) a significant portion (37 to 51%) of colloidal Fe (between 200 kDa and 0.2 µm) within the dissolved organic fraction.

Bergquist *et al.* (2007) suggested that the variability of DFe (in <0.4 µm) was predominantly due to variations in the colloidal Fe as illustrated by the linear regression: $[Fe_{<0.4\ \mu m}] = 1.18\ [Fe_{0.02\ -0.4\ \mu m}] + 0.29$ ($R^2 = 0.85$). Similar results were

found in the Eastern North Atlantic Ocean (Thuróczy *et al.*, 2010b) using the same size fractions as in the present study ($[Fe_{<0.2\ \mu m}] = 1.16\ [Fe_{1000\ kDa-0.2\ \mu m}] + 0.03$; $R^2 = 0.93$; n = 9). However, in the Arctic Ocean, no relationship was found between DFe and larger colloidal Fe, neither in the Atlantic sector of the Southern Ocean (Chapter 5). Thus it appears that such a correlation is not applicable for all oceans. Further investigations are required here.

Nishioka and Takeda (2000) have shown that colloidal Fe (between 200 kDa and 0.2 µm) was the most dynamic fraction during Chaetoceros sp. incubations and was consumed first, instead of soluble Fe (<200 kDa or <0.03 µm). Our results were consistent with their work; indeed, in the Barents Sea and Kara Sea, the concentration of Fe in the larger colloidal fraction (between 1000 kDa and 0.2 µm) was maximal at the fluorescence maximum (at about 40 m depth) and became smaller below this depth. Below 25 m in the Kara Sea (St. 279) and between 1000 and 3000 m in the Makarov Basin (St. 352), ligands in the dissolved fraction were more saturated than those in the fraction <1000 kDa, meaning that ligands in the larger colloidal fraction (between 1000 kDa and 0.2 µm) were almost saturated. If colloids would aggregate, it would lead to a loss of Fe. Wu *et al.* (2001) showed that colloidal Fe (between 0.02-0.4 µm in their study) was important in removal processes when forming aggregates.

The TDFe has been shown to be a good chemical tracer of physical processes in the oceans (Takata *et al.*, 2008 and Thuróczy *et al.*, 2010b). By looking at Fe concentrations in UNF samples (TDFe), Thuróczy *et al.* (2010b) could distinguish the Mediterranean Overflow Water in the Eastern North Atlantic Ocean. In the Amundsen Sea of the Southern Ocean, TDFe concentrations were still high (> 30 nM Fe) up to 100 km away from the glaciers source and where the ligands were highly unsaturated with Fe in the dissolved fraction (Ratio [Lt]/[DFe] >15), indicating solubilisation of Fe processes (Gerringa *et al.*, submitted; Thuróczy *et al.*, submitted). In the present study, high concentrations of TDFe close to the sediment in the shelf seas resulted from the re-suspension of sediments. Similarly, the re-suspension of particles due to down slope processes were seen by elevated TDFe concentrations (St. 255, at 750 m depth) about 100 km away from the

continental shelf of the Nansen Basin. A distinct maximum in [TDFe]/[DFe] (ratio value of 30) was found at the same location likely due to slope processes with sediment re-suspension and a relative enrichment of particulate Fe. These high TDFe concentrations at the Nansen Slope (St. 255) were matched with high concentrations of Mn (Middag *et al.*, 2009) and lower light transmission (Figure 4). These 3 studies suggest a horizontal transport of particles as already demonstrated by Lam *et al.* (2006 and 2008) and Raiswell *et al.* (2008) in other oceans.

4.2. Complexation of Fe

4.2.1. In surface waters

In surface waters, the observed high ligand concentrations can be caused by input of organic matter from rivers as previously reported by Gerringa *et al.* (2007) in the Scheldt estuary, and from the sea-ice formed on the continental shelves. Sea-ice is a potential source of ligands to the surface water because it contains organic matter from the rivers and from micro-organisms. The accumulation of dissolved organic matter within sea-ice was found to be several orders greater than in surface oceanic water as previously reported by Thomas *et al.* (2001), Carlson and Hansell (2003) and Riedel *et al.* (2008). However, we cannot make any conclusions on the sea-ice sources since we could not sample in the vicinity of sea-ice; our first sample were taken at 20 m (St. 255 on the slope of the Nansen Basin) or at 50 m in the deep basins (St. 260, 309 and 352). On the shelf seas, the high ligands concentrations could be due to sediment re-suspension as suggested by Gerringa *et al.* (2008) for the Kerguelen Plateau with samples taken close to the bottom. At the surface and underneath sea-ice, living organisms play a role in the chemistry of Fe. On the one hand, Fe is taken up by most of the living organisms (phytoplankton, bacteria and viruses); on the other hand, their presence generate organic matter (faeces, dead algae), which is degraded and remineralised into possible Fe-binding-ligands. The high DFe concentrations found in surface waters of the central Arctic (St. 309 in the Amundsen Basin and St. 352 in the Makarov Basin) might have not been limiting for the phytoplankton (Timmermans *et al.*, 2005).

However, the thick layer of sea-ice at the surface, source of Fe as discussed above, was most likely responsible for the lack of light leading to the low fluorescence recorded (Timmermans *et al.*, 2001, 2005). Thus Fe uptake by biota should be small resulting in high DFe concentrations.

In the surface waters of the Barents Sea (St. 239) and in the upper layer at the slope of the Nansen Basin (St. 255), relatively high Excess L and slightly weaker ligands (K' value of $10^{21.39}$ and $10^{21.93}$, respectively, Table 1) were measured around the fluorescence maximum (fluorescence >0.3 a.u., Figure 4). A possible explanation for relatively high Excess L concentrations and low conditional stability constant is the presence of exopolymer component like colloidal polysaccharide gels produced by organisms as found in Arctic sea-ice by Meiners *et al.* (2008) and Riedel *et al.* (2007). These colloidal polysaccharides present in relatively high concentration and with a relatively low binding constant (Hassler *et al.*, 2011 and Benner, 2011) may behave as organic ligands thus having a pivotal role in the speciation of Fe in surface waters. Our results are also in line with the results of Rijkenberg *et al.* (2008) who suggested that ligands originating from phytoplankton, or at least found at the the chlorophyll maximum, were relatively weak in contrast to ligands measured at larger depth. However, Rue and Bruland (1995) concluded that ligands originated from phytoplankton are stronger (relatively high K' value). Stronger ligands were measured in the Nansen (St. 260) and Amundsen (St. 309) basins at the chlorophyll maximum; however, the fluorescence signal was lower here (<0.3 a.u.). Thus, there was no proof of a relation between phytoplankton and binding strength of ligands.

4.2.2. Saturation state of the ligands

The ratio [Excess L]/[Fe] (Figure 8) expresses the relative saturation of the ligands with Fe (Chapter 2; Thuróczy *et al.*, 2010b and 2011a). A high ratio means a relatively large excess of ligands, so an extra input of Fe would be easily complexed by the ligands. In this case, ligands have a high buffering capacity. A decrease in Fe also increases the ratio, and thus with respect to biota, an increasing ratio indicates depletion/consumption of Fe. A low ratio, approaching 0, indicates

that the ligands become saturated and shows that possible extra Fe inputs will be preferably removed by precipitation and/or scavenging. The ratio [Excess L]/[Fe] in the dissolved and <1000 kDa fractions decreased with depth, below the surface minimum in the Barents Sea and Amundsen Basin (St. 239 and 309, respectively), in all basins and seas with the exception of the Makarov basin. This decrease with depth was found in the Southern Ocean (Chapter 4; Thuróczy *et al.*, 2011a) and in the Eastern North Atlantic Ocean (Thuróczy *et al.*, 2010b). In both regions, below 450 m depth, low and constant values were found corresponding to relatively constant saturation state of the ligands. These results were supported by the work of Boye *et al.* (2010), who found an increasing portion of colloidal Fe (200 kDa-0.2 μm) as well as an increasing saturation of the ligands from the surface until 1000 m depth. In the deep waters (below 800 m) of the Nansen Basin (St. 260), the ratio [Excess L]/[Fe] was around 3, decreasing with depth. In the Amundsen Basin, the ratio was higher (3-5), showing that here the ligands were less saturated with Fe. Only the Makarov Basin (St. 352) showed the exact opposite trend with depth in the dissolved and <1000 kDa fractions, not yet found anywhere else (Thuróczy *et al.*, 2010b and 2011a). The ratio values increased with depth (less saturation of the ligands with depth) indicating higher potential for Fe solubilisation. The increasing [Excess L]/[Fe] with depth in both dissolved and <1000 kDa fractions were caused by a larger decrease in Fe concentrations than Excess L concentrations. This revealed a possible loss of Fe and ligands towards the bottom as confirmed by increasing [TDFe]/[DFe] (Figure 10) indicating a the relative enrichment of particulate Fe and thus scavenging. Scavenging by settling particles is supported by the fact that the ligands are relatively weak and less reactive in the Makarov Basin compared to the Nansen and Amundsen basins (Figure 9). The combination of scavenging and a lack of Fe sources probably accounted for the net loss of DFe. This net loss was reflected by the increase in both [Excess L]/[Fe] and [TDFe]/[DFe].

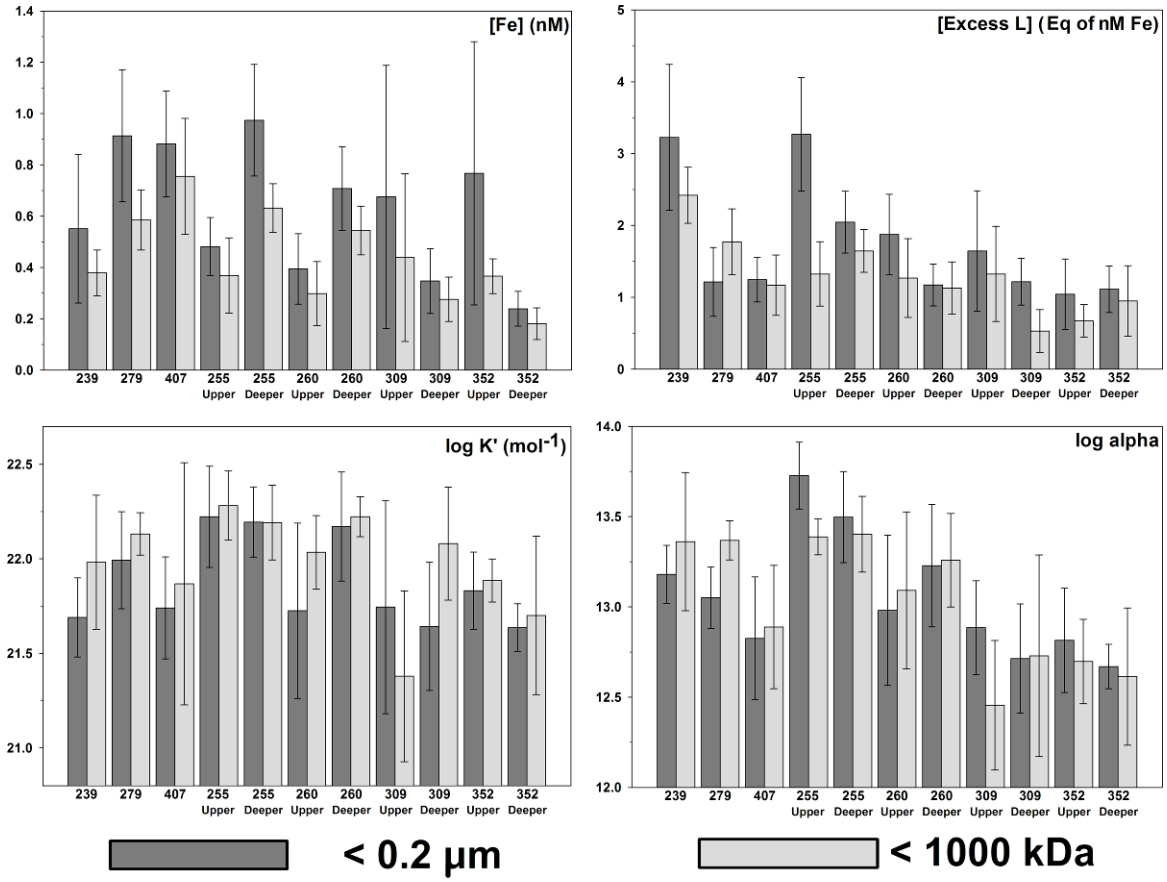

Figure 9: *Average values (±Standard deviation) of Fe concentrations and ligand characteristics, for the dissolved fraction (<0.2 µm, dark grey) and fraction <1000 kDa (light grey), at all the stations sampled, in the seas (St. 239, 279, 407) and in the basins (St. 255, 260, 309, 352): in the upper basins (0-800 m, SW and AW) and in the deeper basins (below 800 m).*

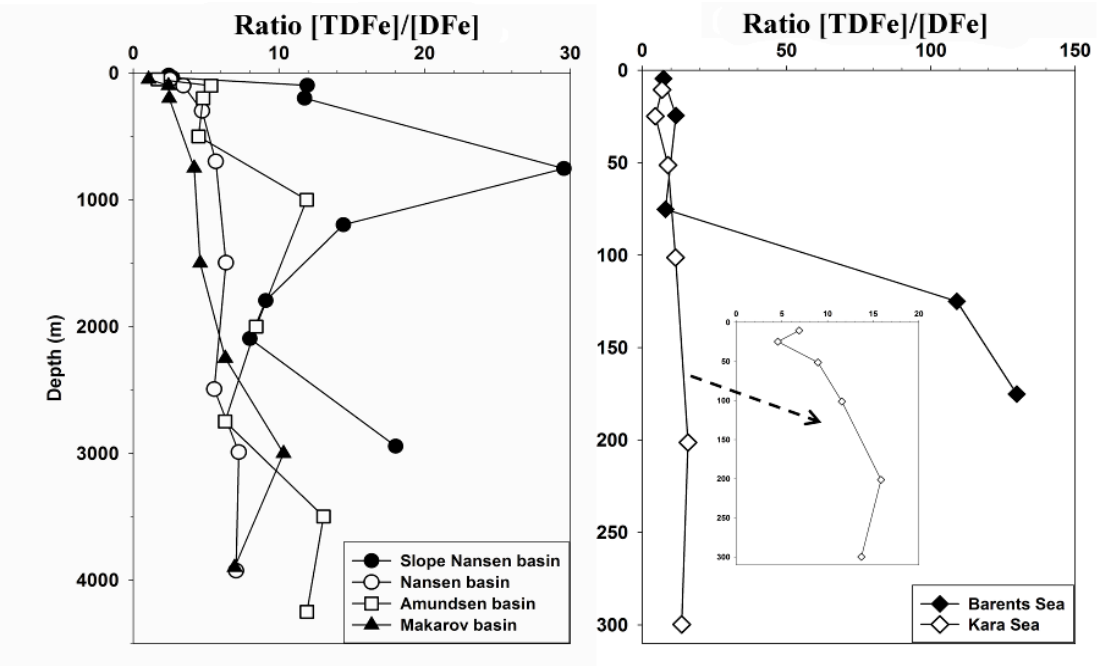

Figure 10: *Ratio [TDFe]/[DFe] with depth. Graphs on the left are the deep basin stations (St. 255, 260, 309 and 352) and graphs at the right are the shelf sea stations (St. 239 and 279). Note the different scales for the ratio values and for the depths. The station in the Kara Sea isalso enlarged (axis of the ratio until 20).*

4.2.3. Complexation of Fe in unfiltered samples

The complexation of Fe in UNF samples is poorly described (Nolting *et al.*, 1998; Thuróczy *et al.*, 2010b), certainly due to the uncertainty of the Fe concentration that is exchangeable. Part of Fe is refractory and irreversibly bound to particles or colloids under natural seawater conditions. The concentration of Fe used in the calculations influences the estimation of Lt and the strength K'. When TDFe is used, these parameters are overestimated; when DFe is used, they are possibly underestimated. However, Excess L is hardly changed when using different Fe concentrations in the calculation, therefore Excess L in UNF samples can be used as discussed by Thuróczy *et al.* (2010b).

Excess L concentrations in UNF samples were similar (within the standard deviations) to those in the smaller fraction at most of the stations indicating a small influence of the particulate fraction on the organic complexation of Fe, except in SW. In surface waters of the Nansen Basin (St. 255 and 260) and of the Kara Sea (St. 279), maximum Excess L in the UNF fraction (Tables 1 and 2, Figure 7) were measured where Excess L was at minimum in the dissolved and <1000 kDa

fractions. Thus, the largest excess of ligands must come from the particulate fraction (>0.2 μm) suggesting that particles could easily bind Fe (reactive) resulting in low excess L. These particles most likely originated from the rivers and sediments, as seen by the low light transmission (Figure 4). In the Makarov Basin, Excess L concentrations in the UNF samples were lower than in the dissolved and <1000 kDa fractions at 1500 and 2250 m depth. This apparent artefact was found in the upper core of the deep waters, just below the limit between the AIW and the AW.

Table 2 (Next pages): *Determination of the ligand characteristics in UNF samples. A: determination of an upper limit using [TDFe]. B: Determination of a lower limit using [DFe].*
** when the model could not fit the data using the lower limit.*
**** The standard deviation for Fe concentrations is missing when there was not enough sample volume to determine the concentration in duplicate or triplicate.*

A	Upper limit										
Station	Depth (m)	[TDFe] (nM)	S.D.	[Lt] (Eq of nM Fe)	S.D.	logK' (mol^{-1})	S.D.	Sensitivity S ($A.mol^{-1}$)	S.D.	[Excess L] (Eq of nM Fe)	[Excess L] / [TDFe]
239											
Barents	**5**	3.01	0.03	4.96	0.41	22.06	0.15	0.90	0.06	1.95	0.7
Sea	**25**	3.61	0.01	7.23	0.22	22.26	0.06	1.14	0.05	3.62	1.0
	75	8.47	0.26	12.25	0.45	22.51	0.11	0.99	0.10	3.78	0.5
	125	54.79	0.54	56.93	0.11	23.66	0.08	1.06	0.03	2.14	0.0
	175	63.08	1.22	65.06	0.29	23.57	0.18	0.29	0.02	1.97	0.0
255											
Nansen	**19**	0.75	0.05	3.73	0.44	21.69	0.10	1.77	0.12	2.98	4.0
Slope	**37**	1.16	0.06	ND	ND	ND	ND	ND	ND	ND	ND
	98	6.28	0.08	8.11	0.32	22.56	0.20	0.78	0.05	1.83	0.3
	200	6.54	0.08	ND	ND	ND	ND	ND	ND	ND	ND
	754	17.35	0.13	ND	ND	ND	ND	ND	ND	ND	ND
	1198	12.72	0.31	ND	ND	ND	ND	ND	ND	ND	ND
	1796	7.78	0.10	ND	ND	ND	ND	ND	ND	ND	ND
	2096	10.41	***	ND	ND	ND	ND	ND	ND	ND	ND
	2944	15.49	0.05	ND	ND	ND	ND	ND	ND	ND	ND
260											
Nansen	**50**	0.69	0.03	4.36	0.22	22.45	0.13	1.27	0.07	3.66	5.3
Basin	**100**	0.95	0.01	3.01	0.23	22.27	0.19	1.27	0.05	2.05	2.2
	300	2.42	0.03	4.04	0.25	23.14	0.43	1.52	0.07	1.62	0.7
	698	2.91	0.06	4.33	0.17	22.66	0.23	0.93	0.03	1.42	0.5
	1497	3.68	0.18	4.88	0.15	22.68	0.16	1.53	0.04	1.20	0.3
	2494	5.26	0.04	6.64	0.09	22.92	0.11	2.06	0.04	1.38	0.3
	2991	4.83	0.13	7.15	0.19	22.59	0.11	1.90	0.07	2.31	0.5
	3926	4.52	0.24	5.12	0.20	23.41	0.39	0.71	0.03	0.60	0.1
279											
Kara	**11**	6.12	0.02	8.30	0.18	22.48	0.08	1.70	0.05	2.19	0.4
Sea	**25**	5.04	***	6.01	0.08	23.19	0.17	1.26	0.02	0.96	0.2
	51	11.87	0.05	12.82	0.14	23.24	0.19	1.56	0.05	0.95	0.1
	101	8.48	0.07	9.42	0.11	23.16	0.15	1.46	0.03	0.94	0.1
	201	10.01	0.06	11.64	0.13	22.84	0.09	1.14	0.03	1.64	0.2
	300	11.00	***	12.26	0.39	22.82	0.29	0.67	0.05	1.26	0.1
309											
Amundsen	**50**	2.44	0.08	3.17	0.07	22.65	0.12	1.04	0.02	0.72	0.3
Basin	**101**	2.39	0.01	4.81	0.48	21.68	0.08	1.82	0.12	2.42	1.0
	201	1.95	0.04	4.51	0.31	22.08	0.11	1.57	0.10	2.55	1.3
	501	1.80	0.05	3.27	0.21	21.93	0.10	1.71	0.06	1.47	0.8
	1001	3.50	0.09	4.12	0.13	22.47	0.13	1.59	0.04	0.62	0.2
	2001	2.83	0.05	4.73	0.38	21.83	0.10	1.83	0.10	1.90	0.7
	2750	3.52	0.09	4.91	0.28	22.27	0.14	2.48	0.11	1.39	0.4
	3499	4.25	0.08	5.86	0.34	22.56	0.28	1.98	0.12	1.61	0.4
	4251	2.66	0.01	3.23	0.08	22.70	0.15	1.73	0.03	0.57	0.2
352											
Makarov	**50**	1.61	0.06	2.74	0.44	21.60	0.16	1.32	0.07	1.13	0.7
Basin	**100**	1.58	0.08	2.50	0.12	22.16	0.10	1.88	0.04	0.92	0.6
	200	1.10	0.04	2.05	0.14	21.95	0.11	1.65	0.04	0.95	0.9
	751	1.89	0.03	2.52	0.12	22.31	0.15	1.67	0.03	0.64	0.3
	1500	1.51	0.06	2.17	0.16	22.23	0.19	1.95	0.05	0.66	0.4
	2251	1.53	0.08	2.47	0.22	22.09	0.18	2.20	0.08	0.94	0.6
	3001	1.72	0.07	2.44	0.05	22.37	0.06	1.98	0.02	0.72	0.4
	3900	1.52	0.01	2.75	0.15	22.07	0.11	1.93	0.05	1.22	0.8

B	Lower limit										
Station	Depth (m)	[DFe] (nM)	S.D.	[Lt] (Eq of nM Fe)	S.D.	logK' (mol^{-1})	S.D.	Sensitivity S ($A.mol^{-1}$)	S.D.	[Excess L] (Eq of nM Fe)	[Excess L] / [DFe]
239											
Barents	5	0.41	0.04	3.46	1.40	21.38	0.25	1.02	0.18	3.05	7.5
Sea	25	0.31	0.03	4.29	0.48	21.80	0.10	1.20	0.11	3.99	12.9
	75	1.05	0.00	4.99	0.72	21.92	0.15	1.00	0.14	3.94	3.8
	125	0.50	0.01	2.88	0.24	22.05	0.13	1.10	0.05	2.38	4.7
	175	0.49	0.02	2.50	0.33	21.93	0.22	0.29	0.02	2.02	4.2
255											
Nansen	19	0.31	0.01	4.00	0.57	21.48	0.08	1.94	0.15	3.69	12.0
Slope	98	0.53	0.01	2.54	0.50	21.80	0.26	0.82	0.06	2.02	3.8
260											
Nansen	50	0.27	0.03	3.96	0.23	22.38	0.14	1.27	0.07	3.68	13.5
Basin	100	0.28	0.04	2.70	0.34	21.91	0.16	1.34	0.08	2.43	8.8
	300	0.51	0.01	2.99	0.48	22.17	0.30	1.92	0.18	2.48	4.8
	698	0.51	0.01	1.99	0.24	22.17	0.29	0.94	0.04	1.48	2.9
	1497	0.58	0.03	2.15	0.24	21.86	0.15	1.61	0.06	1.57	2.7
	2494	0.95	0.01	2.43	0.11	22.28	0.11	2.09	0.04	1.49	1.6
	2991	0.67	0.01	3.30	0.30	21.97	0.12	1.99	0.11	2.64	4.0
	3926	0.64	***	1.24	0.22	22.74	0.44	0.71	0.03	0.60	0.9
279											
Kara	11	0.89	0.01	3.90	0.47	21.65	0.09	1.89	0.13	3.01	3.4
Sea	25	1.10	0.01	2.07	0.09	22.66	0.21	1.26	0.02	0.97	0.9
	51	1.33	0.01	2.80	0.27	22.06	0.18	1.75	0.08	1.48	1.1
	101	0.73	0.01	1.92	0.19	22.11	0.16	1.51	0.04	1.18	1.6
	201	0.63	0.00	2.42	0.24	21.93	0.14	1.16	0.04	1.79	2.8
	300	0.80	0.01	2.91	0.53	21.67	0.16	0.75	0.06	2.11	2.6
309											
Amundsen	50	1.44	0.03	2.16	0.07	22.48	0.13	1.04	0.02	0.72	0.5
Basin	101	0.45	0.00	*	*	*	*	*	*	*	*
	201	0.41	0.01	*	*	*	*	*	*	*	*
	501	0.40	0.01	2.52	0.60	21.39	0.16	1.87	0.14	2.12	5.3
	1001	0.29	***	1.64	0.75	21.19	0.28	1.70	0.12	1.34	4.6
	2001	0.34	0.00	*	*	*	*	*	*	*	*
	2750	0.56	0.02	1.17	0.16	21.93	0.18	1.99	0.06	0.62	1.1
	3499	0.32	0.01	*	*	*	*	*	*	*	*
	4251	0.22	0.01	0.88	0.17	21.79	0.26	1.74	0.04	0.66	3.0
352											
Makarov	50	1.52	0.00	2.70	0.46	21.57	0.16	1.33	0.07	1.17	0.8
Basin	100	0.65	0.02	1.51	0.18	21.84	0.16	1.86	0.05	0.86	1.3
	200	0.44	0.03	1.89	0.32	21.43	0.13	1.74	0.06	1.45	3.3
	751	0.45	0.01	1.26	0.25	21.66	0.22	1.70	0.06	0.81	1.8
	1500	0.33	0.01	0.66	0.17	21.90	0.41	1.75	0.06	0.33	1.0
	2251	0.24	0.01	0.58	0.14	21.85	0.34	1.85	0.05	0.34	1.4
	3001	0.17	0.00	1.18	0.14	21.50	0.10	2.04	0.03	1.01	6.1
	3900	0.22	0.01	1.53	0.28	21.47	0.13	1.85	0.08	1.31	6.0

4.3. Distinct trends in Fe and ligands characteristics

General trends in Fe concentrations and ligand characteristics were observed (Figure 9). By averaging each parameter per environment and per layer: the shelf seas (St. 239, 279 and 407), the upper layer (0-800 m, layer composed of SW and AW) and the deeper layer (<800 m, layer composed of the deep waters, AIW,

CBW and DMBW) of the basins (St. 255, 260, 309 and 352), trends could be distinguished.

The concentrations of DFe and $Fe_{<1000\ kDa}$ became slightly lower in the deeper ocean towards the central Arctic in the Makarov Basin (Figures 6 and 9), as also shown by Klunder *et al.* (submitted a and b). They showed that less Fe sources are present in the Makarov Basin compared to Amundsen Basin and Nansen Basins. The TDFe showed the same geographical trend as DFe (Figure 5): towards the central Arctic, TDFe decreased, from 3-6 nM Fe in the Nansen Basin, to 3 nM Fe in the Amundsen Basin and to 2 nM Fe in the Makarov Basin. This decrease of the particulate fraction towards the central Arctic is related to increasing distance from the shelf and slope sources and thus increasing time for removal processes (export of Fe) such as scavenging. The Deep Makarov Basin Water (DMBW) had different water properties (seen with θ/S diagrams, Figure 3) influenced by water from the Pacific Ocean which most likely explained the different ligand characteristics in deep waters of the Nansen and Amundsen basins (AW, AIW and CBW) and of the Makarov Basin (AW, AIW, CBW and DMBW).

Rue and Bruland (1995) and Buck and Bruland (2007) investigated Fe and ligands in the Central North Pacific Ocean and in the Bering Sea, respectively, and could distinguish two classes of ligands using a different method as the one used in our study. They measured high Excess L concentrations (up to 1.8 Eq of nM Fe) in the surface samples increasing with depth to 2 Eq of nM Fe at 2000 m (Rue and Bruland, 1995), together with lower binding strength at depth. Excess L in our dissolved and <1000 kDa fractions were similar to their values, decreasing from 1.54 and 1.43 Eq of nM Fe, respectively, at 1500 m depth in the DMBW to 0.88 and 0.30 Eq of nM Fe at 3900 m depth, respectively. The ligands were also weaker in the DMBW than in the the upper waters. Overall this suggests the Pacific origin of the ligands in the DMBW.

In the Amundsen and Makarov Basins, Excess L concentrations were lower than in the Nansen Basin (Figure 9). Trends in the binding strength were not obvious; slightly lower values were measured in the Amundsen and Makarov basins compared to the Nansen Basin (Table 1 and Figure 9). However,

considering the stations in the basins, a distinct geographic trend existed in the alpha values (K'*Excess L), which expresses the reactivity of the ligands. Alpha clearly decreased from the continental slope (Figure 9, St. 255, logα >13.5) towards the central Arctic Ocean (St. 352, logα <13). This decrease in the reactivity of the ligands towards the central Arctic means higher potential for Fe export towards the sea-floor in the Makarov Basin. But, does alpha alone control the fate of Fe?

The decrease of alpha in deep waters (below 800 m) towards the central Arctic Ocean fitted the increasing trends of the ligands saturation state (ratio [Excess L]/[Fe]) in the dissolved and <1000 kDa fractions. Ligands were more saturated with Fe (ratio [Excess L]/[Fe] <3) where they were more reactive (higher alpha value) in the Nansen Basin (St. 260). In the Amundsen Basin, they were less saturated (ratio between 3 and 5) where they were less reactive. In the Makarov Basin, the ligands became unsaturated towards the bottom (ratio between 4 and 8) together with a decrease of their reactivity. As mentioned earlier, the decrease of the particulate fraction towards the central Arctic is related to increasing distance from the shelf and slope sources. Ligands can buffer Fe inputs but can also give away Fe when scavenging via sinking particles occurs. In the Nansen Basin where the ligands are reactive, the permanent Fe inputs, which lead to saturate the ligands with Fe, is larger than scavenging and removal processes. Conversely, in the deep Makarov Basin where the ligands are less reactive and where the sources of Fe are limited (Klunder *et al.*, submitted a and b), scavenging of Fe lead to the desaturation of the ligands and to a net export of Fe towards the seafloor because the flux of particles is apparently much larger than the flux of DFe. This highlights the combination of little source of Fe and increasing time for scavenging towards the Makarov Basin.

Trends existed between the seas, with decreasing alpha, decreasing Fe and increasing ratio [Excess L]/[Fe] from the Barents Sea (St. 239), Kara Sea (St. 279) towards the Laptev Sea (St. 407). This Eastwards trend could be due to a dilution of the AW inflow on the shelves, and higher influence from the rivers.

5. Summary and conclusions

Our study presented the first data set on the complexation and size fractionation of Fe in the Arctic Ocean.

Dissolved Fe (DFe) was for 74 to 83% present in the fraction <1000 kDa, except at the chlorophyll maximum depth. Here, only 42 to 64 % of DFe was present in the fraction <1000 kDa, thus a somewhat larger portion of Fe in the larger colloidal fraction (between 1000 kDa and 0.2 μm). Distinct geographical trends in Fe and in ligands characteristics were seen from the shelf seas (Barents Sea) towards the central Arctic Ocean (Makarov Basin). In the surface waters and Atlantic waters (above 800 m depth), the concentrations of DFe and $Fe_{<1000\ kDa}$ were lower in the Nansen Basin (average [DFe] = 0.39 nM ±0.14, n=4; and average [$Fe_{<1000\ kDa}$] = 0.30 nM ±0.12, n=4) than in the Amundsen Basin (average [DFe] = 0.68 nM ±0.51, n=4; and average [$Fe_{<1000\ kDa}$] = 0.44 nM ±0.33, n=4) and in the Makarov Basin (average [DFe] = 0.77 nM ±0.51, n=4; and average [$Fe_{<1000\ kDa}$] = 0.37 nM ±0.07, n=3) as summarised in Figure 9. Below 800 m depth, higher concentrations of Fe were found in the Nansen Basin (average [DFe] = 0.71 nM ±0.16, n=4; and average [$Fe_{<1000\ kDa}$] = 0.54 nM ±0.09, n=4) compared to the Amundsen Basin (average [DFe] = 0.35 nM ±0.13, n=5; and average [$Fe_{<1000\ kDa}$] = 0.28 nM ±0.09, n=5) and in the Makarov Basin (average [DFe] = 0.24 nM ±0.07, n=4; and average [$Fe_{<1000\ kDa}$] = 0.18 nM ±0.06, n=4). A general decrease in excess of ligands (from approximately 3.5 to 1 Eq of nM Fe for the dissolved fraction, and from approximately 1.5 to 0.5 Eq of nM Fe for the fraction <1000 kDa), and in the binding strength (logK' mainly >22 in the Nansen Basin, and logK'<22 in the Amundsen and Makarov basins) resulted in a decrease in alpha. This corresponds to the ligand reactivity (average log α >13.5 in the Nansen Basin, and <13 in the Amundsen and Makarov basins, Figure 9). Total dissolvable iron (TDFe) also decreased from the Nansen Basin where [TDFe] were above 3 nM Fe in the AW and EBDW, towards the Makarov basins where [TDFe] were lower than 2 nM Fe in the AW and DMBW. In addition, a relative enrichment of particulate Fe with depth at all stations was found looking at the ratio [TDFe]/[DFe], revealing removal of Fe via scavenging in the deep basins. Furthermore, in the Nansen and

Amundsen basins, ligands in the dissolved and <1000 kDa fractions were more saturated with Fe with increasing depth (ratio [Excess L]/[Fe] decreasing from 13 at the surface to 1 at depth), which was related to more sources of Fe and to more reactive dissolved ligands (alpha >13.5). Thus, Fe removal might be important here. Conversely, in the Makarov Basin, the dissolved ligands became desaturated with depth (ratio [Excess L]/[Fe] increasing from 0.4 at the surface to 8.5 at depth) as confirmed by their lower reactivity (alpha <13). The Makarov Basin is far from large sources of Fe and ligands, thus increasing the time for scavenging and export of Fe. There, the flux of particles removing Fe is probably larger than the flux of DFe input leading to the desaturation of the ligands.

To conclude, the reactivity (alpha value) and the saturation state (ratio [Excess L]/[Fe]) of the ligands proved to be excellent tools to explain the distribution and the fate of Fe in the different fractions when combining sources of Fe and ligands and removal processes like scavenging.

Chapter 7

Key role of organic complexation of iron in sustaining phytoplankton blooms in the Pine Island and Amundsen Polynyas (Southern Ocean)

This chapter is adapted from: Thuróczy, C.-E., Alderkamp, A.-C., Laan, P., Gerringa, L.J.A., Mills, M.M., Van Dijken, G.L., De Baar, H.J.W., Arrigo, K.R. Key role of organic complexation of iron in sustaining phytoplankton blooms in the Pine Island and Amundsen Polynyas (Southern Ocean). Submitted to Deep-Sea Research II.

Abstract

Primary productivity in the Amundsen Sea (Southern Ocean) is among the highest in Antarctica. The summer phytoplankton bloom in 2009 lasted for >70 days in both the Pine Island and Amundsen Polynyas. Such productive blooms require a large supply of nutrients, including the trace metal iron (Fe). The organic complexation of dissolved Fe was investigated in the Amundsen Sea during the spring of 2009 to better understand the potential role of ligands in enhancing the local stock of soluble Fe. The main sources of Fe and ligands to the Amundsen Sea are the Circumpolar Deep Water (CDW), which is modified by sediment resuspension on the continental shelf and upwells beneath the coastal glaciers and ice-shelves, and melting sea-ice. The upwelling of relatively warm CDW is also responsible for the rapid melting of the Pine Island Glacier (PIG) and surrounding ice-shelves, resulting in the release of Fe into surface waters. At upwelling stations near ice shelves, organic ligands were highly saturated with Fe, increasing the solubility of Fe and enhancing the stock of Fe and its availability to the phytoplankton community. Therefore, at the ice shelf stations, the ligands had little capacity to buffer additional Fe input from glacial melt. In these coastal upwelling regions, much of the glacial Fe supply is lost due to vertical export of Fe via scavenging and precipitation. Conversely, within the phytoplankton bloom in the nearby coastal polynyas, the uptake of Fe combined with the production of organic matter enhanced the abundance of relatively unsaturated organic ligands capable of stabilizing additional Fe supplied from glacial melt. These un-saturated dissolved organic ligands, combined with the continuous input of Fe (dissolved and particulate) from glacial melt, appears to favour the solubilisation of Fe from particulate phase, thus increasing the stock of bioavailable Fe and fuelling the phytoplankton bloom.

1. Introduction

The Southern Ocean plays an important role in the export of anthropogenic CO2 (around 25% of total anthropogenic carbon emission), in part via primary production by phytoplankton (De Baar *et al.*, 1995). Primary productivity is enhanced in polynyas; areas of reduced sea-ice caused typically caused by offshore katabatic winds and seasonal sea-ice (Arrigo *et al.*, 1997; Arrigo and Van Dijken, 2003a). Of the dozens of coastal polynyas circling the Antarctic continent, those located in the Amundsen Sea (Figure 1) exhibit the highest phytoplankton productivity per unit area (Arrigo and Van Dijken, 2003b).

Iron (Fe) is known to limit algal growth in the High Nutrient Low Chlorophyll (HNLC) regions of the world ocean (Martin *et al.*, 1990 and 1991). The abundance of Fe in seawater is controlled by a balance between Fe input (via sediment resuspension, sea-ice and glacial melt, upwelling, atmospheric deposition and hydrothermal inputs), stabilisation processes via organic complexation that keep Fe in the dissolved phase, and by removal processes like (oxidative) precipitation and adsorptive scavenging (Gledhill and Vanden Berg, 1994; Rue and Bruland, 1997; Croot and Johansson, 2000; Boye *et al.*, 2001; Kuma *et al.*, 1996; Nishioka *et al.*, 2000 and 2001; Thuróczy *et al.*, 2010b, 2011 and submitted; Klunder *et al.*, 2011).

Around Antarctica, the two dominant phytoplankton groups include diatoms and the prymnesiophyte *P. antarctica*. On the continental shelf, diatoms are found mainly in the shallow mixed layers whereas *P. antarctica* forms colonies in waters with a deep mixed layer (Arrigo *et al.*, 1999, 2002). Their distributions are governed by their specific requirements for two main growth-limiting factors, Fe and light (De Baar *et al.*, 1990; 2005; Coale *et al.*, 1996; Sunda and Huntsman, 1997; Buma *et al.*, 1991; Timmermans *et al.*, 2001). Diatoms and *P. antarctica* have different nutrient utilisation characteristics (Arrigo *et al.*, 1999) and support very different higher trophic level communities. In the Southern Ocean, Fe controls the magnitude of annual primary productivity while light determines the species distribution (Arrigo *et al.*, 2000; Arrigo *et al.*, 2003; Arrigo and VanDijken, 2003b; Alderkamp *et al.*, submitted). Increase of the air temperature in

Antarctica due to general global warming has an impact on ice melting and subsequent water column stability and thus on the primary productivity and phytoplankton community structure. Furthermore, the inflow of the warm and Circumpolar Deep Water (CDW, Jacobs and Hellmer, 1996) on the Amundsen Sea shelf drives a rapid melting of the Antarctic ice shelves, in particular the Pine Island Glacier. Melting of the Pine Island Glacier could account for 10% of the observed sea-level rise (Rignot *et al.*, 2008) and is an important and continuous source of Fe to surface waters in Pine Island Bay (PIB).

The Amundsen Sea is delimited by the Abbot Ice Shelf in the North-East (Figure 1) and the Crosson, Dotson and Getz Ice Shelves on the west side of the Pine Island Bay (PIB). The Amundsen Sea has a large shelf area, is about 250-400 m deep, and has deep canyons (up to 1600 m depth, Nistche *et al.*, 2007). PIB is surrounded by two main glaciers: the Thwaites Glacier on the western side and the Pine Island Glacier to the south. The Antarctic Circumpolar Current (ACC, Figure 1) flows eastwards around the Antarctic continent and injects relatively warm (~2°C) and saline (Salinity of 34.0-34.5) CDW (Giulivi and Jacobs, 1997) onto the Amundsen Sea contental shelves. This CDW then flows towards the continent and upwells underneath the Pine Island Glacier and the Getz and Dotson Ice Shelves. The CDW inflow is partly responsible for the rapid melting (Jacobs and Hellmer, 1996) of the ice shelves of the Amundsen sea as well as of the Thwaites and Pine Island glaciers (Jenkins *et al.*, 2010). These waters also harbor the two largest and most productive polynyas in the Amundsen Sea, the Pine Island Polynya (PIP) and the Amundsen Polynya (Arrigo and VanDijken, 2003b).

The organic complexation of Fe in the dissolved fraction (<0.2 µm) was studied in the Amundsen Sea during the cruise NBP09-01 onboard the US Research Vessel *Nathaniel B. Palmer* from 5 January until 28 February 2009. The research goal was to gain insight into the role of the ligands in increasing the solubility of Fe by buffering Fe input from upwelling of CDW and glacial melt, and thus indirectly enhancing its bio-availability to the phytoplankton. This work is part of the ”DynaLiFe“ project (Shedding a dynamic light on Fe limitation in the Southern Ocean) which aims to study in situ phytoplankton primary productivity

and carbon uptake (De Baar *et al.*, 2008b) with the main hypothesis: "The interaction between Fe limitation and dynamic irradiance governs phytoplankton distributions in the Southern Ocean" (Alderkamp *et al.*, submitted). Details on the hydrography and on the Fe distribution in the PIB and Pine Island Glacier in the Amundsen Sea are described in Gerringa *et al.* (submitted). The nutrient distributions are described in Alderkamp *et al.* (submitted).

2. Additional details on the materials and methods

Samples for the organic complexation of Fe were taken in the upper 300 m of the water column (at 10, 25, 50, 100, 200, 300 m) at 26 stations, from the January 12th to February 15th (Figure 1, Table 1). Fifteen (15) vertical profiles (St. 3, 7, 13, 16, 23, 55, 81, 91, 92, 102, 106, 107, 113, 114 and 119) were usually collected at 10, 25, 50, 100, 200 and 300 m depth. Moreover at 11 stations (St. 5, 10, 37, 47, 94, 105, 118, 129, 135, 148, 158) only one sample was taken at the chlorophyll maximum (10-15 m depth) for phytoplankton experiments studying the effects of light and ligands additions. These experiments are described by Alderkamp *et al.* (submitted), van Dijken *et al.* (submitted) and Mills *et al.* (submitted).

Chlorophyll-a (Chl a) was quantified using standard JGOFS procedures (JGOFS, 1996). Chlorophyll samples (0.05-1 L) were filtered at ambient seawater temperature under low vacuum pressure. Filters were extracted in 5 ml 90% acetone in the dark at 4°C for 20 hr. The extracted fluorescence was read before and after acidification using a Turner Designs Model 10-AU fluorometer.

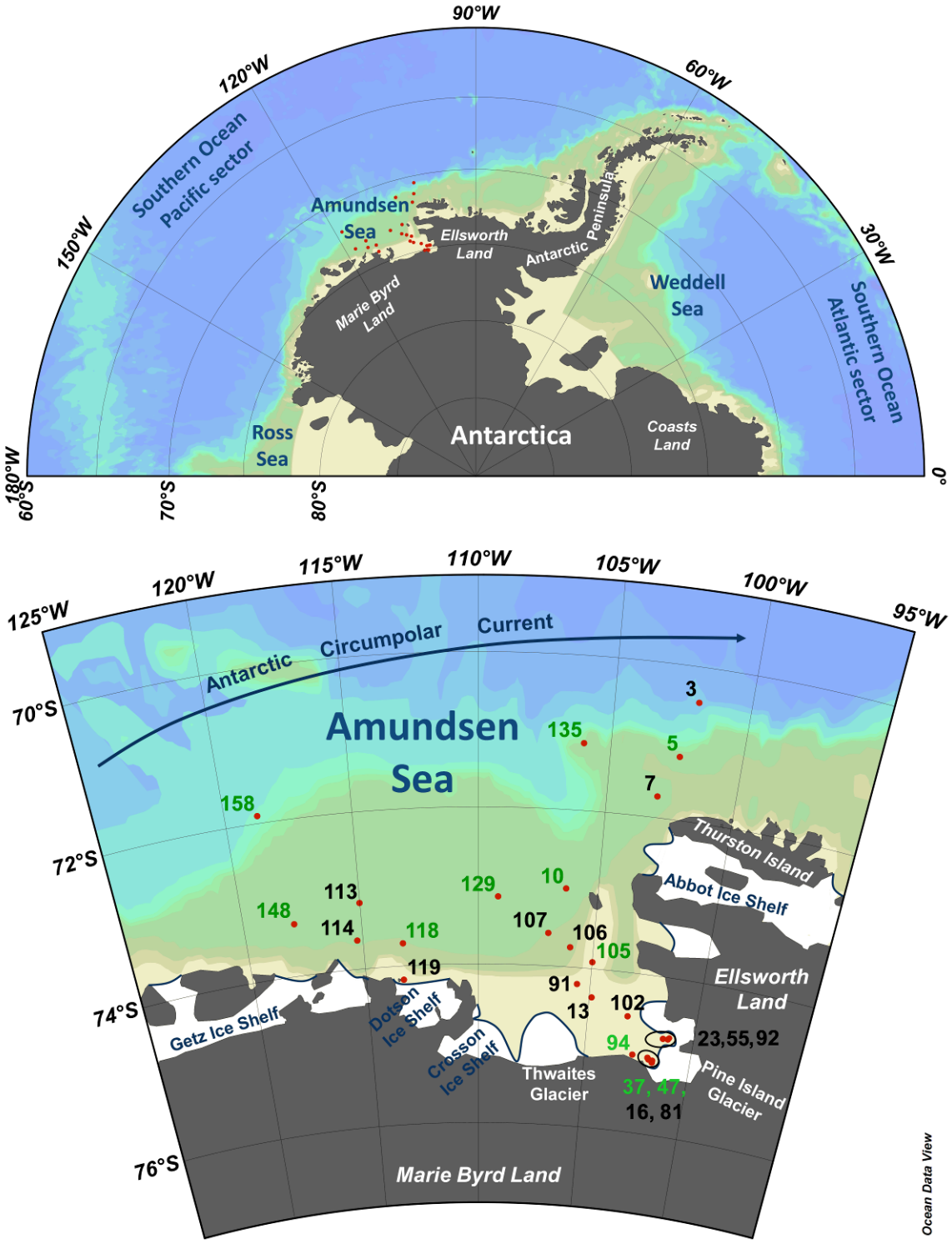

Figure 1: *Map of the Western part of Antarctica (on top) with the studied area (enlarged below). The stations sampled in the Amundsen Sea are shown with red dots and number (Vertical profile in black and sub-surface sampling in green).*

Table 1: *Stations sampled for this study, with number, sampling date, coordinates, location, bottom depth and sea-ice conditions (* 0 = sea-ice free; ½ = partly covered; 1 = completely covered). PIP: Pine Island Polynya; PIG: Pine Island Glacier; AP: Amundsen Polynya; DIS: Dotson Ice Shelf. At the profile stations samples were taken at several depths as listed in table 2. Sub-surface (Sub-S) samples were taken at 10-15 m depth.*

Station	Date	Lat. (°S)	Long. (°W)	Location		Bottom depth (m)	Sea-ice condition*	Sampling type
3	12-Jan	70.46	101.93	Open Ocean		3292	0	Profile
5	13-Jan	71.19	102.38	Slope	Eastern part	1095	½	Sub-S
7	14-Jan	71.73	103.04	Shelf		763	1	Profile
10	15-Jan	73.01	106.35	PIP		763	0	Sub-S
13	16-Jan	74.36	104.89	PIP		1294	0	Profile
16	17-Jan	75.07	101.77	PIG	Southern part	948	0	Profile
23	18-Jan	74.77	101.43	PIG	Northern part	739	0	300 m
37	20-Jan	75.04	102.01	near PIG	Southern part	921	0	Sub-S
47	22-Jan	75.06	101.95	near PIG	Southern part	805	0	Sub-S
55	23-Jan	74.77	101.30	PIG	Northern part	677	0	Profile
81	25-Jan	75.09	101.78	PIG	Southern part	940	0	Profile
91	27-Jan	74.21	105.60	PIP		1028	0	Profile
92	28-Jan	74.77	101.20	PIG	Northern part	670	0	Profile
94	28-Jan	75.02	102.74	near PIG	Southern part	805	0	Sub-S
102	30-Jan	74.55	103.18	PIP		1091	0	Profile
105	31-Jan	73.92	105.00	PIP		318	0	Sub-S
106	31-Jan	73.75	106.02	PIP		873	0	Profile
107	1-Feb	73.58	107.00	PIP		970	0	Profile
113	3-Jan	73.16	115.02	AP		763	0	Profile
114	3-Jan	73.63	115.25	AP		923	0	Profile
118	4-Feb	73.71	113.29	AP		837	0	Sub-S
119	4-Jan	74.17	113.34	DIS		588	0	Profile
129	7-Feb	73.14	109.18	PIP		460	0	Sub-S
135	10-Feb	71.13	106.03	Slope	Eastern part	518	1	Sub-S
148	13-Feb	73.34	117.86	AP		365	0	Sub-S
158	15-Feb	71.90	118.71	Slope	Western part	1118	½	Sub-S

3. Results

3.1. Dissolved iron

Concentrations of dissolved Fe (DFe) in this study ranged between 0.042 nM (= 42 pM) at the chlorophyll maximum (St. 3) and 1.31 nM at the surface near the Pine Island Glacier (St. 55) (Table 2, Figures 2A and 2B). Sub-surface minima in DFe

concentrations were measured just below the chlorophyll maximum (20-25 m depth) at all stations except for those located near the Pine Island Glacier where almost no phytoplankton was present. Surface concentrations (10-15 m depth) were relatively high in the Pine Island Polynya and at St. 3; a much higher concentration (0.4 nM) was measured at St. 7 where sea-ice was abundant (Table 2, Figure 2B). Below the sub-surface minimum, the concentrations of DFe increased with depth to about 0.2 nM at St. 3, 7 and in the Amundsen Polynya, and to 0.2-0.6 nM in the Pine Island Polynya. Stations at or near the Pine Island Glacier had higher DFe concentrations (0.3-1.3 nM) that were relatively constant with depth. At the Dotson Ice Shelf (St. 119), DFe increased with depth from 0.14 nM at 25 m depth to 0.54 nM at 300 m depth (Table 2, Figure 2B).

3.2. Ligand characteristics

The concentrations and depth distributions of dissolved organic ligands (Lt) and excess ligands (L') varied between the different environments sampled. Within the bloom of the Pine Island Polynya (St. 13, 91, 106 and 107), the maximum values of [Lt] were observed at the surface (>0.6 Eq of nM Fe) and minima at 200 m depth (Table 2, Figure 2A). Along the edge of the bloom (St. 102), the maximum [Lt] was measured at 200 m depth (0.9 Eq of nM Fe). The concentrations of L' within the center of the bloom in the Pine Island Polynya (St. 13 and 91), were highest at the surface (0.56 and 0.88 Eq of nM Fe, respectively) and decreased with depth to 0.12 and 0.04 Eq of nM Fe at 300 m depth, respectively (Table 2, Figure 3A). At stations sampled a few days later during the bloom (St. 106 and 107, Figure 3A), [L'] increased from 0.41 to 0.58 Eq of nM Fe at St. 106 and from 0.32 to 0.64 Eq of nM Fe at St. 107. In the Amundsen Polynya, [Lt] and [L'] did not show any consistent trend with depth (Figures 2B and 3B). At St. 3 (open ocean) and St. 7 (sea-ice covered), Lt and L' concentrations were similar except in the upper 50 meters, where lower [Lt] and [L'] were measured at St. 7 than at St. 3 (Figures 2B and 3B).

Near the Pine Island Glacier (St. 16, 55, 81 and 92), [Lt] and [L'] were relatively high (>0.8 Eq of nM Fe) and variable at the surface, with the highest Lt

from this study measured at St. 55 (1.64 Eq of nM Fe). Below 100 m, [Lt] and [L'] were relatively constant, but differed between stations. These differences in [Lt] and [L'] between days presumably reflected the variable currents and hydrography in the vicinity of the Pine Island Glacier (Gerringa *et al.*, submitted). In contrast, at the Dotson Ice Shelf (Figures 2B and 3B), below the surface maximum, [Lt] and [L'] were relatively high and uniform with depth.

The [Lt]/[DFe] ratio highlights the saturation state of the organic ligands (Chapter 2; Thuróczy *et al.*, 2010b and 2011); this ratio is strictly above 1. A low ratio (close to 1) corresponds to ligands relatively saturated with Fe and indicates a low capacity of the ligands to bind and buffer additional Fe input. A relatively high ratio, above 5 for example, indicates that the ligand pool is unsaturated with Fe and can buffer additional Fe input. A high [Lt]/[DFe] therefore increases Fe solubility and maintains Fe in the dissolved phase.

The [Lt]/[DFe] ratios measured here showed consistent trends with depth and location. Polynyas were characterised by having the highest ratio at the surface (5-15), decreasing to values below 4 with depth (Figures 3A, 3B and 5). At the stations influenced by the upwelling of CDW from under the Pine Island Glacier, the ratios were very low (<2.5) and rather constant with depth. At the open ocean (St. 3) and sea-ice covered (St. 7) stations, surface minima in the ratio (1-2) were found above higher values (4-13) at a depth of about 50 m. The ratios from the deepest samples (300 m depth) were always lower than samples taken above in the polynyas.

Lastly, the conditional stability constant (K') varied between $10^{21.14}$ at 300 m at St. 16 (close to the Pine Island Glacier) and $10^{23.04}$ at 50 m depth at St. 114 (in the Amundsen Polynya) (Table 2). The K' values were often maximal at 50 and 100 m depth in the Pine Island Polynya. At St. 3 and 7, K' was maximal at the surface ($10^{22.5}$) and minimal at 50 m depth ($10^{21.5}$). At the Pine Island Glacier stations, K' ranged from $10^{21.14}$ to $10^{22.96}$, varying with depth, location and between days (*e.g.* St. 16 and 81 were taken almost at the same location).

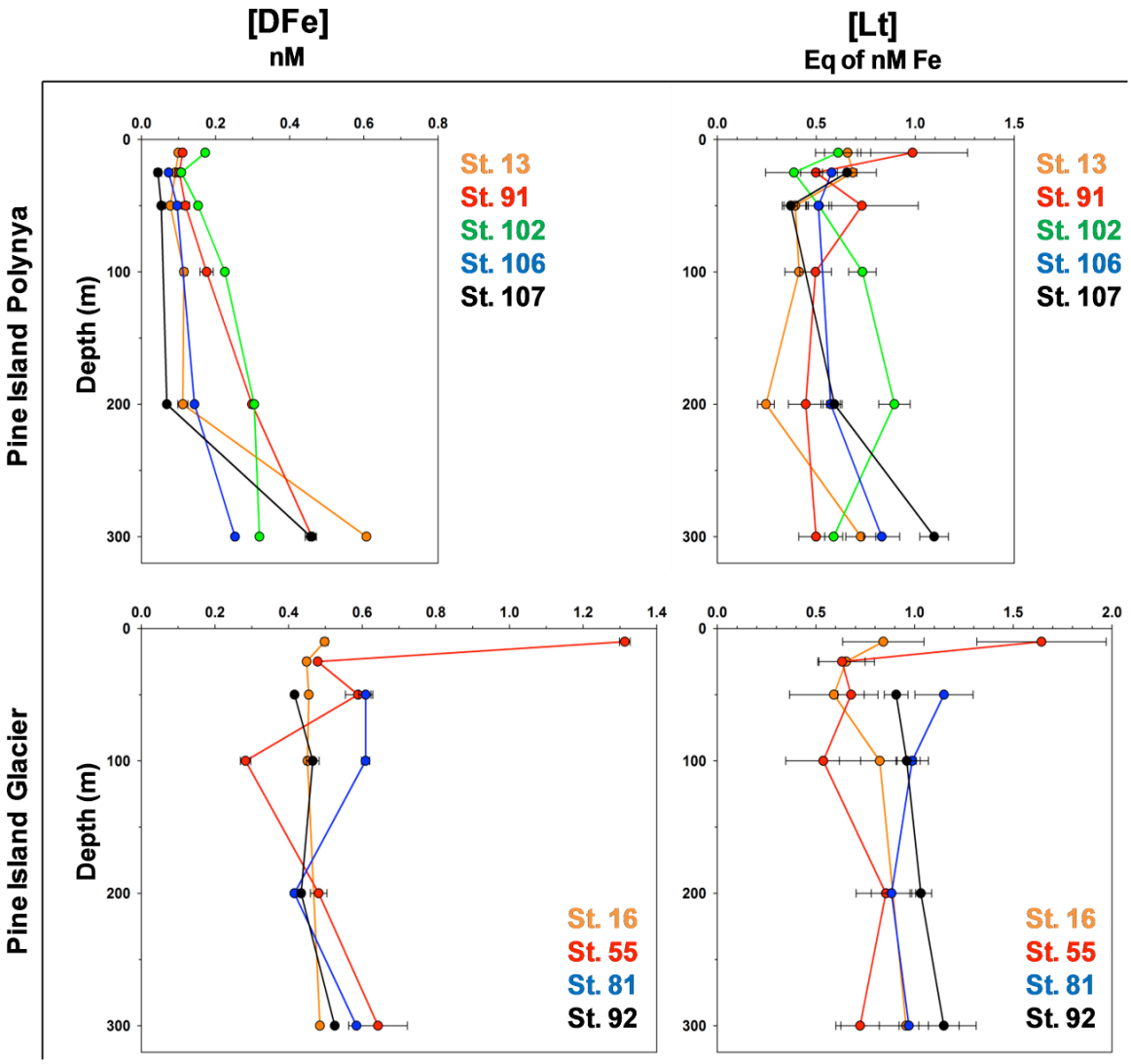

Figure 2A: *Vertical distribution of dissolved Fe (DFe, nM) and dissolved organic ligands (Lt, Eq of nM Fe) over the upper 300 meters (vertical axis, m) per area. Pine Island Polynya (St. 13, 91, 102, 106, 107) and Pine Island Glacier (St. 16, 55, 81, 92). Note the expanded scale (concentrations) at the Pine Island Glacier stations.*

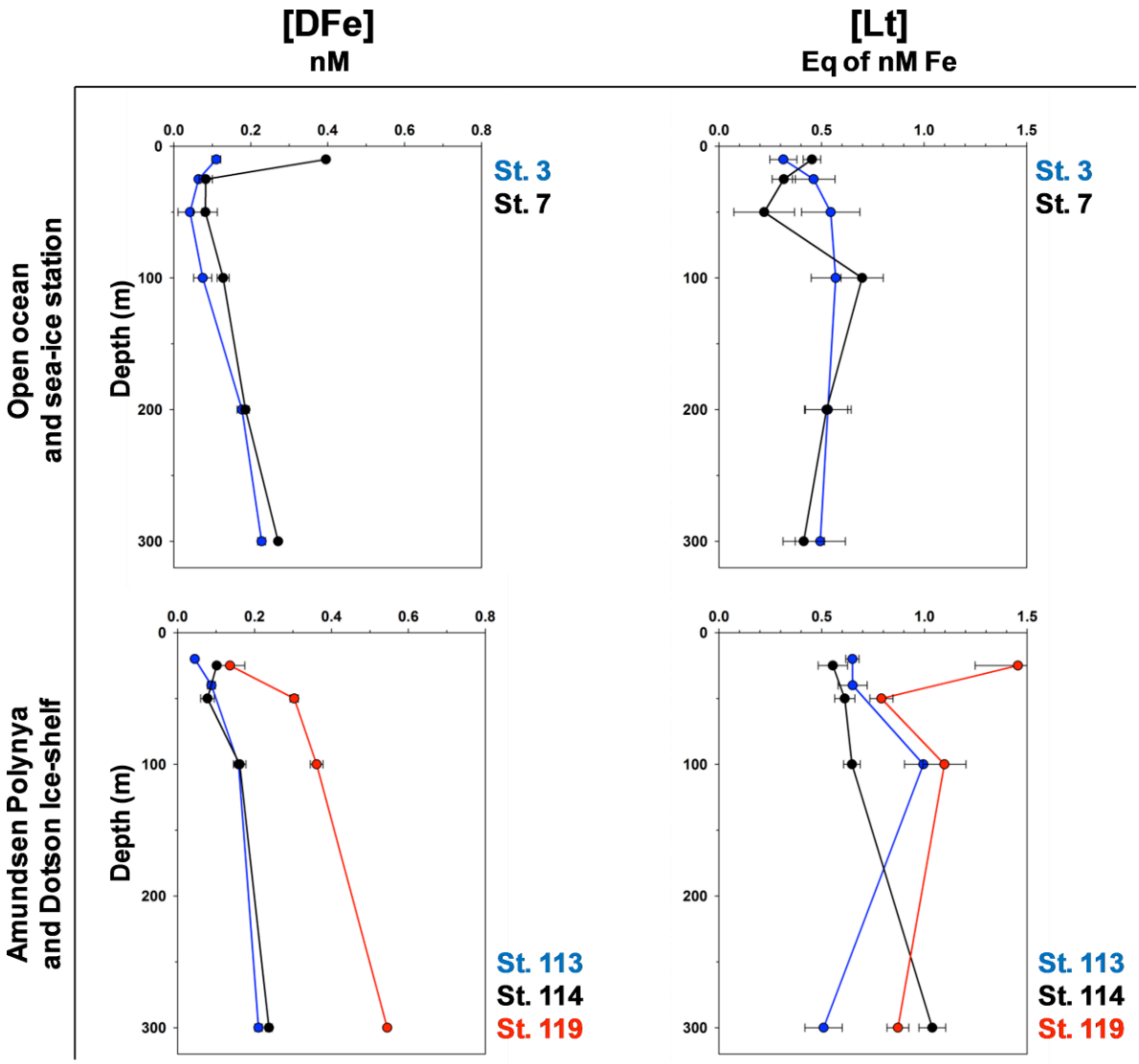

Figure 2B: *Vertical distribution of dissolved Fe (DFe, nM) and dissolved organic ligands (Lt, Eq of nM Fe) over the upper 300 meters (vertical axis, m) per area. Open ocean (St. 3), sea-ice station (St. 7), Amundsen polynya (St. 113 and 114) and Dotson Ice-shelf (St. 119).*

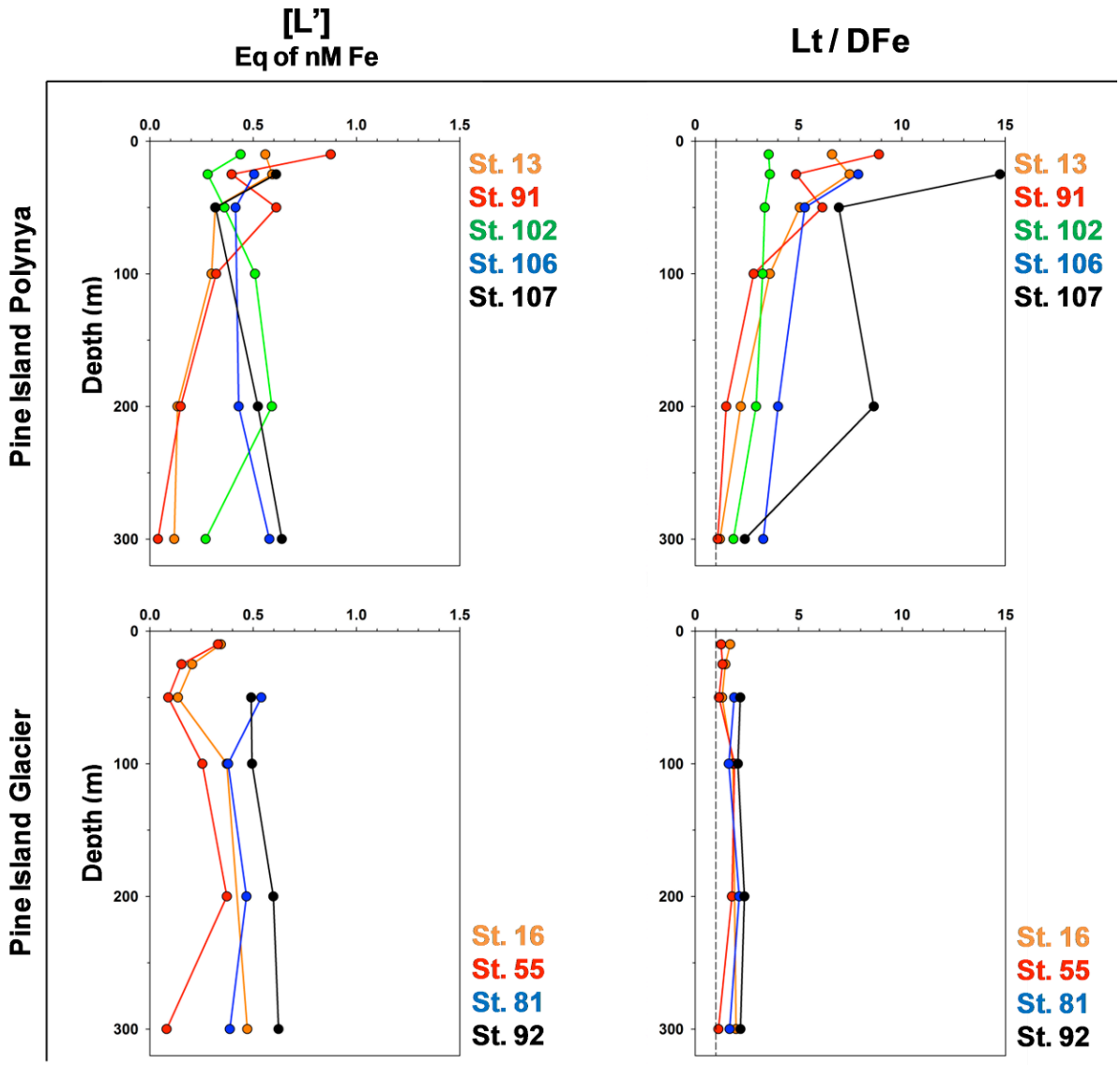

Figure 3A: *Vertical distribution of excess ligand (L', Eq of nM Fe) and ratio [Lt]/[DFe] over the upper 300 meters (vertical axis, m) per area. Pine Island Polynya (St. 13, 91, 102, 106, 107) and Pine Island Glacier (St. 16, 55, 81, 92).*

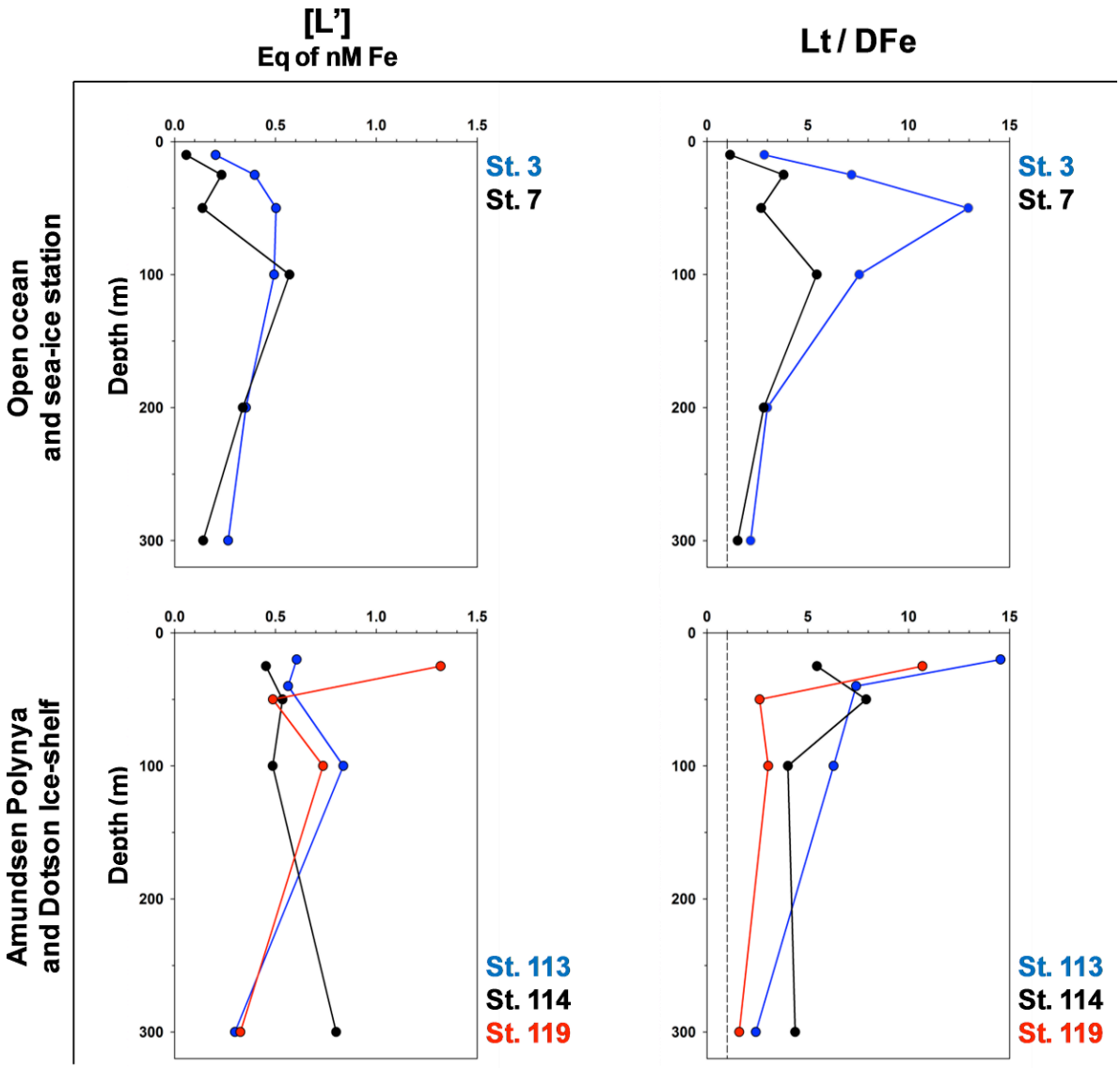

Figure 3B: *Vertical distribution of excess ligand (L', Eq of nM Fe) and ratio [Lt]/[DFe] over the upper 300 meters (vertical axis, m) per area. Open ocean (St. 3), sea-ice station (St. 7), Amundsen polynya (St. 113 and 114) and Dotson Ice-shelf (St. 119).*

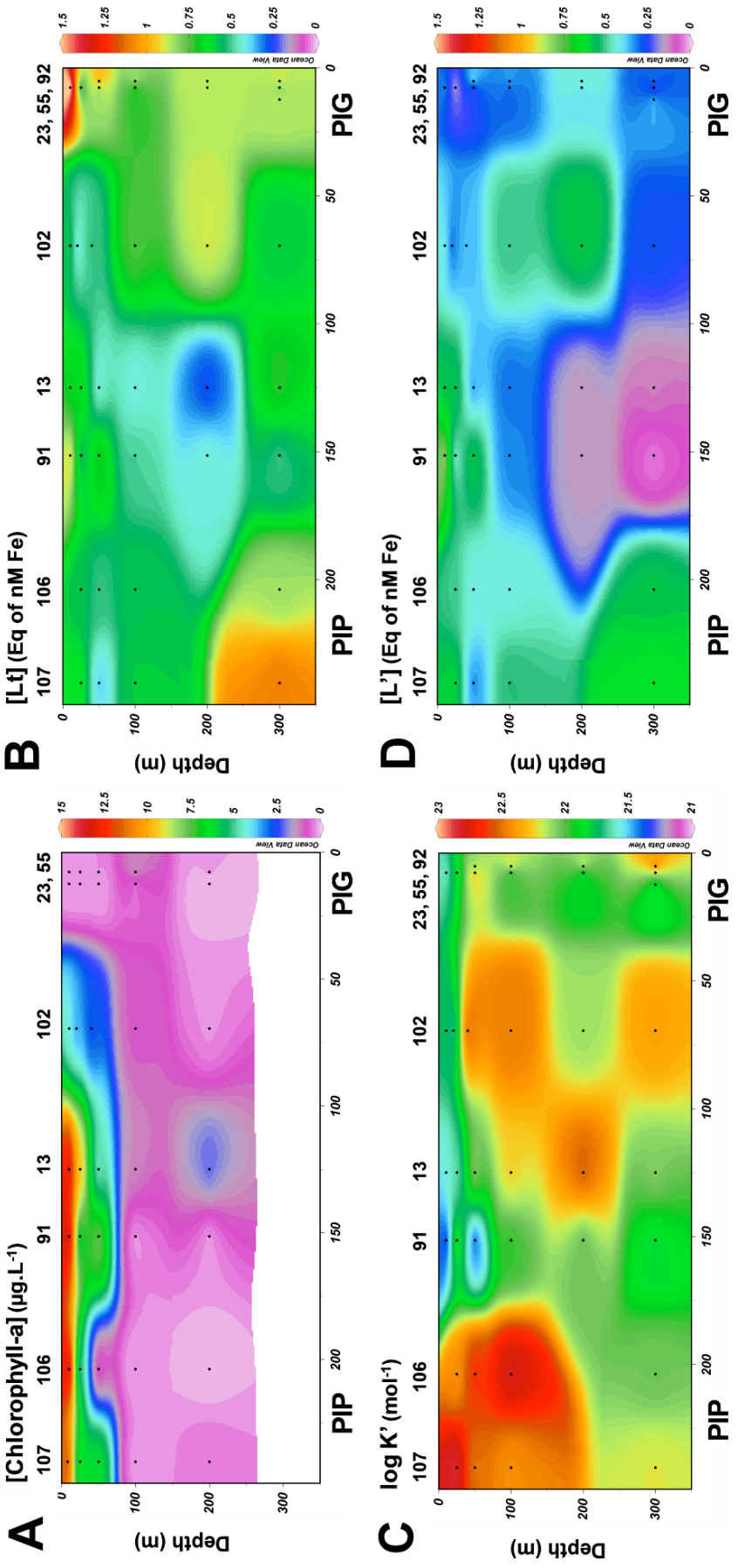
A
[Chlorophyll-a] (µg.L-1)
B
[Lt] (Eq of nM Fe)
C
log K' (mol-1)
D
[L'] (Eq of nM Fe)
Depth (m)
PIP
PIG
107
106
91
13
102
23, 55, 92
Ocean Data View

Figure 4 (Previous page): *Vertical color sections from the Pine Island Polynya (PIP, left) to the Pine Island Glacier (PIG, right) of* ***A:*** *chlorophyll-a concentration,* ***B:*** *Lt concentration,* ***C:*** *log K', and* ***D:*** *L' concentration. The lower horizontal axis represents the distance (km) from the Pine Island Glacier; station numbers are shown in the upper axis. Made using Ocean Data View.*

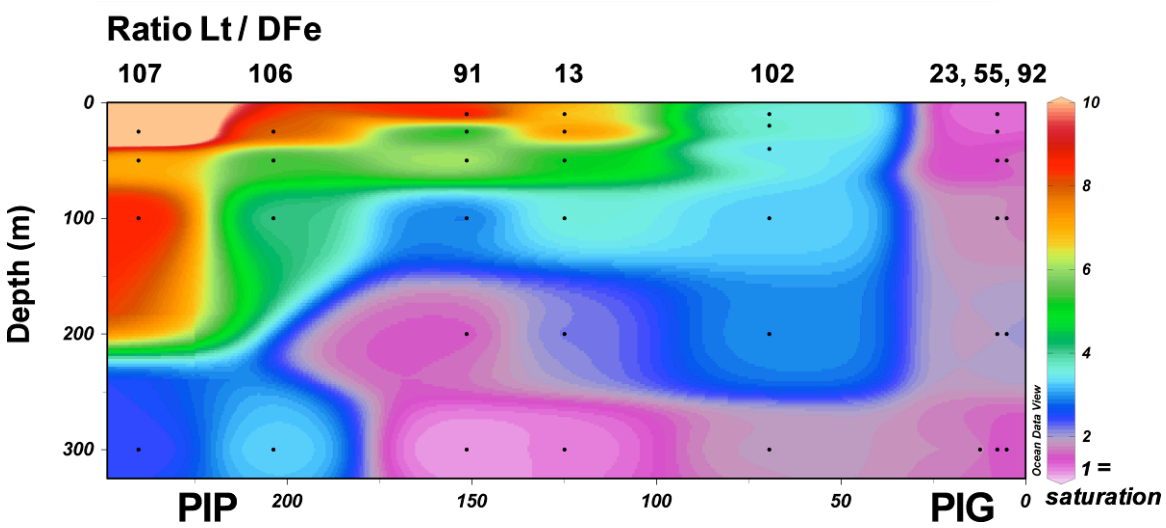

Figure 5: *Vertical color section of the [Lt]/[DFe] ratio from the Pine Island Polynya (PIP, left) to the Pine Island Glacier (PIG, right). The lower horizontal axis represents the distance (km) from the Pine Island Glacier; station numbers are shown in the upper axis. Made using Ocean Data View.*

4. Discussion

In 2009, the austral summer phytoplankton blooms persisted for more than 70 days in the Pine Island and Amundsen Polynyas (Arrigo *et al.*, submitted). Such productive blooms require a large supply of major nutrients (nitrate, phosphate and silicate) but also of the essential trace nutrient Fe. In the Amundsen Sea, the presence of Fe-complexing organic ligands, combined with the various sources of Fe (Gerringa *et al.*, submitted), played an important role in keeping Fe in solution and enhancing its availability to the phytoplankton bloom.

4.1. Upwelling of CDW on the continental shelf and underneath the ice shelves

In the Amundsen Sea, warm and salty CDW at a depth of 200-500 m flows along the continental shelf towards the Antarctic continent. While in transit, the CDW is likely enriched in both ligands and Fe by sediment resuspension and by degradation of settling organic matter produced at the sea surface. The enrichment of ligand concentrations by sediments has been observed previously in deep waters of the Kerguelen Plateau (Gerringa *et al.*, 2008) and on Arctic shelves (Chapter 6; Thuróczy *et al.*, accepted). In the Ross Sea, Fitzwater *et al.* (2000) attributed high concentrations of particulate Fe to re-suspension of sediments from the continental shelf. In this study, only the upper 300 meters were sampled, but because upwelling in the Amundsen Sea brings CDW close to the surface, higher ligand concentration partly due to sediment enrichment was observed at both the Pine Island Glacier ([Lt]>1 Eq of nM Fe, Figure 4-B) and the Dotson Ice Shelf.

Furthermore, this warm CDW drives basal melting of the floating glaciers and ice-shelves. Together with the land erosion caused by glacier and ice shelf motion, terrigenous material is released into the seawater. Terrigenous materials quickly (within 2h, as seen for Co and Zn, Thuróczy *et al.*, 2010a) release metals that are weakly bound to their matrix once in contact with seawater. This likely contributes the elevated concentrations of DFe (>0.4 nM, Table 2 and Figure 2A) and total dissolvable Fe ([TDFe]>30 nM, from unfiltered samples, Gerringa *et al.*, submitted) measured at the ice shelf stations. However, large refractory particles sink before complete dissolution whereas finer particles can be transported away from the glacier and ice-shelf to dissolve over time, thereby releasing their Fe into the seawater. Therefore, land erosion is likely to be a source of Fe but not of ligands (no organic matter input), as confirmed by the [Lt]/[DFe] ratios that are near saturation at the ice shelf stations.

4.2. Phytoplankton bloom

Within the blooms of the Pine Island and Amundsen Polynyas, phytoplankton uptake resulted in low concentrations of DFe (Table 2, Figures 2A and 4-A). On the section from the Pine Island Polynya to the Pine Island Glacier (Figures 4-A and 5) the phytoplankton bloom was accompanied by very high [Lt]/[DFe] ratios (>5, Figures 3A and 5) due to both Fe uptake and ligand production from organic matter generated by the bloom. The ligands, being relatively un-saturated with Fe, enhanced the solubilisation of Fe from outside sources (as described below) via organic complexation. At stations 13 and 91, relatively lower binding strengths were measured (<21.6, Table 2, Figure 4-C) than at stations sampled a little later during the bloom (>22.4, St. 106 and 107). The increase of the binding strength between days indicates that the availability of Fe decreased and also suggests the increased production of siderophores by heterotrophic bacteria in order to enhance the availability of Fe under Fe-stress condition (Barbeau *et al.*, 2001; Butler, 2005; Maldonado *et al.*, 2005). This is consistent with observations by Rue and Bruland (1997), Cullen *et al.* (2006) and Hunter and Boyd (2007) who demonstrated the existence of relatively strong ligands in the presence of phytoplankton.

The presence of phytoplankton and other microorganisms during the spring and summer generates huge quantities of organic matter (Pusceddu *et al.*, 1999). Sarthou *et al.* (2008) suggested that approximately 50% of the Fe used by phytoplankton could be regenerated at the surface. Degradation and remineralisation of organic matter could aid in the regeneration of ligands and Fe in surface waters. This organic matter could be either immediately utilised by plankton or become trapped within the sea-ice later in the season (Kepkay *et al.*, 1994; Sedwick and DiTullio, 1997; Thomas *et al.*, 2001; Grotti *et al.*, 2005; Lannuzel *et al.*, 2007 and 2008) and then released the following season when the sea-ice melts (Lannuzel *et al.*, 2010). Iron and ligands released from melting sea-ice may be pivotal for initiating the spring phytoplankton bloom. Because of the continuous uptake of Fe and production of ligands by phytoplankton blooms in the Pine Island Polynya and Amundsen Polynya, the ligands remain un-saturated with

Fe. This allows any remineralised Fe to be kept in solution and available for further phytoplankton growth.

4.3. Role of the ligands in solubilising Fe from the particulate phase

At stations located near the Pine Island Glacier and Dotson Ice Shelf, high concentrations of DFe (>0.4 nM, Table 2 and Figures 2A and 2B) and TDFe (>30 nM, Gerringa *et al.*, submitted) were measured. Because of these high concentrations of DFe and Lt, the ensuing [Lt]/[DFe] ratio indicated that ligands were near saturation (ratio <2, hence low L' concentrations), consequently removal of non-ligand bound Fe via scavenging may increase. This high potential for scavenging removal of Fe in the vicinity of the Pine Island Glacier is likely to enrich the deep waters in particulate Fe, generating a loop such that when particulate Fe reaches the CDW it upwells from beneath the glacier. On the transect from the Pine Island Glacier to the Pine Island Polynya, the concentrations of TDFe from unfiltered samples still was relatively high up to 100 km away from the Pine Island Glacier (St. 102, 103, 104; Gerringa *et al.*, submitted). This either suggests that particulate Fe can be transported laterally for relatively long distances, as has been seen over the Arctic continental slope (Chapter 6), or simply that particulate Fe close to the glacier is mainly inorganic compared to the particulate Fe within the bloom that is mainly organic (contained in phytoplankton cells). In the upper 50 m of the water column between the Pine Island Glacier and PIB, organic ligands became increasingly desaturated (ratio [Lt]/[DFe], Figures 3A and 5), indicating an increasing capacity to bind and buffer Fe from outside sources. On the same transect, there were a clear decrease in [TDFe] (Gerringa *et al.*, submitted), in [DFe], and [Lt] but an increase in [L'] (Figures 3A and 4). These trends suggest a possible exchange of Fe from the particulate to the dissolved phase (*e.g.* Fe solubilisation), due to the presence of un-saturated organic ligands. This Fe solubilisation process could be responsible for the horizontal transport of particulate Fe away from the glacier.

4.4. Winter hypothesis

During the winter season when little biologic Fe uptake takes place, the ligands will become fully saturated (very low [Lt]/[DFe] ratios) with the continuous input of Fe from the glacier-upwelling. This might lead to export of non-complexed Fe towards the bottom. During the spring, [L'] was very low at the Pine Island Glacier stations (Table 2, Figure 6), leaving few free ligands for new Fe sources. Input of Fe from glacial sources during the winter would be unable to remain in solution and would precipitate when excess ligand concentrations become lower than the solubility product of the Fe oxy-(hydr)oxides. Furthermore, at the stations close to the glaciers, the high TDFe concentrations (Gerringa *et al.*, in prep), together with the presence of saturated organic ligands, might facilitate vertical export of Fe via scavenging as, already suggested by Sedwick *et al.* (2000) in the Ross Sea. The Fe export towards the bottom suggests a "winter enrichment" of the deep waters (the CDW) in the vicinity of the glaciers. Part of the exported Fe might be remineralised and upwelled again after reaching the CDW flow, creating a "loop" pathway for Fe.

Table 2 (Below and next page): *Concentrations of dissolved Fe ([DFe] in nM ± standard deviations, S.D.) and Fe-binding ligand characteristics of all samples. Total ligand and excess ligand concentrations ([Lt] and [L'], respectively) are in Eq of nM Fe (± standard deviations, S.D.). Conditional stability constants K' are in mol^{-1} with S.D.; Sensitivity S with is also given with S.D.*

Location	Station number	Depth (m)	[DFe] (nM)	S.D.	[Lt] (Eq of nM Fe)	S.D.	log K' (mol^{-1})	S.D.	Sensitivity	S.D.	[L'] (Eq of nM Fe)	log alpha L	pFe (M)	Lt/Fe
Open ocean	3	10	0.110	0.011	0.314	0.066	22.49	0.42	1.53	0.01	0.20	12.80	22.75	2.84
		25	0.064	0.007	0.461	0.104	21.78	0.38	2.19	0.03	0.40	12.38	22.57	7.17
		50	0.042	0.031	0.545	0.142	21.40	0.20	2.18	0.04	0.50	12.10	22.48	12.96
		100	0.075	0.024	0.569	0.119	21.63	0.19	1.54	0.03	0.49	12.33	22.45	7.55
		200	0.177	0.013	0.531	0.114	21.95	0.36	2.07	0.04	0.35	12.49	22.25	2.99
		300	0.228	0.010	0.494	0.123	22.07	0.30	1.55	0.03	0.27	12.50	22.14	2.16
Continental slope	5	10-15	0.220	N.D.	0.522	0.270	21.44	0.32	2.18	0.05	0.30	11.92	21.58	2.37
	135	10-15	0.126	N.D.	0.853	0.039	22.31	0.12	1.94	0.01	0.73	13.18	23.08	6.79
	158	10-15	0.087	N.D.	0.908	0.051	22.16	0.11	1.88	0.02	0.82	13.07	23.13	10.44
Shelf	7	10	0.395	0.000	0.453	0.042	22.41	0.27	1.94	0.021	0.06	12.18	21.58	1.15
		25	0.083	0.017	0.316	0.056	22.34	0.31	1.34	0.015	0.23	12.70	22.78	3.80
		50	0.082	0.031	0.220	0.148	21.59	0.41	1.87	0.04	0.14	11.73	21.82	2.69
		100	0.128	0.016	0.698	0.103	21.83	0.15	1.73	0.037	0.57	12.59	22.48	5.44
		200	0.186	0.010	0.524	0.103	22.01	0.38	2.06	0.036	0.34	12.54	22.27	2.81
		300	0.271	0.001	0.413	0.101	22.37	0.38	1.49	0.030	0.14	12.52	22.09	1.52
PIP	10	10-15	0.098	N.D.	0.396	0.186	21.50	0.32	1.41	0.02	0.30	11.98	21.99	4.06
	13	10	0.099	0.004	0.658	0.117	21.56	0.16	1.79	0.03	0.56	12.30	22.31	6.62
		25	0.092	0.005	0.684	0.119	21.61	0.16	1.52	0.02	0.59	12.38	22.42	7.47
		50	0.078	0.013	0.394	0.065	22.12	0.36	1.85	0.02	0.32	12.62	22.73	5.06
		100	0.115	0.009	0.413	0.071	22.27	0.60	1.41	0.02	0.30	12.75	22.69	3.61
		200	0.112	0.014	0.246	0.042	22.58	0.36	1.73	0.01	0.13	12.70	22.66	2.20
		300	0.607	0.004	0.725	0.076	22.08	0.21	1.50	0.02	0.12	12.15	21.37	1.19
	91	10	0.111	0.004	0.986	0.278	21.28	0.21	1.57	0.04	0.88	12.22	22.17	8.89
		25	0.102	0.012	0.498	0.076	21.98	0.25	1.90	0.03	0.40	12.57	22.56	4.88
		50	0.119	0.011	0.731	0.284	21.33	0.34	1.84	0.05	0.61	12.11	22.04	6.15
		100	0.176	0.018	0.496	0.080	21.93	0.29	1.49	0.02	0.32	12.44	22.19	2.83
		200	0.298	0.008	0.447	0.087	21.99	0.37	1.44	0.02	0.15	12.17	21.69	1.50
		300	0.460	0.005	0.499	0.087	21.79	0.25	1.73	0.02	0.04	11.38	20.72	1.08
	102	10	0.172	0.006	0.611	0.114	21.76	0.25	1.90	0.03	0.44	12.40	22.16	3.55
		20	0.107	0.001	0.387	0.144	21.62	0.60	1.39	0.02	0.28	12.07	22.04	3.61
		40	0.153	0.005	0.514	0.063	22.56	0.55	1.45	0.02	0.36	13.12	22.94	3.37
		100	0.225	0.004	0.733	0.069	22.48	0.23	1.86	0.05	0.51	13.18	22.83	3.26
		200	0.304	0.006	0.895	0.079	22.11	0.14	1.48	0.03	0.59	12.88	22.40	2.94
		300	0.318	0.005	0.588	0.046	22.37	0.19	1.39	0.02	0.27	12.80	22.30	1.85
	105	10-15	0.095	0.003	0.222	0.262	21.34	0.42	1.28	0.04	0.13	11.44	21.47	2.35
	106	25	0.073	0.003	0.578	0.061	22.41	0.37	1.66	0.02	0.50	13.11	23.25	7.89
		50	0.096	0.002	0.511	0.053	22.64	0.83	1.48	0.01	0.41	13.26	23.27	5.30
		100	0.143	0.005	0.573	0.049	22.79	0.79	1.68	0.02	0.43	13.42	23.26	4.01
		300	0.252	0.007	0.831	0.091	22.03	0.19	1.51	0.02	0.58	12.79	22.39	3.29
	107	25	0.044	0.010	0.656	0.049	22.85	0.60	1.44	0.01	0.61	13.63	23.99	14.75
		50	0.053	0.005	0.372	0.034	22.49	0.30	1.44	0.01	0.32	12.99	23.26	6.95
		100	0.068	0.002	0.591	0.039	22.42	0.18	1.43	0.01	0.52	13.14	23.31	8.64
		300	0.457	0.015	1.096	0.072	22.20	0.15	1.91	0.02	0.64	13.01	22.35	2.40
	129	10-15	0.081	N.D.	0.912	0.092	21.90	0.15	1.54	0.02	0.83	12.82	22.92	11.31

Location	Station number	Depth (m)	[DFe] (nM)	S.D.	[Lt] (Eq of nM Fe)	S.D.	log K' (mol^{-1})	S.D.	Sensitivity	S.D.	[L'] (Eq of nM Fe)	log alpha L	pFe (M)	Lt/Fe
PIG (Northern part)	23	300	0.446	0.007	0.883	0.135	21.54	0.14	1.56	0.03	0.44	12.18	21.53	1.98
	55	10	1.313	0.014	1.643	0.328	21.59	0.13	2.17	0.13	0.33	12.11	20.99	1.25
		25	0.479	0.003	0.632	0.117	21.80	0.26	1.72	0.02	0.15	11.99	21.31	1.32
		50	0.589	0.035	0.678	0.067	22.41	0.36	1.46	0.02	0.09	12.36	21.59	1.15
		100	0.283	0.014	0.537	0.190	21.66	0.64	1.21	0.03	0.25	12.06	21.61	1.90
		200	0.482	0.022	0.854	0.151	21.58	0.18	1.63	0.03	0.37	12.15	21.47	1.77
		300	0.643	0.080	0.724	0.097	22.04	0.27	1.88	0.03	0.08	11.95	21.14	1.13
	92	50	0.610	0.019	1.149	0.147	21.96	0.22	1.21	0.02	0.54	12.69	21.91	1.88
		100	0.609	0.011	0.988	0.083	22.48	0.21	1.46	0.04	0.38	13.06	22.27	1.62
		200	0.416	0.005	0.883	0.103	22.43	0.24	1.27	0.05	0.47	13.10	22.48	2.12
		300	0.584	0.002	0.971	0.050	22.75	0.24	1.58	0.02	0.39	13.34	22.57	1.66
PIG (Southern part)	16	10	0.498	0.009	0.842	0.206	21.57	0.32	1.86	0.04	0.34	12.11	21.41	1.69
		25	0.449	0.007	0.653	0.144	21.94	0.35	1.67	0.05	0.20	12.25	21.60	1.46
		50	0.455	0.007	0.591	0.224	21.41	0.38	1.57	0.03	0.14	11.54	20.89	1.30
		100	0.451	0.008	0.823	0.204	21.34	0.19	1.79	0.04	0.37	11.91	21.26	1.82
		300	0.485	0.001	0.96	0.36	21.14	0.24	2.04	0.05	0.47	11.82	21.13	1.97
	37	10-15	0.236	0.045	0.640	0.096	22.12	0.41	1.55	0.02	0.40	12.73	22.35	2.71
	47	10-15	0.247	N.D.	0.729	0.148	21.60	0.21	1.89	0.04	0.48	12.28	21.89	2.95
	81	50	0.416	0.001	0.907	0.060	22.36	0.17	1.54	1.50	0.49	13.05	22.43	2.18
		100	0.466	0.017	0.960	0.048	22.96	0.43	1.82	1.78	0.49	13.65	22.98	2.06
		200	0.434	0.008	1.032	0.055	22.33	0.14	1.62	1.59	0.60	13.11	22.47	2.38
		300	0.525	0.006	1.148	0.078	22.18	0.15	2.01	1.95	0.62	12.98	22.26	2.19
	94	10-15	0.094	0.001	0.620	0.173	21.53	0.23	1.79	0.05	0.53	12.25	22.28	6.61
AP	113	20	0.045	0.005	0.650	0.032	22.60	0.20	1.67	0.01	0.61	13.39	23.74	14.56
		40	0.088	0.010	0.651	0.071	22.39	0.33	1.26	0.02	0.56	13.14	23.20	7.39
		100	0.159	0.001	0.995	0.092	21.95	0.13	1.35	0.02	0.84	12.87	22.67	6.28
		300	0.210	0.010	0.509	0.091	21.98	0.31	1.37	0.02	0.30	12.46	22.14	2.42
	114	25	0.102	N.D.	0.554	0.071	22.26	0.37	1.67	0.02	0.45	12.91	22.91	5.45
		50	0.078	0.018	0.613	0.049	23.04	0.36	1.60	0.01	0.53	13.77	23.88	7.89
		100	0.161	0.016	0.647	0.041	22.63	0.30	1.36	0.01	0.49	13.31	23.10	4.01
		300	0.238	0.009	1.038	0.065	22.19	0.15	1.45	0.01	0.80	13.09	22.72	4.37
	118	10-15	0.109	N.D.	1.127	0.174	21.84	0.22	1.74	0.04	1.02	12.84	22.81	10.36
	148	10-15	0.077	N.D.	1.048	0.076	22.02	0.13	1.22	0.01	0.97	13.00	23.12	13.68
DIS	119	25	0.136	0.038	1.455	0.209	21.78	0.11	1.55	0.07	1.32	12.90	22.76	10.68
		50	0.303	0.011	0.791	0.056	22.14	0.12	1.92	0.02	0.49	12.82	22.34	2.61
		100	0.362	0.016	1.097	0.105	21.87	0.11	1.61	0.03	0.74	12.74	22.18	3.04
		300	0.545	0.000	0.871	0.053	22.54	0.16	1.87	0.02	0.33	13.05	22.32	1.60

5. Summary

During the austral summer 2009 in the Amundsen Sea, the organic complexation of Fe proved to be a major process enhancing Fe availability for phytoplankton, thus contributing to the long-lasting bloom.

The inflow of Circumpolar Deep Water onto the Amundsen continental shelf was enriched in both Fe and ligands by the sediment resuspension. Further Fe and ligand enrichment took place when warmer CDW upwelled beneath the Pine Island Glacier causing basal melt of the glacier and releasing terrigenous material containing Fe into the seawater. The upwelling of this modified CDW at the Pine Island Glacier is likely an important source of both Fe and ligands. The high concentrations of organic ligands (despite the low [L'] at the Pine Island Glacier stations) increased Fe solubility, thus maintaining a sufficient stock of Fe in solution, increasing its bioavailability to the phytoplankton. In the Ross Sea Polynya and probably others, low Fe concentration cause the end of the bloom

(Arrigo *et al.*, 2000 and 2003); however in the Amundsen Sea region a prolonged phytoplankton bloom is facilitated through the continuous input of ligands and Fe in modified CDW that upwells from beneath the glaciers and ice shelves that surround the Amundsen and Pine Island Polynyas.

At the ice shelf stations, organic ligands were nearly saturated with Fe, as evidenced by the low [Lt]/[DFe] ratio (<2), corresponding to low excess ligand concentrations. This suggested a high probability for removal of any additional Fe inputs via scavenging and/or precipitation, leading in turn to an enrichment of Fe of the deep waters. Additionally, the massive phytoplankton blooms here produce huge quantities of organic matter, which is degraded and remineralised while sinking out of the water column and enriches the CDW that flows along the continental shelf and eventually upwells from beneath the glaciers and ice shelves. The uptake of Fe by the phytoplankton bloom, together with the production of organic ligands (organic matter and probably siderophores), caused the desaturation of the organic ligands at the surface. This likely favours the solubilisation of Fe from the particulate to the dissolved fraction from the Pine Island Glacier to the Pine Island Polynya. The undersaturation of ligands away from the glacier may play a role in the horizontal transport of Fe from the glacier northwards towards the polynyas by enhancing solubilisation of Fe from the particulate to the dissolved phase.

During the winter, when light is too low to support phytoplankton blooms, Fe is not consumed and organic ligands are saturated with Fe. This halts the solubilisation of Fe from the particulate phase, enhancing the loss of Fe via scavenging. Close to the glacier, the near saturated ligands during the spring become fully saturated, leaving no free space for binding new Fe input, leading to its loss via precipitation. The consequence of this Fe export from the surface to the bottom is winter enrichment of Fe in the CDW inflow, generating a loop pathway as CDW is upwelled beneath the ice shelves.

Chapter 8

Synthesis

1. Major findings

Despite the difficulty of measuring indirectly (titration of empty ligand sites with Fe additions) something that is hardly known (*i.e.* "ligand soup"), and on board a ship, the results obtained during this thesis project proved to be precious for bringing new arguments and hypothesis explaining mechanisms of the Fe cycle in the oceans. Thanks to elaborate equipment and procedures (sampling, filtration, conservation and analyses), the work could be performed in metal clean conditions, without contamination.

1.1. In the Eastern-North Atlantic Ocean

Our results collected during the first expedition (Chapter 3), at a station in the Eastern-North Atlantic Ocean off the coast of Portugal, revealed that unfiltered samples (TDFe concentrations) could be used to distinguish the Mediterranean overflow water (MOW) from other water masses. In addition, we used for the first time the ratio of [Excess L]/[Fe] as relative saturation state of the Fe-binding ligands per fraction. Concentration of Excess L shows a potential to bind Fe, a real amount of free ligand sites that is independent of Fe, whereas the reactivity of the ligands is expressed using the alpha factor ([Excess L] x K'). The ratio of [Excess L]/[Fe] is thus a complementary tool to describe the complexation of Fe in seawater. This parameter allows comparisons between stations, and ocean basins. Finally, the fraction <1000 kDa proved to be the most reactive, hence playing an important role in regulating dissolution, colloid aggregation and scavenging processes.

1.2. In the Atlantic sector of the Southern Ocean

In the Atlantic sector of the Southern Ocean (Chapters 4 and 5), high concentrations of unsaturated ligand were measured in upper waters as found at the station in the Easter-North Atlantic Ocean. This was related to biota with a combination of Fe uptake and ligand production via organic matter, and was especially distinct in HNLC regions. The ligands got more saturated with Fe with increasing depth and reached a constant saturation state at around 450 m depth

characterised by low and constant ratio [Lt]/[DFe] (below 4). This indicates a steady state between ligands and Fe and thus between stabilisation and removal of Fe (scavenging and co-precipitation) towards the seafloor. These dissolved organic ligands have a very strong buffering property, representing a step between sources and export removal of Fe, and their ubiquitous presence reveals the very resistant (refractory) nature of the ligands. Most of the ligands were actually found to exist in the smaller colloidal fraction (<1000 kDa). Along this expedition, we observed for the first time geographical (horizontal) trends in the organic complexation of Fe between different ocean basins by examining the ratio [Lt]/[DFe]. These trends in deep waters were attributed to an increasing distance from Fe sources and to scavenging of Fe. Analyses of the complexation of Fe in unfiltered samples confirmed that the particulate fraction (>0.2 μm) did not contain reversible adsorption sites (no Excess L), at least not within the measuring detection window established by the use of TAC. Therefore, the particulate fraction only has a role in scavenging and removal processes, as seen everywhere with the increasing concentrations of TDFe with depth.

1.3. In the Arctic Ocean

The conclusions on the speciation of Fe in the Arctic Ocean (Chapter 6) brought some rational explanations on the processes involved in the cycle of Fe. There also, distinct trends in Fe concentrations and ligand characteristics were observed vertically and horizontally, from the shelf seas towards the Makarov Basin in the central Arctic Ocean. The use of the ratio [TDFe]/[DFe] revealed a relative enrichment of particulate Fe towards the bottom at all stations, indicating ubiquitous scavenging and export of Fe towards the deep ocean. As expected and as found elsewhere, the organic ligands became nearly saturated with depth in the Amundsen and Nansen Basins. However, an exception was found at the station in the Makarov Basin. Here the ligands got more unsaturated with Fe towards the bottom. This unexpected change in the saturation state of the ligands between the deep basins was explained by a lower reactivity of the ligands (expressed by alpha = [Excess L] x K') and a lack of Fe sources in deep waters towards the central

Arctic. Despite the high potential of the organic ligands to buffer Fe in the deep Makarov Basin, the inputs of Fe from external sources may not be sufficient to counter balance the continuous scavenging of Fe, leading to a net export of Fe to the sediment.

1.4. In the Amundsen Sea, Southern Ocean

During the final expedition to the Southern Ocean in the Amundsen Sea (Chapter 7), the organic complexation of dissolved Fe in the upper 300 m of the water column has proven to play a crucial role in enhancing the local stock of Fe for phytoplankton blooms that lasted 70 days in 2009. There, the natural fertilisation of Fe of the upper waters was carried out by the upwelling of Circumpolar Deep Water (CDW) beneath the coastal glaciers and by subsequent melting of its basal part and of the surrounding sea-ice. Additionally, sediment resuspension may also represent a source of ligands to the CDW upwelling since higher concentrations of ligands were observed at the upwelling stations near the ice shelves. Thanks to the large glacier source, the organic ligands at the upwelling stations were highly saturated with Fe, hence increased the solubility of Fe, and consequently enhanced the stock of dissolved Fe and its transport towards the coastal polynyas. However, in the coastal upwelling regions, much of the glacial Fe supply (up to 90%) must be lost via scavenging and precipitation due to low buffering capacity of the nearly saturated organic ligands in conjunction with the much higher concentration of particulate Fe. Away from the glacier and towards the coastal polynyas, the organic ligands got desaturated with Fe in surface waters due to the uptake of Fe by the phytoplankton blooms. These relatively unsaturated ligands will most likely complex Fe released after remineralisation and may also be able to dissolve Fe from the particulate phase. Additionally, these unsaturated ligands probably buffer Fe from the continuous glacier/upwelling source, thus keeping a sufficient and more bioavailable stock of Fe to the phytoplankton bloom.

2. The organic complexation of Fe in the oceans: a summary

2.1. The size fractionation

Analyses of the complexation of Fe after ultra-filtration showed that most of the ligands present in the dissolved fraction appeared to be in fact in the smaller fraction (<1000 kDa) as shown by the concentrations of Excess L. Thus, changes of the organic ligands in the dissolved fraction were mainly due to changes of the small colloidal ligands. This smaller fraction was found to be most of the time less saturated with Fe but often slightly stronger ligands than the dissolved fraction, thus highlighting the dominance of small colloidal ligands (<1000 kDa) in controlling the distribution of Fe in seawater. Probably the smaller colloidal fraction was the main pool of ligands.

However, looking at the percentage of dissolved Fe actually present in the fraction <1000 kDa, differences were observed between the oceans. In the station in the Eastern-North Atlantic Ocean, approximately 19% of DFe was present in the smaller fraction (truly dissolved and small colloidal Fe, <1000 kDa). Whereas in the Arctic Ocean, 42-64% of DFe was truly dissolved and small colloidal around the chlorophyll maximum, and up to 74-83% of DFe elsewhere in the water column. In the Atlantic sector of the Southern Ocean, similar percentages were found in the upper waters, with approximately 70-80% of DFe actually present as truly dissolved and small colloidal Fe, and between 50 to 70% of DFe in the deeper waters. Only the upper waters in the Drake Passage were found to be similar to the station in the Eastern-North Atlantic Ocean regarding this proportion, with only 17% of DFe as truly dissolved and small colloidal Fe.

The variability in the percentage of Fe between the different colloidal pools reflects the different environments encountered, in terms of external Fe sources and of the different regimes regarding the primary productivity in surface waters. In the deeper ocean, this variable distribution of Fe over the size fractions is likely related to their residence time, which is influenced by the scavenging rates. In the Arctic Ocean, scavenging is relatively high as seen by the relative enrichment of particulate Fe with depth, and as confirmed by a loss of larger colloidal Fe. There, the larger colloidal Fe represented less than 25% of DFe. These large colloids

probably aggregated and can thus be an initiating step to scavenging. In comparison, scavenging appeared to occur at a lower rate in the Southern Ocean, where the percentage of larger colloidal Fe was higher, up to half of DFe, and even higher at the station in the Eastern-North Atlantic Ocean with up to 80% of DFe present as larger colloidal Fe. The circulation of the water masses might also play a role in these processes, and explain the influence of the missing dimension, the time.

2.2. The processes involved

Stabilisation of Fe in seawater is ensured by organic complexation with natural ligands, which increases the residence time of Fe in seawater, hence enhances its potential bioavailability. The reactivity (alpha value) and the saturation state of the ligands (ratio [Lt]/[Fe] or [Excess L]/[Fe]) proved to be excellent tools to explain the distribution and the fate of Fe in the different fractions when associated with the presence and strength of the sources of Fe like continental runoff, melting sea-ice and glaciers or upwelling of deep water. Where sources of Fe were present, the organic ligands got relatively saturated with Fe with increasing depth, whereas where sources of Fe were lacking, the ligands got desaturated with depth revealing a net loss of Fe. Thanks to unfiltered samples, removal processes could be explained. Concentrations of TDFe and the ratio [TDFe]/[DFe] revealed a relative enrichment of particulate Fe with depth and thus removal of Fe via scavenging. Scavenging was found to occur everywhere in all Arctic basins as well as in the Southern Ocean, probably by a permanent rain of particles towards the bottom. The particles with a high affinity to bind Fe will always compete with the dissolved ligands and remove Fe from the water column with the time, unless a source of Fe is present to keep the ligands relatively saturated with Fe. Therefore, the ligands represent a step between the inputs and export of Fe in the oceans. They act as a buffer that controls the solubility of Fe in seawater by their high affinity for Fe, but cannot prevent in the end from the loss via scavenging.

Ligands, sources and scavenging are therefore the three main characters controlling the residence time of Fe in the water column.

3. Discussion on the methods and opened windows on futures investigations

3.1. The organic complexation of Fe in seawater by voltammetry: What about two ligand groups?

The characterisation of the Fe-binding ligands as organic compounds was determined with voltammetric approaches in the middle 90s (Gledhill and Van Den Berg, 1994; Van Den Berg, 1995; Rue and Bruland, 1995). Since then, the knowledge of complexation of Fe in seawater is still predominantly based on results obtained by voltammetry techniques for one ligand group. Nevertheless, the presence of two distinct ligands groups is now widely admitted, with the L_1 siderophore-like ligand attributed to bacterial/microbial activity in upper waters, and the L_2 ligand originating from degradation of organic matter found in the whole water column. However, is the measuring method reliable enough to calculate the concentrations and stability constant of the two supposed ligand groups?

The determination of ligand concentration and stability constant for one group is based on a system with one equation and two unknowns (L' and K', or three together with the sensitivity S). However, the calculations for two groups of ligands are based on a system with a single equation with four unknowns (L'_1, K'_1, L'_2, K'_2, or five unknowns together with S). For the same number of measuring points via the titration, the degrees of freedom are lower in the second case, causing higher uncertainties on the determination of the 5 unknowns.

During our project, the titrations were initially done with 11 Fe additions ranging from 0.33 to 8 nM Fe. Later on, 14 Fe additions ranging from 0.2 to 10 nM Fe were used, with more additions in the low range of Fe additions. This simple change improved considerably the fit of the model and reduced the standard error on the estimated parameters for one ligand group due to an increase of the degrees of freedom. Unfortunately, no improvement was seen for the estimation of two ligand groups, with a very weak or even no fit of the two-ligand-model to the data. Another analytical way of determining two groups should be used, with an

increase of the Fe additions in the titration, a much higher sensitivity of the voltammeter in the low range of Fe addition (higher detection limit) and a wider detection window. The use of larger mercury electrode and other added ligand like salicylaldoxime (SA) proved to be useful to further investigate the two supposed ligand groups (Rue and Bruland, 1995; Buck *et al*., 2007; Buck and Bruland, 2007).

3.2. Filtration, ultra-filtration, unfiltered samples?

So far, filtration and ultra-filtration were used to separate different operationally defined size fractions like the dissolved fraction as <0.2 µm, the colloidal fraction (between 10-200 kDa and 0.2 µm) and soluble fraction (<10-200 kDa). Those fractions are operationally defined by the size cut-off of the filters used. In our study, the size cut-off of 1000 kDa allowed distinguishing the larger colloidal fraction (between 0.2 µm and 1000 kDa) and the fraction <1000 kDa containing small colloidal Fe and the soluble fraction. However, does it reflect the reality? Do we exactly know the effect of filtration? We know that filtration is affected by clogging effects due to aggregation of components on the filter that may be smaller than the size cut-off. Filtration apparently causes disequilibrium in seawater, as found at the station sampled in the Kara Sea of the Arctic Ocean (St. 279) or in deeper waters of the Southern Ocean (St. 128): How to give a rational explanation on the fact that filtration could increase the free ligand sites at these locations other than by concluding that new sites were created by breaking and/or dissociation of ligands, colloids and/or particles during filtration. In order to avoid disturbances generated by filtration and ultra-filtration on the equilibrium in seawater, would it not be needed to develop new separation procedures to study the properties of the ligands in non-disturbed fractions?

Unfiltered samples did bring promising results for concentrations of total dissolvable Fe, and also information that no contribution was given to reversible complexation/adsorption of Fe by the particulate fraction when comparing the concentrations of free ligand sites in both dissolved and unfiltered samples. Unfiltered samples, untouched and close to *in situ* conditions, should be

investigated with more care. The proportion of the different phases in unfiltered samples, like the organic phase, the biota and the mineral phase (refractory), should be estimated for each seawater sample in order evaluate their influence on the real (*i.e. in situ*) equilibrium of Fe between the different species.

3.3. Inter-comparison and future perspective

The determination of Fe complexation could benefit more from some improvements of the method, calculations and inter-comparison between countries and laboratories. The GEOTRACES program successfully initiated inter-comparison work. This common effort should be continued with collaborations, sharing of the knowledge and development of new research topics and techniques.

Finally, will the organic ligands be affected by a more acidic ocean? What will be then the fate of Fe in the ocean and the impact on the primary productivity? New techniques should be developed to study with care the complexation of essential trace metals in phytoplankton cultures at variable pH in order to predict future impact of the rapid changing climate.

References

Alderkamp, A.-C., Mills, M.M., van Dijken, G.L., Laan, P., Thuróczy, C.-E., Gerringa, L.J.A., De Baar, H.J.W., Payne, C., Tortell, P., Visser, R.J.W., Buma, A.G.J., Arrigo, K.R., **submitted**. Iron from melting glaciers fuels phytoplankton blooms in Amundsen Sea (Southern Ocean); phytoplankton characteristics and productivity. Deep-Sea Research Part II.

Alldredge, A., Passow, U., Logan, B., **1993**. The abundance and significance of a class of large, transparent organic particles in the ocean. Deep-Sea Research Part I 40 (6), 1131-1140.

Ambar, I., Serra, N., Neves, F., Ferraira, T., **2008**. Observations of the Mediterranean undercurrent and eddies in the Gulf of Cadiz during 2001. Journal of Marine System 71 (1-2), 195-220.

Anderson, L.G., Björk, G., Holby, O., Jones, E.P., Kattner, G., Koltermann, K.P., Liljeblad, B., Lindegren, R., Rudels, B., Swift, J.H., **1994**. Water masses and circulation in the Eurasian Basin: results from the Oden 91 expedition. Journal of Geophysical Research, Oceans 99 (C2), 3273-3283.

Arrigo, K.R., Worthen, D.L., Lizotte, M.P., Dixon, P., Dieckmann G., **1997**. Primary Production in Antarctic Sea Ice. Science 276 (5311), 394-397.

Arrigo, K.R., Robinson, D. H., Worthen, D. L., Dunbar, R. B., DiTullio, G. R., VanWoert, M., Lizotte, M. P., **1999**. Phytoplankton community structure and the drawdown of nutrients and CO2 in the Southern Ocean. Science 283 (5400), 365-367.

Arrigo, K.R., DiTullio, G.R., Dunbar, R.B., Lizotte, M.P., Robinson, D.H., VanWoert, M., Worthen, D.L., **2000**. Phytoplankton taxonomic variability and nutrient utilization and primary production in the Ross Sea. Journal of Geophysical Research 105 (C4), 8827-8846.

Arrigo, K.R., Dunbar, R.B., Robinson, D.H., Lizotte, M.P, **2002**. Taxon-specific differences in C/P and N/P drawdown for phytoplankton in the Ross Sea, Antarctica. Geophysical Research Letters 29 (19), 1938.

Arrigo, K.R., Van Dijken, G.L., **2003a**. Impact of iceberg C-19 on Ross Sea primary production. Geophysical Research Letters 30 (16), 1836.

Arrigo, K.R., Van Dijken, G.L., **2003b**. Phytoplankton dynamics within 37 Antarctic coastal polynyas systems. Journal of Geophysical Research 108 (C8), 3271.

Arrigo, K.R., Worthen, D.L., Robinson, D. H., **2003**. A coupled ocean-ecosystem model of the Ross Sea: 2. Iron regulation of phytoplankton taxonomic variability and primary production. Journal of Geophysical Research 108 (C7), 3231.

Arrigo, K.R., Lowry, K., van Dijken, G.L., **submitted.** Dynamics of sea ice and phytoplankton in polynyas of the Amundsen Sea, Antarctica. Deep-Sea Research Part II.

Babin, M., Morel, A., Gentili, B., **1996**. Remote sensing of sea surface Sun-induced chlorophyll fluorescence: Consequences of natural variations in the optical characteristics of phytoplankton and the quantum yield of chlorophyll a fluorescence. International Journal of Remote Sensing 17 (12), 2417-2448.

Barbeau, K., Rue, E.L., Bruland, K.W., Butler, A., **2001**. Photochemical cycling of iron in the surface ocean mediated by microbial iron(III)-binding ligands. Nature 413 (6854), 409-413.

Barré, N., Provost, C., Sennechael, N., Lee, J.H., **2008**. Circulation in the Ona Basin, southern Drake Passage. Journal of Geophysical Research 113 (C4), C04033.

Benner, R., **2011**. Loose Ligands and available iron in the Ocean, PNAS, www.pnas.org/cgi/doi/10.1073/pnas.1018163108.

Bergquist, B.A., Boyle, E.A., **2006**. Dissolved iron in the tropical and subtropical Atlantic Ocean. Global Biogeochemical Cycles 20 (1), GB1015.

Bergquist, B.A., Wu, J., Boyle, E.A., **2007**. Variability in oceanic dissolved iron is dominated by the colloidal fraction. Geochimica et Cosmochimica Acta 71 (12), 2960-2974.

Bonnet, S., Guieu, C., **2004**. Dissolution of atmospheric iron in seawater, Geophysical Research Letters 31 (3), L03303.

Bowie, A.R., Whitworth, D.J., Achterberg, E.P., Mantoura, R.F.C., Worsfold, P.J., **2002**. Biogeochemistry of Fe and other trace elements (Al, Co, Ni) in the upper Atlantic Ocean. Deep-Sea Research Part I 49 (4), 605-636.

Boye, M., Van Den Berg, C.M.G., **2000**. Iron availability and the release of iron-complexing ligands by Emiliania huxleyi. Marine Chemistry 70 (4), 277-287.

Boye, M., Van Den Berg, C.M.G., De Jong, J.T.M., Leach, H., Croot, P., De Baar, H.J.W., **2001**. Organic complexation of iron in the Southern Ocean. Deep-Sea Research Part I 48 (6), 1477-1497.

Boye, M., Aldrich, A.P., Van Den Berg, C.M.G., De Jong, J.T.M., Veldhuis, M., De Baar, H.J.W., **2003**. Horizontal gradient of the chemical speciation of iron in surface waters of the northeast Atlantic Ocean. Marine Chemistry 80 (2-3), 129-143.

Boye, M., Nishioka, J., Croot, P.L., Laan, P., Timmermans, K.R., De Baar, H.J.W., **2005**. Major deviations of iron complexation during 22 days of a mesoscale iron enrichment in the open Southern Ocean. Marine Chemistry 96 (3-4), 257-271.

Boye, M., Nishioka, J., Croot, P.L., Laan, P., Timmermans, K.R., Strass, V.H., Takeda, S., De Baar, H.J.W., **2010**. Significant portion of dissolved organic Fe-complexes in fact is Fe colloids. Marine Chemistry 126 (1-4), 20-27.

Breitbarth, E., Achterberg, E.P., Ardelan, M.V., Baker, A.R., Bucciarelli, E., Chever, F., Croot, P.L., Duggen, S., Gledhill, M., Hassellov, M., Hassler, C., Hoffmann, L.J., Hunter, K.A., Hutchins, D.A., Ingri, J., Jickells, T., Lohan, M.C., Nielsdottir, M.C., Sarthou, G., Schoemann, V., Trapp, J.M., Turner, D.R., Ye, Y., 2010. Iron biogeochemistry across marine systems - progress from the past decade. Biogeosciences 7 (3), 1075-1097.

Buck, K.N., Bruland, K.W., **2007**. The physicochemical speciation of dissolved iron in the Bering Sea, Alaska. Limnology and Oceanography 52 (5), 1800-1808.

Buck, K.N., Lohan, M.C., Berger, C.J.M., Bruland, K.W., **2007**. Dissolved iron speciation in two distinct river plumes and an estuary: Implications for riverine iron supply. Limnology and Oceanography 52 (2), 843-855.

Buffle, J., Leppard, G.G., **1995a**. Characterization of aquatic colloids and Macromolecules. 1. Structure and behaviour of colloidal material. Environmental Science and Technology 29 (9), 2169-2175.

Buffle, J., Leppard, G.G., **1995b**. Characterization of aquatic colloids and Macromolecules. 2. Key role of Physical structures on analytical results. Environmental Science and Technology 29 (9), 2176-2184.

Buma, A.G.J., De Baar, H.J.W., Nolting, R.F., Vanbennekom, A.J., **1991**. Metal enrichment experiments in the Weddell-Scotia Seas - Effects of iron and manganese on various plankton communities. Limnology and Oceanography 36 (8), 1865-1878.

Butler, A., **1998**. Acquisition and utilization of transition metal ions by marine organisms. Science 281 (5374), 207-210.

Butler, A., **2005**. Marine siderophores and microbial iron mobilization. BioMetals 18 (4), 369-374.

Carlson, C.A., Hansell, D.A., **2003**. The contribution of DOM on the biogeochemistry ot the Ross Sea. In: Biogeochemical cycles in the Ross Sea, AGU, Antarctic Research Series 78, 123-142.

Carmack, E.C., Foster, T.D., **1975**. On the flow of water out of the Weddell Sea. Deep-Sea Research 22 (11), 711-724.

Carmack, E.C., **1977**. Water characteristics of the Southern Ocean south of the Polar Front. In: Angel, M. (Ed.), A Voyage of Discovery, George Deacon 70th Anniversary Volume. Pergamon Press, Oxford, 15-41.

Chen, M., Wang, W.-X., Guo, L., **2003**. Phase partitioning and solubility of iron in natural seawater controlled by dissolved organic matter. Global Biogeochemistry Cycles 18 (4), GB 4013.

Coale, K.H., Johnson, K.S., Fitzwater, S.E., Gordon, R.M., Tanner, S., Chavez, F.P., Ferioli, L., Sakamoto, C., Rogers, P., Millero, F.J., Steinberg, P., Nightingale, P., Cooper, D., Cochlan, W.P., Landry, M.R., Constantinou, J., Rollwagen, G., Trasvina, A., Kudela, R., **1996**. A massive phytoplankton bloom induced by an ecosystem-scale iron fertilization experiment in the equatorial Pacific Ocean. Nature 383 (6600), 495-501.

Croot, P.L., Johanson, M., **2000**. Determination of iron speciation by cathodic stripping voltammetry in seawater using the competing ligand 2-(2-Thiazolylazo)-p-cresol (TAC). Electroanalysis 12 (8), 565-576.

Croot, P.L., Bowie, A.R., Frew, R.D., Maldonado, M.T., Hall, J.A., Safi, K.A., La Roche, J., Boyd, P.W., Law, C.S., **2001**. Retention of dissolved iron and Fe-II in an iron induced Southern Ocean phytoplankton bloom. Geophysical Research Letters 28 (18), 3425-3428.

Croot, P.L., Streu, P., Baker, A.R., **2004a**. Short residence time for iron in the surface seawater impacted by atmospheric dry deposition from Saharan dust events. Geophysical Research Letters 31 (23), L23S08.

Croot, P.L., Andersson, K., Öztürk, M., Turner, D.R., **2004b**. The distribution and speciation of iron along 6ºE in the Southern Ocean. Deep-Sea Research Part II 51 (22-24), 2857-2879.

Cullen, J.T., Bergquist, B.A., Moffett, J.W., **2006**. Thermodynamic characterization of the partitioning of iron between soluble and colloidal species in the Atlantic Ocean. Marine Chemistry 98 (2-4), 295-303.

Da Silva, J.J.R.F., Williams, R.J.P., **1991**. The Biological Chemistry of the Elements: The Inorganic Chemistry of Life, Oxford University Press, Oxford.

De Baar, H.J.W., Buma, A.G.J., Nolting, R.F., Cadée, G.C., Jacques, G., Tréguer, P.J., **1990**. On iron limitation of the Southern Ocean: experimental observations in the Weddell and Scotia Seas. Marine Ecology Progress Series 65 (2), 105-122.

De Baar, H.J.W., De Jong, J.T.M., Bakker, D.C.E., Löscher, B.M., Veth, C., Bathmann, U., Smetacek, V., **1995**. Importance of iron for plankton blooms and carbon dioxide drawdown in the Southern Ocean. Nature 373 (6513), 412-415.

De Baar, H.J.W., De Jong, J.T.M., **2001**. Distributions, sources and sinks of iron in seawater. In: D.R. Turner and K.A. Hunter (eds.), The Biogeochemistry of Iron in Seawater. Wiley and sons Chapter 5, Fig 5 pp. 135.

De Baar, H.J.W., La Roche, J., **2003**. Metals in the Oceans; Evolution, Biology and Global Change. In: Marine Scientific frontiers for Europe (eds. Lamy, F., Wefer, G.), 79-105, Springer Verlag, Berlin, Germany.

De Baar, H.J.W., Boyd, P.W., Coale, K.H., Landry, M.R., Tsuda, A., Assmy, P., Bakker, D.C.E., Bozec, Y., Barber, R.T., Brzezinski, M.A., Buesseler, K.O., Boye, M., Croot, P.L., Gervais, F., Gorbunov, M.Y., Harrison, P.J., Hiscock, W.T., Laan, P., Lancelot, C., Law, C.S., Levasseur, M., Marchetti, A., Millero, F.J., Nishioka, J., Nojiri, Y., Van Oijen, T., Riebesell, U., Rijkenberg, M.J.A., Saito, H., Takeda, S., Timmermans, K.R., Veldhuis, M.J.W., Waite, A.M., Wong, C.S., **2005**. Synthesis of Iron Fertilization Experiments: From the Iron Age in the Age of Enlightenment. Journal of Geophysical Research 110, C09S16.

De Baar, H.J.W., Timmermans, K.R., Laan, P., De Porto, H.H., Ober, S., Blom, J.J., Bakker, M.C., Schilling, J., Sarthou, G., Smit, M.G., Klunder, M., **2008a**. Titan: A new facility for ultraclean sampling of trace elements and isotopes in the deep oceans in the international Geotraces program. Marine Chemistry 111 (1-2), 4-21.

De Baar H.J.W., Gerringa, L.J.A., Laan, P., Timmermans, K.R., **2008b**. Efficiency of carbon removal per added iron in ocean iron fertilization. Marine Ecology Progress Series 364 , 269-282.

De Jong, J.T.M, Den Das, J., Bathmann, U., Stoll, M.H.C., Kattner, G., Nolting, R.F., De Baar, H.J.W., **1998**. Dissolved iron at subnanomolar levels in the Southern Ocean as determined by ship-board analysis. Analytica Chimica Acta 377 (2-3), 113-124.

Deacon, G.E.R., **1979**. The Weddell Gyre. Deep-Sea Research 26A, 981-995.

Desboeufs, K.V., Losno, R., Colin, J.L., **2001**. Factors influencing aerosol solubility during cloud processes, Atmospheric Environment 35 (20), 3529-3537.

Duce, R.A., Tindale, N.W., **1991**. Atmospheric transport of iron and its deposition in the ocean, Limnology and Oceanography 36 (8), 1715-1726.

Eppley, R.W., Peterson, B.J., **1979**. Particulate organic matter flux and planktonic new production in the deep ocean. Nature 282 (5740), 677-680.

Fahrbach, E., Hoppema, M., Rohardt, G., Schröder, M., Wisotzki, A., **2004**. Decadal-scale variations of water mass properties in the deep Weddell Sea. Ocean Dynamics 54 (1), 77-91.

Fisher, G., Fütterer, D., Gersond, R., Honjo, S., Ostermann, D., Wefer, G., **1988**. Seasonal variability of particle flux in the Weddell Sea and its relation to ice cover. Nature 335, 426-428.

Fitzwater, S.E., Coale, K.H., Gordon, R.M., Johnson, K.S., Ondrusek, M.E., **1996**. Iron deficiency and phytoplankton growth in the equatorial Pacific. Deep-Sea Research II Part 43 (4-6), 995-1015.

Fitzwater, S.E., Johnson, K.S., Gordon, R.M., Coale, K.H., Smith Jr., W.O., **2000**. Trace metal concentrations in the Ross Sea and their relationship with nutrients and phytoplankton growth. Deep-Sea Research II 47 (15-16), 3159-3179.

Flores, H., **2009**. Frozen Desert Alive. Ph.D. Thesis, University of Groningen, The Nettherlands. Electronic version available at: http://www.rug.nl/bibliotheek/catalogibestanden/elekpubrug/dissertaties/index

Foldvik, A., Gammelsrød, T., **1988**. Notes on Southern Ocean hydrography, sea-ice and bottom water formation. Palaeogeography, Palaeoclimatology, Palaeoecology 67 (1-2), 3-17.

GEOTRACES Planning Group, **2006**. GEOTRACES Science Plan. Scientific Committee on Oceanic Research, Baltimore, Maryland.

Gerringa, L.J.A., Herman, P.M.J., Poortvliet, T.C.W., **1995**. Comparison of the linear Van Den Berg/Ružić transformation and a non-linear fit of the Langmuir isotherm applied to Cu speciation data in the estuarine environment. Marine Chemistry 48 (2), 131-142.

Gerringa, L.J.A., Veldhuis, M.J.W., Timmermans, K.R., Sarthou, G., De Baar, H.J.W., **2006**. Co-variance of dissolved Fe-binding ligands with phytoplankton characteristics in the Canary Basin. Marine Chemistry 102 (3-4), 276-290.

Gerringa, L.J.A., Rijkenberg, M.J.A., Wolterbeek, H.Th., Verburg, T.G., Boye, M., De Baar, H.J.W., **2007**. Kinetic study reveals Fe-binding ligand, which affects the solubility of Fe in the Scheldt estuary. Marine Chemistry 103 (1-2), 30-45.

Gerringa, L.J.A., Blain, S., Laan, P., Sarthou, G., Veldhuis, M.J.W., Brussaard, C.P.D., Viollier, E., Timmermans, K.R., **2008**. Fe-binding organic ligands near the Kerguelen Archipelago in the Southern Ocean (Indian sector). Deep-Sea Research Part II 55, 606-621.

Gerringa, L.J.A., Alderkamp, A.-C., Laan, P., Thuróczy, C.-E., De Baar, H.J.W., Mills, M.M., Van Dijken, G.L., Van Haren, H., Arrigo, K.R., **submitted** Fe from melting glacier fuels the algal bloom in Pine Island Bay (Amundsen Sea, Southern Ocean). Deep-Sea Research Part II.

Gledhill, M., Van Den Berg, C.M.G., **1994**. Determination of complexation of iron (III) with natural organic complexing ligands in sea water using cathodic stripping voltammetry. Marine Chemistry 47 (1), 41-54.

Giulivi, C. F., Jacobs, S.S., **1997**. Oceanographic data in the Amundsen and Bellingshausen seas, NB Palmer cruise 9402, Feb–Mar 1994, Tech. Rep. LDEO-97-3, 330 pp., Lamont-Doherty Earth Obs. Of Columbia University, Palisades, N. Y.

Gledhill, M., McCormack, P., Ussher, S., Achterberg, E.P., Mantoura, R.F.C., Worsfold, P.J., **2004**. Production of siderophore type chelates by mixed bacterioplankton populations in nutrient enriched seawater incubations. Marine Chemistry 88 (1-2), 75-83.

Gouretski, V.V., Danilov, A.I., **1993**. Weddell Gyre: structure of the eastern boundary. Deep-Sea Research Part I 40 (3), 561-582.

Grashoff, K., Erhardt, M., Kremling, K., **1983**. Methods in SeawaterAnalyses. Verlag Chemie, Weinheim, Germany. 419 pp.

Grotti, M., Soggia, F., Ianni, C., Frache, R., **2005**.Trace metals distributions in coastal sea ice of Terra Nova Bay, Ross Sea, Antarctica. Antarctic Science 17 (2), 289-300.

Guay, C., Falkner, K., **1997**. Barium as a tracer of Arctic halocline and river waters. Deep-Sea Research Part II (44), 1543-1569.

Hassler, C.S., Schoemann, V., **2009**. Bioavailability of organically bound Fe to model phytoplankton of the Southern Ocean. Biogeosciences 6, 2281-2296.

Hassler, C.S., Alasonati, E., Mancuso Nichols, C.A., Slaveykova, V.I., **2011**. Exopolysaccharides produced by bacteria isolated from the pelagic Southern Ocean - Role in Fe binding, chemical reactivity, and bioavailability. Marine Chemistry 123 (1-4), 88-98.

Hayase, K., Tsubota, H., Sunada, I., Goda, S., Yamazaki, H., **1988**. Vertical distribution of fluorescent organic matter in the North Pacific. Marine Chemistry 25(4), 373.

Hayase, K., Shinozuka, N., **1995**. Vertical distribution of fluorescent organic matter along with AOU and nutrients in the equatorial Central Pacific. Marine Chemistry 48 (3-4), 283-290.

Haygood, M.G., Holt, P.D., Butler, A., **1993**. Aerobactin production by a planktonic marine Vibrio sp. Limnology and Oceanography 38 (5), 1091-1097.

Hirose, K., **2007**. Metal-organic matter interaction: Ecological roles of ligands in oceanic DOM. Applied Geochemistry 22 (8), 1636-1645.

Hudson, R.J.M., Rue, R.L., Bruland, K.W., **2003**. Modeling complexometric titrations of natural water samples. Environmental Science and Technology 37 (8), 1553-1562.

Hunter, K.A., Boyd, P.W., **2007**. Iron-binding ligands and their role in the ocean biogeochemistry of iron. Environmental Chemistry 4 (4), 221-232.

Hutchins, D.A., Witter, A.E., Butler, A., Luther, G.W., **1999a**. Competition among marine phytoplankton for different chelated iron species. Nature 400 (6747), 858-861.

Hutchins, D.A., Franck, V., Brzezinski, M.A., Bruland, K.W., **1999b**. Inducing phytoplankton iron limitation in iron-replete coastal waters with a strong chelating ligand. Limnology and Oceanography 44 (4), 1009-1018.

Jacobs, S.S., Hellmer, H.H., **1996**. Antarctic ice sheet melting in the Southeast Pacific. Geophysical Research Letters 23 (9), 957-960.

Jenkins, A., Dutrieux, P., Jacobs, S.S., McPhail, S.D., Perrett, J.R., Webb, A.T., White D., **2010**. Observations beneath Pine Island Glacier in West Antarctica and implications for its retreat. Nature Geoscience 3 (7), 468-472.

Jickells, T.D., An, Z.S., Andersen, K.K., Baker, A.R., Bergametti, G., Brooks, N., Cao, J.J., Boyd, P.W., Duce, R.A., Hunter, K.A., Kawahata, H., Kubilay, N., La Roche, J., Liss, P.S., Mahowald, N., Prospero, J.M., Ridgwell, A.J., Tegen, I., Torres, R., **2005**. Global iron connections between desert dust, ocean biogeochemistry, and climate. Science 308 (5718), 67-71.

Johnson, K.S., Gordon, R.M., Coale, K.H., **1997**. What controls dissolved iron concentrations in the world ocean? Marine Chemistry 57 (3-4), 137-161.

Johnson, K.S., Boyle, E., Bruland, K., Measures, C., Moffett, J., Aquilarislas, A., Barbeau, K., Cai, Y., Chase, Z., Cullen, J., Doi, T., Elrod, V., Fitzwater, S., Gordon, M., King, A., Laan, P., Laglera-Baquer, L., Landing, W., Lohan, M., Mendez, J., Milne, A., Obata, H., Ossiander, L., Plant, J., Sarthou, G., Sedwick, P., Smith, G.J., Sohst, B., Tanner, S., Van Den Berg, S., Wu, J., **2007**. Developing Standards for Dissolved Iron in seawater. Eos Transactions American Geophysical Union 88 (11), 131-132

Journet, E., Desboeufs, K.V., Caquineau, S., Colin, J.L., **2008**. Mineralogy as a critical factor of dust iron solubility. Geophysical Research Letters 35 (7), 47-51.

Kepkay, P.E., **1994**. Particle aggregation and the biological reactivity of colloids. Marine Ecology Progress Series 109 (2-3), 293-304.

Kiefer, D.A., **1973**. Chlorophyll a fluorescence in marine centric diatoms: Responses of chloroplasts to light and nutrient stress. Marine Biology 23 (1), 39-46.

Klatt, O., Fahrbach, E., Hoppema, M., Rohardt, G., **2005**. The transport of the Weddell Gyre across the Prime Meridian. Deep-Sea Research Part II 52, 513-528.

Klunder, M.B., Laan, P., Middag, R., De Baar, H.J.W., van Ooijen, J.C., **2011**. Dissolved Fe in the Southern Ocean (Atlantic sector). Deep-Sea Research Part II, doi:10.1016/j.dsr2.2010.10.042.

Klunder, M.B., Bauch, D., Laan, P., De Baar, H.J.W., Van Heuven S., Ober, S.. Dissolved iron in the Arctic shelf seas and surface waters of the Central Arctic Ocean: Impact of Arctic river water and ice-melt. **Submitted** to Journal of Geophysical Research-Oceans (a).

Klunder, M.B., Laan, P., Middag, R., De Baar, H.J.W.. Dissolved Fe in the Arctic Ocean: important role of hydrothermal sources, shelf input and scavenging removal. **Submitted** to Journal of Geophysical Research-Oceans (b).

Klunder, M.B., Laan, P., De Baar, H.J.W., **in prep**. Dissolved Fe in the Weddell Sea and in the Drake Passage. Thesis in preparation.

Kondo, Y., Takeda, S., Nishioka, J., Obata, H., Furuya, K., Johnson, W.K., Wong, C.S., **2008**. Organic iron (III) complexing ligands during an iron enrichment experiment in the western subarctic North Pacific. Geophysical Research Letters 35 (12), L12601.

Kuma, K., Nishioka, J., Matsunaga, K., **1996**. Controls on iron(III) hydroxide solubility in seawater: The influence of pH and natural organic chelators. Limnology and Oceanography 41 (3), 396-407.

Kuma, K., **2002**. Variation in iron(III) solubility and iron concentration in the northwestern North Pacific Ocean. Limnology and Oceanography 47(3), 885-892.

Laës, A., Blain, S., Laan, P., Achterberg, E.P., Sarthou, G., De Baar, H.J.W., **2003**. Deep dissolved iron profiles in the eastern North Atlantic in relation to water masses. Geophysical Research Letters 30 (17), 1902.

Laglera, L.M., Van Den Berg, C.M.G., **2007**. Wavelength dependence of the photochemical reduction of iron in Arctic seawater. Environmental Sciences and Technology 41 (7), 2296-2302.

Lam, P.J., Bishop, J.K.B., Henning, C.C., Marcus, M.A., Waychunas, G.A., Fung, I.Y., **2006**. Wintertime phytoplankton bloom in the subarctic Pacific supported by continental margin iron. Global Biogeochemical Cycles 20 (1), GB106.

Lam, P.J., Bishop, J.K.B., **2008**. The continental margin is a key source of iron to the HNLC North Pacific Ocean. Geophysical Research Letters 35 (7), L07608.

Lannuzel, D., Schoemann, V., De Jong, J., Tison, J.L., Chou, L., **2007**. Distribution and biogeochemical behaviour of iron in the East Antarctic sea ice. Marine Chemistry 106 (1-2), 18-32.

Lannuzel, D., Schoemann, V., De Jong, J., Chou, L., Delille, B., Becquevort, S., Tison, J.L., **2008**. Iron study during a time series in the western Weddell pack ice. Marine Chemistry 108 (1-2), 85-95.

Lannuzel, D., Schoemann, V., De Jong, Pasquer, B., Van Der Merwe, P., Masson, F., Tison, J.-L., Bowie, A., **2010**. Distribution of dissolved iron in Antarctic sea ice: Spatial, seasonal, and inter-annual variability. Journal of Geophysical Research 115, G03022.

Lewis, B.L., Holt, P.D., Taylor, S.W., Wilhelm, S.W., Trick, C.G., Butler, A., Luther III, G.W., **1995**. Voltammetric estimation of iron(II1) thermodynamic stability constants for catecholate siderophores isolated from marine bacteria and cyanobacteria. Marine Chemistry 50 (1-4), 179-188.

Liu, X. Millero, F.J., **2002**. The solubility of iron in seawater. Marine Chemistry 77 (1), 43-54.

Logan, B.E., Passow, U., Alldredge, A.L., Grossart, H.-P., Simon, M., **1995**. Rapid formation and sedimentation of large aggregates is predictable from aggregation rates (half lives) of transparent exopolymer particles (TEP). Deep-Sea Research Part II 42 (1), 203-214.

Lohan, M.C., Aguilar-Islas, A.M., Franks, R.P., Bruland, K.W., **2005**. Determination of iron and copper in seawater at pH 1.7 with a new commercially available chelating resin, NTA Superflow. Analytica Chimica Acta 530 (1), 121-129.

Macrellis, H.M., Trick, C.G., Rue, E.L., Smith, G., Bruland, K.W., **2001**. Collection and detection of natural iron-binding ligands from seawater. Marine Chemistry 76 (3), 175-187.

Maldonado, M.T., Strzepek, R.F., Sander, S., Boyd, P.W., **2005**. Acquisition of iron bound to strong organic complexes, with different Fe-binding groups and photochemical reactivities, by plankton communities in Fe-limited subantarctic waters. Global Biogeochemical Cycles 19 (4), GB4S23.

Mantyla, A.W., Reid, J.L., **1983**. Abyssal Characteristics of the World Ocean Waters. Deep-Sea Research Part A 30 (8), 805-833.

Martin, J.H., Gordon, R.M., **1988**. Northeast Pacific iron distributions in relation to phytoplankton productivity. Deep-Sea Research Part A 34 (2), 177-196.

Martin, J.H., Gordon, R.M., Fitzwater, S.E., **1990**. Iron in Antarctic waters. Nature 345 (6271), 156-158.

Martin, J.H., Gordon, R.M., Fitzwater, S.E., **1991**. The case for iron. Limnology and Oceanography 36 (8), 1793-1802.

Martinez, J.S., Butler, A., **2007**. Marine amphiphilic siderophores: Marinobactin structure, uptake, and microbial partitioning. Journal of Inorganic Biochemistry 101 (11-12), 1692-1698.

Measures, C.I., Yeats, P.A., Schmidt, D., **1995**. The hydrographic setting of the IOC base-line cruise to the eastern Atlantic 30-degrees-S to 35-degrees-N. Marine Chemistry 49 (4), 243-252.

Measures, C.I., **1999**. The role of entrained sediments in sea ice in the distribution of aluminium and iron in the surface waters of the Arctic Ocean. Marine Chemistry 68 (1-2), 59-70.

Measures, C.I., Landing, W.M., Brown, M.T., Buck, C.S., **2008**. High-resolution Al and Fe data from the Atlantic Ocean CLIVAR-CO2 repeat hydrography A16N transect: extensive linkages between atmospheric dust and upper ocean geochemistry. Global Biogeochemical Cycles 22 (1), GB1005.

Meiners, K., Krembs, C., Gradinger, R., **2008**. Exopolymer particles: microbial hotspots of enhanced bacterial activity in Arctic fast ice (Chukchi Sea), Aquatic Microbial Ecology 52, 195-207.

Middag, R., Klunder, M.B., Thuróczy, C.-E., Gerringa, L.J.A., De Baar, H.J.W., Timmermans, K.R., Laan, P. Aluminium, iron and manganese in relation to the Silicon cycle in the North East Atlantic Ocean. Personal communication.

Middag, R., De Baar, H.J.W., Laan, P., Baker, K., **2009**. Dissolved aluminium and the silicon cycle in the Arctic Ocean. Marine chemistry 115 (3-4), 176-195.

Middag, R., van Slooten, C., de Baar, H.J.W., Laan, P., **2011a**. Dissolved aluminium in the Southern Ocean. Deep-Sea Research Part II.

Middag, R., De Baar, H.J.W., Laan, P., Cai, P., Van Ooijen, J.C., **2011b**. Dissolved Manganese in the Atlantic sector of the Southern Ocean. Deep-Sea Research Part II, doi:10.1016/j.dsr2.2010.10.043.

Millero, F.J., Yao, W., Aicher, J., **1995**. The speciation of Fe(II) and Fe(III) in natural waters. Marine Chemistry 50 (1-4), 21-39.

Millero, F.J., **1998**. Solubility of Fe(III) in seawater. Earth and Planetary Science Letters 154 (1-4), 323-329.

Mills, M.M., Alderkamp, A.-C., Thuróczy, C.-E., van Dijken, G.L., Laan, P., De Baar, H.J.W., Arrigo, K.R., **submitted**. Phytoplankton biomass and pigment responses to Fe amendments in the Pine Island and Amundsen polynyas. Submitted to Deep-Sea Research Part II.

Moore, J.K., Braucher, O., **2008**. Sedimentary and mineral dust sources of dissolved iron to the world ocean. Biogeosciences 5 (3), 631-656.

Nishioka, J., Takeda, S., **2000**. Change in the concentrations of iron in different size fractions during growth of the oceanic diatom *Chaetoceros sp.*: importance of small colloidal iron. Marine Biology 137 (2), 231-238.

Nishioka, J., Takeda, S., Wong, C.S., Johnson, W.K., **2001**. Sized-fractionated iron concentrations in the northeast Pacific Ocean: distribution of soluble and small colloidal iron. Marine Chemistry 74 (2-3), 157-179.

Nishioka, J., Takeda, S, De Baar, H.J.W., Croot, P.L., Boye, M., Laan, P., Timmermans, K.R., **2005**. Changes in the concentration of iron in different size fractions during an iron enrichment experiment in the open Southern Ocean. Marine Chemistry 95 (1-2), 51-63.

Nistche, F.O., Jacobs, S.S., Larter, R.D., Gohl, K., **2007**. Bathymetry of the Amundsen Sea continental shelf: Implications for geology, oceanography, and glaciology. Geochemistry Geophysics Geosystems 8, Q10009.

Nolting, R.F., Gerringa, L.J.A., Swagerman, M.J.W., Timmermans, K.R., De Baar, H.J.W., **1998**. Fe(III) speciation in the high nutrient, low chlorophyll Pacific region of the Southern Ocean. Marine Chemistry 62 (3-4), 335-352.

Orsi, A.H., Johnson, G.C., Bullister, J.L., **1999**. Circulation, mixing, and production of Antarctic Bottom Water. Progress in Oceanography 43, 55-109.

Passow, U., **1991**. Species**-s**pecific sedimentation and sinking velocities of diatoms. Marine Biology 108 (3), 449-455.

Pollard, R.T., Lucas, M.I., Read, J.F., **2002**. Physical controls on biogeochemical zonation in the Southern Ocean. Deep-Sea Research Part II 49 (16), 3289-3305.

Powell, R.T., Donat, J.R., **2001**. Organic complexation and speciation of iron in the South and Equatorial Atlantic. Deep-Sea Research Part II 48 (13), 2877-2893.

Pusceddu, A., Cattaneo-Vietti, R., Albertelli, G., Fabiano, M., **1999**. Origin, biochemical composition and vertical flux of particulate organic matter under

the pack ice in Terra Nova Bay (Ross Sea, Antarctica) during late summer 1995. Polar Biology 22 (2), 124-132.

Raiswell, R., Benning, L.G., Tranter, M., Tulaczyk, S., **2008**. Bioavailable iron in the Southern Ocean: the significance of the iceberg conveyor belt. Geochemical Transactions 9, 7.

Reid, R.T., Live, D.H., Faulkner, D.J., Butler, A., **1993**. A siderophore from a marine bacterium with an exceptional ferric ion affinity constant. Nature 366 (6454), 455-458.

Reinthaler, T., Van Aken, H., Veth, C., Aristegui, J., Robinson, C., Williams, P.J.Le.B., Lebaron P., Herndl, G., **2006**. Prokaryotic respiration and production in the meso- and bathypelagic realm of the eastern and western North Atlantic basin. Limnology and Oceanography 51 (3), 1262-1273.

Riedel, A., Michel, C., Gosselin, M., LeBlanc, B., **2007**. Enrichment of nutrients, exopolymeric substances and microorganisms in newly formed sea ice on the Mackenzie shelf. Marine Ecology Progress Series 342, 55-67.

Riedel, A., Michel, C., Gosselin, M., LeBlanc, B., **2008**. Winter-spring dynamics in sea ice carbon cycling in the coastal Arctic Ocean. Journal of Marine Systems 74(3-4), 918-932.

Rignot, E., Bamber, J.L., Van Den Broek, M.R., Davis, C., Li, Y.H., Van De Berg, W.J., Van Meijgaard, E., **2008**. Recent Antarctic ice mass loss from radar interferometry and regional climate modelling. Nature Geoscience 1 (2), 106-110.

Rijkenberg, M.J.A., Powell, C.F., Dall'Osto, M., Nielsdottir, M.C., Patey, M.D., Hill, P.G., Baker, A.R., Jickels, T.D., Harrison, R.M., Achterberg, E.P., **2008a**. Changes in iron speciation following a Saharan dust event in the tropical North Atlantic Ocean. Marine Chemistry 110 (1-2), 56-67.

Rijkenberg, M.J.A., Gerringa, L.J.A., Timmermans, K.R., Fischer, A.C., Kroon, K.J., Buma, A.G.J., Wolterbeek, H.Th., De Baar, H.J.W., **2008b**. Enhancement of reactive iron pool by marine diatoms. Marine Chemistry 109 (1-2), 29-44.

Rudels, B., Muench, R.D., Gunn, J., Schauer, U., Friedrich, H.J., **2000**. Evolution of the Arctic Ocean boundary current north of the Siberian Shelves. Journal of Marine Systems 25 (1), 77-99.

Rue, E.L., Bruland, K.W., **1995**. Complexation of iron(III) by natural organic ligands in the Central North Pacific as determined by a new competitive ligand

equilibration/adsorptive cathodic stripping voltammetric method. Marine Chemistry 50 (1-4), 117-138.

Rue, E.L., Bruland, K.W., **1997**. The role of organic complexation on ambient iron chemistry in the equatorial Pacific Ocean and the response of a mesoscale iron addition experiment. Limnology and Oceanography 42 (5), 901-910.

Saito, M.A., Sigman, D.M., Morel, F.M.M., **2003**. The bioinorganic chemistry of the ancient ocean: the co-evolution of cyanobacterial metal requirements and biogeochemical cycles at the Archean-Proterozoic boundary? Inorganica Chimica Acta 356, 308-318.

Sarthou, G., Baker, A.R., Kramer, J., Laan, P., Laës, A., Ussher, S., Achterberg, E.P., De Baar, H.J.W., Timmermans, K.R., Blain, S., **2007**. Influence of atmospheric inputs on the iron distribution in the subtropical North-East Atlantic Ocean. Marine Chemistry 104 (3-4), 186-202.

Sarthou, G., Vincent, D., Christaki, U., Obernosterer, I., Timmermans, K.R., Brussaard, C.P.D., **2008**. The fate of biogenic iron during a phytoplankton bloom induced by natural fertilisation: Impact of copepod grazing. Deep-Sea Research Part II 55 (5-7), 734-751.

Sedwick, P.N., DiTullio, G.R., 1997. Regulation of algal blooms in Antarctic shelf waters by release of iron from melting sea ice. Geophysical Research Letters 24 (20), 2515-2518.

Sedwick, P.N., DiTullio, G.R., Mackey, D.J., **2000**. Iron and manganese in the Ross Sea, Antarctica: seasonal iron limitation in Antarctic shelf waters. Journal of Geophysical Research 105 (C5), 11 321-11 336.

Sievers, H.A., Nowlin, W.D., **1984**. The stratification and water masses at Drake Passage. Journal of Geophysical Research 89 (NC6), 489-514.

Sunda, W.G., Swift, D.G., Huntsman, S.A., **1991**. Low iron requirement for growth in oceanic phytoplankton. Nature 351 (6321), 55-57.

Sunda, W.G., Huntsman, S.A., **1997**. Interrelated influence of iron, light and cell size on marine phytoplankton growth. Nature 390 (6658), 389-392.

Sunda, W.G., **2001**. Bioavailability and Bioaccumulation of Iron in the Sea. Chapter 3 in: Turner, D.R., Hunter, K.A. (eds.). The Biogeochemstry of Iron in Seawater. Wiley and sons. 7, 41-84

Takata H., Kuma, K., Isoda, Y., Otosaka, S., Senjyu, T., Minagawa, M., **2008**. Iron in the Japan Sea and its implications for the physical processes in deep water. Geophysical Research Letters 35, L02606.

Tani, H., Nishioka, J., Kuma, K., Takata, H., Yamashita, Y., Tanque, Y., Tanoue, E., Midorikawa, T., **2003**. Iron(III) hydroxide solubility and humic-type fluorescent organic matter in the deep water column of the Okhotsk Sea and the northwestern North Pacific Ocean. Deep-Sea Research Part I 50, 1063-1078.

Taylor, S.R., **1964**. Abundance of chemical elements in the continental crust: a new table. Geochimica et Cosmochimica Acta 28 (8), 1273-1285.

Tomas, D.N., Kennedy, H., Kattner, G., Gerdes, D., Gough, C., Dieckmann, G.S., **2001**. Biogeochemistry of platelet ice: its influence on particle flux under fast ice in the Weddell Sea, Antarctica. Polar Biology 24 (7), 486-496

Tomczak, M., Godfrey, J.S., 2001. Regional oceanography: An introduction. First Edition (1994), Pergamon Edition. http://www.cmima.csic.es/mirror/mattom/regoc/pdfversion.html.

Thuróczy, C.-E., Boye, B., Losno, R., **2010a**. Dissolution of cobalt and zinc from natural and anthropogenic dusts in seawater. Biogeosciences 7 (6), 1927-1936.

Thuróczy, C.-E., Gerringa, L.J.A., Klunder, M.B., Middag, R., Laan, P., Timmermans, K.R., De Baar, H.J.W., **2010b**. Speciation of Fe in the Eastern North Atlantic Ocean. Deep-Sea Research Part I 57 (11), 1444-1453.

Thuróczy, C.-E., Gerringa, L.J.A., Klunder, M.B., Laan, P., De Baar, H.J.W., **2011a**. Observation of consistent trends in the organic complexation of dissolved iron in the Atlantic sector of the Southern Ocean. Deep-Sea Research Part II, in press.

Thuróczy, C.-E., Gerringa, L.J.A., Klunder, M.B., Laan, P., Le Guitton, M., De Baar, H.J.W., **2011b**. Distinct trends in the speciation of iron between the shelf seas and the deep basins of the Arctic Ocean. Journal of Geophysical Research-Oceans, in press.

Thuróczy, C.-E., Alderkamp, A.-C., Laan, P., Gerringa, L.J.A., M.M. Mills, G.L. Van Dijken, De Baar, H.J.W., Arrigo, K.R. Key role of organic complexation of iron in sustaining phytoplankton blooms in the Pine Island and Amundsen Polynyas (Southern Ocean). **Submitted** to Deep-Sea Research Part II.

Timmermans, K.R., Gledhill, M., Nolting, R.F., Veldhuis, M.J.W., De Baar, H.J.W., Van Den Berg, C.M.G., **1998**. Responses of marine phytoplankton in

iron enrichment experiments in the northern North Sea and northeast Atlantic Ocean. Marine Chemistry 61 (3-4), 229-242.

Timmermans, K.R., Davey, M.S., Van Der Wagt, B., Snoek, J., Geider, R.J., Veldhuis, M.J.W., Gerringa, L.J.A., De Baar, H.J.W., **2001**. Co-limitation by iron and light of Chaetoceros brevis, C. dichaeta and C. calcitrans Bacillariophyceae. Marine Ecology Progress Series 217, 287-297.

Timmermans, K.R., Van Der Wagt, B., De Baar, H.J.W., **2004**. Growth rates, half-saturation constants, and silicate, nitrate, and phosphate depletion in relation to iron availability of four large, open-ocean diatoms from the Southern Ocean. Limnology and Oceanography 49 (6), 2141-2151.

Timmermans, K.R., Van Der Wagt, B., Veldhuis, M.J.W., Maatman, A., De Baar, H.J.W., **2005**. Physiological responses of three species of marine pico-phytoplankton to ammonium, phosphate, iron and light limitation. Journal of Sea Research 53 (1-2), 109-120.

Tortell, P.D., Maldonado, M.T., Price, N.M., **1996**. The role of heterotrophic bacteria in iron-limited ocean ecosystems. Nature 383, (6598) 330-332.

Tortell, P.D., Maldonado, M.T., Granger, J., Price, N.M., **1999**. Marine bacteria and biogeochemical cycling of iron in the oceans. FEMS Microbiology and Ecology 29 (1), 1-11.

Turner, D.R., Hunter, K.A., De Baar, H.J.W, **2001**. Introduction in: Turner, D.R., Hunter, K.A. (eds.). The Biogeochemstry of Iron in Seawater. Wiley and sons. 7, 41-84.

Turoczy, N.J., Sherwood, J.E., **1997**. Modification of the Van Den Berg/Ruzic method for the investigation of complexation parameters of natural waters. Analytica Chimica Acta 354 (1-3), 15-21.

Ussher, S.J., Achterberg, E.P., Worsfold, P.J., **2004**. Marine Biogeochemistry of Iron. Environmental Chemistry 1, 67-80.

Ussher, S.J., Worsfold, P.J., Achterberg, E.P., Laës, A., Blain, S., Laan, P., De Baar, H.J.W., **2007**. Distribution and redox speciation of dissolved iron on the European continental margin. Limnology and Oceanography 52 (6), 2530-2539.

Van Aken, H.M., **2001**. The hydrography of the mid-latitude Northeast Atlantic Ocean-Part III: the subducted thermocline water mass. Deep-Sea Research Part I 48 (1), 237-267.

Van Der Merwe, P., Lannuzel, D., Mancuso Nichols, C.A., Meiners, K., Heil, P., Norman, L., Thomas, D.N., Bowie, A.R., **2009**. Biogeochemical observations during the winter-spring transition in East Antarctic sea ice: Evidence of iron and exopolysaccharide controls. Marine Chemistry 115 (3-4), 163-175.

Van Haren, H., Mills, D.K., Wetsteyn, L.P.M.J., **1998**. Detailed observations of the phytoplankton spring bloom in the stratifying central North Sea. Journal of Marine Research 56 (3), 655-680.

Van Leeuwen, H.P., Jansen, S., **2005**. Dynamic aspects of metal speciation by competitive ligand exchange–adsorptive stripping voltammetry (CLE–AdSV). Journal of Electroanalytical Chemistry 579, 337–342

Van Leeuwen, H.P., Raewyn, M.T., **2005**. Kinetic Limitations in Measuring Stabilities of Metal Complexes by Competitive Ligand Exchange-Adsorptive Stripping Voltammetry (CLE-AdSV). Environmental Science and Technology 39 (18), 7217-7225.

Verdugo, P., Alldredge, A.L., Azam, F., Kirchman, D.L., Passow, U., Santschi, P.H., **2004**. The oceanic gel phase: a bridge in the DOM-POM continuum. Marine Chemistry 92, 67-85.

Völker, C., Wolf-Gladrow, D.A., **1999**. Physical limits on iron uptake mediated by siderophores or surface reductases. Marine Chemistry 65 (3-4), 227-244.

Vraspir, J.M., Butler, A., **2009**. Chemistry of marine ligands and siderophores. Annual Review of Marine Science 1, 43-63.

Wells, M.L., Goldberg, E.D., **1993**. Colloid aggregation in seawater. Marine Chemistry 41 (4), 353-358.

Wells, M.L., Goldberg, E.D., **1994**. The distribution of colloids in the North Atlantic and Southern Oceans. Limnology and Oceanography 39 (2), 286-302.

Wells, M.L., Smith, G.J., Bruland, K.W., **2000**. The distribution of colloidal and particulate bioactive metals in Narragansett Bay, RI. Marine Chemistry 71 (1-2), 143-163.

Whitworth III, T., Nolwin Jr., W.D., **1987**. Water masses and Currents of the Southern Ocean at the Greenwich Meridian. Journal of Geophysical Research 92 (C6), 6462-6476.

Wilhelm, S.W., Trick, C.G., **1994**. Iron-limited growth of cyanobacteria: multiple siderophore production is a common response. Limnology and Oceanography 39 (8), 1979-1984.

Wilhelm, S.W., **1995**. Ecology of iron-limited cyanobacteria: a review of physiological responses and implications for aquatic systems. Aquatic Microbiology and Ecology 9, 295-303.

Wilhelm, S.W., Maxwell, D.P., Trick, C.G., **1996**. Response of the cyanobacterium Synechococcus PCC 7002 to iron-limitation: growth, iron requirements and siderophore production. Limnology and Oceanography 41, 89-97.

Wilhelm, S.W., MacAuley, K., Trick, C.G., **1997**. Evidence for the importance of catechol-type siderophores in the iron-limited growth of a cyanobacterium. Limnology and Oceanography 43, 992-997.

Witter, A.E., Luther III, G.W., **1998**. Variation in Fe-organic complexation with depth in the Northwestern Atlantic Ocean as determined using a kinetic approach. Marine Chemistry 62 (3-4), 241-258.

Witter, A.E., Hutchins, D.A., Butler, A., Luther III, G.W., **2000**. Determination of conditional stability constants and kinetic constants for strong model Fe-binding ligands in seawater. Marine Chemistry 69 (1-2), 1-17.

Wu, J., Luther III, G.W., **1995**. Complexation of Fe(III) by natural organic ligands in the Northwest Atlantic Ocean by a competitive ligand equilibration method and a kinetic approach. Marine Chemistry 50 (1-4), 159-177.

Wu, J., Boyle, E., Sunda, W., Wen, L.-S., **2001**. Soluble and colloidal iron in the oligotrophic north Atlantic and north Pacific. Science 293 (5531), 847-849.

Yamamoto-Kawai, M., Tanaka, N., Pivovarov, S., **2005**. Freshwater and brine behaviors in the Arctic Ocean deduced from historical data of d18O and alkalinity (1929-2002 A.D.). Journal of Geophysical Research 110 (C10), C10003.

Nerderlandse Samevatting

Fysische en Chemische Speciatie van IJzer in Polaire Wateren

1. Over ijzer en complexatie

IJzer (Fe) is vierde op de lijst van meest voorkomende elementen in de aardkorst (5 gewichtsprocent). Echter, de concentraties in zeewater zijn bijzonder laag. Tijdens de evolutie van de aarde ontstonden algen die fotosynthese konden doen. Dit introduceerde zuurstof in de oceanen zodat Fe op grote schaal neersloeg. Heden ten dage is Fe zo'n schaars element dat in 40% van de oceanen fytoplankton (algen) gelimiteerd worden in hun groei door gebrek aan ijzer. We noemen dat HNLC (hoog nutriënt, laag chlorofyl) gebieden.

Ondanks de lage concentratie, is Fe een essentieel element voor de groei van fytoplankton in de bovenste laag van de oceaan. Het wordt gebruikt in enzymen and belangrijke processen zoals fotosynthese. Fytoplankton is de basis van de voedselketen in de oceaan en is ook verantwoordelijk voor de vastlegging van het broeikasgas CO2. Microbes zoals bacteriën en archaea hebben ook Fe nodig om te kunnen leven. Deze organismen zijn in tegenstelling tot fytoplankton aanwezig in de gehele waterkolom. Zij zijn verantwoordelijk voor de afbraak en remineralisatie van naar beneden zinkend organisch materiaal.

Toch kan opgelost Fe aanwezig zijn in concentraties boven het oplosbaarheidsproduct van Fe-oxides en -hydroxides door de aanwezigheid van natuurlijke liganden. Deze liganden binden het opgeloste Fe en houden het daarmee in oplossing. Ze zijn voornamelijk organisch, afkomstig van organismen. De binding van Fe met deze liganden noemen we ook wel complexatie.

De verdeling van Fe over zijn opgeloste en vaste fases in zeewater hangt af van de competitie tussen processen die het oplossen en neerslaan bepalen en van de aanwezigheid van externe Fe bronnen. De binding door liganden zorgt voor het in oplossing gaan en blijven van Fe. Dit proces vergroot de verblijftijd van Fe in zeewater en verhoogt de potentiële beschikbaarheid van Fe voor organismen. Het verdwijnen uit de opgeloste fase wordt voornamelijk bepaald door neerslaan als oxide of als hydroxide en door "scavenging". Scavenging is een Engelse term die moeilijk te vertalen is, stofzuigen komt nog het meest in de buurt. Deeltjes groter dan 0.2 micron (>0.2 μm) die in de oceanen naar beneden zakken adsorberen Fe op de weg naar beneden. Dit adsorberen wordt scavenging genoemd. Van fijne

colloidale deeltjes is het bekend dat ze erg reactief zijn en dat de verblijftijd in zeewater lang kan zijn omdat ze niet zinken. Deze colloidale deeltjes kunnen echter een eerste stap vormen in het verdwijnen uit de opgeloste fase, omdat ze kunnen samenklonteren en als grotere aggregaten wel kunnen zinken.

2. De speciatie van Fe in dit onderzoek

In dit onderzoek werd de speciatie van Fe, de verdeling over de verschillende vormen waarin Fe voorkomt, bestudeerd. Dit werd gedaan door middel van filtratie in drie verschillende groottes (fysische speciatie) en door middel van chemische speciatie in iedere onderscheiden grootte. De studie van chemische speciatie bestond uit de karakterisering van de Fe bindende liganden door het bepalen van de bindingsterkte en van de concentratie van liganden.

De Fe speciatie werd bestudeerd in het kader van het internationale programma GEOTRACES tijdens het Internationale Polaire Jaar (International Polar Year, IPY). De eerste vaartocht vond plaats in 2007 in het oostelijk deel van de Atlantische Oceaan voor de kust van Portugal (Hoofdstuk 3). Hierna volgden drie vaartochten in polaire gebieden, de eerste in 2007 naar de Noordelijke IJszee (Hoofdstuk 6), een tweede in 2008 naar het Atlantische deel van de Zuidelijke Oceaan (Hoofdstukken 4 en 5) en de derde in 2009 naar de Amundsen Zee (Zuidelijke Oceaan) ten westen van het Antarctisch Schiereiland (Hoofdstuk 7). De belangrijkste conclusies worden hieronder besproken.

Drie fracties zijn onderscheiden in dit onderzoek: 1) de totale fractie waarmee het natuurlijke monster bedoeld wordt, dit bevat ook het particulaire deel (>0.2 μm), hierin wordt TDFe gemeten (dat gedeelte van het Fe in het gehele ongefiltreerde monster, dat kan oplossen na een half jaar aangezuurd te zijn geweest tot pH=2); 2) de opgeloste fractie (<0.2 μm) met DFe (opgelost Fe); en 3) de fractie kleiner dan 1000 kDa (<1000 kDa) die Fe in de zogenaamde werkelijk opgeloste fractie bevat (<10 kDa) en de kleine colloidale fractie bevat. Nadat scheiding in fracties zijn in de monsters Fe gemeten en zijn met behulp van voltammetrie de concentratie van de liganden bepaald en de sterkte waarmee ze Fe

binden, de conditionele bindingssterkte K'. De filtratie en andere analytische methodes worden beschreven in Hoofdstuk 2.

3. Belangrijkste resultaten

3.1. De oostelijk Noord-Atlantische Oceaan

De resultaten uit de eerste expeditie (Hoofdstuk 3) betreffen onderzoek aan een station in het oostelijk deel van de Atlantische Oceaan voor de kust van Portugal. Hier werd aangetoond dat met Fe in ongefiltreerde monsters (TDFe) het water dat uit de Middellandse Zee komt onderscheiden kan worden van andere watermassa's. Bovendien werd de verhouding tussen de concentratie van lege (niet met Fe gevulde) ligand plaatsen en de concentratie Fe uitgedrukt als: [Excess L]/[Fe] geïntroduceerd. De concentratie lege ligand -plaatsen geeft het potentieel aan om Fe te kunnen binden, terwijl deze concentratie onafhankelijk is van de Fe concentratie zelf. De reactiviteit van de liganden kan worden uitgedrukt met de zogenaamde alfa coefficient, het product van de conditionele bindingsterkte K' en de concentratie lege ligand plaatsen (alfa = [Excess L] x K'). De verhouding [Excess L]/[Fe] is daarmee een extra middel om de complexatie van Fe in oceaanwater te beschrijven. Deze parameter bleek erg nuttig te zijn om stations en zelfs oceaanbekkens met elkaar te vergelijken.

De fijne fractie (<1000 kDa) bleek de meest reactieve te zijn en speelde daarom een belangrijke rol in processen van oplossen, colloid aggregatie en scavenging.

3.2. De Atlantische sector van de Zuidelijke Oceaan

In de Atlantische sector van de Zuidelijke Oceaan (Hoofdstukken 4 en 5) werden hoge concentraties ligand-plaatsen gemeten in het bovenste deel van de waterkolom. Dit werd veroorzaakt door levende organismes, o.a. fytoplankton en bacteria, aan de ene kant door opname van Fe, aan de andere kant door de productie van organisch materiaal en daarmee ook organische liganden. Deze hoge concentratie aan lege ligand -plaatsen was vooral duidelijk in HNLC gebieden. Met toenemende diepte raakten de liganden meer verzadigd met Fe en bereikten rond 450 meter een evenwicht, dat gekarakteriseerd kan worden door [Excess

L]/[Fe] < 4. Het bereiken van een min of meer lage en constante waarde geeft aan dat er een soort evenwicht, steady state, bestaat tussen complexatie door liganden, scavenging en neerslaan, en dus tussen in oplossing blijven van Fe en export naar de oceaanbodem. De liganden hebben hier een sterk bufferende werking en vertragen de export van Fe. Omdat ze overal aanwezig blijken moeten ze resistent zijn tegen afbraak. De hoogste concentratie liganden werd gemeten in de kleinste fractie (<1000 kDa).

Tijdens deze expeditie werd voor de eerste keer een geografische trend gevonden in de karakteristieken van de organische Fe complexatie met behulp van de verhouding [Excess L]/[Fe]. Deze horizontale trend in het diepe gedeelte (>450 m) van de oceaan werd toegeschreven aan de afstand tot Fe bronnen en aan scavenging. Analyse van de ongefiltreerde fractie liet zien dat in de fractie >0.2 μm geen meetbare reversibele binding of adsorptie van Fe plaatsvindt. Dit terwijl TDFe met de diepte toeneemt, hetgeen toegewezen wordt aan scavenging.

3.3. De Noordelijke IJszee

Conclusies uit het onderzoek in de Noordelijke IJszee brachten inzicht in de processen die de cyclus van Fe in de oceaan bepalen. Ook hier waren duidelijke trends in de concentraties Fe en liganden aanwezig, zowel vertikaal als horizontaal vanaf de Russische shelf-zeeën naar het Makarov bekken in de centrale Noordelijke IJszee. De verhouding [TDFe]/[DFe] liet zien dat er een relatieve verrijking van particulair Fe met de diepte optrad, een sterke indicatie voor scavenging en export van Fe naar de bodem van de oceaan. Zoals ook elders is gevonden, raakten de liganden meer verzadigd met de diepte in de Amundsen en Nansen bekkens. Een uitzondering werd gevormd door een station in het Makarov bekken, waar de liganden Fe kwijtraakten met de diepte. Dit onverwachte verschijnsel kon verklaard worden door een relatief lage reactiviteit van de liganden (alfa) in het Makarov bekken in combinatie met een gebrek aan Fe bronnen in de nabijheid. Ondanks een hoge concentratie aan lege ligand plaatsen werd er zo weinig Fe van elders aangevoerd dat het verlies door scavenging niet

gecompenseerd kon worden. Dit had ook hier een netto export van Fe tot gevolg richting oceaan bodem.

3.4. De Amundsen Zee, Zuidelijke Oceaan

Tijdens de laatste expeditie naar de Zuidelijke Oceaan, in de Amundsen Zee (Hoofdstuk 7) bleek dat de organische complexatie van Fe in de bovenste 300 m van de oceaan een cruciale rol speelde om de grote fytoplankton bloei, die meer dan 70 dagen duurde, van Fe te voorzien. In de Amundsen Zee treedt een natuurlijke bemesting met Fe op door warm Circumpolair Diep Water (CDW) dat opstroomt tot onder gletsjers, die van land in zee uitkomen. De gletschers smelten hierdoor aan de onderkant extra af waarbij veel Fe vrijkomt. Bovendien fungeert opwerveling van sediment als een bron van liganden tijdens het opstromen van het CDW, aangezien hoge ligand concentraties werden waargenomen in stations bij de gletschers. Dankzij de aanwezigheid van de liganden kon Fe uit het smeltwater gecomplexeerd worden. De liganden waren compleet verzadigd nabij de gletsjers. Het overige vrijgekomen Fe (>99%) sloeg neer en/of werd “gescavenged” en verdween naar de bodem. Via lateraal transport kon het gecomplexeerde Fe naar de fytoplankton bloei in de polynya (ijsvrij gebied met specifieke eigenschappen) bereiken.

Met toenemende afstand vanaf de gletschers nam de concentratie lege ligand plaatsen toe, wat indicatief is voor opname van Fe door fytoplankton. Deze lege plaatsen zullen waarschijnlijk een rol spelen wanneer Fe vrijkomt na afbraak van organisch materiaal.

5. Hoogtepunten uit het onderzoek

De analyse van de organische complexering van Fe na ultra-filtratie toonde aan, via de concentratie van ongebonden, lege ligand plaatsen (Excess L), dat de meeste opgeloste liganden (<0.2 μm) voorkomen in de fijnste fractie (<1000 kDa). Veranderingen in de concentratie van organische liganden in de opgeloste fase worden dus veroorzaakt door veranderingen in de kleine colloïdale fractie. De liganden in deze <1000 kDa fractie waren over het algemeen iets minder verzadigd

met Fe dan in opgeloste fractie (<0.2 µm) en waren sterker. Beide eigenschappen wijzen er op dat de kleine colloidale fractie de verdeling van Fe bepaalde over de fracties in zeewater.

Wanneer de verdeling van Fe over de fracties beschouwd wordt, valt op dat er een grote verscheidenheid is tussen de bestudeerde oceanen. De reden van dit verschil ligt in de variatie in natuurlijke omstandigheden, zoals externe bronnen van Fe en verschillen in primaire productie. In de diepe lagen van de oceanen is de verdeling van Fe over de fracties gerelateerd aan de verblijftijd. De verblijftijd van Fe wordt op zijn beurt weer geregeerd door de mate van "scavenging". In de Noordelijke IJszee was de mate van scavenging tamelijk hoog. Dit werd geconcludeerd uit de relatieve verrijking van particulair Fe met de diepte en het daarmee gepaard gaande verlies van Fe in fractie met grote colloïdale deeltjes. Het percentage grotere colloidale deeltjes bedroeg slechts 25% van het opgeloste Fe (DFe). Waarschijnlijk zijn deze grotere colloidale deeltjes samengeklonterd tot particulaire deeltjes en gaan daarom uitzinken en dus ook "scavengen". In de oceaan rond Antarctica, de Zuidelijke Oceaan, daarentegen, was de mate van scavenging lager hetgeen weerspiegeld werd door een hoger percentage grotere colloidale deeltjes (50% van DFe). In de Atlantische Oceaan bij Portugal was zelfs 80% van DFe aanwezig als grotere colloïdale deeltjes. De circulatie van water massa's speelde hierin ongetwijfeld ook een rol en hiermee wordt ook de hier ontbrekende dimensie tijd geintroduceerd.

Indien er Fe bronnen aanwezig zijn, worden met de diepte de liganden verzadigd met Fe. Maar als er geen bronnen in de buurt zijn, worden de liganden steeds meer onder-verzadigd aan Fe als functie van de diepte, hetgeen een indicatie is voor een verlies van Fe uit de opgeloste fase naar de particulaire fase. De resultaten uit ongefiltreerde monsters bieden uitkomst. TDFe (totaal oplosbaar Fe) en de verhouding TDFe/DFe (totaal oplosbaar Fe/opgelost Fe) ondersteunen de hypothese van een toename van particulair Fe met de diepte en dus van export van Fe uit de opgeloste fase van de oceaan.

Scavenging speelde overal een belangrijke rol, zowel in alle Arctische bekkens als in de Zuidelijke Oceaan, waarschijnlijk door het continue karakter van de regen van deeltjes naar de bodem van de oceaan. De deeltjes hebben een grote affiniteit voor Fe en zullen altijd concurreren met de opgeloste liganden. Als er geen bron van Fe in de nabijheid is, zullen de deeltjes uiteindelijk winnen en Fe uit de liganden halen. De liganden dienen als buffer, ze controleren de oplosbaarheid van Fe in zeewater, vertragen scavenging en neerslag van Fe-oxiden, maar uiteindelijk kunnen ze niet verhinderen dat Fe via scavenging uit de opgeloste fase verdwijnt.

Opgeloste liganden, Fe bronnen and scavenging zijn daarom de drie voornaamste factoren die de verblijftijd van Fe in de oceanen bepalen.

Acknowledgments

First and foremost, I want to express my full gratitude and my best feelings to Hein De Baar and Loes Gerringa who offered me the great opportunity to start and achieve this unique thesis, for their help and advices and for the many kilometers spend all around the globe by boat and by plane!

This work would not have been possible without the help and the participation of my colleagues Maarten Klunder and Patrick Laan, thank you. I am also very grateful to Anne-Carlijn Alderkamp and Kevin Arrigo for giving us the opportunity to join the DynaLiFe team in the Amundsen Sea. I want to acknowledge Marie Boyé for motivating me to start this thesis and for her many advices. I give many thanks to those who surrounded me during these 4 years spent on Texel and at sea, I won't forget them, the great time I had with them and their constant support; hereby I think of Astrid, Rob, Célia, Claire, Véronique, Jeroen and Louise, Leslie, Frank, Joost, John, Luis and Sofia, Eva, Antoine and Béa, and my dear roommates Catarina, Sabine, Taichi and Daniele. I greatly thank Marc, Suzanne, Arjen and Annabelle for joining successfully my research project.

We want to send our recognition and gratefulness to Jun Nishioka for sharing his knowledge and for helping us with getting the filters.

I also acknowledge Joke Mulder for helping me trough many administrative tasks, and the workshop team for building us amazing customised tools. We thank Jan van Ooyen, Karel Baker and Sven Ober for the nutrients and the CTD data. We are most grateful to Captain John Ellen of R.V. *Pelagia,* Captain Stefan Schwarze of R.V. *Polarstern* and Captain Mike Watson of R.V. *Nathaniel B. Palmer* and their respective crew as well as the respective chiefs scientists, Klaas Timmermans, Ursula Schauer, Eberhard Fahrbach and Stanley Jacobs.

Acknowledgments

It is an honor for me to have my colleagues, but before all friends, Astrid and Maarten to my sides as paranimfs during the ceremony, thank you so much.

My final thank, but not the least, goes to my Marie for her permanent and lovely support, for believing in me and for giving me motivation and energy when it was needed, despite the many kilometers between us.

<3

I dedicate this thesis to my family and in memory of my godmother and grandmother. I will also never forget our colleagues Willem Polman and Stefan Winter who did not return from Antarctica.

This whole project was funded by NWO. Geotraces sub-project: 851.40.102.

Borned on 21st January 1983 in Bois-Colombes, France, I finished my university education in 2006, in Marine Biology and Environmental Chemistry at the European Institute for Sea Research (IUEM) in Brest. In 2005, I had my first experience as research assistant in marine phytoplantonnic eco-toxicology with Prof. Annick Hourmant, University of Western Britany, France. The next year, my interest for marine geochemistry increased considerably so I did my second internship with dr. Marie Boyé (IUEM) in collaboration with Prof. Rémi Losno from the Laboratory of Atmospheric Systems (LISA), Paris. From this work on the dissolution of cobalt and zinc from natural and anthropogenic dusts in seawater followed my first publication. After graduating, I got the opportunity to start this fantastic PhD thesis with Prof. Hein De Baar and dr. Loes Gerringa at the Royal Netherlands Institut for Sea Research.

Thuróczy, C.-E., Boye, B., Losno, R. 2010a. Dissolution of cobalt and zinc from natural and anthropogenic dusts in seawater. Biogeosciences 7 (6), 1929-1936. doi: 10.5194/bg-7-1927-2010.

Thuróczy, C.-E., Gerringa, L.J.A., Klunder, M.B., Middag, R., Laan, P., Timmermans, K.R., De Baar, H.J.W. 2010b. Speciation of Fe in the Eastern North Atlantic Ocean. Deep-Sea Research I 57 (11), 1444-1453. doi: 10.1016/j.dsr.2010.08.004.

Thuróczy, C.-E., Gerringa, L.J.A., Klunder, M.B., Laan, P., De Baar, H.J.W. 2011a. Observation of consistent trends in the organic complexation of iron in the Atlantic sector of the Southern Ocean. Deep-Sea Research II. doi: 10.1016/j.dsr2.2011.01.002.

Thuróczy, C.-E., Gerringa, L.J.A., Klunder, M.B., Laan, P., Le Guitton, M., De Baar, H.J.W., 2011b. Distinct trends in the speciation of iron between the shelf seas and the deep basins of the Arctic Ocean. Journal of Geophysical Research. doi:10.1029/2010JC006835.

Thuróczy, C.-E., Alderkamp, A.-C., Laan, P., Gerringa, L.J.A., De Baar, H.J.W., Arrigo, K.R. Key role of organic complexation of iron in sustaining phytoplankton blooms in the Pine Island and Amundsen Polynyas (Southern Ocean). Submitted to Deep-Sea Research II.